Universidad Carlos III de Madrid
www.uc3m.es

TESIS DOCTORAL

Mechanical and multifunctional properties of polymer composites based on nano-structures

Autor:

Luis Carlos Herrera Ramírez

Director/es:

Dr. Roberto Guzmán de Villoria

Tutor:

Dr. Jon Mikel Molina Aldareguía

Departamento de Ciencia e Ingeniería de Materiales e Ingeniería Química

Leganés, octubre 2017

Abbreviations

0D	Zero-dimensional
1D	One-dimensional
2D	Two-dimensional
3D	Three-dimensional
3PB	Three-point bending
BSE	Back-scattered electrons
CB	Carbon black
CFRP	Carbon fibre-reinforced polymer
CNT	Carbon nanotube
CMF	Carbon microfiller
CNF	Carbon nanofiber
DC	Direct current
DMA	Dynamic mechanical analysis
DSC	Differential scanning calorimetry
EDS	Energy dispersive spectroscopy
FRP	Fibre-reinforced polymer
GNP	Graphite nanoplatelet
G_{IC}	Mode I critical strain energy release rate
HGM	Hollow glass microsphere
HGM-CNF	Hollow glass microsphere/Carbon nanofiber
h-NP	Alumina nanoparticle/Carbon nanotube
K_{IC}	Plane-strain mode I fracture toughness
E''	Loss modulus
MWNT	Multi-walled carbon nanotube
NP	Alumina spherical nanoparticle
PP	Polypropylene
SE	Secondary electrons
SEM	Scanning electron microscopy
SENB	Single-edge-notch bend specimen
SWNT	Single-walled carbon nanotube
E'	Storage modulus
TEM	Transmission electron microscopy
T_g	Glass transition temperature
TGA	Thermogravimetric analysis
X_C	Degree of crystallinity

Abstract

The continuous development of industries, such as aerospace, automobile or energy, requires a new generation of polymer composites with novel functionalities, i.e. desired values of thermal and electrical conductivities, while maintaining their mechanical properties to be used in structural applications. One example of this new generation of composites could be hybrid fibre-reinforced polymers, consisting in fibre-reinforced polymers in which the matrix is appropriately modified with fillers.

As a first step in the above mentioned approach, in this thesis the modification of polymers with different carbon-based fillers is analysed. Graphite nanoplatelets and carbon nanotubes were used to prepare polypropylene composites. Both fillers provided modest improvements on mechanical properties, while the electrical conductivity of the CNT composites was comparable to similar materials previously reported. The third filler was a novel micron-scaled carbon material which exhibited potential to perform as reinforcing agent in polymeric matrices. It was found that the filler significantly enhanced the thermal stability of the composites, while having modest effect on their thermal conductivity and mechanical behaviour.

In order to produce polymer composites with specific combination of properties, hybrid carbon-based fillers, using spherical micro- and nano-particles as substrates, were obtained by the chemical vapour deposition technique (CVD).

The first developed hybrid filler consisted in alumina nanoparticles and carbon nanotubes and it was used as filler for epoxy matrix composites. The obtained composites showed enhanced thermal and electrical conductivity compared with the neat matrix, although having similar mechanical behaviour. Finally, hollow glass microspheres with carbon nanofibres grown on its surface were obtained and then dispersed within a urethane acrylate resin. The main characteristic of the resulting composites is their low density and thermal conductivity while having higher electrical conductivity, compared to the neat resin.

Resumen

El continuo desarrollo de industrias como la aeroespacial, del automóvil o de la energía, requiere una nueva generación de materiales compuestos poliméricos con nuevas características, como niveles deseados de conductividades térmicas y eléctricas, y que al mismo tiempo mantengan unos niveles de propiedades mecánicas adecuados para ser usados en aplicaciones estructurales. Un ejemplo de materiales compuestos poliméricos mejorados podrían ser los materiales compuestos híbridos de matriz polimérica reforzados con fibras, en los cuales la matriz polimérica está modificada con los refuerzos apropiados.

Como primera etapa en el desarrollo de los materiales anteriormente mencionados, en ésta tesis se han analizado varios polímeros modificados con diferentes refuerzos basados en carbono. Se han empleado nanoplaquetas de grafito y nanotubos de carbono para la preparación de materiales compuestos de matriz polipropileno. Ambos refuerzos proporcionaron ligeros aumentos de las propiedades mecánicas, mientras que la conductividad eléctrica de los materiales con nanotubos de carbono es comparable a la de materiales similares reportados en la literatura disponible. El tercer material es un novedoso refuerzo micrométrico basado en carbono, que ha sido empleado para el procesado de materiales compuestos de polipropileno. Éste refuerzo mejoró significativamente la estabilidad térmica del polipropileno al mismo tiempo que produjo mejoras más modestas en conductividad térmica y propiedades mecánicas.

Con el objetivo de obtener materiales compuestos con las combinaciones deseadas de propiedades, se han obtenido materiales híbridos en estructuras de carbono por medio de un proceso de deposición química en fase vapor. Para ello se han empleado partículas cerámicas micro y nanométricas.

En primer lugar se ha desarrollado un material híbrido compuesto por nanopartículas de alúmina y nanotubos de carbono, usado como refuerzo para una resina epoxi. Los materiales compuestos obtenidos presentaron mayores niveles de conductividad térmica y eléctrica mayores comparados con la matriz sin modificar, sin embargo su comportamiento mecánico era similar al de la resina.

En segundo lugar se han obtenido microesferas de vidrio huecas con nanofibras de carbono sintetizadas en su superficie. Éste material se ha usado como refuerzo de materiales compuestos con una resina uretano acrilato. Las principales características de los materiales desarrollados son su baja densidad y conductividad térmica y alta conductividad eléctrica, comparada con la resina pura.

Table of Contents

1 Motivation and thesis outline

1.1 Motivation

Fibre-reinforced polymers (FRPs) are a specific type of polymer composite designed to provide superior strength-to-weight and stiffness-to-weight ratios than steels or aluminium. In structural applications, FRPs generally adopt a two-dimensional configuration of laminates composed by carbon fibre plies held together by a polymer, intended to maximize the in-plane specific stiffness and specific strength. However, the interlayer region of these laminates are matrix-rich regions that can crack easily and reduce the electrical and thermal conductivity in the through-thickness direction, compared to the in-plane direction.

A possible approach to overcome these drawbacks is to modify the matrix of the FRPs with appropriate fillers to yield desired levels of electrical and thermal conductivity, while maintaining or improving the mechanical behaviour of the matrix.

In the las two decades carbon-based fillers, as carbon nanotubes, carbon nanofibres, graphene and its derivatives, have been extensively studied to be fillers in polymer composites due to their outstanding electrical, thermal and mechanical properties.

The first main objective of this thesis was to study the effect of different carbon fillers on the properties of a polypropylene (PP) matrix.

- Objective 1: In first place, PP composites with graphite nanoplatelets, a graphene-based filler, were studied. Due to the lack of extensive research done in the field of quasistatic fracture behaviour of PP, the objective of this works was to provide a detailed analysis of the fracture mechanism of the resulting composites.

- Objective 2: In second place, the mechanical and electrical properties of PP composites with CNTs were assessed. In this case, the objective was to

study the effect of the processing approach on the resulting morphology of the composites. Moreover, the identification of fracture mechanism of the resulting composites was also addressed.

- Objective 3: In this thesis a novel carbon microfiller was developed. This filler showed potential to be used as filler for polymer composites. Thus, the third objective of this thesis was to analyse the effect of the carbon microfiller on the mechanical and thermal properties of polypropylene.

In spite of the outstanding properties of carbon fillers, some applications may require composites with certain properties which are extremely difficult to obtain with a single filler. Therefore, the combination of carbon materials with a secondary material, to obtain hybrid polymer composites, is a promising approach to achieve new materials with an unusual combination of properties or higher properties improvements, compared to the composites with the isolated fillers.

The second main objective of this thesis was to develop hybrid fillers based on spherical micro- and nano-particles. To do so, the chemical vapour deposition technique (CVD) was used for the synthesis of carbon-based nano-structures.

- Objective 4: In first place, the attention was focused on the development of a hybrid filler composed by nanoparticles and carbon materials, since there were no reported works concerning hybrid fillers obtained by CVD using nanoparticles as substrate. The second objective was to study the applicability of this hybrid material as filler for epoxy composites.

- Objective 5: Some applications required polymeric materials with high levels of electrical conductivity while maintaining or improving their thermal insulating behaviour. Therefore, the last objective of this thesis was to provide an approach to satisfy that requirement. This was done by the combination of hollow glass microspheres and carbon nanofibres to obtain a hybrid filler.

1.2 Thesis outline

This thesis is organized in the following chapters:

Chapter 2 Introduction

The background of polymer composites and fibre-reinforced polymers is given. The modification of the matrix with carbon-based fillers is presented as an approach to overcome the drawbacks of fibre-reinforced polymers. Therefore, a review of carbon fillers, especially carbon nanotubes, nanofibres, graphene and graphene nanoplatelets, was done.

Since the combination of fillers is a promising approach to obtain multifunctional composites with the desired properties, the background of hybrid fillers is presented. The next section deals with the state-of-the-art of hybrid fillers obtained by the synthesis of carbon nanotubes on different substrates (micron-scaled fibres, two- and three-dimensional particles) by chemical vapour deposition.

Chapter 3 How do graphite nanoplatelets affect the fracture toughness of polypropylene composites?

From a mechanical perspective, graphene and its derivatives, such as graphite nanoplates, graphite oxide, carbon nanofibers, or nanotubes, are envisioned as ideal nanofillers for polymer composites. Thus, tremendous research effort have been invested in order to determine the reinforcing mechanism of these nanofillers in the matrix: crack bridging, crystallization enhancement or crack deflection are some possible mechanisms proposed. In this work, a detailed analysis of the fracture mechanism of graphite nanoplates (GNPs)/polypropylene composites was performed. Commercially available graphite nanoplates, composed of multiple graphene layers stacked together, were used to produce polypropylene nanocomposites by following a masterbatch technique. The fracture toughness was determined applying the S_{pb} parameter method and the fracture mechanism was identified as void nucleation and growth. In this work is demonstrated that GNPs affect the fracture toughness of polypropylene, by improving it. The

mechanism responsible for this improvement is the debonding of the GNP agglomerates, which promotes the matrix plastic deformation during the fracture process.

Chapter 4 The effect of a semi-industrial masterbatch process on the carbon nanotube agglomerates and its influence in the properties of thermoplastic carbon nanotube composites

The present study details an industrial process to prepare polypropylene (PP) composites reinforced with different loadings (0.5-10wt.%) of carbon nanotubes (CNTs) from a direct dilution of a masterbatch produced by an optimised extrusion compounding process. The work demonstrates how the anisotropy in the distribution of CNTs can have a positive effect on the electrical conductivity and fracture toughness of the resulting composites. The composite with the highest loading of CNTs had an electrical conductivity of 10^{-2} S/m comparable to those reported in the available literature. The composites showed anisotropy in their properties that seems to be caused by the non-homogeneous distribution of the agglomerates produced by the orientation of the flow direction during the injection process. The composites produced in this work exhibited a fracture toughness up to 55% higher than neat PP and failed by polymer ductile tearing. It was found that the CNT agglomerates distributed throughout the matrix increased the toughness of PP by promoting plastic deformation of the matrix during the fracture process and by a slight load transfer between the polymer matrix and the CNTs of the agglomerates.

Chapter 5 Polypropylene composites with enhanced mechanical and thermal properties thanks to a novel carbon microfiller

The potential of a novel carbon micron-scaled material to be used as filler in polypropylene (PP) composites was analysed in this work. The filler exhibited high growth yield, being a promising filler to be produced at large-scale, and a fibre-like structure with a highly rough surface morphology, being also a promising filler to improve the mechanical properties due to mechanical interlocking. Although after the processing of the composites by a masterbatch approach, the fibre-like structures that were obtained after the synthesis were broken, the resulting

carbon microfiller (CMF) was homogeneously distributed within the matrix. Moreover, the resulting composites exhibited improved thermal stability and conductivity. It was found that, likely due to its surface morphology, the CMF acted as nucleating agent for the crystalline phase of PP and some degree of mechanical interlocking effect took place, since the addition of CMF resulted in composites with enhanced mechanical properties. Further work should be done to understand the effect of the filler on the crystalline morphology of PP and their effect on the plastic deformation, e.g. strain at break and fracture behaviour, of composites. The obtained results make the CMF/PP composite very attractive for the development of commercially available polymer composites with improved mechanical and thermal properties.

Chapter 6 Alumina nanoparticle/carbon nanotube hybrid filler and its application to epoxy composites

Hybrid materials offer the opportunity to obtain polymer composites with desired properties which cannot be obtain when using a single material as filler. In this work a nano-scaled hybrid material composed by spherical alumina nanoparticles and carbon nanotubes was developed. An aerospace-grade epoxy resin was used as matrix for nanocomposites filled with the hybrid material and the as-received nanoparticles for comparison purposes. The resulting composites showed similar mechanical behaviour but enhanced thermal conductivity, compared to the neat epoxy and the composites with nanoparticles without carbon nanotubes. The presence of CNTs in the hybrid filler resulted in a composite with an electrical conductivity of $1 \pm 0.3 \times 10^{-3}$ S/m, compared with the electrically insulating matrix and nanoparticle composites.

Chapter 7 Low thermal and high electrical conductivity in hollow glass microspheres covered with carbon nanofiber–polymer composites

To take advantage of both the low density and thermal conductivity of hollow glass microspheres, and the high mechanical and electrical conductivity of carbon-based nanofillers, micro- and nanosized fillers can be combined into a single composite material. Here we prepared composite materials from hollow glass microspheres (HGMs) and from the same microspheres surrounded by carbon nanofibers

(CNFs). By adding 10% wt. of HGM-CNFs to a high-temperature resin we can obtain a low density (0.8 g/cm^3), low thermally (0.17 W/mK) and high electrically conductive ($7 \pm 3 \times 10^{-4}$ S/m) composite. This novel method demonstrates the possibility to achieve an unusual combination of properties such as low thermal and high electrical conductivity which, along with their light weight and thermal stability, makes these materials promising for aerospace applications or thermoelectric devices.

Chapter 8 Concluding remarks and future work

Finally, this chapter summarizes the conclusions obtained from the work done during this thesis. Further work to be done in order to complete or develop the presented results is proposed.

2 Introduction

2.1 Background

Polymers are materials composed by long chains of repeating groups of atoms joined to each other by covalent bonds [1]. Depending on their molecular structure and properties they can be divided in three categories: thermoplastics, thermosets and elastomers. The different properties will determine the application where they are used. In spite of their differences, in general, polymers provide a wide number of advantages over metals or ceramics such as lower cost, lower densities, ease of fabrication and chemical resistance. However due to the low level of their mechanical properties (Figure 2.1) the use of polymers in structural applications is limited [2,3].

In order to overcome the limitations of polymers, composites has been developed. Composites are the result of the combination of two or more materials, retaining their chemical and physical properties and having an identifiable interface between them [4]. The combination of the different materials is done in a way that allows to obtain superior or different properties than their constituents [2]. Therefore, when polymers are combined with one or more materials, producing polymer-matrix composites, they can give the best overall and desired performance.

2.1.1 Fibre-reinforced polymers (FRPs)

The most commonly used polymer composite, designed to provide superior strength-to-weight and stiffness-to-weight ratios than steels or aluminium, are continuous fibre-reinforced polymers (FRPs) [5,6] (Figure 2.1). FRPs are highly demanded for a variety of applications in industries as transport (aerospace, marine, automobile), sport or even civil engineering [7,8]. As an example of the importance that FRPs have in aerospace industries, the new A350 of Airbus has up to 52% in weight made of composite materials and also Boeing claimed to have developed the first aircraft with a full-scale one-piece composite fuselage section (Boeing 787) [9].

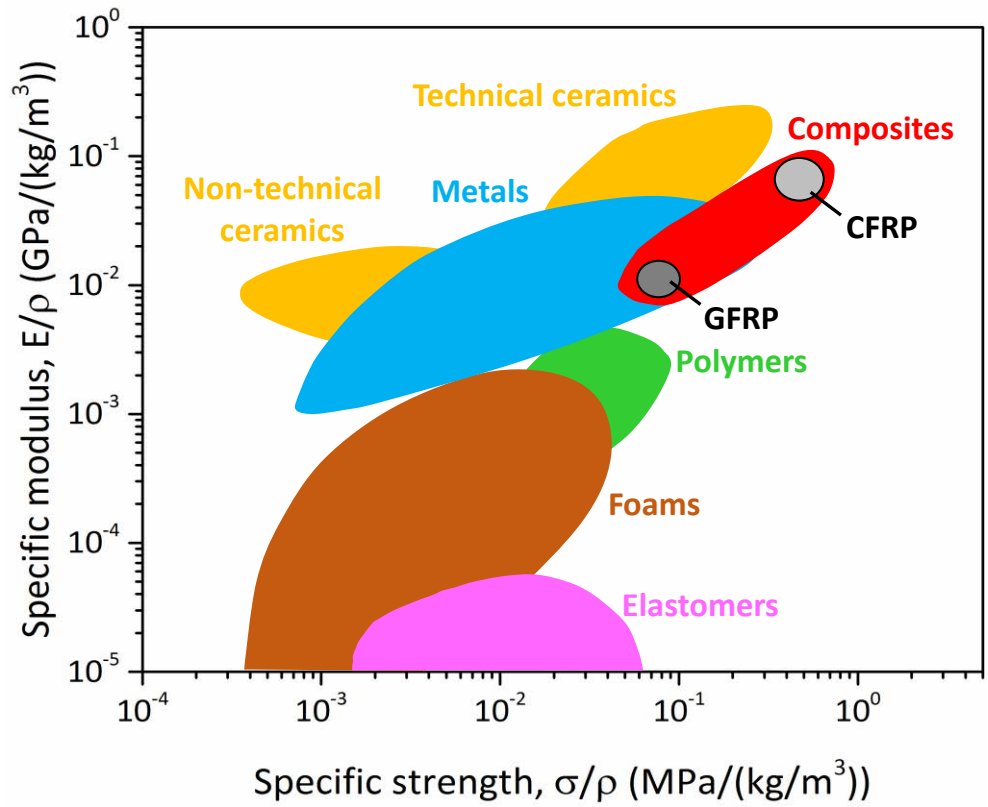

Figure 2.1 Specific modulus as a function of the specific strength for different groups of materials (adapted from [6]).

From a mechanical point of view, FRPs for structural applications generally adopt a two-dimensional (2D) configuration of laminates composed by fibre plies held together by a polymer, intended to maximize the in-plane specific stiffness and specific strength (Figure 2.2). In this configuration, the in-plane direction is defined by the axes 1 and 2; and the though-thickness direction, by the axis 3. However, the interlayer region of these laminates are matrix-rich regions that are extremely susceptible to crack initiation and propagation due to the relatively poor properties of the matrix and the weak matrix-fibre interface. This problem is known as delamination and is one of the most important limitations for the implementation of FRPs on a wide scale and range of structural applications [4,5].

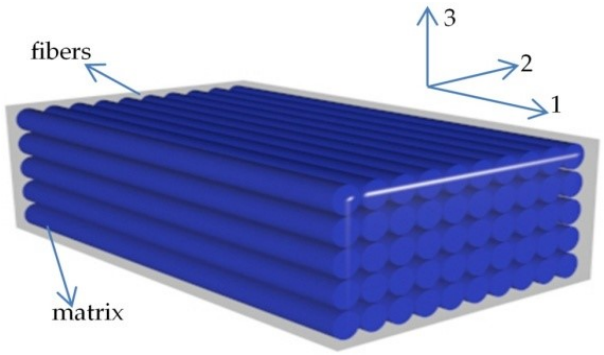

Figure 2.2 Schematic of an unidirectional 2D fibre-reinforced polymer [10]. In-plane direction (axes 1 and 2) and trhough-thickness direction (axis 3).

Regarding other properties different from mechanical, in general, fibre-reinforced polymers have low thermal and electrical conductivities, similar to those of the matrix. However, since carbon fibres possess high thermal (10-100 W/mK) and electrical conductivities (10^4 -10^5 S/m) [5], carbon fibre-reinforced polymers (CFRPs) have higher thermal and electrical conductivities compared to glass or ceramic FRPs. Furthermore, due to their two-dimensional configuration, the properties of FRPs in the through-thickness direction are highly matrix-property dominated. For instance, carbon fibre-reinforced polymers (CFRPs) usually present relatively lower thermal (≈1 W/mK) and electrical (10^{-2}-10^0 S/m) conductivity in the through-thickness direction compared to those in the in-plane direction (≈10 W/mK, ≈10^4 S/m) [5,11–13].

Materials used for aerospace structures require a certain level of electrical conductivity to protect the structures from the damage caused by common environmental occurrences as lightning strikes [12,14,15]. Therefore, the development of FRPs with enhanced through-thickness electrical conductivity is of great interest. Other possible applications for polymer composites with improved electrical and thermal conductivity is the development of self-sensing capability for health monitoring of damages [16] or the effective heat dissipation in aerodynamically heated areas or those near electronic devices or engines [5].

2.2 Polymer composites

An approach to overcome the low mechanical properties and lack of multifunctionality (i.e. thermal and electrical conductivity) in the through-

thickness direction of conventional two-dimensional FRPs, consists in the modification of the polymeric matrix by adding appropriate micro- or nano-sized fillers. The resulting material can be defined as a hybrid polymer composite as it is reinforced with fibres and a secondary filler.

Polymers reinforced with nanosized fillers, namely nanocomposites, has focused the interest of materials researchers since the late 1980s. For instance, the Toyota research group demonstrated enhanced mechanical and thermal stability in nylon 6-clay nanocomposites [17–19].

The most important advantage of nano-scaled fillers over conventional micron-scaled fillers is that significant properties (i.e. mechanical, electrical, thermal) improvements can be achieved at very low amounts of nanofillers (<5 wt.%), instead of the higher additions (10-30 wt.%) of micron-sized fillers [20].

In order to enhance the mechanical properties of a polymer, it can be modified with polymeric (elastomer or thermoplastic) particles [21,22]. However, depending on the material and processing, the addition of a polymeric dispersed phase could lead to the lowering the glass transition temperature (T_g) of the matrix [23–25] or the decrease of strength and modulus of the composite with increasing the rubber content [23,26–29].

An alternative approach to obtain improvements in mechanical properties without compromising other properties is to add rigid inorganic particles. This type of filer has proved to be effective fillers to improve the mechanical properties of polymer composites. Furthermore, due to the relatively higher thermal conductivity of inorganic (bulk) materials, compared to that of polymers, the resulting composites usually exhibits enhanced thermal conductivity. However, these fillers failed when an electrically conducting material is needed, due to their inherent insulating behaviour.

In order to increase the electrical conductivity of polymers, the use of metallic particles as fillers has been explored [30]. Due to the relatively higher density of these particles, compared to polymer, the increase in the electrical conductivity is obtained at expenses of the increased weight of the resulting composites.

In this context, carbon-based fillers are envisioned as ideal candidates to be used as fillers due to their low densities (≈2 g/cm^3) and superior mechanical, electrical and thermal properties. Therefore, a review of carbon fillers and their use for the development of polymer composites is presented in the following section.

2.3 Carbon-based fillers

Since the 70s, carbon based fillers, such as carbon black, has been used as nanofiller to produce polymer composites, especially elastomeric matrix, with enhanced electrical conductivity and mechanical properties while maintaining light weight [31,32]. Recently, carbon nanotubes, graphene and its derivatives had become promising nanofillers due to their excellent mechanical, electrical and thermal properties.

2.3.1 Carbon black

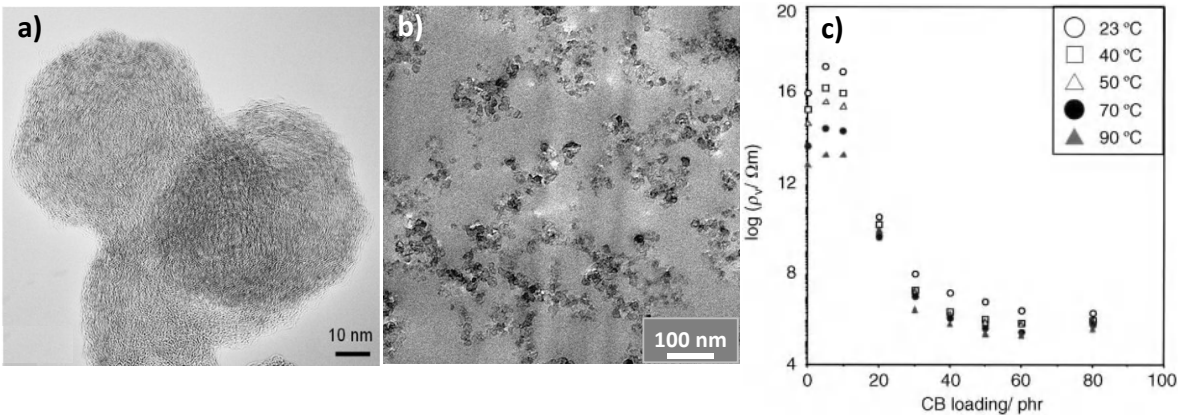

Figure 2.3 TEM images of a) carbon black particles [33], b) epoxy resin with 3 wt.% of carbon black [34] and c) volume resisitivity of nafural rubber filled with carbon black. At various vulcanizates temperatures, as a fucntion fot he CB loading, in parts per hundred resin (phr) [32].

Carbon black is obtained from partial combustion and thermal degradation of hydrocarbons [31]. It consists in near-spherical particles composed by amorphous carbon and small domains of graphitic carbon, with a size in the range of 5-100 nm (Figure 2.3a). This particles forms agglomerates (1-40 μm) due to chemical and physical interactions. Once they are mixed with a polymeric matrix, the carbon black agglomerates are broken up down to smaller agglomerates (100-500 nm) (Figure 2.3b). Carbon black has been long used for the reinforcement of elastomers to increase tear and abrasion resistance, tensile strength, modulus or hardness

[32,34]. It has also been used in the production of electrically conductive polymers [35–37] (Figure 2.3c).

2.3.2 Carbon nanotubes and nanofibres (CNTs and CNFs)

A single-walled carbon nanotube (SWNT) can be described as a single-atom layer of sp^2-hybridized carbon atoms, i.e. a graphene sheet, rolled up in a seamless tube with diameters between 0.4 to 10 nm and length of up to several micrometres (Figure 2.4a). A multi-walled carbon nanotube (MWNT) consists in multiple concentric layers of graphene separated by approximately 0.34 nm, similar to the interlayer distance in graphite (Figure 2.4b), with diameter between 10 and 100 nm, depending on the number of walls [38–40]. Although the properties of carbon nanotubes depend on their structure (diameter, number of layers, chirality), impurities and defects, these materials have outstanding thermal, electrical and mechanical properties due to the covalent sp^2 bond between carbon atoms. A value of *ca.* 2500 W/mK was measured for the intrinsic thermal conductivity of individual MWNT [41], while values in the range of 1750-5800 W/mK were obtained for crystalline ropes of SWNTs [42]. In addition, SWNTs have electrical conductivity $>10^6$ S/m [43] and $>10^5$ S/m for MWNTs [44]. The tensile strength of individual MWNT was found to be in the range 11-63 GPa, while the Young's modulus varied from 270 to 950 GPa [45].

An alternative filler to carbon nanotubes are carbon nanofibers (CNFs) [46–48], which consist in high aspect ratio filaments, with diameters on the order of 50-200 nm and lengths of up to mm. CNFs can present a wide range of morphologies, some of them are shown in Figure 2.4. In general, CNFs have lower mechanical properties, higher diameter and densities than CNTs, however they have higher availability and lower price. Additionally, due to the presence of reactive carbon edges in the CNF surface, they can be easily functionalized, compared with CNTs, to enhance the dispersion and stress transfer to the matrix [46–49].

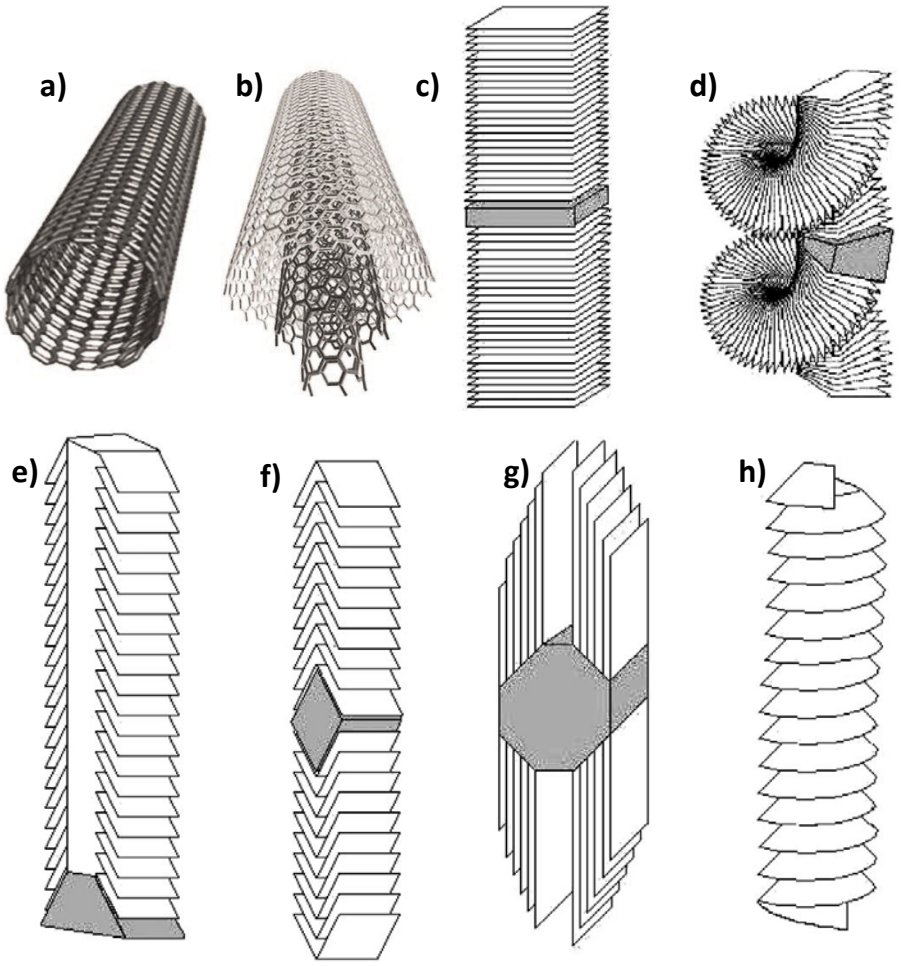

Figure 2.4 Schematic of a) single-walled, b) multi-walled carbon nanotubes [50] and carbon nanofibers with different structures: c) platelet, d) spiral platelet, e) fishbone with hollow core, f) solid fishbone, g) ribbon and h) stacked-cup [51].

Carbon nanotubes and nanofibres have been extensively studied to be part of a novel generation of composite materials [46–48,52–56].

The effect of carbon nanotubes and nanofibers on the resulting mechanical properties of polymer composites are greatly influenced by many parameters, e.g. filler type, aspect ratio, orientation, synthesis method, surface pre-treatment, functionalization and/or morphology, processing approach or polymer matrix [52]. Nonetheless, probably the main concerns to fully take advantage of the outstanding strength and stiffness of CNTs and CNFs are to achieve a homogeneous dispersion of the filler and a strong interaction filler-matrix to enhance the stress transfer [48,55]. In general, there is an optimum filler content until which the properties increase with increasing the filler content. At higher contents than the optimum one, agglomeration of the filler may take place and, thus, the composite

processing becomes more difficult. This may result in composites exhibiting a drop in mechanical properties, in some cases even below those of the neat matrix [57–59].

It is worth to note that some authors suggest that the reinforcing efficiency of CNTs and CNFs is higher when the matrix has a ductile behaviour, such as polyolefins, than in brittle matrices, such as epoxies [5,52]. An example of this effect has been reported for glassy (brittle) and rubbery (ductile) epoxy composites with carbon nanotubes [60]. In the glassy composite with 4 wt.% of multi-walled CNTs, the tensile modulus increased only 4%, while the strength and strain at break decreased by 4 and 50%, respectively, compared to the neat glassy epoxy. In the case of the rubbery epoxy composite with the same filler content, the modulus, strength and strain at break were significantly improved, being a 23, 34 and 13% higher, respectively, than those of the rubbery epoxy.

In fracture mechanics, the energy required for the propagation or growth of a pre-existing crack within a material is defined as fracture toughness [3]. During the fracture process of a polymer composite, different sub-processes related with the filler may take place. These processes may dissipate a certain amount of energy, which contribute to increase the total energy required for the sample's final failure. In this case, the process is known as toughening mechanism [61].

Regarding the fracture behaviour of polymer composites with CNTs or CNFs, generally the dominant mechanism in the total energy dissipation process is the filler pull-out [62,63]. When the sample is loaded, the stress concentration in the process zone ahead the crack tip induces the filler debonding. As the crack propagates, the filler is pulled out from the matrix (Figure 2.5a). In this process the energy is dissipated through the work of friction of the interfacial shear stresses between the debonded filler and the matrix. Crack bridging is another possible toughening mechanism that can take place after filler debonding in polymer composites with CNFs and CNTs (Figure 2.5b) [64–66]. It takes place behind the crack front and consists in the connection of botch crack surfaces by the fibrous nanofillers. Some authors reported that in the case of randomly oriented fillers, only 23% of them will contribute to the bridging mechanism [67]. Additional

energy is dissipated through the filler breakage (Figure 2.5a), the sword-in-sheath of CNTs (Figure 2.5a) [45,68,69] and the unravelling or uncoiling of stacked-cup CNFs [65,66].

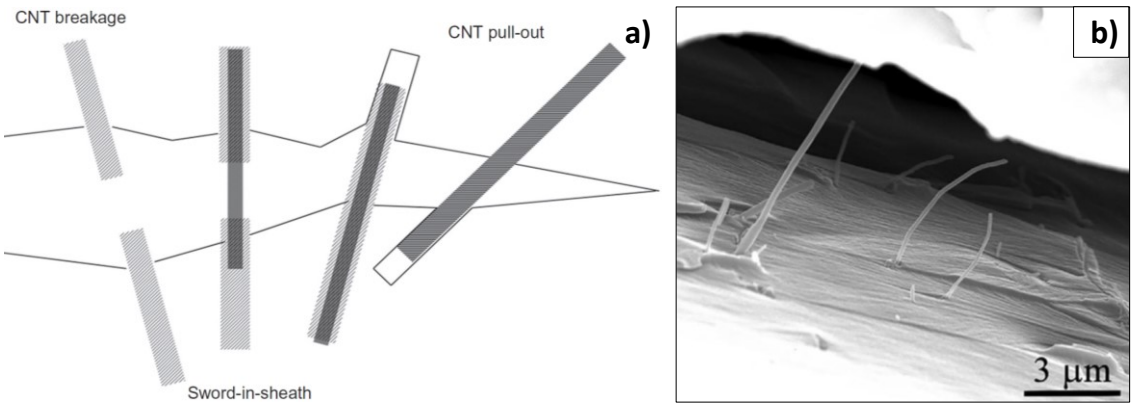

Figure 2.5 a) Toughening mechanisms consisting in carbon nanotube breakage, sword-in-sheath of a CNT and CNT pull-out [61]. b) SEM image of crack bridging in an epoxy composite with CNFs [66].

Concerning the cure behaviour of thermosets, as epoxy resins, it may be affected upon the addition of CNFs and CNTs. In general, the curing process of epoxies can be divided in an initial chemically controlled stage followed by a diffusion-controlled stage [70,71]. In one hand, the residual catalyst particles, present in the carbon filler, may accelerate the reaction during the first stage of the curing process [70,71]. Furthermore, some authors claimed that the accelerating effect may be also due to the high thermal conductivity of carbon filler [72,73] and/or to their high specific surface area [74]. On the other hand, the addition of filler generally results in an increased viscosity of the mixture, thus the diffusion control of the cure process is favoured [70,71].

Regarding the glass transition temperature (T_g), several parameters may contribute to the reduction of the T_g. The lowering of the cross-linking degree, taking place with both untreated [75,76] and surface modified CNTs [77], the presence of dispersion-aiding agents or solvents [78] and the agglomeration of the filler [70] are some mechanisms that contribute to the reduction of the T_g. On the other hand, once the resin is cured, the filler could restrict the mobility of the polymeric chains, thus contributing to increase the T_g [48,73,79,80]. Even if the amount of nanofiller added to the polymer is not really large, the combination of the mentioned effects may also lead to composites with slightly affected T_g

[48,60,81,82]. A review on the effect of carbon nanotubes on the cure reaction and the T_g can be found elsewhere [70].

In polypropylene, a semi-crystalline thermoplastic, CNTs may act as nucleating agents for the crystalline phase of the matrix while they seem to have no significant effect on the degree of crystallinity nor on the appearance of new crystalline phases, as reported by some authors [58,83–88]. Furthermore, it has also been reported a reduction in the crystallite size, resulting from a similar degree of crystallinity and a higher number of nucleating sites in composites, compared to the neat matrix [58,86,89] and a more uniform distribution of crystallite size than in neat polymer [86,90].

Regarding the electrical properties, from the available literature it is clear that the conductivity can be improved by several orders of magnitude upon the addition of a small amount of CNTs or CNFs [46,52,56,91]. In order to change the behaviour of a polymer composite from insulator to conductor, electrically conducting fillers are added to the matrix. Starting with the insulating matrix, with increasing the filler content there is a region, known as percolation threshold, in which the electrical conductivity suddenly increases by several orders of magnitude. In Figure 2.6a this region is located between 1 and 3 wt.% of filler for the CNF composites. The percolation threshold is related with the formation of a continuous filler path, i.e. conducting network, through the composite (Figure 2.6a) [56].

In general, higher values of electrical conductivity and lower percolation thresholds are obtained when CNTs are used to modify polymers, compared to CNFs. An example of this behaviour can be observed in Figure 2.6a, where the direct current electrical conductivity of polystyrene composites with CNFs and CNTs, respectively, are shown. This effect may be due to several factors, as the relatively higher electrical conductivity, aspect ratio and surface area of CNTs compared to that of CNFs, making filler-filler contacts to be more likely to occur for the CNTs than for the CNFs at the same filler content [92,93]. In Figure 2.6a it can be observed that the percolation threshold of CNT composites is reached at lower filler contents compared to the CNF composites.

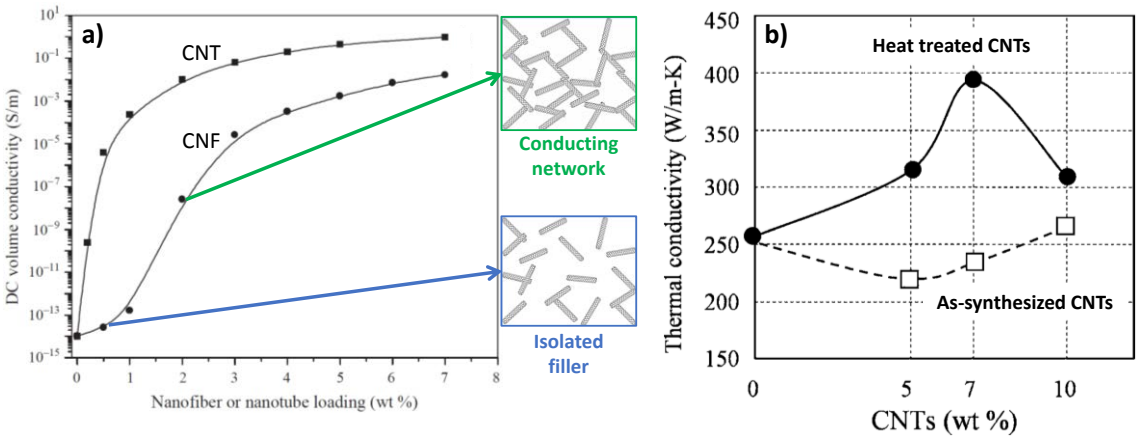

Figure 2.6 a) Direct current (DC) electrical conductvity, as a function of filler content, of polystyrene composites with CNFs and CNTs [92]. The schematic of the filler distribution within the matrix and its effect on the electrical behaviour of the composite [46]. B) Thermal conductivity, as a function of filler content, of CF/phenolic resin composites containing as-synthesized and heat treated CNTs, respectively [94].

Similarly to the electrical conductivity behaviour, the addition of CNTs and CNFs to a polymer would lead to composites with improved thermal conductivities. However, the majority of reported results are not even close to those expected from the intrinsic thermal conductivities of CNTs, approximately between 1000 and 6000 W/mK [41,42], and CNFs [54], higher than those of polymers, in the range between 0.1 and 1 W/mK [95]. Impurities and defects in the structure of the filler may reduce their intrinsic conductivity [96,97]. As an example, some authors have reported a significant enhancement in the thermal conductivity of CF/phenolic resin composites by adding heat treated CNTs compared to the same CNTs but used as-synthesized (Figure 2.6b) [94]. The main heat conduction mechanism in polymers is through elastic vibrations of the lattice, i.e. phonons, therefore defects in the polymer structure, interface between the filler and the matrix and contacts between fillers are regions where phonon scattering takes place, therefore contributing to increase the thermal resistance [97]. However, other parameters that affect the resulting thermal conductivity are the nature of the matrix (amorphous, semi-crystalline), filler morphology (shape and size) and distribution within the matrix (orientation, agglomeration, formation of conducting network) [95].

2.3.3 Graphene and graphite nanoplatelets (GNPs)

Probably the material that has generated the greatest interest in the last decade to be used as filler for polymer composites is graphene. Considered as the building block of all graphitic materials (Figure 2.7), graphene is a single-atom-thick flat layer of sp^2-hybridized carbon atoms joined together forming a two-dimensional honeycomb lattice [98].

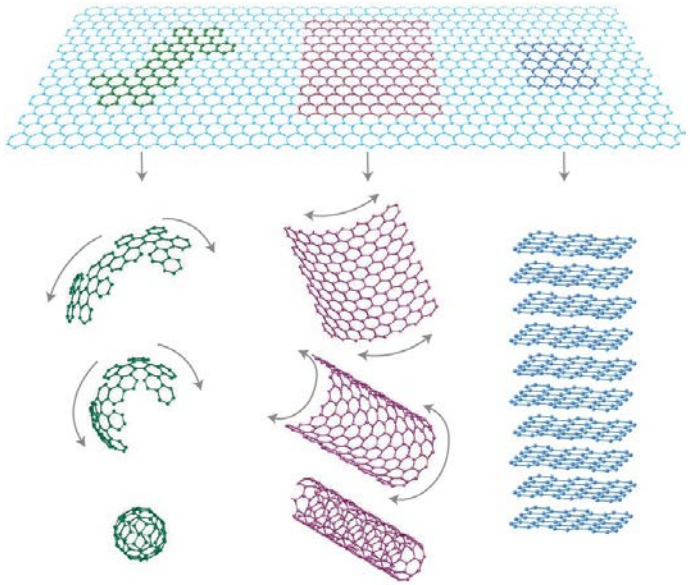

Figure 2.7 A graphene layer (2D) can be wrapped to form buckyballs or fullerenes (0D), rolled into nanotubes (1D) or stacked into graphite (3D) [98].

Graphene has been envisioned an excellent filler for polymer composites due to its outstanding in-plane properties. A defect-free graphene layer could exhibit an Young's modulus of 1 TPa, having a breaking strength of 42 N/m [99], which corresponds to an intrinsic strength of 130 GPa. It also has very high electrical conductivity, up to 6000 S/cm [100], and room-temperature carrier mobility of about 104 cm^2/Vs [101]. The extremely high values of thermal conductivity, in the range of 4800-5300 W/mK [102], exceed those of the diamond, which is in the range 800-2000 W/mK [103].

Since graphene production is still really far to be efficiently scaled up, graphene-based materials have been developed as a solution for the lack of availability of graphene in large quantities. Graphite oxide is a common precursor for the cost-effective and scalable production of chemically modified graphene and other

graphene-based materials [104,105]. It can be prepared by treatment of graphite flakes with oxidizing agents so that epoxide and hydroxyl groups are attached within the layer and carboxyl and carbonyl groups are attached at the layer edges (Figure 2.8a). Due to its polar functional groups it can be easily dispersed in water and organic solvents [106] and exfoliated by sonication or shear mixing [107]. Thus, producing single layer or nanoplatelets of graphene oxide [105,108] that can be functionalized [109] or reduced to obtain materials similar to graphene [108,110]. For example, graphene oxide is electrically insulating while the material obtained after reducing it is electrically conductive, like graphene.

Graphite nanoplatelets (GNP) are composed by multiple graphene layers that are stacked together (Figure 2.8b). Thus, the thickness of the platelet depends on the number of layers [111]. This material has in-plane properties similar to the in-plane properties of graphite (e.g. mechanical, thermal and electrical) [112] and can be obtained by cost-effective methods involving exfoliation of natural flaky graphite, by mechanical milling or chemical approaches involving graphene oxide, graphite intercalation compounds or expanded graphite [113].

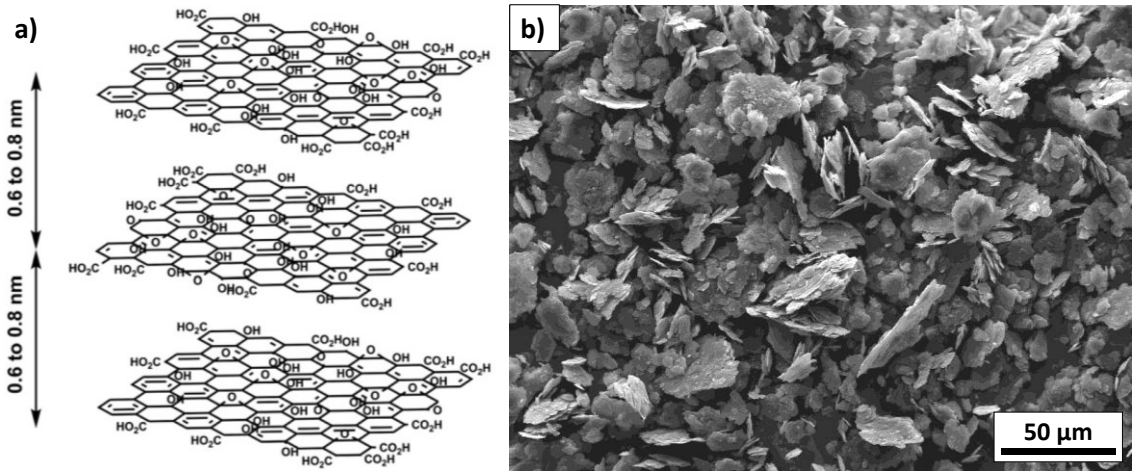

Figure 2.8 a) Schematic of graphite oxide [108], b) SEM image of graphite nanoplatelets.

Graphene and graphene-based fillers have been widely used for the processing of polymer composites [59,108,114–117]. The main characteristic of these two-dimensional structures is their large surface areas which allow high interaction between the filler and the matrix and high levels of stress transfer from the matrix to the filler [118]. Some authors reported that having different types of GNPs with similar thickness but different flakes sizes, those with the highest lateral size

provide higher toughening and reinforcing efficiency in the resulting composites [119–121]. An example of this effect can be observed in Figure 2.9.

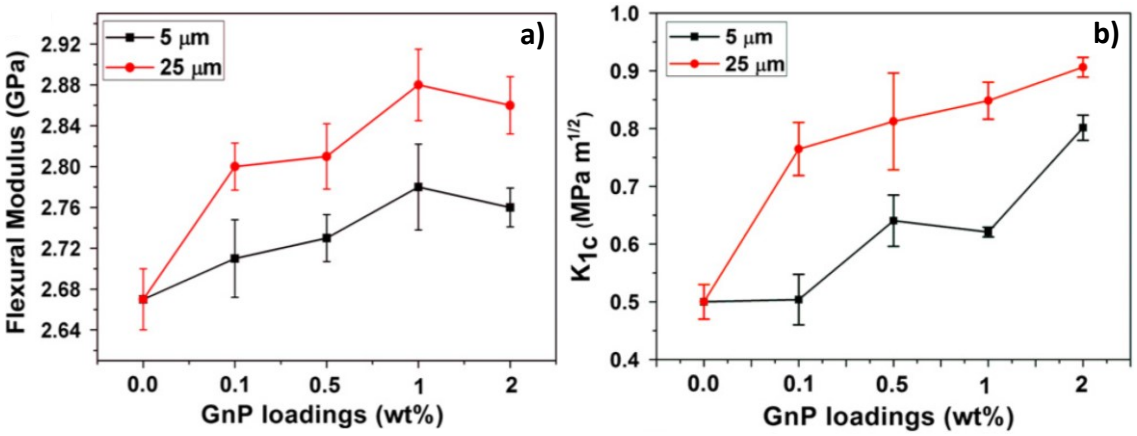

Figure 2.9 a) Flexural modulus and b) mode I fracture toughness of epoxy composites with GNPs with a flake size of 5 and 25 μm, respectively [121].

As it has been mentioned, a homogenous dispersion of the filler is a key parameter to obtain significant improvements of properties [122]. Carbon nanofillers tend to agglomerate due to van der Waals forces. Moreover, graphene-based fillers are difficult to homogeneously disperse within the matrix due to the strong interplanar π-π interactions and their large surface areas [59,123].

In some of the few reported works where the authors compare the effect of the CNTs and GNPs, the CNTs outperform the GNPs in terms of mechanical behaviour of the resulting composites [121,124]. In [125], the authors reported an improvement of 13%, compared to the neat epoxy, in the tensile strength of epoxy composites with 1 wt.% of CNTs, while the tensile strength of the composite with 1 wt.% of GNPs was similar to that of the neat epoxy.

If a uniform dispersion is achieved, graphene and GNPs show potential to provide higher improvements in mechanical properties compared to composites with other carbon fillers, as CNTs or CNFs, at the same filler content [59,125–127]. For instance, it has been reported that epoxy composites with 0.1 wt.% of GNPs showed an improvement on tensile strength of about 40%, compared to that of neat resin. However, by adding the same amount of CNTs resulted in an improvement of only 14%. The same effect was found for the tensile modulus and the mode I fracture toughness [126].

The fracture behaviour of graphene and GNPs have also been extensively studied, providing the identification of the main toughening mechanisms involved during the failure of composites [128–130]. Crack deflection may take place by tilting and twisting of the advancing crack front as it reaches a graphene-based filler [126,127,129,131]. The deflection of the crack results in an increased roughness of the fracture surface, as shown in Figure 2.10. The fracture surface of neat epoxy (Figure 2.10a) is smooth, indicative of brittle fracture. However, the fracture surface of the composite with 1 wt.% of GNPs (Figure 2.10b) exhibits a rougher surface, than that of neat epoxy.

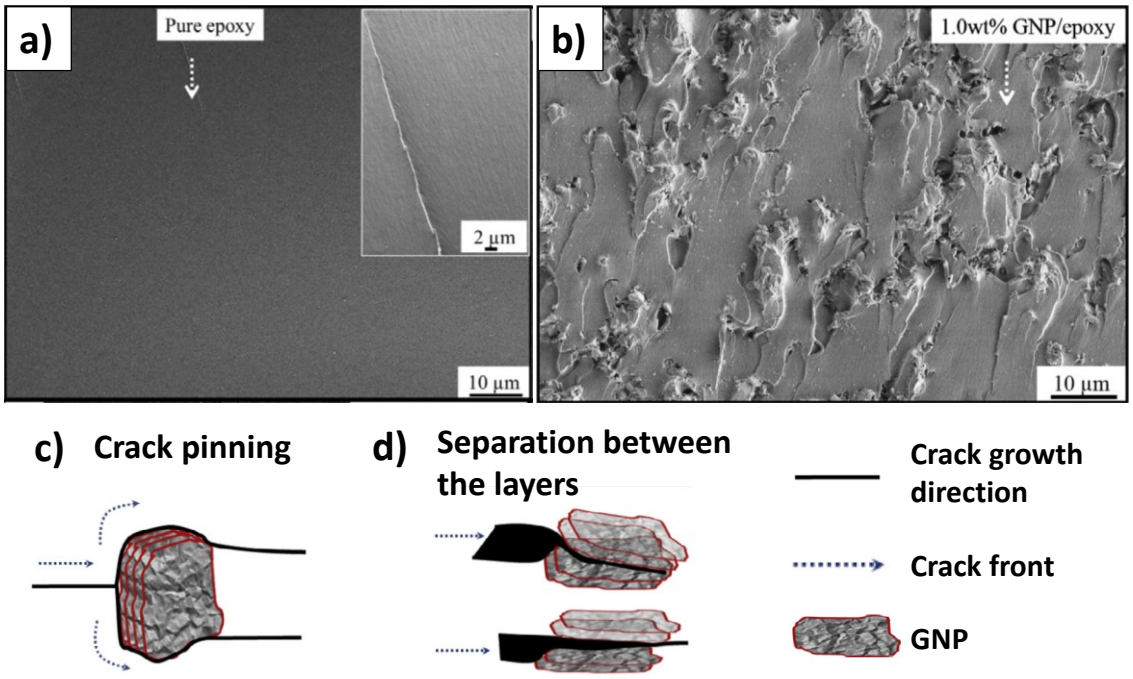

Figure 2.10 SEM images of the fracture surface of a) neat epoxy and b) composite with 1 wt.% of GNP. Schematic of the toughening mechanisms consisting in c) crack pinning and d) separation between layers [128].

Based on the analysis of adjacent fracture surfaces, some authors have also identified features related to filler pull-out, crack bridging, crack pinning (Figure 2.10c) and separation between the GNP layers as the crack propagates through the GNP particle (Figure 2.10d) [122,128,130]. Other authors have suggested that void nucleation and plastic deformation of the matrix, due to the debonding of the filler, are possible toughening mechanisms [122,130,132]. Regarding the pull out mechanism, it is worth to note that some authors have reported significant

improvements on strain and toughness in epoxy composites with graphene flakes as the lateral size of the filler increases [119]. They suggested that this behaviour could be due to the increased friction between the filler and the matrix, as the filler lateral size increased, during the pull-out of the filler.

The addition of graphene-based fillers to polymers as polycarbonate [133], polypropylene [134], polyimide [135] or epoxy [136] may result in no changes on T_g. It has also been reported T_g shifted towards higher temperatures in polymers as epoxy [122,132,137], polymethyl methacrylate [120,138], polyvinyl alcohol [139], polypropylene [140] or ethylene-propylene-diene rubber [141]. Conversely, some authors reported T_g shifted towards lower temperatures in polymers as polycarbonate [133]. Nonetheless, it should be taken into account that the effect of graphene or its derivatives on the glass transition of the matrix also depends on the size of the platelets [120], their degree of dispersion [122] or interaction with the host polymer [139]. Another important parameter is the surface morphology, as the presence of defects and roughness may induce a certain degree of mechanical interlocking with the matrix, thus reducing the segmental mobility of polymeric chains [118].

Graphene or GNPs may have a nucleating effect on the crystallisation of the semi-crystalline polymers and may even induce the crystallisation of different crystalline phases, as those present in neat polymer [108]. For instance, in [142], Kalaitzidou *et al.* found that GNPs act as nucleating agents and promote the nucleation of the β-phase, rather than the α-phase of neat PP. As a result of the addition of graphene or GNPs, the degree of crystallinity may be increased, not significantly affected or decreased, compared to the unmodified polymer. Moreover, the crystalline structure may suffer changes, e.g. in crystallite thickness or spherulite size [108,142].

The addition of graphene and graphite nanoplatelets results in composites with improved electrical, once the percolation threshold has been reached, and thermal conductivities [95,113,134,143–145]. As in the case of other properties, the electrical and thermal conductivities of the resulting composites depend especially on the dispersion degree of the filler [122,136]. For instance, in [136], the authors

dispersed GNPs in epoxy resin by two different approaches, i.e. three-roll milling and sonication plus high speed mixing [136]. In one hand, the composites prepared by three-roll milling showed the characteristic percolating behaviour. The electrical conductivity increased by 4 orders of magnitude at the percolation threshold, which was approximately 0.3 wt.%. On the other hand, the composites obtained by sonication and high shear mixing showed the worst electrical behaviour. The electrical conductivity of the composites did not show the characteristic shape of the percolating behaviour, instead it steadily increased with increasing the filler content, reaching lower conductivity values compared to the composites obtained after three-roll milling.

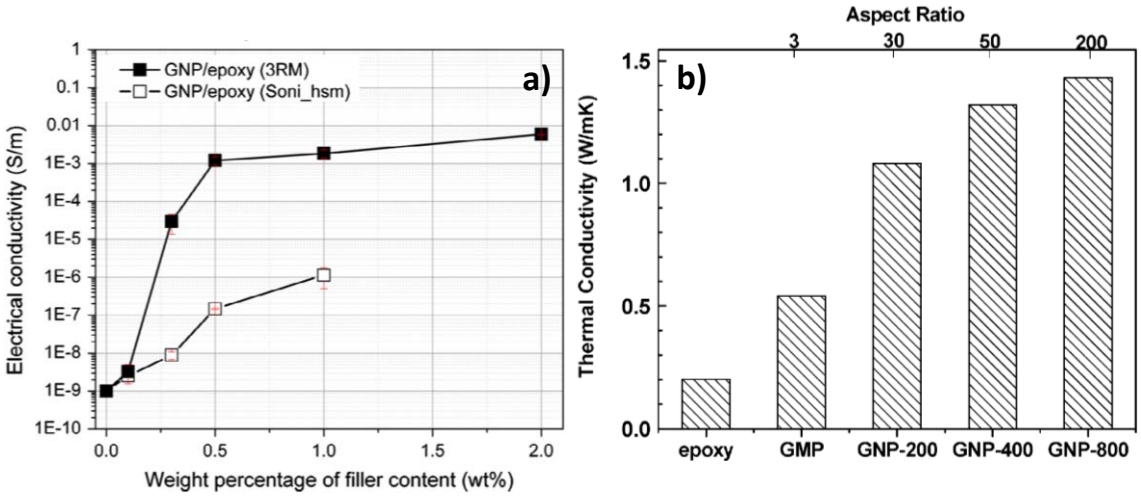

Figure 2.11 a) Electrical conductivity, as a function of the filler content, of epoxy composites with GNPs prepared by three-roll milling (3RM) or by sonication and high speed mixing (Soni_hsm) [136]. b) Thermal conductivities of epoxy composites with 5.4 vol.% of graphite microfiller (GMP) and GNPs with different sizes, i.e. aspect ratios [145].

Regarding the thermal conductivity, the filler morphology, i.e. lateral length or aspect ratio, also plays a crucial role on the resulting composites [121,145]. This can be clearly seen in Figure 2.11b, where the thermal conductivities of epoxy composites with 5.4 vol.% of graphite microfiller and GNPs with different aspect ratios are shown [145]. The authors concluded that the efficiency of the graphitic filler on the improvement of the thermal conductivity increased as the aspect ratio increased. The composite with GNPs with an aspect ratio of ≈200 (length≈ 0.35 μm, thickness≈ 1.7 nm) has a thermal conductivity a 620% higher than that of neat epoxy. However, the improvement in the composite with graphite microfiller with

an aspect ratio of ≈3 (length≈30 μm, thickness≈10 μm) is only a 170%, compared to neat epoxy.

To sum up, carbon materials are excellent candidates to be added to polymers in order to obtain composites with improved mechanical, electrical and thermal properties. Thus, in the following three chapters of this thesis, the effect of graphite nanoplatelets, carbon nanotubes and a novel carbon microfiller in polypropylene matrices is studied and discussed.

In spite of the outstanding properties of carbon fillers, some applications may require composites with certain properties which are extremely difficult to obtain with a single filler. For instance, in electronic packaging applications, electrically insulating materials with high thermal conductivity are required [146]. Some authors had reported that by covering carbon nanotubes with a layer of silica (Figure 2.12a), the resulting epoxy composites showed enhanced thermal conductivity while retaining the electrically insulating behaviour of the matrix [147], as it can be observed in Figure 2.12b.

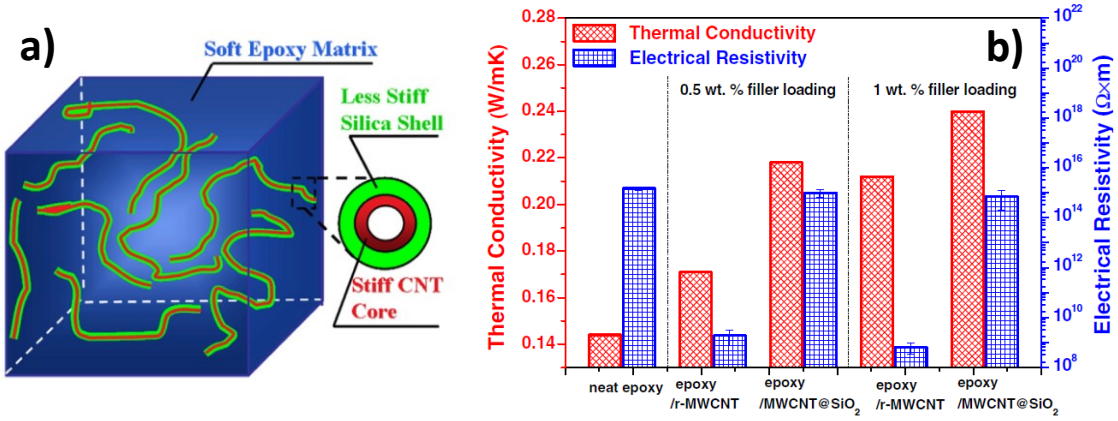

Figure 2.12 a) Schematic of the composite consisting in carbon nanotubes, covered by a silica shell, dispersed within an epoxy resin, b) Thermal conductivities and electical resistivities of the neat epoxy and the composites with "as-received" CNTs (r-MWCNT) and carbon nanotubes covered by a silica shell (MWCNT@SiO_2) [147].

Therefore, the combination of carbon materials with a secondary material, to obtain hybrid polymer composites, is a promising approach to achieve new materials with an unusual combination of properties or higher properties improvements, compared to the composites with the isolated fillers. Therefore, in

the next section a brief review of hybrid fillers for polymer composites was done. In Chapter 6, the hybrid filler obtained after growing carbon nanotubes in the presence of alumina nanoparticles is presented. The effect of this filler on the mechanical, thermal and electrical properties of an epoxy matrix is studied and discussed. In Chapters 7, the hybrid filler consisting in hollow glass microspheres with carbon nanofibres grown on their surface is presented. The effect of this hybrid filler the thermal and electrical behaviour of a high temperature resin is studied and discussed.

2.4 Hybrid polymer composites

The definition of hybrid material it is still not clear. It can be a material that commonly includes an inorganic and an organic compound blended at the molecular scale [148]. This definition is similar to that given by the IUPAC, which states that hybrids are composed by a mixture of organic, inorganic or both types of components, interpenetrating on a sub-micron scale [149]. In this work, it will be assumed that "a hybrid material is a combination of two or more materials in a predetermined geometry and scale, optimally serving a specific engineering purpose" [150] and that a hybrid polymer composite is the material obtained by dispersing two or more materials within a polymeric matrix. For instance, a hybrid polymer composite could be the fibre-reinforced polymer in which the matrix has been modified with a nanofiller. In this review, the attention will be focused on hybrid composites where at least one of the components is a carbon-based material.

In the available literature, the most straightforward approach to obtain hybrid polymer composites is by directly adding two or more different fillers to the matrix. Moreover, the fillers can have sizes in different scales, what is known as the multi-scale approach [151].

There are several works reporting hybrid composites made up of conventional fibres and carbon-based fillers embedded within a polymeric matrix to give hybrid FRPs. Thus, the fillers could be dispersed within the matrix [66,152,153], sprayed-up (Figure 2.13a) [154–156] or placed by electrophoretic deposition (Figure 2.13b) [157,158] on the surface of the fibres. Other approaches consist in using

CNTs or CNFs to obtain yarns or fibres that are braided around fibre bundles (Figure 2.13c) [53,159] or mats, layers or forests which are placed between the laminate plies (Figure 2.13d) [160–163].

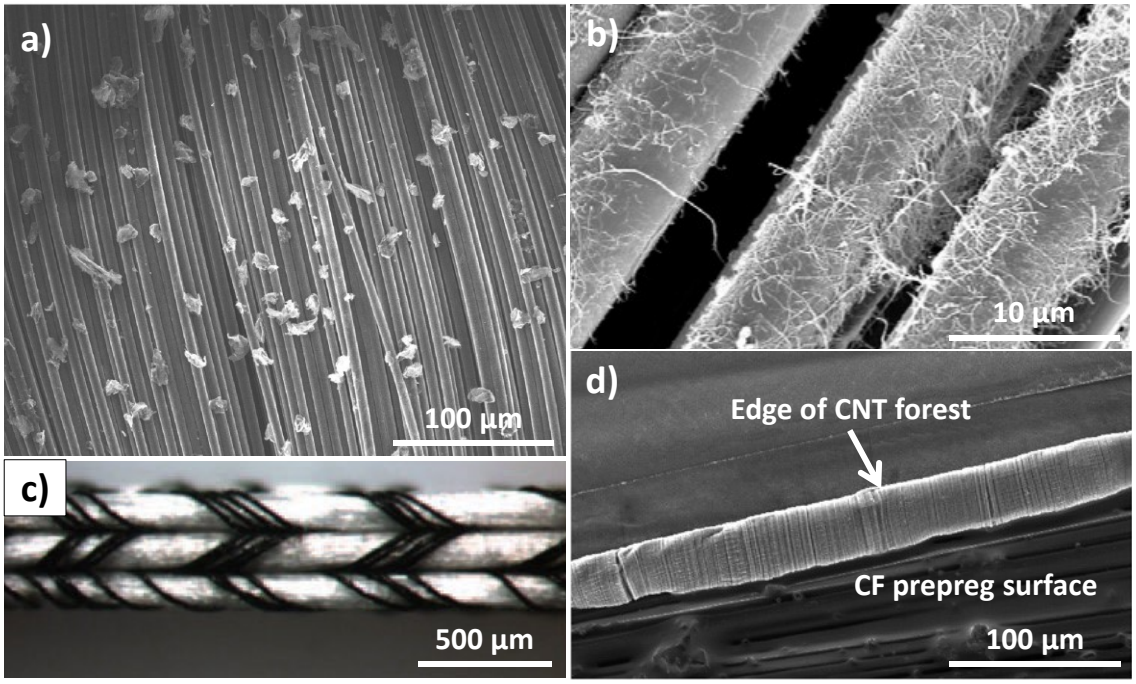

Figure 2.13 Several examples of hybrid polymer composites. SEM images of a) GNPs sprayed on the surface of CFs [155], b) CF with CNTs deposited by electrophoresis [164], image of c) glass fibre bundle braided with a CNT yarn [159], and d) SEM image of a CNT forest placed on the surface of a CF prepreg ply [161].

In general, the resulting hybrid composites exhibit enhanced mechanical properties, especially mode I and II interlaminar fracture and interlaminar shear strength. As an example, some authors have transferred aligned CNT forests to pre-impregnated plies of carbon fibre reinforced polymer in a way such they were located at the interlaminar crack front [163]. The modified laminate showed improvements on mode I and mode II fracture toughness of 31 and 161%, respectively, compared to those of the unmodified laminate. Other authors reported improvements in both the flexural and interlaminar shear strength of 11 and 86%, respectively, for carbon fibre-epoxy composites with mats of carbon nanofibers at the interlaminar region [160]. In these composites, the authors also reported improvements in the through-thickness electrical conductivity of approximately 150%, compared to the unmodified composite. However, the

improvement in the in-plane direction was only of ≈20%. Thus, in the case of two-dimensional carbon-fibre reinforced polymers upon the addition of a secondary carbon filler, the electrical conductivity in the through-thickness direction can be more significantly increased than in the in-plane direction [155,160].

Hybrid polymer composites can also be obtained by mixing particles of different materials, shapes and/or sizes. A common system used in the rubber industry consists in a rubber matrix with carbon black and silica particles [165] or clay platelets [166]. Recently, a review on the reinforcement of epoxy resins with thermoplastic or elastomer microparticles and different nano-scaled fillers (as silica nanoparticles, clay nanoplatelets, CNTs, graphene and GNPs) has been published [21]. In a similar work, the results of hybrid epoxy composites with soft (rubber) and rigid (silica, clay, CNTs, graphene) particles have also been reviewed [167].

An important characteristic of polymer composites with a mixture of fillers is the possible synergistic effect that can take place, especially in the formation of a filler conductive network [168–170]. An example of this effect can be found in [169], where the authors reported that the thermal conductivity increased by adding up to 30 vol.% of either silane-modified SiC nanoparticles or functionalized CNTs. Moreover, the later gave the highest results. Interestingly, when they prepared composites with the mixture of both types of filler, in a 1:1 ratio, the resulting thermal conductivity was the highest, compared to that of the composites with the same amount of functionalized CNTs.

Hybrid polymer composites can also be obtained by mixing two or more types of carbonaceous fillers. In this sense, the effect of carbon nanotubes and graphene-based fillers on the mechanical [121,124,171], thermal [172–174] and electrical [124,171,174,175] properties of polymer composites has been extensively studied.

The CNTs may act as obstacles and reduce the agglomeration of the graphene-based fillers. This could explain the higher reinforcing efficiency of the CNT+GNP mixture, reported in [121]. The epoxy composites with 0.5 wt.% of the mixture (CNT:GNP ratio of 9:1) exhibited the highest improvement in flexural modulus, a 17%, compared to that of the composites with the same amount of neat CNT, a 9%,

and GNP, a 5%. A similar synergistic effect was reported for epoxy composites with 0.1 wt.% of the CNT+GNP mixture (CNT:GNP ratio of 4:1) [124]. The achieved improvements, compared to neat epoxy, were a 17.5 and a 12.5% in flexural modulus and strength, respectively, which were the highest compared to the composites with the mixture at other ratios or with the pure CNTs and GNPs. In this work [124], the authors claimed that by combining one-dimensional CNTs with two-dimensional GNPs, the percolation threshold could be reached at lower filler content, i.e. 0.62 wt.%, than in the case of the single CNTs, a 0.84 wt.%, or GNPs, a 0.88 wt.%.

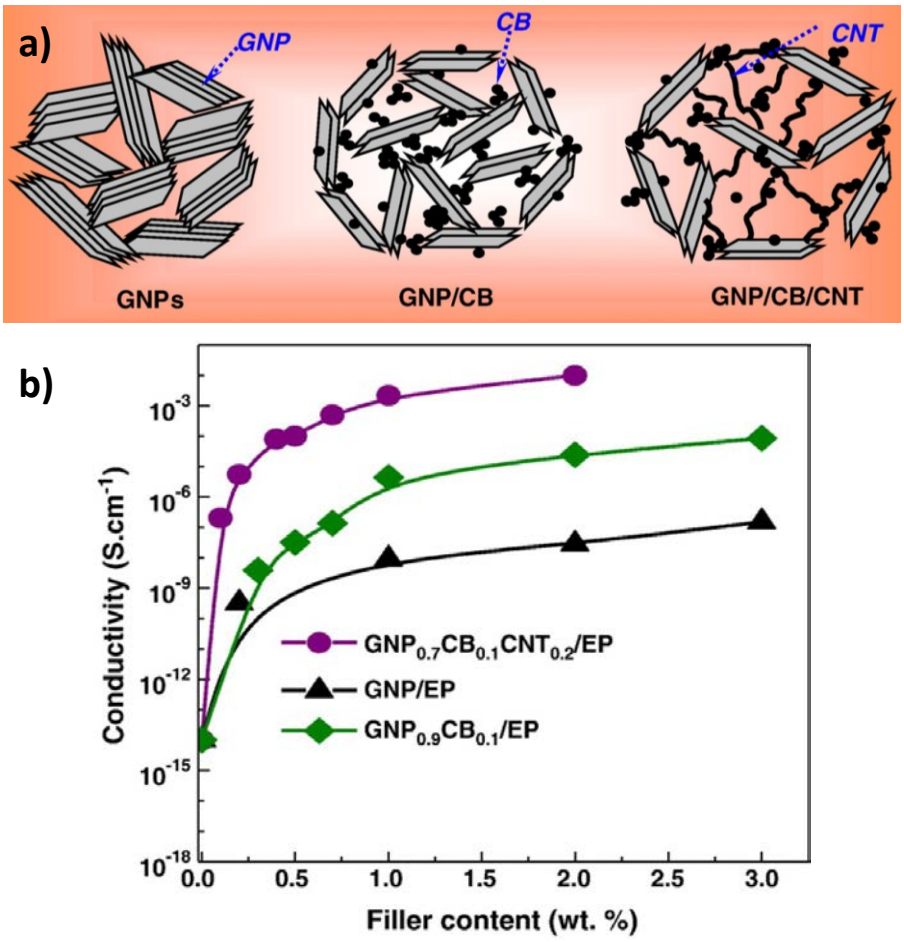

Figure 2.14 a) Schematic of fillers and their mixtures and b) electrical conductivity, as a function of the total filler content, of composites with GNPs, GNPs+CB mixture and GNPs+CB+CNTs mixture as a function of the total filler content [176].

Furthermore, it has been reported that the addition of a third filler, in this case CNTs, to the mixture of GNPs and CB could lead to higher values of electrical conductivity than composites with the same filler content of the GNP+CB mixture,

as shown in Figure 2.14. The synergistic effect can also be obtained for the thermal conductivity [172]. For epoxy composites with 10 wt.% of CNTs and GNPs, the thermal conductivities were 0.85 and 1.49 W/mK, compared to 0.201 W/mK of neat epoxy. However, when the authors added 10 wt.% of the GNP+CNT mixture (in a GNP:CNT ratio of 3:1), the resulting composite exhibited a thermal conductivity of 1.75 W/mK, corresponding to an enhancement of 800% compared to neat epoxy.

Apart from the simple mixture of fillers, another approach to obtain hybrid polymer composites is to obtain a hybrid filler which can be thought of as a single material and then dispersing it within the matrix. An example of hybrid fillers are the core-shell structures consisting in a CNT as core and a polymeric shell, which could be obtained through in situ chemical polymerization [177]. Metallic particles covered by a carbon shell are also available, in this case, by thermolysis of metal-containing monomers [178]. Oxide nanoparticles could be grown on the surface of CNTs by a precipitation method, showing these nanospheres better interaction than those mixed with the CNTs [179]. By means of a sol-gel process, carbon nanotubes covered by a layer of silica could be obtained as shown in Figure 2.12a [180]. In a similar approach, GNPs can be coated with alumina nanoparticles or nanolayers [181].

All the above mentioned techniques have in common that the initial material is the carbon-based filler and the synthesized one is the inorganic filler. However, hybrid fillers can also be obtained by synthesizing carbon structures. When dealing with the synthesis of carbon materials, the chemical vapour deposition (CVD) process is one of the most used techniques for the synthesis of carbon-based fillers because of the relatively low cost of the equipment, it is easily scalable and it can provide high production yields [182]. Therefore, it was the approach chosen to obtain the hybrid fillers presented in this thesis.

2.5 Hybrid fillers obtained by chemical vapour deposition (CVD)

Among all the approaches for the synthesis of carbon structures, the chemical vapour deposition is one of the most popular and widely used [182–184]. During the chemical vapour deposition process, the thermal decomposition of a carbon-containing molecule, as hydrocarbons, in the vapour phase, takes place at the surface of a catalyst. The result of this reaction is the deposition of a solid carbon-based material. Due to the catalytic nature of the reaction involved in this process it is usually known as catalytic chemical vapour deposition (CCVD) [183,185]. The chemical vapour deposition process can be used to obtain a hybrid filler by using one material as substrate while the second one, i.e. the carbon-based, is grown during the CVD process.

In the next sections, an overview of different hybrid materials obtained by CVD is presented. The hybrid fillers are classified depending on whether the substrate used was a micron-scaled conventional fibre (Figure 2.15a), a two-dimensional particle (Figure 2.15b) or a three-dimensional (spherical and non-spherical) particle (Figure 2.15c).

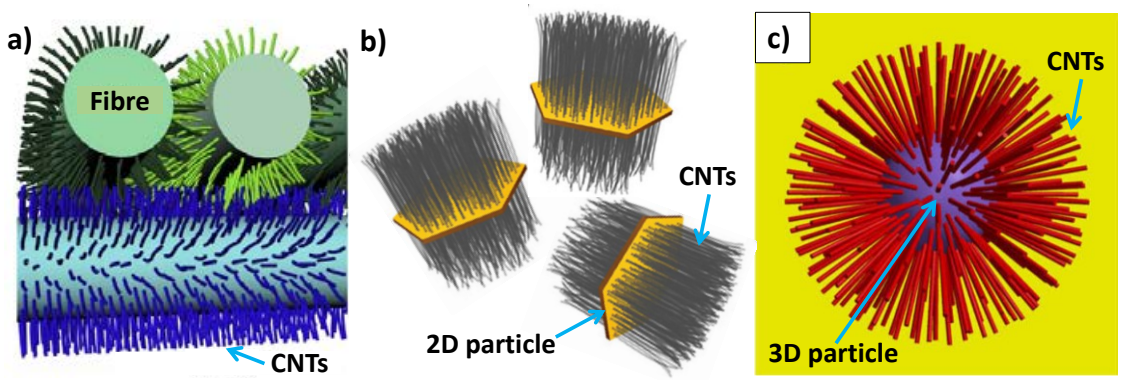

Figure 2.15 Examples of different hybrid fillers consisting in a) micron-scaled fibres and CNTs [186], b) two-dimensional particles and CNTs [187] and c) three-dimensional particles and CNTs [188].

2.5.1 Micron-scaled fibres as substrates

During the last decade, the synthesis of carbon nanotubes using micron-scaled fibres as substrate has been extensively studied (Figure 2.16a). An early work regarding the synthesis of carbon nanofibers on the surface of CFs [189] is the starting point of this approach.

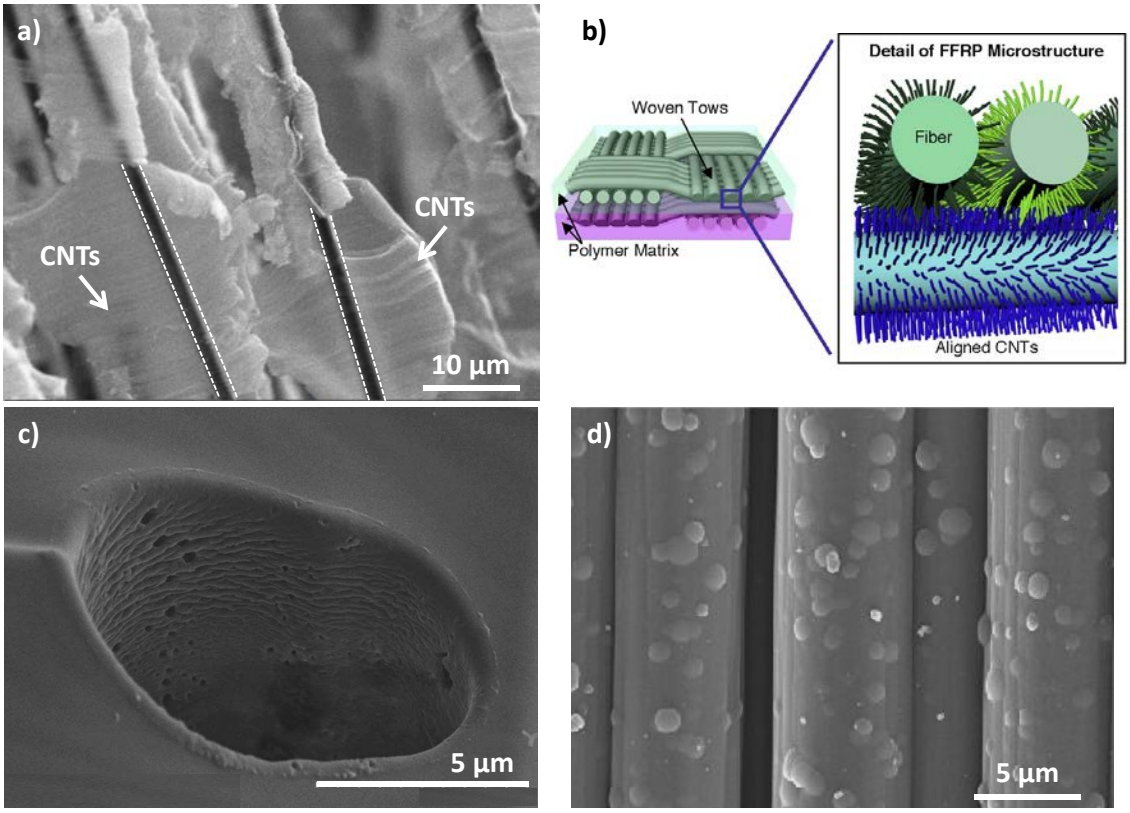

Figure 2.16 a) SEM image of CNTS grown by CVD on the surface of alumina fibres, b) schematic of a hybrid FRP comprosed by micron-sized fibers with aligned CNTs attahced to their surface [186], SEM images of c) micron-scaled hole left in an epoxy matrix by a pulled-out carbon fibre where the nano-scaled holes left by pulled-out CNTs could be observed [190] and d) carbon fibres with structures imilar to carbon black grown on their surface by CVD [191].

Later, multifunctional brushes were developed by synthesising CNTs on selected areas, i.e. fibre ends, of SiC fibres [192]. This idea was further extended to the growth of CNTs on the surface of SiC fibre fabric to obtain an architecture similar to that shown in Figure 2.16b [193]. This proved to be a promising approach to improve the capability of energy dissipation by adding toughening mechanisms as CNT pull-out (Figure 2.16c). Furthermore, the hybrid composites showed significant improvements of thermal and electrical conductivity in all directions,

compared to the base composite, indicating an effective formation of a conductive network throughout the composite. The synthesis of CNTs on the surface of alumina an silica fibres [194–197] as well as the resulting hybrid composites have been investigated [194,198,199]. The thermal stability of ceramic fibres allows their use as substrates during the CVD process without significantly damaging the fibres. However, carbon fibres has also been explored as substrate for the growth of carbon fillers [190,200–203]. By selecting an appropriate catalyst treatment and processing conditions significant damage of the fibres could be avoided [204–206]. Recently, the growth of structures similar to carbon black on the surface of carbon fibres has been reported (Figure 2.16d) [191]. The resulting composites showed modest improvements on interlaminar shear and impact strength due to an increased interfacial adhesion between the CB-modified fibres and matrix.

2.5.2 Two-dimensional particles as substrates

Carbon nanotubes have been synthesized on different substrates since the late 90s, just few years after their discovery by Iijima in 1991 [39]. Alumina, silica, zeolite or $CaCO_3$ microparticles have been used as supports for the growth of CNTs through the decomposition of different hydrocarbons [207–209]. SWNTs have been synthesized using alumina and silica nanoparticles as support for metallic particles acting as catalyst [210,211]. There is also a work reporting the synthesis of CNTs using a mixture of CB and a Co precursor [212]. However, in the above mentioned works the interest was not on the hybrid structures consisting in CNTs/substrate rather than in the subsequent purification of the CNTs, i.e. isolation of the CNTs from the catalyst/substrate.

The literature related with hybrid fillers, obtained by the synthesis of carbon structures on particles, is scarce. However it has been slowly growing in the last years. In 2002, Gournis *et al.* reported the synthesis of CNTs on the surface of 2D clay platelets [213], claiming that the resulting hybrid material would be attractive for the processing of polymer composites with outstanding functionalities. Since then, several research groups have developed the synthesis of CNTs on 2D particles of clay [214–221], layered double hydroxide [187], SiC [222–225] or

graphite nanoplatelets [226,227] to obtain hybrid structures similar to those shown in Figure 2.17.

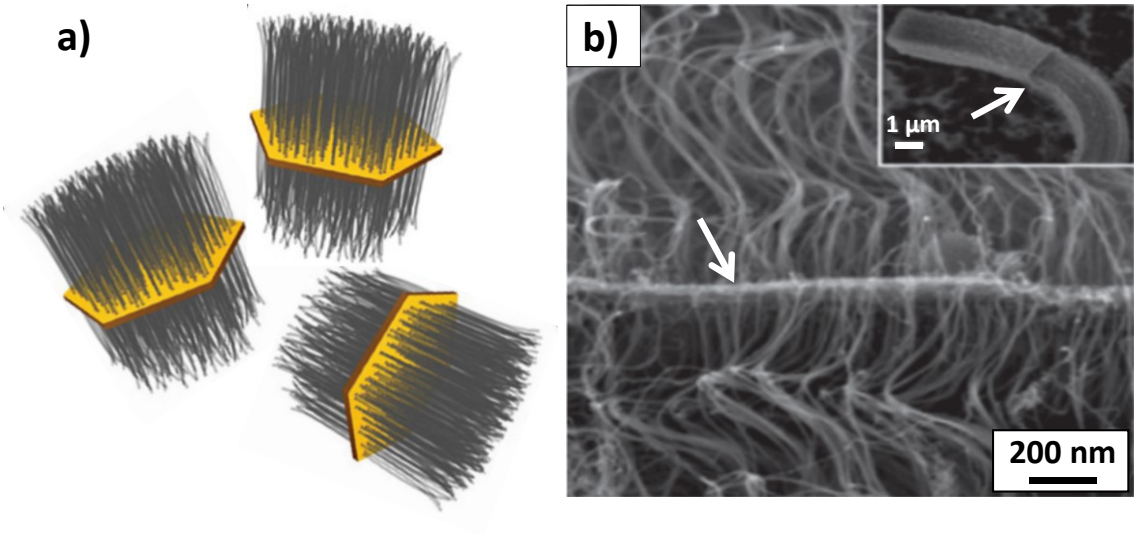

Figure 2.17 a) Schematic of a hybrid filler consisint in layered double hydroxide platelets with CNTs grown on its surfaces [187]. and b) SEM image of a hybrid filler obtained after the CVD synthesis of CNTs from catalysts supported on the surfaces of graphite nanoplatelets (indicated by the arrow). The inset shows a lower magnification image of the hybrid filler [227].

In Table 2.1, the main results obtained for polymer composites with hybrid fillers based on two- and three-dimensional particles are summarized in terms of mechanical properties, DMA properties, glass transition temperature, electrical and thermal conductivity and other results of interest. It should be taken into account that hybrid filler refers to the hybrid material which can be thought of as a single material, instead of the simple mixture of components.

From the results shown in Table 2.1, it can be said that the addition of hybrid fillers to different polymers usually leads to improved mechanical properties. The homogeneous dispersion and strong interaction between the filler and the matrix seem to be the responsible for this effect [228].

Polyurethane nanocomposites foams were prepared with as-received clay, as-received CNTs and the hybrid filler. As it can be observed in Table 2.1, the later showed improvements in specific compressive modulus and strength of 33 and 22%, respectively, compared to the unmodified foam. Thus, the hybrid filler

showed a synergistic effect, since clays and CNTs did not show any reinforcing effect in their corresponding composites [218,229].

In [187], the authors studied polyimide films reinforced with just 0.4 wt.% of layered double hydroxide-CNTs (Figure 2.17a). They reported significant improvements on the mechanical properties, especially in the strain at break which was enhanced by 124%. The tensile modulus and tensile strength were enhanced by 18 and 40%, respectively (Table 2.1).

This effect was also observed, except of the strain at break which in this case decreased, on polyamide 6 composites with similar hybrid fillers, in this case clay-CNTs, processed by a simple melt mixing [215]. In both works, the hybrid filler exhibited strong interaction with the polymeric matrix and a homogenous dispersion within the matrix, attributed to the three-dimensional structure of the filler, rather than the one- and two-dimensional structure of CNTs and clay platelets, respectively. The benefit provided by the hybrid fillers was evident from the fact that mechanical properties improvements were relatively higher when compared to those obtained in composites reinforced with neat CNTs or neat clay. This effect has also been observed on epoxy composites with hybrid nanoclay-CNTs [230]. The hardness of composites with 2 wt.% of CNTs, nanoclay, mixture nanoclay/CNTs and the hybrid material increased by 19, 16, 21 and 40%, respectively, compared to that that of neat epoxy (Table 2.1). As it can be observed, the composite with the hybrid material rendered the highest improvement, which was even higher than that of the composite with the mixture of fillers.

Concerning the glass transition, the hybrid filler could increase the mobility of the segments of the polymeric chains in the amorphous phase, thus lowering the T_g [231]. However, the opposite effect is also possible. The strong interfacial interaction between the hybrid filler and matrix could increase the hindrance of the segmental motion of polymer chains [228,232]. Finally, the addition of clay/CNTs hybrid fillers could also result in no significant changes on the T_g of the resulting composites [233]. Regarding the electrical conductivity, percolation thresholds as low as 0.57 wt.% of hybrid clay/CNTs can be achieved due to its three-dimensional structure [231].

The addition of hybrid fillers seems to have a thermal stabilising effect during the decomposition process of the composites, as reported in Table 2.1. The stabilising effect could be explained due to a barrier effect of the filler for the diffusion of volatile degradation products or to the entrapping of free radicals during the oxidation/degradation process [231,234,235].

As it can be observed in Table 2.1, the hybrid clay/CNTs seems to act as nucleating agent for the crystallization of polymers as polyethylene terephthalate [231], polyvinyl alcohol [232], polylactic acid [233] or polyamide 6 [228]. In the last case, it seems to promote the nucleation of a different phase. In general, it can be said that the addition of the hybrid clay/CNTs do not significantly affects the degree of crystallinity [228,231,233].

Regarding the multifunctional properties (Table 2.1), hybrid fillers (0.6-1.2 wt.%) consisting in SiC microplatelets with vertically aligned CNTs grown on their surface, were dispersed in an epoxy resin to obtain conductive composites [223]. Thanks to the electrically conductive network formed by the filler, the authors were able to perform electrical resistance measurements, during a tensile test, to identify the elastic and plastic behaviour. Furthermore, the hybrid SiC-CNTs could be used to increase the dielectric permittivity and loss of polymers, as polyvinylidene fluoride [236]. The CVD process can be controlled to obtain CNTs on one or both sides of the SiC [222]. In polyvinylidene fluoride composites, the percolation thresholds are 0.7 vol.% for hybrid filler with CNTs mainly grown in one face, and 1.47 for hybrid filler with CNTs grown on both faces. These percolation thresholds are significantly lower than the 10 vol.% of similar composites with neat CNTs.

The advantages of the hybrid fillers over the isolated fillers or their mixtures is clear from the results presented in Figure 2.18 [227,237]. In the first example (Figure 2.18a), by adding the same amount, i.e. 6.6 wt.%, of CNTs or GNPs to polyvinylidene fluoride, the AC conductivity of the resulting composites is similar to that of the matrix. When the CNT+GNP mixture is added, there is an increase in the AC conductivity of about one order of magnitude. However, the composites remain exhibiting an insulating behaviour. Finally, when the hybrid filler, i.e. CNT-

GNP thought of as a single filler, is added, the conductivity significantly increases up to 10^{-4} S/m. The same effect can be found in the mechanical properties of epoxy composites (Figure 2.18b). Upon the addition of CNTs or GNPs (0.5 wt.%), a slight improvement of the tensile modulus and strength, compared to those of neat epoxy, takes place. By adding a mixture of 0.24 wt.% CNTs and 0.26 wt.% GNPs, the increase is somewhat higher than in the previous two cases. However, the strain at break significantly decrease with any filler or mixture of fillers. Interestingly, the composites with the hybrid CNT-GNP presents the highest improvements in tensile modulus and strength, while maintaining a strain at break similar to that of neat epoxy.

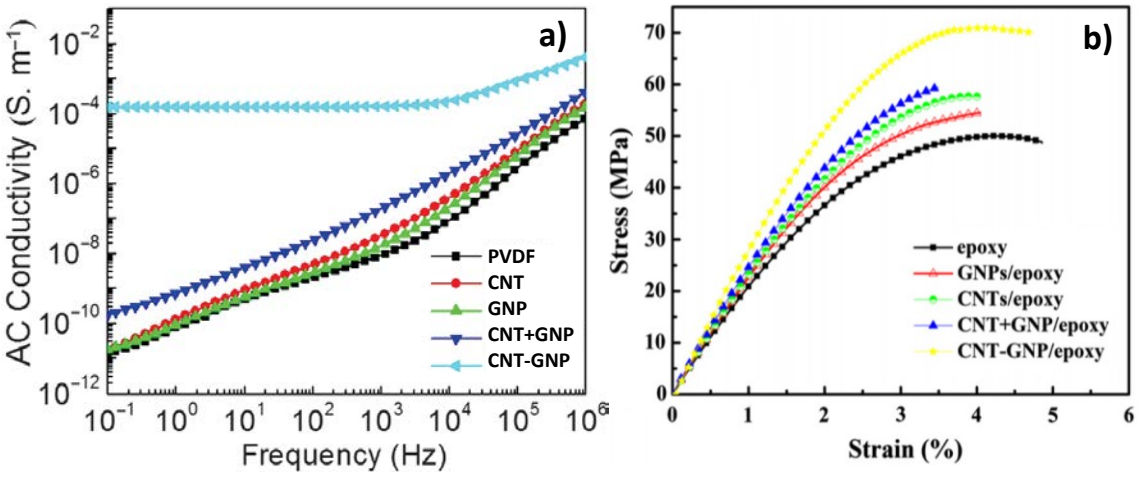

Figure 2.18 a) AC conductivity, as a function of the frequency, of PVDF and its composites with 6.6 wt.% of GNPs, CNTs and hybrid CNG-CNT, respectively, as well as the compossite with the mixture 3.46 wt.% CNTs and 3.14 wt.% GNPs [227], b) Strain-stress cruves of a tensile test of neat epoxy and its composites with 0.5 wt.% of GNPs, CNTs and hybrid CNT-GNP, respectively, as well as the composite with the mixture 0.24 wt.% CNTs and 0.26 wt.% GNPs [237].

2.5.3 Three-dimensional particles as substrates

As it has been mentioned, the hybrid fillers developed in this thesis were obtained by using alumina nanoparticles and hollow glass microspheres as substrates.

The addition of ceramic particles of TiO_2 [238–242], alumina (Al_2O_3) [243–245], silica (SiO_2) [246–249] or calcium carbonate ($CaCO_3$) [250–253], has proved to be an effective approach to improve mechanical properties, among others, of polymers. In general, the modulus (tensile and flexural) of the resulting composites

increase as the modulus of the filler is relatively higher than that of the matrix. If the interface matrix-filler is weak, the addition of particles tends to reduce the strength [240,241]. Regarding the fracture process of polymers reinforced with inorganic ceramic particles, the toughening mechanisms due to the presence of particles have been extensively studied [61,243,253–258]. Crack deflection [61,243,259], crack pinning [61,243,260], shear yielding of the matrix [61,246,256,261] or debonding of the particles from the matrix and subsequent plastic void growth [246,262–264] are energy dissipating mechanisms responsible for the generally enhanced fracture toughness of polymer composites with rigid particles.

Regarding the multifunctional properties, inorganic ceramic particles are electrically insulating materials [265]. Although the addition of this type of particles to polymeric matrices may result in a slightly increased electrical conductivity [242,266], the resulting composites exhibit an electrically insulating behaviour. Therefore, they have been studied for the development of advanced insulating materials to be used in the electronic industry [266–271].

In inorganic materials as ceramics, the heat is propagated through atomic vibrations (phonons), while the contribution of electron movement to the thermal conductivity can be neglected. This means that their thermal conductivity is lower than that of metals and carbon-based materials, where free electrons are more efficient in the heat propagation than phonons. However due to their structure, the thermal conductivity of inorganic (boron nitride, aluminium nitride, alumina, etc.) particles is higher than that of polymers [95,97,265,272]. Thus, the addition of this type of fillers to polymers is a very common approach followed to obtain thermally conductive, yet electrically insulating, composites to be used in electronic packaging and printed circuit board substrates [95,97,268,270,273].

Ceramic particles are available in different morphologies, for instance they can be hollow and filled by a gas. In this sense, hollow glass microspheres (HGMs) have been widely used in polymer composites due to their resulting low density, low thermal conductivity and dielectric constant, low moisture absorption and low coefficient of thermal expansion [274–278]. However, in thermoset composites,

the addition of the HGMs often results in decreased tensile, compressive or flexural strength. Regarding the modulus, it can be maintained or even increased by controlling the density, i.e. the wall thickness, of HGMs [279–281].

In conclusion, inorganic particles have proved to be effective fillers to improve the mechanical properties of polymer composites. If an appropriate filler-matrix interaction is achieved. Furthermore, due to the relatively higher thermal conductivity of inorganic (bulk) materials, compared to that of polymers, the resulting composites usually exhibits enhanced thermal conductivity.

However, these fillers failed when an electrically conducting materials is needed, due to their inherent insulating behaviour. The hybridization with carbon materials is a promising approach to increase the electrical conductivity of polymer composites with inorganic ceramic particles. As it was mentioned for composites with hybrid fillers based on two-dimensional particles and CNTs, the resulting hybrid fillers seemed to have strong interfacial interaction with the matrix [187,228]. Therefore, the hybrid fillers obtained with three-dimensional inorganic particles may also benefit from an enhanced interaction with the polymeric matrix.

In the available literature there are works reporting the synthesis of carbon nanotubes on mm-sized inorganic oxide (SiO_2, Al_2O_3 and ZrO_2) spheres [282–284], micron- and sub-micron-sized silica spheres [285,286], porous silica microspheres [287], alumina microspheres [188,224,225,288,289], stainless steel nanospheres [290], nanospheres of alumina and iron oxide [291]. Furthermore, it has also been reported the synthesis of hybrid structures consisting in micron-scaled irregular SiC particles-CNTs [292], fibrous hydroxyapatite-CNTs [293], micron-sized alumina particles [294,295] or micron-scaled $BaTiO_3$ particles [296].

An example of the different morphologies of the grown CNTs that can be obtain by controlling the parameters of the CVD process are shown in Figure 2.19.

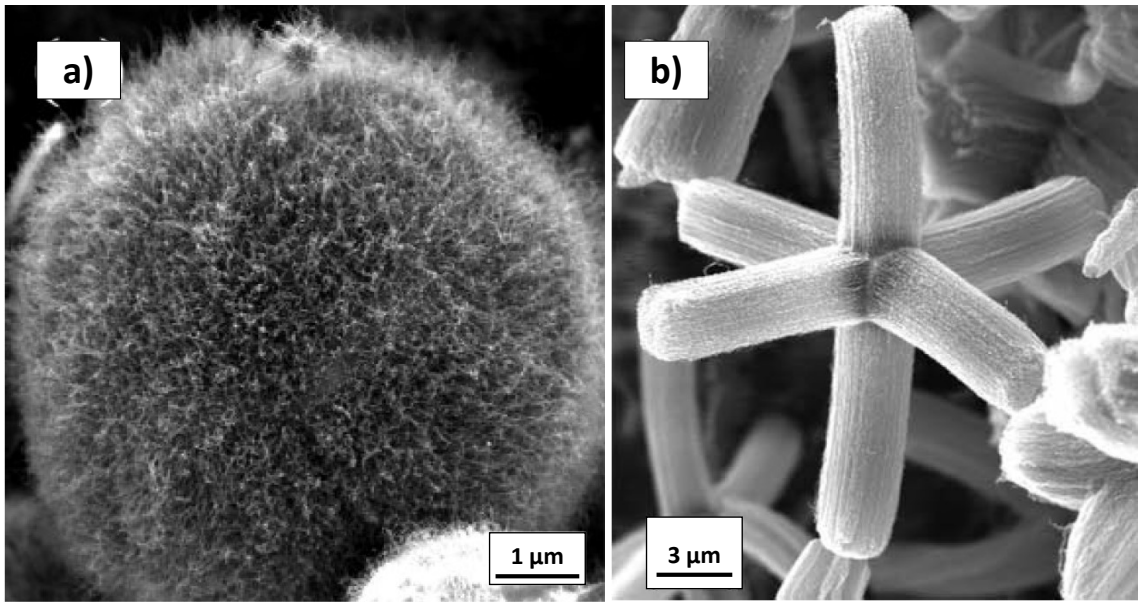

Figure 2.19 SEM images of CNTs grown on alumina microparticles showing a) short CNTs covering the whole surface of the microparticle and b) CNTs forming independent branches uniformly distributed in six directions [188,288].

As shown in Table 2.1, some authors have reported the synthesis of hybrid fillers consisting in alumina microspheres and CNTs with different aspect ratios, i.e. CNT content, [297]. They performed the tensile characterization of epoxy composites with 0.5 wt.% of filler and found that both the tensile modulus and strength increased for all aspect ratios analysed. However, the optimum aspect ratio was 2000, i.e. 26 wt.% of CNTs, which resulted in improvements of 27 and 38% in modulus and strength, respectively, compared to neat epoxy. Interestingly, the hybrid filler with aspect ratio of 2000 also yielded the lowest percolation threshold of the CNTs in the composites, a 0.12 wt.% (Table 2.1). The composites with the hybrid fillers with the highest aspect ratios, i.e. 2000 and 3200, showed the possibility to be monitored during the tensile tests to identify the elastic and the plastic behaviour. This strain sensing ability is similar to that previously reported for composites with SiC-CNTs [223] and GNPs-CNTs [237] (Table 2.1).

Zakaria *et al.* have developed a hybrid filler composed by alumina microparticles and carbon nanotubes, which they used as filler in epoxy composites [298–300]. As it can be observed in Table 2.1, they reported the reinforcing effect of the hybrid filler in the tensile, flexural and compressive properties; being this last case the one in which the filler exhibited its best reinforcing effect. At a filler loading of 5

wt.%, the compressive modulus and strength increased by 148 and 117%, respectively, compared to neat epoxy [300]. Moreover, this composite showed improved thermal stability [300] and a thermal conductivity a 20% higher than that of the unmodified resin [298].

The main characteristic of the hybrid fillers analysed on Table 2.1 is that the substrates (i.e. two- and three-dimensional particles) have sizes in the micron-scale. First, the CNTs grown in the surface of the micron-scaled particles may help to improve the interfacial strength between the filler and the matrix. In second place, the substrates may reduce the agglomeration of CNTs and helping to obtain a homogenous distribution of the nanofiller within the matrix [290]. Furthermore, the three-dimensional morphology of the hybrid filler may result in the formation of the conducting network at lower fillers content, compared to the neat CNTs [287,301] or the simple mixture of components [298].

As it has been reviewed, none of the reported works deals with the synthesis of hybrid fillers using nano-scaled particles as substrates.

In chapter 6 a novel hybrid filler composed by alumina nanoparticles and carbon nanotubes is presented. The homogeneous dispersion of the resulting hybrid nanofiller proved to be difficult, and agglomerates were observed in the produced composites. This poor dispersion resulted in epoxy composites with similar or slightly improved flexural and fracture behaviour, compared to neat epoxy. However, the composites with the hybrid filler showed enhanced thermal and electrical conductivity compared to the epoxy resin and the composites with the as-received nanoparticles.

Finally, a novel hybrid filler based on hollow glass microspheres and carbon nanofibres grown on their surface are developed to obtain lightweight polymer composites with increased electrical conductivity while maintaining or improving their thermal insulting behaviour.

Table 2.1 Summary of main properties of polymer composites with hybrid fillers based on CNTs grown on 2D, spherical and non-spherical particles.

Matrix	Hybrid substrate-grown filler (wt.% of grown filler)	Mechanical properties	DMA properties	Glass transition temperature	Electrical and thermal conductivity	Others	Ref.
Epoxy	Clay-CNTs (-)	↑ HV as ↑wt.%, +40% for 2 wt.%, (HV_0=10.8)	-	-	-	-	[230]

PA-6	Clay-CNTs (40 wt.%)	↑E_T and σ_T, ↓ε_b as ↑wt.%, +290% and +153%, >-20% respectively, for 1 wt.% (E_{T0}=0.4 GPa and σ_{T0}=18.5 MPa, ε_{b0}>200%)	-	-	-	-	[215]
Epoxy	Clay-CNTs (48.5 wt.%)	↑ Vicker's hardness +36% for 1 wt.% (HV_0=16), ↑ Impact strength a 110% for 1 wt.% (I_0=20.2 kJ/m^2)	-	-	-	-	[302]

PVA	Clay-CNTs (-)	-	↑E' as ↑wt.%, @50°C +138% for 7 wt.% (E'_0=2 GPa)	↑ T_g as ↑wt.%, +14°C for 7 wt.% (T_{g0}=57.5°C)	-	↑$T_{5\%}$ (N_2) as ↑wt.%, +16°C for 2 wt.% ($T_{5\%\,0}$=230°C) Nucleating effect of the filler, higher X_C for all wt.%	[232]
PI	LDHs-CNTs (36 wt.%)	↑E_T, σ_T and ε_b as ↑wt.%, +18%, +40% and +124%, respectively, for 0.4 wt.% (E_{T0}=0.65 GPa, σ_{T0}=78.1 MPa, ε_{b0}=26.6%)	-	-	-	-	[187]

PA-6	Clay-CNTs (40 wt.%)	↑E_T and σ_T as ↑wt.%, +325% and +170%, respectively, for 2 wt.% (E_{T0}=0.4 GPa and σ_{T0}=18.5 MPa)	↑E' as ↑wt.%, +55% (-50°C) +120% (100°C) for 2 wt.% (E'_0=3 GPa(-50°C), E'_0=0.3 GPa (100°C))	↑T_g as ↑wt.%, +17.2°C for 2 wt.% (T_{g0}=27.2°C)	-	↑$T_{5\%}$ (air and N_2) as ↑wt.%, +26°C (air) and +18°C (N_2) for 2 wt.% ($T_{5\%\ 0}$=382°C (air), 393 (N_2)). Filler acts as α-phase nucleating agent	[228]
PLA	Clay-CNTs (58.1 wt.%)	↑E as ↑wt.%, +17% for 3 wt.% (G'_0=2.2 GPa)	-	No significant changes with the addition of filler (T_{g0}=58°C)	σ_{DC}=0.7 S/m for 5 wt.%	↓$T_{5\%}$ (air) with hybrid filler, -41°C for 5 wt.% ($T_{5\%\ 0}$=321°C) Nucleating effect of the filler, no changes in X_C	[233]

PU	Clay-CNTs (22 wt.%)	↑E_C/ρ and σ_C/ρ as ↑wt.%, +33% and +22%, respectively, for 1 wt.% (E_{C0}/ρ_0=0.33 MPa/kgm^3, σ_{C0}/ρ_0=9.8 kPa/kgm^3)	-	-	-	↑T_i (N_2) as ↑wt.%, +8°C for 1 wt.% ($T_{i\,0}$=274°C)	[229]
PET	Clay-CNTs (58.1 wt.%)	-	↑E' @RT a +27% and +46% for 1 and 3 wt.%, respectively (E'_0=260 Pa)	↓T_g as ↑wt.%, ≈-5°C for 3 wt.% (T_{g0}=68°C)	σ_{DC}=3x10^{-7} S/m for 3 wt.%; ϕ_C=0.57 wt.% (0.33 wt.% CNTs)	↑$T_{5\%}$ (air) as ↑wt.%, +16°C for 2 wt.% ($T_{5\%\,0}$=382°C) Nucleating effect of the filler, no significant changes in X_C	[231]

Epoxy	Clay-CNTs (30 wt.%)	↑E_T and σ_T as ↑wt.%, +135% and +87%, respectively, for 5 wt.% (E_{T0}=0.9 GPa and σ_{T0}=34 MPa), ↑ mHV as ↑wt.%, +14% for 5 wt.%, (mHV_0=14.6)	-	-	-	-	[303]
PVDF	2D SiC-CNTs (27 wt.%)	-	-	-	σ_{AC}=10^{-2} S/m for 8.8 wt.%, ϕ_C=5.65 wt.% (1.53 wt.% CNTs)	↑ε_r for high charge storage capacitors, or ↑ε_r and ↑ loss tangent for EM-wave absorption	[236]

Epoxy	2D SiC-CNTs (-)	-	-	-	Electrically conductive composites for 0.6-1.2 wt.%	*in situ* strain sensing (identification of elastic and plastic behaviour during tensile test)	[223, 297]
PVDF	2D SiC with CNTs in one or both faces (-)	-	-	-	σ_{AC}=10^{-3} S/m for 1.5 vol.%, CNTs, ϕ_C=0.7 vol.% CNTs (one side), σ_{AC}=10^{-2} S/m for 2.25 vol.% CNTs, ϕ_C=1.47 vol.% CNTs (both sides)	ϕ_C can be adjusted by controlling the synthesis of CNTs on SiC: CNTs grown on one side or on both sides	[222]

PVDF	GNPs-CNTs (52 wt.%)	-	-	-	σ_{AC}=10^{-4} S/m for 6.6 wt.%	↓T_i with hybrid filler, -15°C for 6.6 wt.%, ($T_{i\,0}$=464°C) Reduced X_C, competition between nucleating effect and restricted motion of polymer chains	[227]
Epoxy	GNPs-CNTs (48 wt.%)	↑E_T and σ_T as ↑wt.%, +40% and +36%, respectively, for 0.5 wt.% (E_{T0}=2.2 GPa and σ_{T0}=50 MPa), similar ε_b to that of neat epoxy	-	-	Electrically conductive composites for 0.5 wt.%	*in situ* strain sensing (identification of elastic and plastic behaviour during tensile test)	[237, 297]

Epoxy	Alumina microspheres-CNTs (20 wt.%)	-	-	No significant changes up to 0.15 wt.% CNTs, ↑ for higher wt.%, +46°C for 0.36 wt.% (T_{g0}=74°C)	↑k and α as ↑wt.%, +130% and +115%, respectively, for 0.15 wt.% CNTs (k_0=0.17 W/mK, α_0=0.13 mm^2/s)	-	[301]
PVA	Silica microspheres-CNTs (33.6 wt.%)	-	-	-	σ_{AC}=10^{-2} S/m for 20 wt.%, ϕ_C=0.62 wt.% (0.20 wt.% CNTs),	-	[287]

Epoxy	Alumina microspheres-CNTs with different AR: 500, 1200, 2000 and 3200 (14, 25, 26 and 62.5 wt.%, respectively)	↑E_T and σ_T with hybrid filler addition for all AR, +27% and +38%, respectively, for 0.5 wt.% hybrid with AR=2000 (26 wt.% CNTs) (E_{T0}=2.2 GPa and σ_{T0}=50 MPa)	-	-	ϕ_C=0.27, 0.24, 0.12 and 0.25 wt.% CNTs for hybrids with AR of 500, 1200, 2000 and 3200, respectively	For composites with hybrids with AR of 2000 and 3200: *in situ* strain sensing (identification of elastic and plastic behaviour during tensile test)	[297]
PVDF	$BaTiO_3$ microspheres-CNTs (11 wt.%)	-	-	-	-	↑ε_r and ↑ loss tangent as ↑wt.%, ϕ_C=10 vol.%	[296]

Epoxy	Alumina microspheres-CNTs (20 wt.%)	↑E_T and ↓ε_b as ↑wt.%, +26% and -20%, respectively, for 10 wt.%, (E_{T0}=2.12 GPa and ε_{b0}=n.a.), similar σ_T to that of neat epoxy	-	-	σ_{AC}=10^{-3} S/m for 10 wt.% (2 wt.% CNTs), ϕ_C=0.76 vol.% CNTs (1.3 wt.% CNTs), ↑k and α as ↑wt.%, +56% and +92%, respectively, for 10 wt.% (k_0=0.25 W/mK, α_0=0.147 mm^2/s)	↑ε_r and ↑ loss tangent as ↑wt.%	[304]

PU	Stainless steel nanospheres-CNTs (-)	↑E_T and σ_T with hybrid filler, +34% and +19%, respectively, for 5 wt.% (E_{T0}=2.18 GPa and σ_{T0}=52.5 MPa)	-	-	-	-	[290]
Epoxy	Alumina microparticles-CNTs (60 wt.%)	↑E_T and σ_T with hybrid filler, +47% and +34%, respectively, for 1 wt.% (E_{T0}=1.12 GPa and σ_{T0}=19.6 MPa), similar ε_b to that of neat epoxy	-	-	-	-	[294]

HDPE	Alumina microparticles-CNTs (60 wt.%)	↑E_T and σ_T, ↓ε_b as ↑wt.%, +100% and +66%, -87% respectively, for 5 wt.% (E_{T0}=0.36 GPa and σ_{T0}=17.5 MPa, ε_{b0}=67%)	-	-	-	-	[305]
Epoxy	Alumina microparticles-CNTs (12 wt.%)	↑E_T and σ_T with addition of hybrid, +39% and +30%, respectively, for 3 wt.% (E_{T0}=1.92 GPa and σ_{T0}=51 MPa) similar ε_b to that of neat epoxy	-	↑T_g as ↑wt.%, +25°C for 5 wt.% (T_{g0}=101°C)	↑k as ↑wt.%, +20% for 5 wt.% (k_0=0.2 W/mK)	↓CTE as ↑wt.% in both the glassy and rubbery state, -11.5% and -3%, respectively, for 5 wt.%	[298]

Epoxy	Alumina microparticles-CNTs (12 wt.%)	↑E_F and σ_F, ↓ε_b with addition of hybrid, +35% and +30%, -38%, respectively, for 5 wt.% (E_{F0}=3.7 GPa, σ_{F0}=102 MPa, ε_{b0}=9%)	-	-	-	↑ε_r as ↑wt.%	[299]
Epoxy	Alumina microparticles-CNTs (12 wt.%)	↑E_C and σ_C with addition of hybrid, +148% and +117%, respectively, for 5 wt.% (E_{C0}=1.04 GPa and σ_{C0}=33.7 MPa)	-	-	-	↑T_i with hybrid filler, +25°C for 5 wt.%, ($T_{i\,0}$=295°C)	[300]

The sub-index 0 indicates the value for the neat polymer

HV: Vicker's hardness, mHV: Vicker's microhardness

E_T: Tensile modulus, σ_T: Tensile strength, ε_b: Strain at break

E_F: Flexural modulus, σ_F: flexural strength, ε_b: Strain at break.

E_C: Compressive modulus, σ_C : Compressive strength

ρ: Density, AR: aspect (length to diameter) ratio

E': Storage modulus, T_g: Glass transition temperature

σ_{DC}: Direct current (DC) electrical conductivity, σ_{AC}: Alternating current (AC) electrical conductivity, ϕ_C: Percolation threshold

k: Thermal conductivity, α: Thermal diffusivity, $T_{5\%}$: Temperature at which a 5 wt.% loss takes place, T_i=Starting temperature for decomposition

X_C: Degree of crystallinity, ε_r: Dielectric permittivity

CTE: Coefficient of thermal expansion

2.6 References

[1] R.J. Young, P.A. Lovell, Introduction to Polymers, 2nd ed., Chapman and Hall, London, 1991.

[2] J.P. Jose, S.K. Malhotra, Advances in Polymer Composites: Macro- and Microcomposites – State of the Art, New Challenges, and Opportunities, in: S. Thomas, J. Kuruvilla, S. Kumarlhotra, K. Goda, M.S. Sreekala (Eds.), Polym. Compos., Wiley-VCH Verlag GmbH & Co. KGaA, 2012: pp. 1–16. doi:10.1002/9783527645213.ch1.

[3] T.L. Anderson, Fracture Mechanics: Fundamentals and Applications, Third Edition, CRC Press, 2005.

[4] D.B. Miracle, S.L. Donaldson, ASM Handbook. Volume 21, ASM International, Materials Park, OH, 2001.

[5] P.K. Mallick, Fiber-Reinforced Composites: Materials, Manufacturing, and Design, Third Edition, CRC Press, 2007.

[6] M. Ashby, Materials Selection in Mechanical Design, 3rd ed., Butterworth-Heinemann, 2005.

[7] U. Meier, Strengthening of structures using carbon fibre/epoxy composites, Constr. Build. Mater. 9 (1995) 341–351. doi:10.1016/0950-0618(95)00071-2.

[8] I.A. Sharaky, L. Torres, J. Comas, C. Barris, Flexural response of reinforced concrete (RC) beams strengthened with near surface mounted (NSM) fibre reinforced polymer (FRP) bars, Compos. Struct. 109 (2014) 8–22. doi:10.1016/j.compstruct.2013.10.051.

[9] A milestone for composites in aviation, J. Fail. Anal. Prev. 5 (2005) 5–7. doi:10.1361/154770205X55009.

[10] R. Younes, A. Hallal, F. Fardoun, F. Hajj, Comparative Review Study on Elastic Properties Modeling for Unidirectional Composite Materials, in: N. Hu (Ed.), Compos. Their Prop., InTech, 2012. doi:10.5772/50362.

[11] M.W. Pilling, B. Yates, M.A. Black, P. Tattersall, The thermal conductivity of carbon fibre-reinforced composites, J. Mater. Sci. 14 (1979) 1326–1338. doi:10.1007/BF00549304.

[12] Y. Hirano, S. Katsumata, Y. Iwahori, A. Todoroki, Artificial lightning testing on graphite/epoxy composite laminate, Compos. Part Appl. Sci. Manuf. 41 (2010) 1461–1470. doi:10.1016/j.compositesa.2010.06.008.

[13] S. Han, D.D.L. Chung, Increasing the through-thickness thermal conductivity of carbon fiber polymer–matrix composite by curing pressure increase and filler incorporation, Compos. Sci. Technol. 71 (2011) 1944–1952. doi:10.1016/j.compscitech.2011.09.011.

[14] M. Gagné, D. Therriault, Lightning strike protection of composites, Prog. Aerosp. Sci. 64 (2014) 1–16. doi:10.1016/j.paerosci.2013.07.002.

[15] C. Karch, C. Metzner, Lightning protection of carbon fibre reinforced plastics-An overview, in: 2016 33rd Int. Conf. Light. Prot. ICLP, 2016: pp. 1–8. doi:10.1109/ICLP.2016.7791441.

[16] J. Wen, Z. Xia, F. Choy, Damage detection of carbon fiber reinforced polymer composites via electrical resistance measurement, Compos. Part B Eng. 42 (2011) 77–86. doi:10.1016/j.compositesb.2010.08.005.

[17] A. Okada, M. Kawasumi, A. Usuki, Y. Kojima, T. Kurauchi, O. Kamigaito, Nylon 6–Clay Hybrid, in: MRS Proc., Cambridge Univ Press, 1989. http://journals.cambridge.org/abstract_S1946427400362807 (accessed January 28, 2014).

[18] A. Usuki, Y. Kojima, M. Kawasumi, A. Okada, Y. Fukushima, T. Kurauchi, O. Kamigaito, Synthesis of nylon 6-clay hybrid, J. Mater. Res. 8 (1993) 1179–1184. doi:10.1557/JMR.1993.1179.

[19] Y. Kojima, A. Usuki, M. Kawasumi, A. Okada, Y. Fukushima, T. Kurauchi, O. Kamigaito, Mechanical properties of nylon 6-clay hybrid, J. Mater. Res. 8 (1993) 1185–1189. doi:10.1557/JMR.1993.1185.

[20] K.I. Winey, R.A. Vaia, Polymer Nanocomposites, MRS Bull. 32 (2007) 314–322. doi:10.1557/mrs2007.229.

[21] P. Vijayan P., D. Puglia, M.A.S.A. Al-Maadeed, J.M. Kenny, S. Thomas, Elastomer/thermoplastic modified epoxy nanocomposites: The hybrid effect of “micro” and “nano” scale, Mater. Sci. Eng. R Rep. 116 (2017) 1–29. doi:10.1016/j.mser.2017.03.001.

[22] J.Z. Liang, R.K.Y. Li, Rubber toughening in polypropylene: a review, J. Appl. Polym. Sci. 77 (2000) 409–417.

[23] R. Bagheri, B.T. Marouf, R.A. Pearson, Rubber-Toughened Epoxies: A Critical Review, Polym. Rev. 49 (2009) 201–225. doi:10.1080/15583720903048227.

[24] L. Becu, A. Maazouz, H. Sautereau, J.F. Gerard, Fracture behavior of epoxy polymers modified with core-shell rubber particles, J. Appl. Polym. Sci. 65 (1997) 2419–2431.
[25] G. Giannakopoulos, K. Masania, A.C. Taylor, Toughening of epoxy using core–shell particles, J. Mater. Sci. 46 (2011) 327–338. doi:10.1007/s10853-010-4816-6.
[26] M.R. Dadfar, F. Ghadami, Effect of rubber modification on fracture toughness properties of glass reinforced hot cured epoxy composites, Mater. Des. 47 (2013) 16–20. doi:10.1016/j.matdes.2012.12.035.
[27] G. Liu, G. Qiu, Study on the mechanical and morphological properties of toughened polypropylene blends for automobile bumpers, Polym. Bull. 70 (2013) 849–857. doi:10.1007/s00289-012-0880-1.
[28] S.H. Jafari, A.K. Gupta, Impact strength and dynamic mechanical properties correlation in elastomer-modified polypropylene, J. Appl. Polym. Sci. 78 (2000) 962–971. doi:10.1002/1097-4628(20001031)78:5<962::AID-APP40>3.0.CO;2-5.
[29] A.K. Gupta, B.K. Ratnam, K.R. Srinivasan, Impact toughening of polypropylene by ethylene vinyl acetate copolymer, J. Appl. Polym. Sci. 45 (1992) 1303–1312. doi:10.1002/app.1992.070450718.
[30] B. Garnier, B. Agoudjil, A. Boudenne, Metallic Particle-Filled Polymer Microcomposites, in: S. Thomas, J. Kuruvilla, S. Kumarlhotra, K. Goda, M.S. Sreekala (Eds.), Polym. Compos., Wiley-VCH Verlag GmbH & Co. KGaA, 2012: pp. 575–612. doi:10.1002/9783527645213.ch19.
[31] J.-B. Donnet, Carbon Black: Science and Technology, Second Edition, CRC Press, 1993.
[32] A. Kato, Y. Ikeda, S. Kohjiya, Carbon Black-Filled Natural Rubber Composites: Physical Chemistry and Reinforcing Mechanism, in: S. Thomas, J. Kuruvilla, S. Kumarlhotra, K. Goda, M.S. Sreekala (Eds.), Polym. Compos., Wiley-VCH Verlag GmbH & Co. KGaA, 2012: pp. 515–543. doi:10.1002/9783527645213.ch17.
[33] H. Ning, Y. Li, J. Li, N. Hu, Y. Liu, L. Wu, F. Liu, Toughening effect of CB-epoxy interleaf on the interlaminar mechanical properties of CFRP laminates, Compos. Part Appl. Sci. Manuf. 68 (2015) 226–234. doi:10.1016/j.compositesa.2014.09.030.
[34] B.C. Kim, S.W. Park, D.G. Lee, Fracture toughness of the nano-particle reinforced epoxy composite, Compos. Struct. 86 (2008) 69–77. doi:10.1016/j.compstruct.2008.03.005.
[35] R. Schueler, J. Petermann, K. Schulte, H.-P. Wentzel, Agglomeration and electrical percolation behavior of carbon black dispersed in epoxy resin, J. Appl. Polym. Sci. 63 (1997) 1741–1746. doi:10.1002/(SICI)1097-4628(19970328)63:13<1741::AID-APP5>3.0.CO;2-G.
[36] I. Balberg, A comprehensive picture of the electrical phenomena in carbon black–polymer composites, Carbon. 40 (2002) 139–143.
[37] H. Tang, Z.Y. Liu, J.H. Piao, X.F. Chen, Y.X. Lou, S.H. Li, Electrical behavior of carbon black-filled polymer composites: Effect of interaction between filler and matrix, J. Appl. Polym. Sci. 51 (1994) 1159–1164. doi:10.1002/app.1994.070510701.
[38] A. Krueger, Carbon Nanotubes, in: Carbon Mater. Nanotechnol., Wiley-VCH Verlag GmbH & Co. KGaA, 2010: pp. 123–281. doi:10.1002/9783527629602.ch3.
[39] S. Iijima, Helical microtubules of graphitic carbon, Nature. 354 (1991) 56–58.
[40] Y. Gogotsi, Nanomaterials Handbook, CRC Press, 2006.
[41] M.K. Samani, N. Khosravian, G.C.K. Chen, M. Shakerzadeh, D. Baillargeat, B.K. Tay, Thermal conductivity of individual multiwalled carbon nanotubes, Int. J. Therm. Sci. 62 (2012) 40–43. doi:10.1016/j.ijthermalsci.2012.03.003.
[42] J. Hone, M. Whitney, C. Piskoti, A. Zettl, Thermal conductivity of single-walled carbon nanotubes, Phys. Rev. B. 59 (1999) R2514–R2516. doi:10.1103/PhysRevB.59.R2514.
[43] A. Thess, R. Lee, P. Nikolaev, H. Dai, P. Petit, J. Robert, C. Xu, Y.H. Lee, S.G. Kim, A.G. Rinzler, D.T. Colbert, G.E. Scuseria, D. Tománek, J.E. Fischer, R.E. Smalley, Crystalline Ropes of Metallic Carbon Nanotubes, Science. 273 (1996) 483–487. doi:10.1126/science.273.5274.483.
[44] Y. Ando, X. Zhao, H. Shimoyama, G. Sakai, K. Kaneto, Physical properties of multiwalled carbon nanotubes, Int. J. Inorg. Mater. 1 (1999) 77–82. doi:10.1016/S1463-0176(99)00012-5.
[45] M.-F. Yu, O. Lourie, M.J. Dyer, K. Moloni, T.F. Kelly, R.S. Ruoff, Strength and Breaking Mechanism of Multiwalled Carbon Nanotubes Under Tensile Load, Science. 287 (2000) 637–640. doi:10.1126/science.287.5453.637.
[46] M.H. Al-Saleh, U. Sundararaj, A review of vapor grown carbon nanofiber/polymer conductive composites, Carbon. 47 (2009) 2–22. doi:10.1016/j.carbon.2008.09.039.

[47] G.G. Tibbetts, M.L. Lake, K.L. Strong, B.P. Rice, A review of the fabrication and properties of vapor-grown carbon nanofiber/polymer composites, Compos. Sci. Technol. 67 (2007) 1709–1718. doi:10.1016/j.compscitech.2006.06.015.
[48] M.H. Al-Saleh, U. Sundararaj, Review of the mechanical properties of carbon nanofiber/polymer composites, Compos. Part Appl. Sci. Manuf. 42 (2011) 2126–2142. doi:10.1016/j.compositesa.2011.08.005.
[49] N. Hiremath, G. Bhat, High-performance carbon nanofibers and nanotubes, in: Struct. Prop. High-Perform. Fibers, Elsevier, 2017: pp. 79–109. doi:10.1016/B978-0-08-100550-7.00004-8.
[50] V. Choudhary, A. Gupta, Polymer/carbon nanotube nanocomposites, in: Carbon Nanotub.-Polym. Nanocomposites, Intech, 2011.
[51] I. Martin-Gullon, J. Vera, J.A. Conesa, J.L. González, C. Merino, Differences between carbon nanofibers produced using Fe and Ni catalysts in a floating catalyst reactor, Carbon. 44 (2006) 1572–1580. doi:10.1016/j.carbon.2005.12.027.
[52] Z. Spitalsky, D. Tasis, K. Papagelis, C. Galiotis, Carbon nanotube–polymer composites: Chemistry, processing, mechanical and electrical properties, Prog. Polym. Sci. 35 (2010) 357–401. doi:10.1016/j.progpolymsci.2009.09.003.
[53] T.-W. Chou, L. Gao, E.T. Thostenson, Z. Zhang, J.-H. Byun, An assessment of the science and technology of carbon nanotube-based fibers and composites, Compos. Sci. Technol. 70 (2010) 1–19. doi:10.1016/j.compscitech.2009.10.004.
[54] Z. Han, A. Fina, Thermal conductivity of carbon nanotubes and their polymer nanocomposites: A review, Prog. Polym. Sci. 36 (2011) 914–944. doi:10.1016/j.progpolymsci.2010.11.004.
[55] P.-C. Ma, N.A. Siddiqui, G. Marom, J.-K. Kim, Dispersion and functionalization of carbon nanotubes for polymer-based nanocomposites: A review, Compos. Part Appl. Sci. Manuf. 41 (2010) 1345–1367. doi:10.1016/j.compositesa.2010.07.003.
[56] W. Bauhofer, J.Z. Kovacs, A review and analysis of electrical percolation in carbon nanotube polymer composites, Compos. Sci. Technol. 69 (2009) 1486–1498. doi:10.1016/j.compscitech.2008.06.018.
[57] V. Realinho, M. Antunes, D. Arencón, J.I. Velasco, Mechanical–Viscoelastic Characterization in Nanocomposites, in: S. Thomas, K. Joseph, S. Kumarlhotra, K. Goda, M.S. Sreekala (Eds.), Polym. Compos., Wiley-VCH Verlag GmbH & Co. KGaA, 2013: pp. 117–146. doi:10.1002/9783527652372.ch5.
[58] M. Morcom, G. Simon, 17 - Polyolefin–carbon nanotube composites, in: Polym. Nanotube Compos., Woodhead Publishing, 2011: pp. 511–544. doi:10.1533/9780857091390.2.511.
[59] G. Mittal, V. Dhand, K.Y. Rhee, S.-J. Park, W.R. Lee, A review on carbon nanotubes and graphene as fillers in reinforced polymer nanocomposites, J. Ind. Eng. Chem. 21 (2015) 11–25. doi:10.1016/j.jiec.2014.03.022.
[60] Z. Yang, K. McElrath, J. Bahr, N.A. D'Souza, Effect of matrix glass transition on reinforcement efficiency of epoxy-matrix composites with single walled carbon nanotubes, multi-walled carbon nanotubes, carbon nanofibers and graphite, Compos. Part B Eng. 43 (2012) 2079–2086. doi:10.1016/j.compositesb.2012.01.049.
[61] M.M. Shokrieh, S.M. Ghoreishi, M. Esmkhani, 11 - Toughening mechanisms of nanoparticle-reinforced polymers, in: Q.Q. Ye (Ed.), Toughening Mech. Compos. Mater., Woodhead Publishing, 2015: pp. 295–320.
[62] H.D. Wagner, P.M. Ajayan, K. Schulte, Nanocomposite toughness from a pull-out mechanism, Compos. Sci. Technol. 83 (2013) 27–31. doi:10.1016/j.compscitech.2013.04.017.
[63] J.-K. Kim, Y. Mai, High strength, high fracture toughness fibre composites with interface control—A review, Compos. Sci. Technol. 41 (1991) 333–378. doi:10.1016/0266-3538(91)90072-W.
[64] B. Fiedler, F.H. Gojny, M.H.G. Wichmann, M.C.M. Nolte, K. Schulte, Fundamental aspects of nano-reinforced composites, Compos. Sci. Technol. 66 (2006) 3115–3125. doi:10.1016/j.compscitech.2005.01.014.
[65] M.J. Palmeri, K.W. Putz, L.C. Brinson, Sacrificial Bonds in Stacked-Cup Carbon Nanofibers: Biomimetic Toughening Mechanisms for Composite Systems, ACS Nano. 4 (2010) 4256–4264. doi:10.1021/nn100661a.
[66] R.B. Ladani, S. Wu, A.J. Kinloch, K. Ghorbani, J. Zhang, A.P. Mouritz, C.H. Wang, Improving the toughness and electrical conductivity of epoxy nanocomposites by using aligned carbon

nanofibres, Compos. Sci. Technol. 117 (2015) 146–158. doi:10.1016/j.compscitech.2015.06.006.
[67] V. Mirjalili, P. Hubert, Modelling of the carbon nanotube bridging effect on the toughening of polymers and experimental verification, Compos. Sci. Technol. 70 (2010) 1537–1543. doi:10.1016/j.compscitech.2010.05.016.
[68] M.-F. Yu, B.I. Yakobson, R.S. Ruoff, Controlled Sliding and Pullout of Nested Shells in Individual Multiwalled Carbon Nanotubes, J. Phys. Chem. B. 104 (2000) 8764–8767. doi:10.1021/jp002828d.
[69] J. Blanco, E.J. García, R.G. de Villoria, B.L. Wardle, Limiting Mechanisms of Mode I Interlaminar Toughening of Composites Reinforced with Aligned Carbon Nanotubes, J. Compos. Mater. 43 (2009) 825–841. doi:10.1177/0021998309102398.
[70] A. Allaoui, N. El Bounia, How carbon nanotubes affect the cure kinetics and glass transition temperature of their epoxy composites? – A review, Express Polym. Lett. 3 (2009) 588–594. doi:10.3144/expresspolymlett.2009.73.
[71] H. Xie, B. Liu, Z. Yuan, J. Shen, R. Cheng, Cure kinetics of carbon nanotube/tetrafunctional epoxy nanocomposites by isothermal differential scanning calorimetry, J. Polym. Sci. Part B Polym. Phys. 42 (2004) 3701–3712. doi:10.1002/polb.20220.
[72] D. Puglia, L. Valentini, J.M. Kenny, Analysis of the cure reaction of carbon nanotubes/epoxy resin composites through thermal analysis and Raman spectroscopy, J. Appl. Polym. Sci. 88 (2003) 452–458.
[73] L. Guadagno, L. Vertuccio, A. Sorrentino, M. Raimondo, C. Naddeo, V. Vittoria, G. Iannuzzo, E. Calvi, S. Russo, Mechanical and barrier properties of epoxy resin filled with multi-walled carbon nanotubes, Carbon. 47 (2009) 2419–2430. doi:10.1016/j.carbon.2009.04.035.
[74] J. Wu, D.D.L. Chung, Calorimetric study of the effect of carbon fillers on the curing of epoxy, Carbon. 42 (2004) 3039–3042. doi:10.1016/j.carbon.2004.07.010.
[75] J.D. Fidelus, E. Wiesel, F.H. Gojny, K. Schulte, H.D. Wagner, Thermo-mechanical properties of randomly oriented carbon/epoxy nanocomposites, Compos. Part Appl. Sci. Manuf. 36 (2005) 1555–1561. doi:10.1016/j.compositesa.2005.02.006.
[76] A. Montazeri, N. Montazeri, Viscoelastic and mechanical properties of multi walled carbon nanotube/epoxy composites with different nanotube content, Mater. Des. 32 (2011) 2301–2307. doi:10.1016/j.matdes.2010.11.003.
[77] H. Miyagawa, L.T. Drzal, Thermo-physical and impact properties of epoxy nanocomposites reinforced by single-wall carbon nanotubes, Polymer. 45 (2004) 5163–5170. doi:10.1016/j.polymer.2004.05.036.
[78] Y.-H. Liao, O. Marietta-Tondin, Z. Liang, C. Zhang, B. Wang, Investigation of the dispersion process of SWNTs/SC-15 epoxy resin nanocomposites, Mater. Sci. Eng. A. 385 (2004) 175–181. doi:10.1016/j.msea.2004.06.031.
[79] Y.-K. Choi, K. Sugimoto, S.-M. Song, Y. Gotoh, Y. Ohkoshi, M. Endo, Mechanical and physical properties of epoxy composites reinforced by vapor grown carbon nanofibers, Carbon. 43 (2005) 2199–2208. doi:10.1016/j.carbon.2005.03.036.
[80] Y. Zhou, F. Pervin, L. Lewis, S. Jeelani, Experimental study on the thermal and mechanical properties of multi-walled carbon nanotube-reinforced epoxy, Mater. Sci. Eng. A. 452–453 (2007) 657–664. doi:10.1016/j.msea.2006.11.066.
[81] A.S. dos Santos, T. de O.N. Leite, C.A. Furtado, C. Welter, L.C. Pardini, G.G. Silva, Morphology, thermal expansion, and electrical conductivity of multiwalled carbon nanotube/epoxy composites, J. Appl. Polym. Sci. 108 (2008) 979–986. doi:10.1002/app.27614.
[82] T.M. Herceg, S.-H. Yoon, M.S.Z. Abidin, E.S. Greenhalgh, A. Bismarck, M.S.P. Shaffer, Thermosetting nanocomposites with high carbon nanotube loadings processed by a scalable powder based method, Compos. Sci. Technol. 127 (2016) 62–70. doi:10.1016/j.compscitech.2016.01.017.
[83] A.R. Bhattacharyya, T.V. Sreekumar, T. Liu, S. Kumar, L.M. Ericson, R.H. Hauge, R.E. Smalley, Crystallization and orientation studies in polypropylene/single wall carbon nanotube composite, Polymer. 44 (2003) 2373–2377. doi:10.1016/S0032-3861(03)00073-9.
[84] C. Marco, M. Naffakh, M.A. Gómez, G. Santoro, G. Ellis, The crystallization of polypropylene in multiwall carbon nanotube-based composites, Polym. Compos. 32 (2011) 324–333. doi:10.1002/pc.21059.
[85] M.-K. Seo, J.-R. Lee, S.-J. Park, Crystallization kinetics and interfacial behaviors of polypropylene composites reinforced with multi-walled carbon nanotubes, Mater. Sci. Eng. A. 404 (2005) 79–84. doi:10.1016/j.msea.2005.05.065.

[86] G.-W. Lee, S. Jagannathan, H.G. Chae, M.L. Minus, S. Kumar, Carbon nanotube dispersion and exfoliation in polypropylene and structure and properties of the resulting composites, Polymer. 49 (2008) 1831–1840. doi:10.1016/j.polymer.2008.02.029.
[87] M. Ganß, B.K. Satapathy, M. Thunga, R. Weidisch, P. Pötschke, D. Jehnichen, Structural interpretations of deformation and fracture behavior of polypropylene/multi-walled carbon nanotube composites, Acta Mater. 56 (2008) 2247–2261. doi:10.1016/j.actamat.2008.01.010.
[88] E. Assouline, A. Lustiger, A.H. Barber, C.A. Cooper, E. Klein, E. Wachtel, H.D. Wagner, Nucleation ability of multiwall carbon nanotubes in polypropylene composites, J. Polym. Sci. Part B Polym. Phys. 41 (2003) 520–527.
[89] H. Zhang, Z. Zhang, Impact behaviour of polypropylene filled with multi-walled carbon nanotubes, Eur. Polym. J. 43 (2007) 3197–3207. doi:10.1016/j.eurpolymj.2007.05.010.
[90] M. Razavi-Nouri, M. Ghorbanzadeh-Ahangari, A. Fereidoon, M. Jahanshahi, Effect of carbon nanotubes content on crystallization kinetics and morphology of polypropylene, Polym. Test. 28 (2009) 46–52. doi:10.1016/j.polymertesting.2008.10.001.
[91] J.K.W. Sandler, J.E. Kirk, I.A. Kinloch, M.S.P. Shaffer, A.H. Windle, Ultra-low electrical percolation threshold in carbon-nanotube-epoxy composites, Polymer. 44 (2003) 5893–5899. doi:10.1016/S0032-3861(03)00539-1.
[92] Y. Yang, M.C. Gupta, K.L. Dudley, R.W. Lawrence, A Comparative Study of EMI Shielding Properties of Carbon Nanofiber and Multi-Walled Carbon Nanotube Filled Polymer Composites, J. Nanosci. Nanotechnol. 5 (2005) 927–931. doi:10.1166/jnn.2005.115.
[93] D. Zhu, Y. Bin, M. Matsuo, Electrical conducting behaviors in polymeric composites with carbonaceous fillers, J. Polym. Sci. Part B Polym. Phys. 45 (2007) 1037–1044. doi:10.1002/polb.21115.
[94] Y.A. Kim, S. Kamio, T. Tajiri, T. Hayashi, S.M. Song, M. Endo, M. Terrones, M.S. Dresselhaus, Enhanced thermal conductivity of carbon fiber/phenolic resin composites by the introduction of carbon nanotubes, Appl. Phys. Lett. 90 (2007) 093125. doi:10.1063/1.2710778.
[95] H. Chen, V.V. Ginzburg, J. Yang, Y. Yang, W. Liu, Y. Huang, L. Du, B. Chen, Thermal conductivity of polymer-based composites: Fundamentals and applications, Prog. Polym. Sci. 59 (2016) 41–85. doi:10.1016/j.progpolymsci.2016.03.001.
[96] J. Che, T. Cagin, W.A. Goddard III, Thermal conductivity of carbon nanotubes, Nanotechnology. 11 (2000) 65.
[97] N. Burger, A. Laachachi, M. Ferriol, M. Lutz, V. Toniazzo, D. Ruch, Review of thermal conductivity in composites: Mechanisms, parameters and theory, Prog. Polym. Sci. 61 (2016) 1–28. doi:10.1016/j.progpolymsci.2016.05.001.
[98] A.K. Geim, K.S. Novoselov, The rise of graphene, Nat. Mater. 6 (2007) 183–191.
[99] C. Lee, X. Wei, J.W. Kysar, J. Hone, Measurement of the Elastic Properties and Intrinsic Strength of Monolayer Graphene, Science. 321 (2008) 385–388. doi:10.1126/science.1157996.
[100] X. Du, I. Skachko, A. Barker, E.Y. Andrei, Approaching ballistic transport in suspended graphene, Nat. Nanotechnol. 3 (2008) 491–495. doi:10.1038/nnano.2008.199.
[101] K.S. Novoselov, Electric Field Effect in Atomically Thin Carbon Films, Nature. 428 (2004) 153.
[102] A.A. Balandin, S. Ghosh, W. Bao, I. Calizo, D. Teweldebrhan, F. Miao, C.N. Lau, Superior Thermal Conductivity of Single-Layer Graphene, Nano Lett. 8 (2008) 902–907. doi:10.1021/nl0731872.
[103] A.V. Sukhadolau, E.V. Ivakin, V.G. Ralchenko, A.V. Khomich, A.V. Vlasov, A.F. Popovich, Thermal conductivity of CVD diamond at elevated temperatures, Diam. Relat. Mater. 14 (2005) 589–593. doi:10.1016/j.diamond.2004.12.002.
[104] S. Park, R.S. Ruoff, Chemical methods for the production of graphenes, Nat. Nanotechnol. 4 (2009) 217–224. doi:10.1038/nnano.2009.58.
[105] Y. Zhu, S. Murali, W. Cai, X. Li, J.W. Suk, J.R. Potts, R.S. Ruoff, Graphene and graphene oxide: synthesis, properties, and applications, Adv. Mater. 22 (2010) 3906–3924.
[106] J.I. Paredes, S. Villar-Rodil, A. Martínez-Alonso, J.M.D. Tascón, Graphene Oxide Dispersions in Organic Solvents, Langmuir. 24 (2008) 10560–10564. doi:10.1021/la801744a.
[107] K.R. Paton, E. Varrla, C. Backes, R.J. Smith, U. Khan, A. O'Neill, C. Boland, M. Lotya, O.M. Istrate, P. King, T. Higgins, S. Barwich, P. May, P. Puczkarski, I. Ahmed, M. Moebius, H. Pettersson, E. Long, J. Coelho, S.E. O'Brien, E.K. McGuire, B.M. Sanchez, G.S. Duesberg, N. McEvoy, T.J.

Pennycook, C. Downing, A. Crossley, V. Nicolosi, J.N. Coleman, Scalable production of large quantities of defect-free few-layer graphene by shear exfoliation in liquids, Nat. Mater. advance online publication (2014). doi:10.1038/nmat3944.
[108] J.R. Potts, D.R. Dreyer, C.W. Bielawski, R.S. Ruoff, Graphene-based polymer nanocomposites, Polymer. 52 (2011) 5–25. doi:10.1016/j.polymer.2010.11.042.
[109] P. Steurer, R. Wissert, R. Thomann, R. Mülhaupt, Functionalized Graphenes and Thermoplastic Nanocomposites Based upon Expanded Graphite Oxide, Macromol. Rapid Commun. 30 (2009) 316–327. doi:10.1002/marc.200800754.
[110] S. Stankovich, D.A. Dikin, R.D. Piner, K.A. Kohlhaas, A. Kleinhammes, Y. Jia, Y. Wu, S.T. Nguyen, R.S. Ruoff, Synthesis of graphene-based nanosheets via chemical reduction of exfoliated graphite oxide, Carbon. 45 (2007) 1558–1565. doi:10.1016/j.carbon.2007.02.034.
[111] D.D.L. Chung, Review Graphite, J. Mater. Sci. 37 (2002) 1475–1489. doi:10.1023/A:1014915307738.
[112] B.Z. Jang, A. Zhamu, Processing of nanographene platelets (NGPs) and NGP nanocomposites: a review, J. Mater. Sci. 43 (2008) 5092–5101. doi:10.1007/s10853-008-2755-2.
[113] R. Sengupta, M. Bhattacharya, S. Bandyopadhyay, A.K. Bhowmick, A review on the mechanical and electrical properties of graphite and modified graphite reinforced polymer composites, Prog. Polym. Sci. 36 (2011) 638–670. doi:10.1016/j.progpolymsci.2010.11.003.
[114] H. Kim, A.A. Abdala, C.W. Macosko, Graphene/Polymer Nanocomposites, Macromolecules. 43 (2010) 6515–6530. doi:10.1021/ma100572e.
[115] T. Kuilla, S. Bhadra, D. Yao, N.H. Kim, S. Bose, J.H. Lee, Recent advances in graphene based polymer composites, Prog. Polym. Sci. 35 (2010) 1350–1375. doi:10.1016/j.progpolymsci.2010.07.005.
[116] R. Verdejo, M.M. Bernal, L.J. Romasanta, M.A. Lopez-Manchado, Graphene filled polymer nanocomposites, J. Mater. Chem. 21 (2011) 3301–3310. doi:10.1039/C0JM02708A.
[117] B. Li, W.-H. Zhong, Review on polymer/graphite nanoplatelet nanocomposites, J. Mater. Sci. 46 (2011) 5595–5614. doi:10.1007/s10853-011-5572-y.
[118] A. Kumar, D.K. Chouhan, P.S. Alegaonkar, T.U. Patro, Graphene-like nanocarbon: An effective nanofiller for improving the mechanical and thermal properties of polymer at low weight fractions, Compos. Sci. Technol. 127 (2016) 79–87. doi:10.1016/j.compscitech.2016.02.028.
[119] J. Kim, J. Kim, S. Song, S. Zhang, J. Cha, K. Kim, H. Yoon, Y. Jung, K.-W. Paik, S. Jeon, Strength dependence of epoxy composites on the average filler size of non-oxidized graphene flake, Carbon. 113 (2017) 379–386. doi:10.1016/j.carbon.2016.11.023.
[120] C. Vallés, A.M. Abdelkader, R.J. Young, I.A. Kinloch, The effect of flake diameter on the reinforcement of few-layer graphene–PMMA composites, Compos. Sci. Technol. 111 (2015) 17–22. doi:10.1016/j.compscitech.2015.01.005.
[121] S. Chatterjee, F. Nafezarefi, N.H. Tai, L. Schlagenhauf, F.A. Nüesch, B.T.T. Chu, Size and synergy effects of nanofiller hybrids including graphene nanoplatelets and carbon nanotubes in mechanical properties of epoxy composites, Carbon. 50 (2012) 5380–5386. doi:10.1016/j.carbon.2012.07.021.
[122] L.-C. Tang, Y.-J. Wan, D. Yan, Y.-B. Pei, L. Zhao, Y.-B. Li, L.-B. Wu, J.-X. Jiang, G.-Q. Lai, The effect of graphene dispersion on the mechanical properties of graphene/epoxy composites, Carbon. 60 (2013) 16–27. doi:10.1016/j.carbon.2013.03.050.
[123] S. Chatterjee, F.A. Nüesch, B.T.T. Chu, Comparing carbon nanotubes and graphene nanoplatelets as reinforcements in polyamide 12 composites, Nanotechnology. 22 (2011) 275714. doi:10.1088/0957-4484/22/27/275714.
[124] L. Yue, G. Pircheraghi, S.A. Monemian, I. Manas-Zloczower, Epoxy composites with carbon nanotubes and graphene nanoplatelets – Dispersion and synergy effects, Carbon. 78 (2014) 268–278. doi:10.1016/j.carbon.2014.07.003.
[125] S.-Y. Yang, W.-N. Lin, Y.-L. Huang, H.-W. Tien, J.-Y. Wang, C.-C.M. Ma, S.-M. Li, Y.-S. Wang, Synergetic effects of graphene platelets and carbon nanotubes on the mechanical and thermal properties of epoxy composites, Carbon. 49 (2011) 793–803. doi:10.1016/j.carbon.2010.10.014.
[126] M.A. Rafiee, J. Rafiee, Z. Wang, H. Song, Z.-Z. Yu, N. Koratkar, Enhanced Mechanical Properties of Nanocomposites at Low Graphene Content, ACS Nano. 3 (2009) 3884–3890. doi:10.1021/nn9010472.
[127] M.A. Rafiee, W. Lu, A.V. Thomas, A. Zandiatashbar, J. Rafiee, J.M. Tour, N.A. Koratkar, Graphene Nanoribbon Composites, ACS Nano. 4 (2010) 7415–7420. doi:10.1021/nn102529n.

[128] S. Chandrasekaran, N. Sato, F. Tölle, R. Mülhaupt, B. Fiedler, K. Schulte, Fracture toughness and failure mechanism of graphene based epoxy composites, Compos. Sci. Technol. 97 (2014) 90–99. doi:10.1016/j.compscitech.2014.03.014.
[129] Q. Meng, S. Araby, J. Ma, 3 - Toughening mechanisms in epoxy/graphene platelets composites, in: Q.Q. Ye (Ed.), Toughening Mech. Compos. Mater., Woodhead Publishing, 2015: pp. 73–112.
[130] M.M. Shokrieh, S.M. Ghoreishi, M. Esmkhani, Z. Zhao, Effects of graphene nanoplatelets and graphene nanosheets on fracture toughness of epoxy nanocomposites, Fatigue Fract. Eng. Mater. Struct. 37 (2014) 1116–1123. doi:10.1111/ffe.12191.
[131] X. Wang, J. Jin, M. Song, An investigation of the mechanism of graphene toughening epoxy, Carbon. 65 (2013) 324–333. doi:10.1016/j.carbon.2013.08.032.
[132] I. Zaman, T.T. Phan, H.-C. Kuan, Q. Meng, L.T. Bao La, L. Luong, O. Youssf, J. Ma, Epoxy/graphene platelets nanocomposites with two levels of interface strength, Polymer. 52 (2011) 1603–1611. doi:10.1016/j.polymer.2011.02.003.
[133] M. Yoonessi, J.R. Gaier, Highly Conductive Multifunctional Graphene Polycarbonate Nanocomposites, ACS Nano. 4 (2010) 7211–7220. doi:10.1021/nn1019626.
[134] P. Song, Z. Cao, Y. Cai, L. Zhao, Z. Fang, S. Fu, Fabrication of exfoliated graphene-based polypropylene nanocomposites with enhanced mechanical and thermal properties, Polymer. 52 (2011) 4001–4010. doi:10.1016/j.polymer.2011.06.045.
[135] M. Yoonessi, Y. Shi, D.A. Scheiman, M. Lebron-Colon, D.M. Tigelaar, R.A. Weiss, M.A. Meador, Graphene Polyimide Nanocomposites; Thermal, Mechanical, and High-Temperature Shape Memory Effects, ACS Nano. 6 (2012) 7644–7655. doi:10.1021/nn302871y.
[136] S. Chandrasekaran, C. Seidel, K. Schulte, Preparation and characterization of graphite nano-platelet (GNP)/epoxy nano-composite: Mechanical, electrical and thermal properties, Eur. Polym. J. 49 (2013) 3878–3888. doi:10.1016/j.eurpolymj.2013.10.008.
[137] S.G. Prolongo, A. Jimenez-Suarez, R. Moriche, A. Ureña, In situ processing of epoxy composites reinforced with graphene nanoplatelets, Compos. Sci. Technol. 86 (2013) 185–191. doi:10.1016/j.compscitech.2013.06.020.
[138] T. Ramanathan, S. Stankovich, D.A. Dikin, H. Liu, H. Shen, S.T. Nguyen, L.C. Brinson, Graphitic nanofillers in PMMA nanocomposites—An investigation of particle size and dispersion and their influence on nanocomposite properties, J. Polym. Sci. Part B Polym. Phys. 45 (2007) 2097–2112. doi:10.1002/polb.21187.
[139] H.J. Salavagione, G. Martínez, M.A. Gómez, Synthesis of poly(vinyl alcohol)/reduced graphite oxide nanocomposites with improved thermal and electrical properties, J. Mater. Chem. 19 (2009) 5027. doi:10.1039/b904232f.
[140] M.A. Milani, D. González, R. Quijada, N.R.S. Basso, M.L. Cerrada, D.S. Azambuja, G.B. Galland, Polypropylene/graphene nanosheet nanocomposites by in situ polymerization: Synthesis, characterization and fundamental properties, Compos. Sci. Technol. 84 (2013) 1–7. doi:10.1016/j.compscitech.2013.05.001.
[141] S. Araby, I. Zaman, Q. Meng, N. Kawashima, A. Michelmore, H.-C. Kuan, P. Majewski, J. Ma, L. Zhang, Melt compounding with graphene to develop functional, high-performance elastomers, Nanotechnology. 24 (2013) 165601. doi:10.1088/0957-4484/24/16/165601.
[142] K. Kalaitzidou, H. Fukushima, P. Askeland, L.T. Drzal, The nucleating effect of exfoliated graphite nanoplatelets and their influence on the crystal structure and electrical conductivity of polypropylene nanocomposites, J. Mater. Sci. 43 (2008) 2895–2907. doi:10.1007/s10853-007-1876-3.
[143] M.A. Raza, A. Westwood, A. Brown, N. Hondow, C. Stirling, Characterisation of graphite nanoplatelets and the physical properties of graphite nanoplatelet/silicone composites for thermal interface applications, Carbon. 49 (2011) 4269–4279. doi:10.1016/j.carbon.2011.06.002.
[144] C.-C. Teng, C.-C.M. Ma, C.-H. Lu, S.-Y. Yang, S.-H. Lee, M.-C. Hsiao, M.-Y. Yen, K.-C. Chiou, T.-M. Lee, Thermal conductivity and structure of non-covalent functionalized graphene/epoxy composites, Carbon. 49 (2011) 5107–5116. doi:10.1016/j.carbon.2011.06.095.
[145] A. Yu, P. Ramesh, M.E. Itkis, E. Bekyarova, R.C. Haddon, Graphite Nanoplatelet−Epoxy Composite Thermal Interface Materials, J. Phys. Chem. C. 111 (2007) 7565–7569. doi:10.1021/jp071761s.
[146] X.C. Tong, Advanced Materials for Thermal Management of Electronic Packaging, Springer New York, New York, NY, 2011. http://link.springer.com/10.1007/978-1-4419-7759-5 (accessed December 4, 2015).

[147] W. Cui, F. Du, J. Zhao, W. Zhang, Y. Yang, X. Xie, Y.-W. Mai, Improving thermal conductivity while retaining high electrical resistivity of epoxy composites by incorporating silica-coated multi-walled carbon nanotubes, Carbon. 49 (2011) 495–500. doi:10.1016/j.carbon.2010.09.047.
[148] G. Kickelbick, Introduction to Hybrid Materials, in: G. Kickelbick (Ed.), Hybrid Mater., Wiley-VCH Verlag GmbH & Co. KGaA, 2006: pp. 1–48. doi:10.1002/9783527610495.ch1.
[149] M. Nič, J. Jirát, B. Košata, A. Jenkins, A. McNaught, eds., hybrid material, in: IUPAC Compend. Chem. Terminol., 2.1.0, IUPAC, Research Triagle Park, NC, 2009. doi:10.1351/goldbook.GT07553.
[150] M.F. Ashby, Y.J.M. Bréchet, Designing hybrid materials, Acta Mater. 51 (2003) 5801–5821. doi:10.1016/S1359-6454(03)00441-5.
[151] A.M. Díez-Pascual, M. Naffakh, C. Marco, M.A. Gómez-Fatou, G.J. Ellis, Multiscale fiber-reinforced thermoplastic composites incorporating carbon nanotubes: A review, Curr. Opin. Solid State Mater. Sci. 18 (2014) 62–80. doi:10.1016/j.cossms.2013.06.003.
[152] J.S. Fenner, I.M. Daniel, Hybrid nanoreinforced carbon/epoxy composites for enhanced damage tolerance and fatigue life, Compos. Part Appl. Sci. Manuf. 65 (2014) 47–56. doi:10.1016/j.compositesa.2014.05.023.
[153] J. Qiu, C. Zhang, B. Wang, R. Liang, Carbon nanotube integrated multifunctional multiscale composites, Nanotechnology. 18 (2007) 275708. doi:10.1088/0957-4484/18/27/275708.
[154] J. Zhu, A. Imam, R. Crane, K. Lozano, V. Khabashesku, E. Barrera, Processing a glass fiber reinforced vinyl ester composite with nanotube enhancement of interlaminar shear strength, Compos. Sci. Technol. 67 (2007) 1509–1517. doi:10.1016/j.compscitech.2006.07.018.
[155] H.S. Kim, H.T. Hahn, Graphite Nanoplatelets Interlayered Carbon/Epoxy Composites, AIAA J. 47 (2009) 2779–2784. doi:10.2514/1.39522.
[156] S.U. Khan, J.-K. Kim, Improved interlaminar shear properties of multiscale carbon fiber composites with bucky paper interleaves made from carbon nanofibers, Carbon. 50 (2012) 5265–5277. doi:10.1016/j.carbon.2012.07.011.
[157] S.-B. Lee, O. Choi, W. Lee, J.-W. Yi, B.-S. Kim, J.-H. Byun, M.-K. Yoon, H. Fong, E.T. Thostenson, T.-W. Chou, Processing and characterization of multi-scale hybrid composites reinforced with nanoscale carbon reinforcements and carbon fibers, Compos. Part Appl. Sci. Manuf. 42 (2011) 337–344. doi:10.1016/j.compositesa.2010.10.016.
[158] J.K. Park, I.-H. Do, P. Askeland, L.T. Drzal, Electrodeposition of exfoliated graphite nanoplatelets onto carbon fibers and properties of their epoxy composites, Compos. Sci. Technol. 68 (2008) 1734–1741. doi:10.1016/j.compscitech.2008.02.002.
[159] P.D. Bradford, A.E. Bogdanovich, Electrical Conductivity Study of Carbon Nanotube Yarns, 3-D Hybrid Braids and their Composites, J. Compos. Mater. 42 (2008) 1533–1545. doi:10.1177/0021998308092206.
[160] Q. Chen, L. Zhang, A. Rahman, Z. Zhou, X.-F. Wu, H. Fong, Hybrid multi-scale epoxy composite made of conventional carbon fiber fabrics with interlaminar regions containing electrospun carbon nanofiber mats, Compos. Part Appl. Sci. Manuf. 42 (2011) 2036–2042. doi:10.1016/j.compositesa.2011.09.010.
[161] E.J. Garcia, B.L. Wardle, A. John Hart, Joining prepreg composite interfaces with aligned carbon nanotubes, Compos. Part Appl. Sci. Manuf. 39 (2008) 1065–1070. doi:10.1016/j.compositesa.2008.03.011.
[162] M. Arai, Y. Noro, K. Sugimoto, M. Endo, Mode I and mode II interlaminar fracture toughness of CFRP laminates toughened by carbon nanofiber interlayer, Compos. Sci. Technol. 68 (2008) 516–525. doi:10.1016/j.compscitech.2007.06.007.
[163] B.G. Falzon, S.C. Hawkins, C.P. Huynh, R. Radjef, C. Brown, An investigation of Mode I and Mode II fracture toughness enhancement using aligned carbon nanotubes forests at the crack interface, Compos. Struct. 106 (2013) 65–73. doi:10.1016/j.compstruct.2013.05.051.
[164] E. Bekyarova, E.T. Thostenson, A. Yu, H. Kim, J. Gao, J. Tang, H.T. Hahn, T.-W. Chou, M.E. Itkis, R.C. Haddon, Multiscale Carbon Nanotube−Carbon Fiber Reinforcement for Advanced Epoxy Composites, Langmuir. 23 (2007) 3970–3974. doi:10.1021/la062743p.
[165] N. Rattanasom, T. Saowapark, C. Deeprasertkul, Reinforcement of natural rubber with silica/carbon black hybrid filler, Polym. Test. 26 (2007) 369–377. doi:10.1016/j.polymertesting.2006.12.003.

[166] J. Ayippadath Gopi, S.K. Patel, A.K. Chandra, D.K. Tripathy, SBR-clay-carbon black hybrid nanocomposites for tire tread application, J. Polym. Res. 18 (2011) 1625–1634. doi:10.1007/s10965-011-9567-9.
[167] B.T. Marouf, Y.-W. Mai, R. Bagheri, R.A. Pearson, Toughening of Epoxy Nanocomposites: Nano and Hybrid Effects, Polym. Rev. 56 (2016) 70–112. doi:10.1080/15583724.2015.1086368.
[168] G.-W. Lee, M. Park, J. Kim, J.I. Lee, H.G. Yoon, Enhanced thermal conductivity of polymer composites filled with hybrid filler, Compos. Part Appl. Sci. Manuf. 37 (2006) 727–734. doi:10.1016/j.compositesa.2005.07.006.
[169] K. Yang, M. Gu, Enhanced thermal conductivity of epoxy nanocomposites filled with hybrid filler system of triethylenetetramine-functionalized multi-walled carbon nanotube/silane-modified nano-sized silicon carbide, Compos. Part Appl. Sci. Manuf. 41 (2010) 215–221. doi:10.1016/j.compositesa.2009.10.019.
[170] T. Zhou, X. Wang, X. Liu, D. Xiong, Improved thermal conductivity of epoxy composites using a hybrid multi-walled carbon nanotube/micro-SiC filler, Carbon. 48 (2010) 1171–1176. doi:10.1016/j.carbon.2009.11.040.
[171] J. Li, P.-S. Wong, J.-K. Kim, Hybrid nanocomposites containing carbon nanotubes and graphite nanoplatelets, Mater. Sci. Eng. A. 483–484 (2008) 660–663. doi:10.1016/j.msea.2006.08.145.
[172] A. Yu, P. Ramesh, X. Sun, E. Bekyarova, M.E. Itkis, R.C. Haddon, Enhanced Thermal Conductivity in a Hybrid Graphite Nanoplatelet - Carbon Nanotube Filler for Epoxy Composites, Adv. Mater. 20 (2008) 4740–4744. doi:10.1002/adma.200800401.
[173] H. Im, J. Kim, Thermal conductivity of a graphene oxide–carbon nanotube hybrid/epoxy composite, Carbon. 50 (2012) 5429–5440. doi:10.1016/j.carbon.2012.07.029.
[174] M. Safdari, M.S. Al-Haik, Synergistic electrical and thermal transport properties of hybrid polymeric nanocomposites based on carbon nanotubes and graphite nanoplatelets, Carbon. 64 (2013) 111–121. doi:10.1016/j.carbon.2013.07.042.
[175] M. Verma, S.S. Chauhan, S.K. Dhawan, V. Choudhary, Graphene nanoplatelets/carbon nanotubes/polyurethane composites as efficient shield against electromagnetic polluting radiations, Compos. Part B Eng. 120 (2017) 118–127. doi:10.1016/j.compositesb.2017.03.068.
[176] T. Wei, L. Song, C. Zheng, K. Wang, J. Yan, B. Shao, Z.-J. Fan, The synergy of a three filler combination in the conductivity of epoxy composites, Mater. Lett. 64 (2010) 2376–2379. doi:10.1016/j.matlet.2010.07.061.
[177] Y. Yang, Y. Hao, J. Yuan, L. Niu, F. Xia, In situ preparation of caterpillar-like polyaniline/carbon nanotube hybrids with core shell structure for high performance supercapacitors, Carbon. 78 (2014) 279–287. doi:10.1016/j.carbon.2014.07.004.
[178] A. Zotti, A. Borriello, S. Zuppolini, V. Antonucci, M. Giordano, A.D. Pomogailo, V.A. Lesnichaya, N.D. Golubeva, A.N. Bychkov, G.I. Dzhardimalieva, M. Zarrelli, Fabrication and characterization of metal-core carbon-shell nanoparticles filling an aeronautical composite matrix, Eur. Polym. J. 71 (2015) 140–151. doi:10.1016/j.eurpolymj.2015.07.052.
[179] Y. Hou, Y. Cheng, T. Hobson, J. Liu, Design and Synthesis of Hierarchical MnO2 Nanospheres/Carbon Nanotubes/Conducting Polymer Ternary Composite for High Performance Electrochemical Electrodes, Nano Lett. 10 (2010) 2727–2733. doi:10.1021/nl101723g.
[180] Y. Yang, S. Qiu, W. Cui, Q. Zhao, X. Cheng, R.K.Y. Li, X. Xie, Y.-W. Mai, A facile method to fabricate silica-coated carbon nanotubes and silica nanotubes from carbon nanotubes templates, J. Mater. Sci. 44 (2009) 4539–4545. doi:10.1007/s10853-009-3687-1.
[181] R. Sun, H. Yao, H.-B. Zhang, Y. Li, Y.-W. Mai, Z.-Z. Yu, Decoration of defect-free graphene nanoplatelets with alumina for thermally conductive and electrically insulating epoxy composites, Compos. Sci. Technol. 137 (2016) 16–23. doi:10.1016/j.compscitech.2016.10.017.
[182] M. Kumar, Y. Ando, Chemical vapor deposition of carbon nanotubes: a review on growth mechanism and mass production, J. Nanosci. Nanotechnol. 10 (2010) 3739–3758.
[183] V. Jourdain, C. Bichara, Current understanding of the growth of carbon nanotubes in catalytic chemical vapour deposition, Carbon. 58 (2013) 2–39. doi:10.1016/j.carbon.2013.02.046.
[184] R. Guzmán de Villoria, A.J. Hart, B.L. Wardle, Continuous High-Yield Production of Vertically Aligned Carbon Nanotubes on 2D and 3D Substrates, ACS Nano. 5 (2011) 4850–4857. doi:10.1021/nn2008645.

[185] H.O. Pierson, 1 - Introduction and General Considerations, in: Handb. Chem. Vap. Depos. CVD Second Ed., William Andrew Publishing, Norwich, NY, 1999: pp. 25–35. doi:10.1016/B978-081551432-9.50004-8.
[186] S.S. Wicks, R.G. de Villoria, B.L. Wardle, Interlaminar and intralaminar reinforcement of composite laminates with aligned carbon nanotubes, Compos. Sci. Technol. 70 (2010) 20–28. doi:10.1016/j.compscitech.2009.09.001.
[187] M.-Q. Zhao, Q. Zhang, X.-L. Jia, J.-Q. Huang, Y.-H. Zhang, F. Wei, Hierarchical Composites of Single/Double-Walled Carbon Nanotubes Interlinked Flakes from Direct Carbon Deposition on Layered Double Hydroxides, Adv. Funct. Mater. 20 (2010) 677–685. doi:10.1002/adfm.200901522.
[188] D. He, M. Bozlar, M. Genestoux, J. Bai, Diameter- and length-dependent self-organizations of multi-walled carbon nanotubes on spherical alumina microparticles, Carbon. 48 (2010) 1159–1170. doi:10.1016/j.carbon.2009.11.039.
[189] W.B. Downs, R.T.K. Baker, Novel carbon fiber-carbon filament structures, Carbon. 29 (1991) 1173–1179.
[190] K.H. Hung, W.S. Kuo, T.H. Ko, S.S. Tzeng, C.F. Yan, Processing and tensile characterization of composites composed of carbon nanotube-grown carbon fibers, Compos. Part Appl. Sci. Manuf. 40 (2009) 1299–1304. doi:10.1016/j.compositesa.2009.06.002.
[191] J. Dong, C. Jia, M. Wang, X. Fang, H. Wei, H. Xie, T. Zhang, J. He, Z. Jiang, Y. Huang, Improved mechanical properties of carbon fiber-reinforced epoxy composites by growing carbon black on carbon fiber surface, Compos. Sci. Technol. 149 (2017) 75–80. doi:10.1016/j.compscitech.2017.06.002.
[192] A. Cao, V.P. Veedu, X. Li, Z. Yao, M.N. Ghasemi-Nejhad, P.M. Ajayan, Multifunctional brushes made from carbon nanotubes, Nat. Mater. 4 (2005) 540–545. doi:10.1038/nmat1415.
[193] V.P. Veedu, A. Cao, X. Li, K. Ma, C. Soldano, S. Kar, P.M. Ajayan, M.N. Ghasemi-Nejhad, Multifunctional composites using reinforced laminae with carbon-nanotube forests, Nat. Mater. 5 (2006) 457–462. doi:10.1038/nmat1650.
[194] E.J. Garcia, B.L. Wardle, A. John Hart, N. Yamamoto, Fabrication and multifunctional properties of a hybrid laminate with aligned carbon nanotubes grown In Situ, Compos. Sci. Technol. 68 (2008) 2034–2041. doi:10.1016/j.compscitech.2008.02.028.
[195] N. Yamamoto, A. John Hart, E.J. Garcia, S.S. Wicks, H.M. Duong, A.H. Slocum, B.L. Wardle, High-yield growth and morphology control of aligned carbon nanotubes on ceramic fibers for multifunctional enhancement of structural composites, Carbon. 47 (2009) 551–560. doi:10.1016/j.carbon.2008.10.030.
[196] L.J. Ci, Z.G. Zhao, J.B. Bai, Direct growth of carbon nanotubes on the surface of ceramic fibers, Carbon. 43 (2005) 883–886. doi:10.1016/j.carbon.2004.11.010.
[197] H. Qian, A. Bismarck, E.S. Greenhalgh, M.S.P. Shaffer, Synthesis and characterisation of carbon nanotubes grown on silica fibres by injection CVD, Carbon. 48 (2010) 277–286. doi:10.1016/j.carbon.2009.09.029.
[198] N. Yamamoto, R. Guzman de Villoria, B.L. Wardle, Electrical and thermal property enhancement of fiber-reinforced polymer laminate composites through controlled implementation of multi-walled carbon nanotubes, Compos. Sci. Technol. 72 (2012) 2009–2015. doi:10.1016/j.compscitech.2012.09.006.
[199] R.G. de Villoria, N. Yamamoto, A. Miravete, B.L. Wardle, Multi-physics damage sensing in nano-engineered structural composites, Nanotechnology. 22 (2011) 185502. doi:10.1088/0957-4484/22/18/185502.
[200] S. Rahmanian, A.R. Suraya, R. Zahari, E.S. Zainudin, Synthesis of vertically aligned carbon nanotubes on carbon fiber, Appl. Surf. Sci. 271 (2013) 424–428. doi:10.1016/j.apsusc.2013.01.207.
[201] J. Zhao, L. Liu, Q. Guo, J. Shi, G. Zhai, J. Song, Z. Liu, Growth of carbon nanotubes on the surface of carbon fibers, Carbon. 46 (2008) 380–383. doi:10.1016/j.carbon.2007.11.021.
[202] M.A. Shazed, A.R. Suraya, S. Rahmanian, M.A. Mohd Salleh, Effect of fibre coating and geometry on the tensile properties of hybrid carbon nanotube coated carbon fibre reinforced composite, Mater. Des. 1980-2015. 54 (2014) 660–669. doi:10.1016/j.matdes.2013.08.063.
[203] Z.-G. Zhao, L.-J. Ci, H.-M. Cheng, J.-B. Bai, The growth of multi-walled carbon nanotubes with different morphologies on carbon fibers, Carbon. 43 (2005) 663–665. doi:10.1016/j.carbon.2004.10.013.

[204] T.R. Pozegic, I. Hamerton, J.V. Anguita, W. Tang, P. Ballocchi, P. Jenkins, S.R.P. Silva, Low temperature growth of carbon nanotubes on carbon fibre to create a highly networked fuzzy fibre reinforced composite with superior electrical conductivity, Carbon. 74 (2014) 319–328. doi:10.1016/j.carbon.2014.03.038.
[205] V.G. de Resende, E.F. Antunes, A. de Oliveira Lobo, D.A.L. Oliveira, V.J. Trava-Airoldi, E.J. Corat, Growth of carbon nanotube forests on carbon fibers with an amorphous silicon interface, Carbon. 48 (2010) 3655–3658. doi:10.1016/j.carbon.2010.06.006.
[206] N. De Greef, L. Zhang, A. Magrez, L. Forró, J.-P. Locquet, I. Verpoest, J.W. Seo, Direct growth of carbon nanotubes on carbon fibers: Effect of the CVD parameters on the degradation of mechanical properties of carbon fibers, Diam. Relat. Mater. 51 (2015) 39–48. doi:10.1016/j.diamond.2014.11.002.
[207] K. Hernadi, A. Fonseca, J.B. Nagy, D. Bernaerts, A.A. Lucas, Fe-catalyzed carbon nanotube formation, Carbon. 34 (1996) 1249–1257. doi:10.1016/0008-6223(96)00074-7.
[208] E. Couteau, K. Hernadi, J.W. Seo, L. Thiên-Nga, C. Mikó, R. Gaál, L. Forró, CVD synthesis of high-purity multiwalled carbon nanotubes using CaCO3 catalyst support for large-scale production, Chem. Phys. Lett. 378 (2003) 9–17. doi:10.1016/S0009-2614(03)01218-1.
[209] R. Philippe, B. Caussat, A. Falqui, Y. Kihn, P. Kalck, S. Bordère, D. Plee, P. Gaillard, D. Bernard, P. Serp, An original growth mode of MWCNTs on alumina supported iron catalysts, J. Catal. 263 (2009) 345–358. doi:10.1016/j.jcat.2009.02.027.
[210] J.H. Hafner, M.J. Bronikowski, B.R. Azamian, P. Nikolaev, A.G. Rinzler, D.T. Colbert, K.A. Smith, R.E. Smalley, Catalytic growth of single-wall carbon nanotubes from metal particles, Chem. Phys. Lett. 296 (1998) 195–202. doi:10.1016/S0009-2614(98)01024-0.
[211] J. Kong, A.M. Cassell, H. Dai, Chemical vapor deposition of methane for single-walled carbon nanotubes, Chem. Phys. Lett. 292 (1998) 567–574. doi:10.1016/S0009-2614(98)00745-3.
[212] K. Dasgupta, R. Venugopalan, D. Sathiyamoorthy, The production of high purity carbon nanotubes with high yield using cobalt formate catalyst on carbon black, Mater. Lett. 61 (2007) 4496–4499. doi:10.1016/j.matlet.2007.02.042.
[213] D. Gournis, M.A. Karakassides, T. Bakas, N. Boukos, D. Petridis, Catalytic synthesis of carbon nanotubes on clay minerals, Carbon. 40 (2002) 2641–2646. doi:10.1016/S0008-6223(02)00165-3.
[214] A. Bakandritsos, A. Simopoulos, D. Petridis, Carbon Nanotube Growth on a Swellable Clay Matrix, Chem. Mater. 17 (2005) 3468–3474. doi:10.1021/cm0482131.
[215] W.-D. Zhang, I.Y. Phang, T.X. Liu, Growth of Carbon Nanotubes on Clay: Unique Nanostructured Filler for High-Performance Polymer Nanocomposites, Adv. Mater. 18 (2006) 73–77. doi:10.1002/adma.200501217.
[216] M.K.S. Li, P. Gao, P.-L. Yue, X. Hu, Synthesis of exfoliated CNT–metal–clay nanocomposite by chemical vapor deposition, Sep. Purif. Technol. 67 (2009) 238–243. doi:10.1016/j.seppur.2009.03.038.
[217] E. Esmizadeh, A.A. Yousefi, G. Naderi, C. Milone, Drastic increase in catalyst productivity of nanoclay-supported CVD-grown carbon nanotubes by organo-modification, Appl. Clay Sci. 118 (2015) 248–257. doi:10.1016/j.clay.2015.06.022.
[218] L. Madaleno, R. Pyrz, L.R. Jensen, J.J. Pinto, A.B. Lopes, V. Dolomanova, J. Schjødt-Thomsen, J.C.M. Rauhe, Synthesis and characterization of montmorillonite-carbon nanotubes hybrid fillers for nanocomposites, Polym. Polym. Compos. 20 (2012) 693.
[219] M. Lu, K.T. Lau, J.Q. Qi, D.D. Zhao, Z. Wang, H.L. Li, Novel nanocomposite of carbon nanotube–nanoclay by direct growth of nanotubes on nanoclay surface, J. Mater. Sci. 40 (2005) 3545–3548.
[220] Q. Zhang, M. Zhao, Y. Liu, A. Cao, W. Qian, Y. Lu, F. Wei, Energy-Absorbing Hybrid Composites Based on Alternate Carbon-Nanotube and Inorganic Layers, Adv. Mater. 21 (2009) 2876–2880. doi:10.1002/adma.200900123.
[221] L. Madaleno, R. Pyrz, L.R. Jensen, J.J.C. Pinto, A.B. Lopes, V. Dolomanova, J. Schjødt-Thomsen, J.C.M. Rauhe, Synthesis of clay–carbon nanotube hybrids: Growth of carbon nanotubes in different types of iron modified montmorillonite, Compos. Sci. Technol. 72 (2012) 377–381. doi:10.1016/j.compscitech.2011.11.027.
[222] W. Li, J. Yuan, Y. Lin, S. Yao, Z. Ren, H. Wang, M. Wang, J. Bai, The controlled formation of hybrid structures of multi-walled carbon nanotubes on SiC plate-like particles and their synergetic effect as a filler in poly(vinylidene fluoride) based composites, Carbon. 51 (2013) 355–364. doi:10.1016/j.carbon.2012.08.064.

[223] W. Li, J. Yuan, A. Dichiara, Y. Lin, J. Bai, The use of vertically aligned carbon nanotubes grown on SiC for in situ sensing of elastic and plastic deformation in electrically percolative epoxy composites, Carbon. 50 (2012) 4298–4301. doi:10.1016/j.carbon.2012.05.011.
[224] A. Dichiara, J. Bai, The growth of carbon nanotube multilayers on ceramic μ-particles by catalytic chemical vapour deposition, Diam. Relat. Mater. 29 (2012) 52–58. doi:10.1016/j.diamond.2012.07.010.
[225] A.B. Dichiara, J. Yuan, S. Yao, A. Sylvestre, L. Zimmer, J. Bai, Effective synergistic effect of Al2O3 and SiC microparticles on the growth of carbon nanotubes and their application in high dielectric permittivity polymer composites, J. Mater. Chem. A. 2 (2014) 7980. doi:10.1039/c4ta00369a.
[226] Z. Fan, J. Yan, L. Zhi, Q. Zhang, T. Wei, J. Feng, M. Zhang, W. Qian, F. Wei, A Three-Dimensional Carbon Nanotube/Graphene Sandwich and Its Application as Electrode in Supercapacitors, Adv. Mater. 22 (2010) 3723–3728. doi:10.1002/adma.201001029.
[227] A. Dichiara, J.-K. Yuan, S.-H. Yao, A. Sylvestre, J. Bai, Chemical Vapor Deposition Synthesis of Carbon Nanotube-Graphene Nanosheet Hybrids and Their Application in Polymer Composites, J. Nanosci. Nanotechnol. 12 (2012) 6935–6940. doi:10.1166/jnn.2012.6573.
[228] C. Zhang, W.W. Tjiu, T. Liu, W.Y. Lui, I.Y. Phang, W.-D. Zhang, Dramatically Enhanced Mechanical Performance of Nylon-6 Magnetic Composites with Nanostructured Hybrid One-Dimensional Carbon Nanotube–Two-Dimensional Clay Nanoplatelet Heterostructures, J. Phys. Chem. B. 115 (2011) 3392–3399. doi:10.1021/jp112284k.
[229] L. Madaleno, R. Pyrz, A. Crosky, L.R. Jensen, J.C.M. Rauhe, V. Dolomanova, A.M.M.V. de Barros Timmons, J.J. Cruz Pinto, J. Norman, Processing and characterization of polyurethane nanocomposite foam reinforced with montmorillonite–carbon nanotube hybrids, Compos. Part Appl. Sci. Manuf. 44 (2013) 1–7. doi:10.1016/j.compositesa.2012.08.015.
[230] M. Lu, K. Lau, W.-Y. Tam, K. Liao, Enhancement of Vicker's hardness of nanoclay-supported nanotube reinforced novel polymer composites, Carbon. 44 (2006) 383–386. doi:10.1016/j.carbon.2005.09.007.
[231] G. Gorrasi, S. D'Ambrosio, G. Patimo, R. Pantani, Hybrid clay-carbon nanotube/PET composites: Preparation, processing, and analysis of physical properties, J. Appl. Polym. Sci. 131 (2014) 40441. doi:10.1002/app.40441.
[232] Y.-Q. Zhao, K.-T. Lau, Z. Wang, Z.-C. Wang, H.-Y. Cheung, Z. Yang, H.-L. Li, Fabrication and properties of clay-supported carbon nanotube/poly (vinyl alcohol) nanocomposites, Polym. Compos. 30 (2009) 702–707. doi:10.1002/pc.20698.
[233] G. Gorrasi, C. Milone, E. Piperopoulos, M. Lanza, A. Sorrentino, Hybrid clay mineral-carbon nanotube-PLA nanocomposite films. Preparation and photodegradation effect on their mechanical, thermal and electrical properties, Appl. Clay Sci. 71 (2013) 49–54. doi:10.1016/j.clay.2012.11.004.
[234] T.Y. Zhou, G.C.P. Tsui, J.Z. Liang, S.Y. Zou, C.Y. Tang, V. Mišković-Stanković, Thermal properties and thermal stability of PP/MWCNT composites, Compos. Part B Eng. 90 (2016) 107–114. doi:10.1016/j.compositesb.2015.12.013.
[235] C.-C. Chu, K.L. White, P. Liu, X. Zhang, H.-J. Sue, Electrical conductivity and thermal stability of polypropylene containing well-dispersed multi-walled carbon nanotubes disentangled with exfoliated nanoplatelets, Carbon. 50 (2012) 4711–4721. doi:10.1016/j.carbon.2012.05.063.
[236] J.-K. Yuan, W.-L. Li, S.-H. Yao, Y.-Q. Lin, A. Sylvestre, J. Bai, High dielectric permittivity and low percolation threshold in polymer composites based on SiC-carbon nanotubes micro/nano hybrid, Appl. Phys. Lett. 98 (2011) 032901. doi:10.1063/1.3544942.
[237] W. Li, A. Dichiara, J. Bai, Carbon nanotube–graphene nanoplatelet hybrids as high-performance multifunctional reinforcements in epoxy composites, Compos. Sci. Technol. 74 (2013) 221–227. doi:10.1016/j.compscitech.2012.11.015.
[238] P. Carballeira, F. Haupert, Toughening effects of titanium dioxide nanoparticles on TiO_2/epoxy resin nanocomposites, Polym. Compos. (2009) NA-NA. doi:10.1002/pc.20911.
[239] Y. Zhou, E. White, M. Hosur, S. Jeelani, Effect of particle size and weight fraction on the flexural strength and failure mode of TiO2 particles reinforced epoxy, Mater. Lett. 64 (2010) 806–809. doi:10.1016/j.matlet.2010.01.016.
[240] D. Pinto, L. Bernardo, A. Amaro, S. Lopes, Mechanical properties of epoxy nanocomposites using titanium dioxide as reinforcement – A review, Constr. Build. Mater. 95 (2015) 506–524. doi:10.1016/j.conbuildmat.2015.07.124.

[241] P. Supaphol, P. Thanomkiat, J. Junkasem, R. Dangtungee, Non-isothermal melt-crystallization and mechanical properties of titanium(IV) oxide nanoparticle-filled isotactic polypropylene, Polym. Test. 26 (2007) 20–37. doi:10.1016/j.polymertesting.2006.07.011.
[242] M. Forhad Mina, S. Seema, R. Matin, M. Jellur Rahaman, R. Bijoy Sarker, M. Abdul Gafur, M. Abu Hashan Bhuiyan, Improved performance of isotactic polypropylene/titanium dioxide composites: Effect of processing conditions and filler content, Polym. Degrad. Stab. 94 (2009) 183–188. doi:10.1016/j.polymdegradstab.2008.11.006.
[243] B. Wetzel, P. Rosso, F. Haupert, K. Friedrich, Epoxy nanocomposites – fracture and toughening mechanisms, Eng. Fract. Mech. 73 (2006) 2375–2398. doi:10.1016/j.engfracmech.2006.05.018.
[244] S. Zhao, L.S. Schadler, R. Duncan, H. Hillborg, T. Auletta, Mechanisms leading to improved mechanical performance in nanoscale alumina filled epoxy, Compos. Sci. Technol. 68 (2008) 2965–2975. doi:10.1016/j.compscitech.2008.01.009.
[245] H. Zhao, R.K.Y. Li, Crystallization, mechanical, and fracture behaviors of spherical alumina-filled polypropylene nanocomposites, J. Polym. Sci. Part B Polym. Phys. 43 (2005) 3652–3664. doi:10.1002/polb.20654.
[246] T.H. Hsieh, A.J. Kinloch, K. Masania, A.C. Taylor, S. Sprenger, The mechanisms and mechanics of the toughening of epoxy polymers modified with silica nanoparticles, Polymer. 51 (2010) 6284–6294. doi:10.1016/j.polymer.2010.10.048.
[247] Y.L. Liang, R.A. Pearson, Toughening mechanisms in epoxy–silica nanocomposites (ESNs), Polymer. 50 (2009) 4895–4905. doi:10.1016/j.polymer.2009.08.014.
[248] M.Z. Rong, M.Q. Zhang, Y.X. Zheng, H.M. Zeng, K. Friedrich, Improvement of tensile properties of nano-SiO2/PP composites in relation to percolation mechanism, Polymer. 42 (2001) 3301–3304. doi:10.1016/S0032-3861(00)00741-2.
[249] M.F. Omar, H.M. Akil, Z.A. Ahmad, Particle size – Dependent on the static and dynamic compression properties of polypropylene/silica composites, Mater. Des. 45 (2013) 539–547. doi:10.1016/j.matdes.2012.09.026.
[250] L. Li, H. Zou, L. Shao, G. Wang, J. Chen, Study on mechanical property of epoxy composite filled with nano-sized calcium carbonate particles, J. Mater. Sci. 40 (2005) 1297–1299.
[251] Q. Shi, L. Wang, H. Yu, S. Jiang, Z. Zhao, X. Dong, A Novel Epoxy Resin/CaCO3 Nanocomposite and its Mechanism of Toughness Improvement, Macromol. Mater. Eng. 291 (2006) 53–58. doi:10.1002/mame.200500223.
[252] W.C.. Zuiderduin, C. Westzaan, J. Huétink, R.. Gaymans, Toughening of polypropylene with calcium carbonate particles, Polymer. 44 (2003) 261–275. doi:10.1016/S0032-3861(02)00769-3.
[253] Z. Bartczak, A.S. Argon, R.E. Cohen, M. Weinberg, Toughness mechanism in semi-crystalline polymer blends: II. High-density polyethylene toughened with calcium carbonate filler particles, Polymer. 40 (1999) 2347–2365. doi:10.1016/S0032-3861(98)00444-3.
[254] B.B. Johnsen, A.J. Kinloch, R.D. Mohammed, A.C. Taylor, S. Sprenger, Toughening mechanisms of nanoparticle-modified epoxy polymers, Polymer. 48 (2007) 530–541. doi:10.1016/j.polymer.2006.11.038.
[255] M. Quaresimin, K. Schulte, M. Zappalorto, S. Chandrasekaran, Toughening mechanisms in polymer nanocomposites: From experiments to modelling, Compos. Sci. Technol. 123 (2016) 187–204. doi:10.1016/j.compscitech.2015.11.027.
[256] B. Cotterell, J.Y.H. Chia, K. Hbaieb, Fracture mechanisms and fracture toughness in semicrystalline polymer nanocomposites, Eng. Fract. Mech. 74 (2007) 1054–1078. doi:10.1016/j.engfracmech.2006.12.023.
[257] D. Arencón, J.I. Velasco, Fracture Toughness of Polypropylene-Based Particulate Composites, Materials. 2 (2009) 2046–2094. doi:10.3390/ma2042046.
[258] B. Lauke, On the effect of particle size on fracture toughness of polymer composites, Compos. Sci. Technol. 68 (2008) 3365–3372. doi:10.1016/j.compscitech.2008.09.011.
[259] K.T. Faber, A.G. Evans, Crack deflection processes—I. Theory, Acta Metall. 31 (1983) 565–576. doi:10.1016/0001-6160(83)90046-9.
[260] F.F. Lange, The interaction of a crack front with a second-phase dispersion, Philos. Mag. 22 (1970) 0983–0992. doi:10.1080/14786437008221068.
[261] M. Salviato, M. Zappalorto, M. Quaresimin, Plastic shear bands and fracture toughness improvements of nanoparticle filled polymers: A multiscale analytical model, Compos. Part Appl. Sci. Manuf. 48 (2013) 144–152. doi:10.1016/j.compositesa.2013.01.006.

[262] M. Zappalorto, M. Salviato, M. Quaresimin, A multiscale model to describe nanocomposite fracture toughness enhancement by the plastic yielding of nanovoids, Compos. Sci. Technol. 72 (2012) 1683–1691. doi:10.1016/j.compscitech.2012.07.010.
[263] J.G. Williams, Particle toughening of polymers by plastic void growth, Compos. Sci. Technol. 70 (2010) 885–891. doi:10.1016/j.compscitech.2009.12.024.
[264] K. Friedrich, U.A. Karsch, Failure processes in particulate filled polypropylene, J. Mater. Sci. 16 (1981) 2167–2175. doi:10.1007/BF00542377.
[265] G. Wypych, 5 - PHYSICAL PROPERTIES OF FILLERS AND FILLED MATERIALS, in: Handb. Fill. Fourth Ed., ChemTec Publishing, 2016: pp. 303–371. doi:10.1016/B978-1-895198-91-1.50007-5.
[266] S. Singha, M.J. Thomas, Dielectric properties of epoxy nanocomposites, IEEE Trans. Dielectr. Electr. Insul. 15 (2008).
[267] A. Mohanty, V.K. Srivastava, Dielectric breakdown performance of alumina/epoxy resin nanocomposites under high voltage application, Mater. Des. 47 (2013) 711–716. doi:10.1016/j.matdes.2012.12.052.
[268] A. Agrawal, A. Satapathy, Thermal and dielectric behavior of epoxy composites filled with ceramic micro particulates, J. Compos. Mater. (2013). doi:10.1177/0021998313513205.
[269] S. Virtanen, H. Ranta, S. Ahonen, M. Karttunen, J. Pelto, K. Kannus, M. Pettersson, Structure and dielectric breakdown strength of nano calcium carbonate/polypropylene composites, J. Appl. Polym. Sci. 131 (2014) 39504. doi:10.1002/app.39504.
[270] A. Agrawal, A. Satapathy, Thermal and dielectric behaviour of polypropylene composites reinforced with ceramic fillers, J. Mater. Sci. Mater. Electron. 26 (2015) 103–112. doi:10.1007/s10854-014-2370-8.
[271] T. Ramu, H. Nagamani, Alumina and silica based epoxy nano-composites for electrical insulation, IEEE Trans. Dielectr. Electr. Insul. 21 (2014) 236–243. doi:10.1109/TDEI.2013.003555.
[272] T.M. Tritt, Thermal conductivity: theory, properties, and applications, Springer Science & Business Media, 2005.
[273] C.P. Wong, R.S. Bollampally, Thermal conductivity, elastic modulus, and coefficient of thermal expansion of polymer composites filled with ceramic particles for electronic packaging, J. Appl. Polym. Sci. 74 (1999) 3396–3403.
[274] N. Gupta, S.E. Zeltmann, V.C. Shunmugasamy, D. Pinisetty, Applications of Polymer Matrix Syntactic Foams, JOM. 66 (2014) 245–254. doi:10.1007/s11837-013-0796-8.
[275] K.C. Yung, B.L. Zhu, T.M. Yue, C.S. Xie, Preparation and properties of hollow glass microsphere-filled epoxy-matrix composites, Compos. Sci. Technol. 69 (2009) 260–264. doi:10.1016/j.compscitech.2008.10.014.
[276] B. Zhu, J. Ma, J. Wang, J. Wu, D. Peng, Thermal, dielectric and compressive properties of hollow glass microsphere filled epoxy-matrix composites, J. Reinf. Plast. Compos. 31 (2012) 1311–1326. doi:10.1177/0731684412452918.
[277] B.L. Zhu, H. Zheng, J. Wang, J. Ma, J. Wu, R. Wu, Tailoring of thermal and dielectric properties of LDPE-matrix composites by the volume fraction, density, and surface modification of hollow glass microsphere filler, Compos. Part B Eng. 58 (2014) 91–102. doi:10.1016/j.compositesb.2013.10.029.
[278] J.Z. Liang, F.H. Li, Measurement of thermal conductivity of hollow glass-bead-filled polypropylene composites, Polym. Test. 25 (2006) 527–531. doi:10.1016/j.polymertesting.2006.02.007.
[279] N. Gupta, R. Nagorny, Tensile properties of glass microballoon-epoxy resin syntactic foams, J. Appl. Polym. Sci. 102 (2006) 1254–1261. doi:10.1002/app.23548.
[280] N. Gupta, E. Woldesenbet, P. Mensah, Compression properties of syntactic foams: effect of cenosphere radius ratio and specimen aspect ratio, Compos. Part Appl. Sci. Manuf. 35 (2004) 103–111. doi:10.1016/j.compositesa.2003.08.001.
[281] C. Swetha, R. Kumar, Quasi-static uni-axial compression behaviour of hollow glass microspheres/epoxy based syntactic foams, Mater. Des. 32 (2011) 4152–4163. doi:10.1016/j.matdes.2011.04.058.
[282] R. Xiang, G.H. Luo, W.Z. Qian, Y. Wang, F. Wei, Q. Li, Large Area Growth of Aligned CNT Arrays on Spheres: Towards Large Scale and Continuous Production, Chem. Vap. Depos. 13 (2007) 533–536. doi:10.1002/cvde.200704249.

[283] Q. Zhang, J. Huang, F. Wei, G. Xu, Y. Wang, W. Qian, D. Wang, Large scale production of carbon nanotube arrays on the sphere surface from liquefied petroleum gas at low cost, Chin. Sci. Bull. 52 (2007) 2896–2902. doi:10.1007/s11434-007-0458-8.
[284] Q. Zhang, J.-Q. Huang, M.-Q. Zhao, W.-Z. Qian, Y. Wang, F. Wei, Radial growth of vertically aligned carbon nanotube arrays from ethylene on ceramic spheres, Carbon. 46 (2008) 1152–1158. doi:10.1016/j.carbon.2008.04.017.
[285] S. Huang, Growing carbon nanotubes on patterned submicron-size SiO2 spheres, Carbon. 41 (2003) 2347–2352. doi:10.1016/S0008-6223(03)00275-6.
[286] S. Agrawal, A. Kumar, M.J. Frederick, G. Ramanath, Hybrid Microstructures from Aligned Carbon Nanotubes and Silica Particles, Small. 1 (2005) 823–826. doi:10.1002/smll.200500023.
[287] R.N. Othman, I.A. Kinloch, A.N. Wilkinson, Synthesis and characterisation of silica–carbon nanotube hybrid microparticles and their effect on the electrical properties of poly(vinyl alcohol) composites, Carbon. 60 (2013) 461–470. doi:10.1016/j.carbon.2013.04.062.
[288] D. He, J. Bai, Acetylene-Enhanced Growth of Carbon Nanotubes on Ceramic Microparticles for Multi-Scale Hybrid Structures, Chem. Vap. Depos. 17 (2011) 98–106. doi:10.1002/cvde.201006878.
[289] D. He, H. Li, W. Li, P. Haghi-Ashtiani, P. Lejay, J. Bai, Growth of carbon nanotubes in six orthogonal directions on spherical alumina microparticles, Carbon. 49 (2011) 2273–2286.
[290] X.H. Nguyen, Y.B. Lee, C.H. Lee, D.-S. Lim, Synthesis of sea urchin-like particles of carbon nanotubes directly grown on stainless steel cores and their effect on the mechanical properties of polymer composites, Carbon. 48 (2010) 2910–2916. doi:10.1016/j.carbon.2010.04.027.
[291] Z.H. Han, B. Yang, S.H. Kim, M.R. Zachariah, Application of hybrid sphere/carbon nanotube particles in nanofluids, Nanotechnology. 18 (2007) 105701.
[292] L. Ci, J. Bai, Novel Micro/Nanoscale Hybrid Reinforcement: Multiwalled Carbon Nanotubes on SiC Particles, Adv. Mater. 16 (2004) 2021–2024. doi:10.1002/adma.200400379.
[293] V. Kosma, T. Tsoufis, T. Koliou, A. Kazantzis, K. Beltsios, J.T.M. De Hosson, D. Gournis, Fibrous hydroxyapatite–carbon nanotube composites by chemical vapor deposition: In situ fabrication, structural and morphological characterization, Mater. Sci. Eng. B. 178 (2013) 457–464. doi:10.1016/j.mseb.2012.11.026.
[294] C.N. He, F. Tian, A carbon nanotube–alumina network structure for fabricating epoxy composites, Scr. Mater. 61 (2009) 285–288. doi:10.1016/j.scriptamat.2009.04.003.
[295] M.H.A. Kudus, H.M. Akil, H. Mohamad, L.E. Loon, Effect of catalyst calcination temperature on the synthesis of MWCNT–alumina hybrid compound using methane decomposition method, J. Alloys Compd. 509 (2011) 2784–2788. doi:10.1016/j.jallcom.2010.11.099.
[296] B. Fan, J. Bai, Composites of hybrids BaTiO 3 /carbon nanotubes/polyvinylidene fluoride with high dielectric properties, J. Phys. Appl. Phys. 48 (2015) 455303. doi:10.1088/0022-3727/48/45/455303.
[297] W. Li, D. He, J. Bai, The influence of nano/micro hybrid structure on the mechanical and self-sensing properties of carbon nanotube-microparticle reinforced epoxy matrix composite, Compos. Part Appl. Sci. Manuf. 54 (2013) 28–36. doi:10.1016/j.compositesa.2013.07.002.
[298] M.R. Zakaria, H.M. Akil, M.H.A. Kudus, S.S.M. Saleh, Enhancement of tensile and thermal properties of epoxy nanocomposites through chemical hybridization of carbon nanotubes and alumina, Compos. Part Appl. Sci. Manuf. 66 (2014) 109–116. doi:10.1016/j.compositesa.2014.07.008.
[299] M.R. Zakaria, H. Md. Akil, M.H. Abdul Kudus, A.H. Kadarman, Improving flexural and dielectric properties of MWCNT/epoxy nanocomposites by introducing advanced hybrid filler system, Compos. Struct. 132 (2015) 50–64. doi:10.1016/j.compstruct.2015.05.020.
[300] M.R. Zakaria, H.M. Akil, M.H. Abdul Kudus, M.B.H. Othman, Compressive properties and thermal stability of hybrid carbon nanotube-alumina filled epoxy nanocomposites, Compos. Part B Eng. 91 (2016) 235–242. doi:10.1016/j.compositesb.2016.01.013.
[301] M. Bozlar, D. He, J. Bai, Y. Chalopin, N. Mingo, S. Volz, Carbon Nanotube Microarchitectures for Enhanced Thermal Conduction at Ultralow Mass Fraction in Polymer Composites, Adv. Mater. 22 (2010) 1654–1658. doi:10.1002/adma.200901955.
[302] Z. Wang, C. Xu, Y. Zhao, D. Zhao, Z. Wang, H. Li, K. Lau, Fabrication and mechanical properties of exfoliated clay–CNTs/epoxy nanocomposites, Mater. Sci. Eng. A. 490 (2008) 481–487. doi:10.1016/j.msea.2008.01.040.

[303] N.S.A.A. Bakhtiar, H.M. Akil, M.R. Zakaria, M.H.A. Kudus, M.B.H. Othman, New generation of hybrid filler for producing epoxy nanocomposites with improved mechanical properties, Mater. Des. 91 (2016) 46–52. doi:10.1016/j.matdes.2015.11.081.
[304] D. He, B. Fan, H. Zhao, M. Yang, H. Wang, J. Bai, W. Li, X. Zhou, J. Bai, Multifunctional polymer composites reinforced by carbon nanotubes–Alumina hybrids with urchin-like structure, Mater. Today Commun. 11 (2017) 94–102. doi:10.1016/j.mtcomm.2017.03.001.
[305] F. Tian, C.N. He, Processing and mechanical properties of carbon nanotube–alumina hybrid reinforced high density polyethylene composites, Mater. Res. Bull. 46 (2011) 1143–1147. doi:10.1016/j.materresbull.2011.03.013.

3 How do graphite nanoplates affect the fracture toughness of polypropylene composites?

3.1 Introduction

In the last decade, graphene-based nanostructures have been extensively studied as part of a novel generation of composite materials. Their outstanding mechanical properties and extraordinary surface area make these nanoscaled materials ideal as nanofillers. Although recent efforts have been made to scale-up the production of graphene [1] or modified graphene [2], only graphite nanoplates (GNPs), which consist of stacked graphene layers bound to each other by van der Waals forces, can currently be produced at the scales needed for use in composite materials and structural applications.

The addition of a small amount of nanofiller can lead to a significant improvement in mechanical properties. Stiffness and strength can be enhanced when nanofillers are homogeneously dispersed [3] and a strong interphase between nanofillers and polymer matrix exists [4,5]. Tremendous research effort have been invested to determine how the nanofiller affects the mechanical and fracture behaviour of a polymer [6–11]. The most effective way to toughen semi-crystalline polymers is the cavitation or nucleation of voids [12,13]. One approach to achieve this toughening effect is the addition of nanoparticles. However, if these nanoparticles have a strong interaction with the host matrix then the cavitation or debonding and consequent void nucleation could be hindered [14]. Such materials would have extrinsic rather than intrinsic toughening mechanisms, i.e., crack bridging [15], crack deflection [16], etc.

One of the main problems in analysing the effect of a nanofiller in a thermoplastic matrix is the difficulty in characterizing the fracture toughness. In the case of ductile polymers, fracture toughness is generally determined by the *J*-integral versus crack growth resistance (*J–R)* curve, in which the value of the *J*-integral is plotted against the crack extension. To measure the *J–R* curve, a multi-specimen

technique is commonly used [17]. A set of pre-cracked test specimens of the same size, geometry and material are tested until the crack grows to a certain length. As a single test is needed for each point of the *J*–*R* curve, a large number of tests and specimens are needed to obtain the whole curve. Additionally, in the case of polypropylene (PP), measurement of the crack extension is extremely difficult because of the presence of fine-scale fracture-surface features or microstructural inhomogeneities [18]. To overcome these drawbacks, Sharobeam and Landes proposed the S_{pb} parameter method [19–21], in which the crack length is estimated indirectly throughout the whole mechanical test; only one single pre-cracked specimen plus one notched specimen are used to measure the whole *J*–*R* curve. This low material consumption makes this method ideal for materials produced in small batches, such as nanocomposites.

In the work presented here, we analyse the toughening effect of graphite nanoplates in a polypropylene matrix made by a simple extrusion-compounding process, followed by an injection-moulding process. The S_{pb} parameter method is used to analyse the fracture toughness of the resulting PP composites. To identify the plastic deformation zone that appears ahead of the crack tip in the specimen during the fracture test, a full-field strain analysis is carried out by digital image correlation. The fracture mechanism is identified by scanning electron microscopic (SEM) analysis of the fracture surfaces.

3.2 Methods

3.2.1 Materials and preparation of nanocomposites

A commercial polypropylene homopolymer (Borealis HB601WG), with a density of 900 kg/m^3 and a melt flow index (230°C/2.16 kg) of 2.2 g/10 min, was used for the production of PP/GNP nanocomposites. Graphite nanoplates were purchased from Avanzare (Logroño, Spain) and used with no further treatment. The individual GNPs have a particle size of 2 × 5 µm and are less than 10 nm thick.

Compounding and injection molding

Polypropylene masterbatch with a content of 5 wt.% GNP was prepared using an industrial extrusion-compounding machine (Coperion ZSK 26, 26 mm diameter co-

rotating twin-screw). The polymer pellets and the GNPs were introduced through the extruder's main gravimetric feeder and side-feeder, respectively. The screw speed was 500 rpm and the temperature of mixture was increased from 170 °C in the feeding zone up to 190 °C at the nozzle. The compounding was extruded through a 2 mm diameter die at a constant output rate of 5 Kg/h, producing 10 kg of masterbatch. The extruded material was quenched immediately in a water bath at room temperature, dried, and cut into pellets.

Masterbatch pellets were dried at 80 °C for 4 h prior to processing. Composites of different GNP weight fractions were prepared by diluting the masterbatch with neat PP using an injection moulding machine (JSW 85 EL II) with a 35 mm diameter reciprocating screw, at a screw speed of 120 rpm. The temperature profile was increased from 225 °C at the barrel up to 255 °C at the nozzle. A specific steel mould was used at 30 °C to obtain normalized specimens for flexural tests, by following the specifications of the standard ISO 178, in the form of prismatic bars with dimensions of 125 ×13 × 5 mm^3.

3.2.2 Analysis of the particle size and dispersion of the graphite nanoplates

SEM analysis of the as received GNP was performed using an EVO MA15 Zeiss scanning electron microscope. The agglomerate size distribution was analysed with the help of the image processing software ImageJ. The lateral size and the thickness of a minimum of 200 GNP agglomerates were measured. For the analysis of the degree of dispersion, samples of the produced materials were cooled in liquid nitrogen and immediately broken at high speed by impacting with a Charpy pendulum. The cryo-fractured surfaces were analysed by using scanning electron microscopy (EVO MA15, Zeiss) after they had been sputter-coated with a thin layer of gold.

3.2.3 Differential scanning calorimetry and dynamic mechanical analysis

Differential scanning calorimetry (DSC) was performed on a DSC Q200 (TA Instruments), to obtain information about the effect of the nanofiller on the

crystallization behaviour of the PP matrix. During the measurements, the samples were heated from 20 to 220 °C at a rate of 10 °C/min, held at 220 °C for 0.5 min to eliminate any previous thermal history, and then cooled to 20 °C at a rate of 10 °C/min. Then, after being kept at 20 °C for 0.5 min, the samples were heated to 220 °C at a rate of 10 °C/min.

Dynamic mechanical analysis (DMA) were carried out by using specimens with dimensions of 17.5 × 13 × 5 mm in single cantilever mode. The tests were performed on a Q800 (TA Instruments) in a temperature range of –150 to 150 °C, at a frequency of 3 Hz, and a heating rate of 1.5 °C/min.

3.2.4 Mechanical characterization

Characterization of flexural properties was conducted under ambient conditions by using a Zwick Roell Z 10KN. At least ten specimens of each composition were measured. Tests were carried out following standard ISO 178 with a cross-head speed of 2 mm/min. Specimens were tested in a three-point bending configuration with 57 mm between supports.

The characterization of the fracture behaviour of PP nanocomposites was carried out by using a three-point bending test, at room temperature, using an Instron 3384 at a cross-head speed of 1 mm/min. Single-edge-notch bending (SENB) specimens, with dimensions of 62.5×13×5 mm^3, were tested with a span-to-width ratio of 4. To apply the S_{pb} parameter method two types of specimens were tested, reference and pre-cracked specimens. A schematic representation of the SENB specimens tested is shown in Figure 3.4a. In this work, one reference and three pre-cracked specimens were tested for each GNP concentration. All the specimens had blunt notches machined with a disk-cutting machine. In the case of the references specimens the blunt notch length, a_b, was 10.4 ± 0.1 mm. For the pre-cracked specimens the blunt notch length, a_b, was 3.3 ± 0.1 mm. Then, in the pre-cracked specimens, the notch was sharpened by tapping with a razor blade to extend the crack length with a sharp crack with a length, a_{sp}, of 1 mm. Thus, the pre-cracked specimens had total crack lengths, a_p, of 4.3 ± 0.2 mm, as was confirmed by examining every specimen with an optical microscope. A detailed explanation of the S_{pb} parameter method can be found in [19–22].

3.2.5 Fractographic analysis and digital image correlation

To perform a digital image correlation (DIC) study, one side of every SENB specimen was painted white and then lightly sprayed with black paint to obtain the random speckle pattern that is required for DIC analysis. Images were taken every 3 s during the test. The area of analysis (13×6.5 mm^2) was located immediately ahead the root of the blunt notch (Figure 3.4a). The acquired images were evaluated by using the Vic-2D 2009 Digital Image Correlation software (VicSNAP, Correlated Solutions Inc., Columbia, SC, USA).

After fracture tests, specimens were cooled in liquid nitrogen and immediately broken at high speed by impacting with a Charpy pendulum. This procedure ensured that brittle fracture surfaces were generated, to allow the easy identification of the ductile fracture surface generated during the fracture test. The surfaces of broken specimens were analysed by using scanning electron microscopy after they had been sputter-coated with a thin layer of gold.

3.3 Results and discussion

3.3.1 Agglomerate size distribution and dispersion of the graphite nanoplates

Morphology of the as-received GNPs was characterized by SEM (Figure 3.1a). It was observed that GNPs were in an agglomerated state. The circle-equivalent diameter was calculated from the area of these GNP agglomerates. In the inset of Figure 3.1a is shown the equivalent diameter and thickness distribution. It was found that the agglomerates have an average equivalent diameter of 21 μm and an average thickness of 11 μm.

The cryogenically fractured surfaces of neat PP and the nanocomposites with 0.5 and 5 wt.% of GNPs are presented in Figure 3.1b-d. In the surface of a neat PP sample, the presence of some particles composed of silicon and oxygen among other elements can be observed; these elements may have been used to enhance the processability or heat stability of the particles. Figure 3.1c reveals that in the material with 0.5 wt.% of GNPs, the agglomerates have not been dispersed into individual plates, however they are well distributed within the matrix. In the case

of the nanocomposite with 5 wt.% GNP (Figure 3.1d), the highest nanofiller content produced in this study, contains more and bigger GNP agglomerates (with a diameter of between ca. 20 and 50 μm) than those observed in samples with lower GNP amount, as expected [7,23,24].

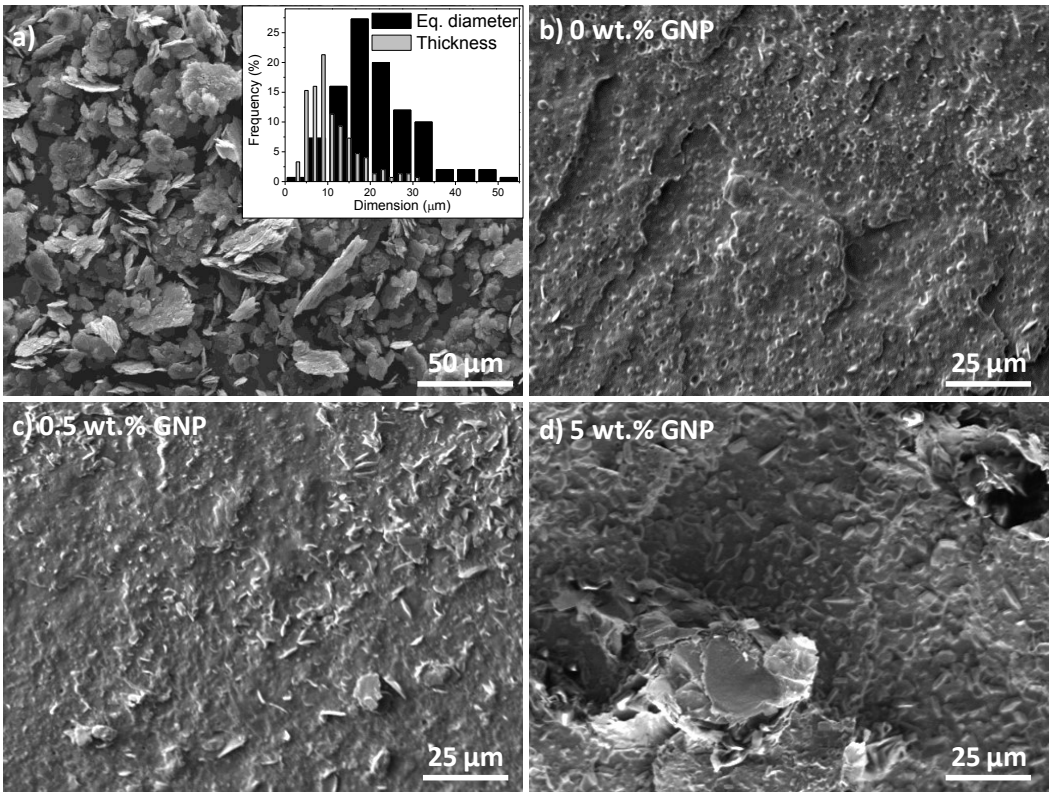

Figure 3.1 SEM images of a) the as-received GNP. The inset shows the equivalent diameter and thickness distribution of the GNP agglomerates. b) The cryogenically fractured surfaces of PP and nanocomposites with c) 0.5 and d) 5 wt.% of GNP are shown. In c) a good distribution of the GNPs can be seen, and small agglomerates are observable. However, in d) large GNP agglomerates can be observed.

This analysis of the dispersion degree seems to indicate that the processing requires other parameters to achieve a higher dispersion degree of the agglomerates (e.g., melt temperature, mixing time, screw rotational speed, screw profile and diameter) to promote their break up [25–29]. Another approach to achieve the dispersion of the agglomerates would be to maintain the processing parameters but combining with other techniques as three roll mill, as suggested by Pötschke et al [30] or adding extra steps (i.e., extrusion compounding), However, it has to be taken into account that re-agglomeration of the nanofiller can occur,

being thermally-driven and shear-induced during the re-melting of the material. This effect has been reported by Alig et al.[24] and Jamali et al.[31].

3.3.2 DSC and DMA measurements

The thermograms obtained from the DSC measurements are shown in Figure 3.2a. The melting and crystallization temperatures were taken as those corresponding to the maximum of the melting and crystallization peaks, respectively, of these thermograms. There is no change either in the crystallization (123.9 ± 0.3°C) or the melting (163.8 ± 0.6°C) temperature and peak profiles upon the addition of nanofiller. The degree of crystallinity (X_c) of the nanocomposites was calculated by following (Eq. 3.1) [32,33]:

$$X_C(\%) = \frac{\Delta H_s}{(1-\phi)\Delta H_0} \times 100 \qquad \text{Eq. 3.1}$$

where ΔH_s is the heat of fusion of the measured sample (obtained by integration of melting peaks [34]), ϕ is the weight fraction per unit of mass of the nanofiller, and ΔH_0 is the heat of fusion of 100 % crystalline PP, taken as 209 J/g [32,35].

The degree of crystallinity of the matrix remained unaffected by the addition of nanofiller, with a value of 26.6 ± 0.3 % for all the different weight fractions. These results agree with previously reported results and confirm that, although GNPs may act as a nucleating agents for PP crystallization [33], X_c does not change with the addition of the nanofiller. The results obtained by DSC may indicate that the GNP–PP interphase does not significantly affect the crystallization or melting process, thus the intrinsic properties of the PP matrix do not seem to be affected by the addition of GNPs.

Results obtained from the dynamic mechanical analysis are shown in Figure 3.2b. The three characteristic relaxations of polypropylene, α, β, and γ, have been observed for the loss tangent, tan δ [36]. The α relaxation peak is related to the motion within the crystalline phase of PP, particularly to the diffusion of defects in the crystals [36]. The β relaxation peak is associated with the glass transition of the amorphous fraction of PP. Finally, the γ relaxation peak varies little with the

crystallinity and has been attributed to local motions of the methyl groups within the amorphous phase of PP [36]. No significant changes are found in the relaxations described above for the different nanocomposites. For the nanocomposites with high GNP loads only, tan δ shows higher values, mainly after the γ peak. This rise in the tan δ could be associated with the mobility of the polymer chains in the surroundings of the GNP agglomerates, due to poor interaction between the nanofiller and the host matrix.

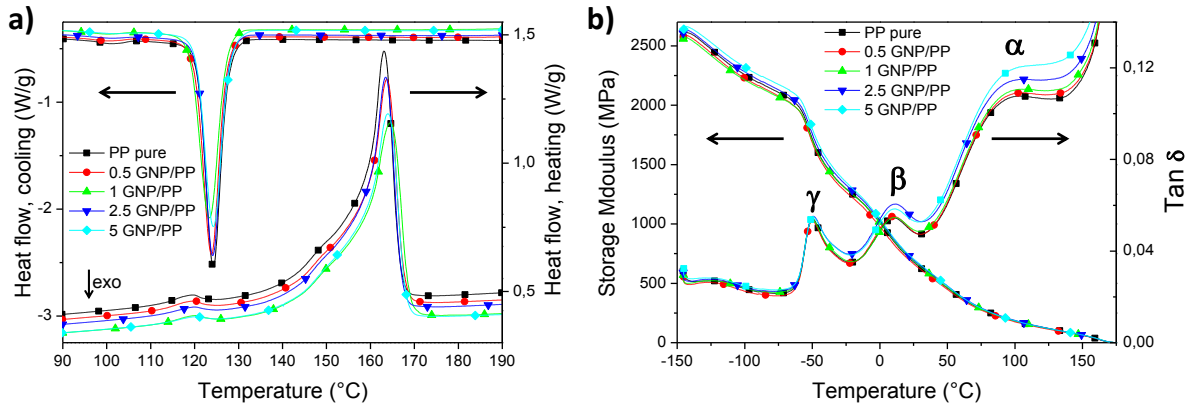

Figure 3.2 a) DSC thermograms showing heating and cooling curves of GNP/PP nanocomposites. b) Storage modulus and tan δ (at a frequency of 3Hz) of the GNP/PP nanocomposites as a function of temperature.

The amount of GNP present in the nanocomposite slightly affects the storage modulus at low temperatures. However, after the modulus drop due to the γ and β peaks, the storage modulus is quite similar in all nanocomposites. No significant modification of the polymeric matrix was detected due to the addition of GNP. Similar behaviour was also observed in other thermoplastic/clay composites [37]. In the case of a PP/GNP nanocomposite [32], a reduction in the storage modulus was reported. In both cases there was a slight variation of the crystallization and glass transition temperatures, which was explained in terms of a weak particle–matrix interface and nanofiller agglomeration.

3.3.3 Flexural and fracture toughness tests

Results obtained from three-point-bending tests (Figure 3.3a) show no significant effect on the flexural and fracture toughness upon the addition of the GNP to the PP matrix, which could be attributed to a low dispersion degree of the nanofiller and/or poor interfacial bonding and interaction between the polymeric matrix and

the nanofiller [4]. However, there was a slight decrease in the flexural strength and modulus, for GNP content up to 1 wt.%, being this GNP amount a transition point as for higher GNP amount, both properties increases.

The average value of the fracture toughness J_{IC} calculated from the three specimens tested for each GNP loading is presented in Figure 3.3b. The analysis of the fracture behaviour of the GNP/PP nanocomposites shows that increasing the amount of GNPs, up to a maximum of 2.5 wt.%, increases the energy required for the initiation of the crack growth. An improvement of 25 % is achieved for a loading of 1 wt.% of GNPs. However, a further increase in the proportion of GNPs leads to a significant decrease in this energy; the 5 wt.% GNP nanocomposite has a fracture toughness that is 20 % lower than that of neat PP. This decrease in mechanical properties for high volume fraction is expected and it is strongly related with the poor dispersion of the nanofiller in the matrix, as is widely reported in the literature [3,5].

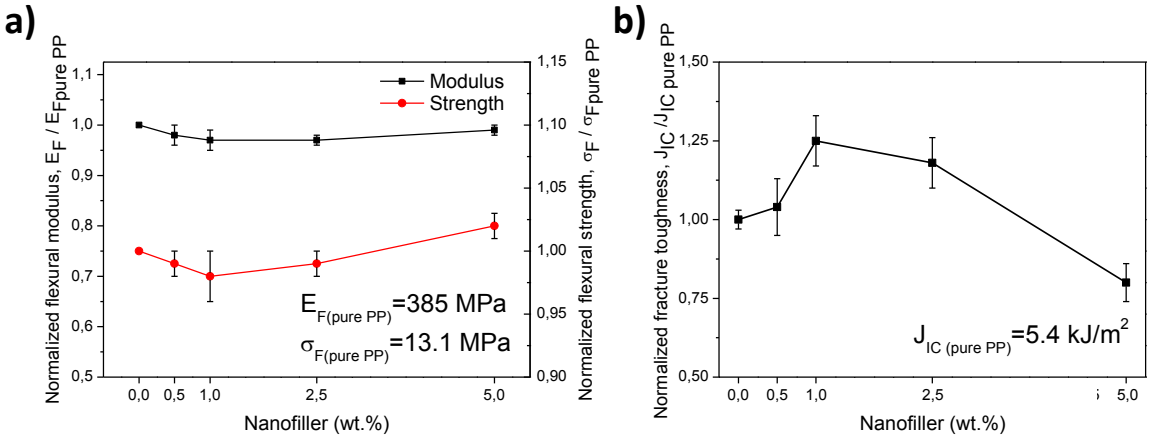

Figure 3.3 Normalized flexural modulus and strength as a function of the nanofiller content for the GNP/PP nanocomposites a). Crack-growth initiation energy, JIC, for the GNP/PP nanocomposites b). The fracture toughness increases for GNP loadings up to 2.5 wt.%, reaching its maximum for the nanocomposite with 1 wt.%. The fracture toughness of the material with the highest amount of GNPs has a value that is a 20 % lower than that of the neat PP.

3.3.4 DIC study and SEM analysis of the fracture surfaces

The strain in the principal direction, ε_1, was calculated by using digital image correlation images from the pictures taken during the fracture test. This is the direction in which the major principal stresses take place, and in this case, is

approximately equal to the longitudinal direction of the single edge-notched bent specimen. Comparison between the full-field strain measurements obtained for PP (Figure 3.4b) and the nanocomposites with 1 and 5 wt.% of GNPs (Figure 3.4c and d, respectively), at the moment of the fracture initiation, shows a change in size of the deformation zone ahead the crack tip. It must be taken into account that as the DIC images were obtained during the test, thus the strain provided by them has both an elastic and plastic component. However, the S_{pb} parameter method, for the identification of the crack growth initiation, is correctly applied when plastic behaviour is fully achieved [19,20], so that the plastic component can be assumed to be the predominant component of the deformation shown in Figure 3.4. Additionally, for this comparison it was assumed that the plastic zone has a cylindrical shape along the thickness of the single edge-notched bend specimen, although it is well known that the shape of this zone changes with the transition from plain stress (at the specimen surface) to plain strain conditions (in the central interior portion of the sample) [38]. For comparison purposes, we have analysed the size of a region with a fixed deformation (4.5% for all the samples).

In the case of neat PP, the size of the region with a deformation smaller or equal to 4.5% is 90 mm^3 (Figure 3.4b). The size of this region increases by 35%, up to 123 mm^3, in the nanocomposite with 1 wt.% of GNPs (Figure 3.4c). This increase in size may indicate that a large amount of plastic strain took place in the zone ahead of the crack tip. This result seems to be in agreement with those obtained from the flexural characterization; the nanocomposite with 1 wt.% of GNPs has the lowest value of strength and modulus out of neat PP and all our nanocomposites, which may suggest a lower plastic resistance [13]. In the case of the nanocomposite with 5 wt.% of GNPs (Figure 3.4d), the size of this region decreases by 12 % compared to the case of neat PP, with a size of approximately 80 mm^3.

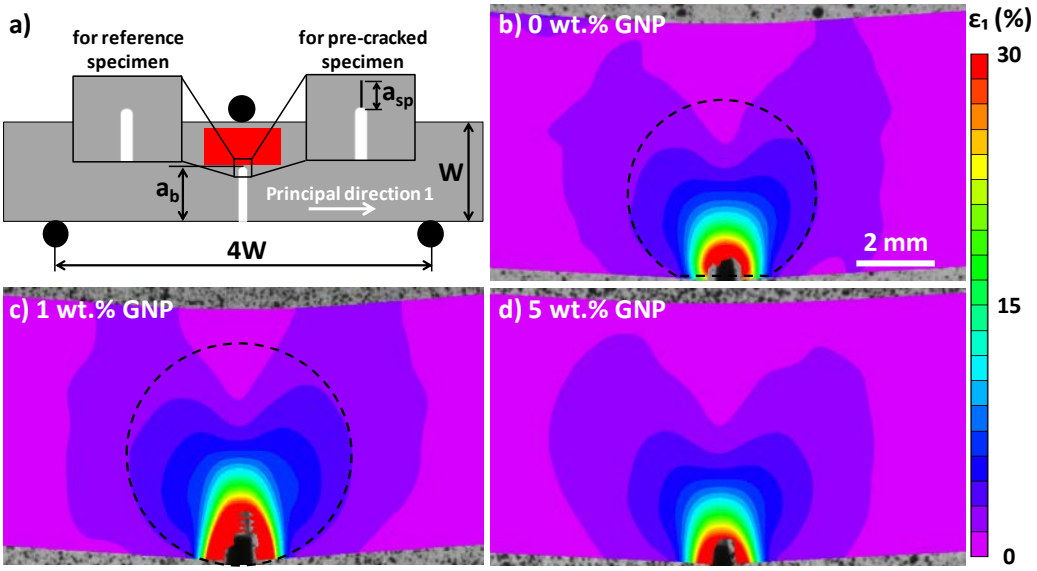

Figure 3.4 Schematic representation of the two types of single-edge-notch bending specimens tested for the application of the S_{pb} parameter method. The insets show the differences between the reference and the pre-cracked specimen. The reference specimen has a blunt notch with a length a_b=10.4 mm and the precracked specimen has a blunt notch with a length a_b=3.3 mm plus a sharp pre-crack with a length of a_{sp}=1 mm, giving a total crack length a_p=4.3 mm. The red rectangle is the area of interest (AOI) analyzed by digital image correlation. The principal direction is approximately equal to the longitudinal direction of the single edge-notched bend specimen. The strain field in the principal direction, ε_1, was obtained from the DIC study at the moment of fracture initiation during the fracture toughness tests for neat PP b), nanocomposite with 1 wt.% of GNP c); the material with the highest fracture toughness, and the 5 wt.% GNP nanocomposite d); the material with the lowest fracture toughness.

A detailed analysis of the fracture surfaces of neat PP and nanocomposites was performed by using scanning electron microscopy. At low magnification, all the materials tested appear to have the same fracture surface features. As an example, the fracture surface of neat PP and the nanocomposite with 0.5 wt.% GNP is shown in Figure 3.5a and b. The region of the surface ahead the initial pre-crack can be divided into three different zones. First, there is a zone characterized by stretched polymeric fibrils (zone 1 in Figure 3.5a and b). Immediately after this first zone, there is a region where voids in the polymer are clearly observable (zone 2 in Figure 3.5b and c). Finally, a third zone with a smooth surface is observed, which is representative of a brittle fracture (zone 3 in Figure 3.5c).

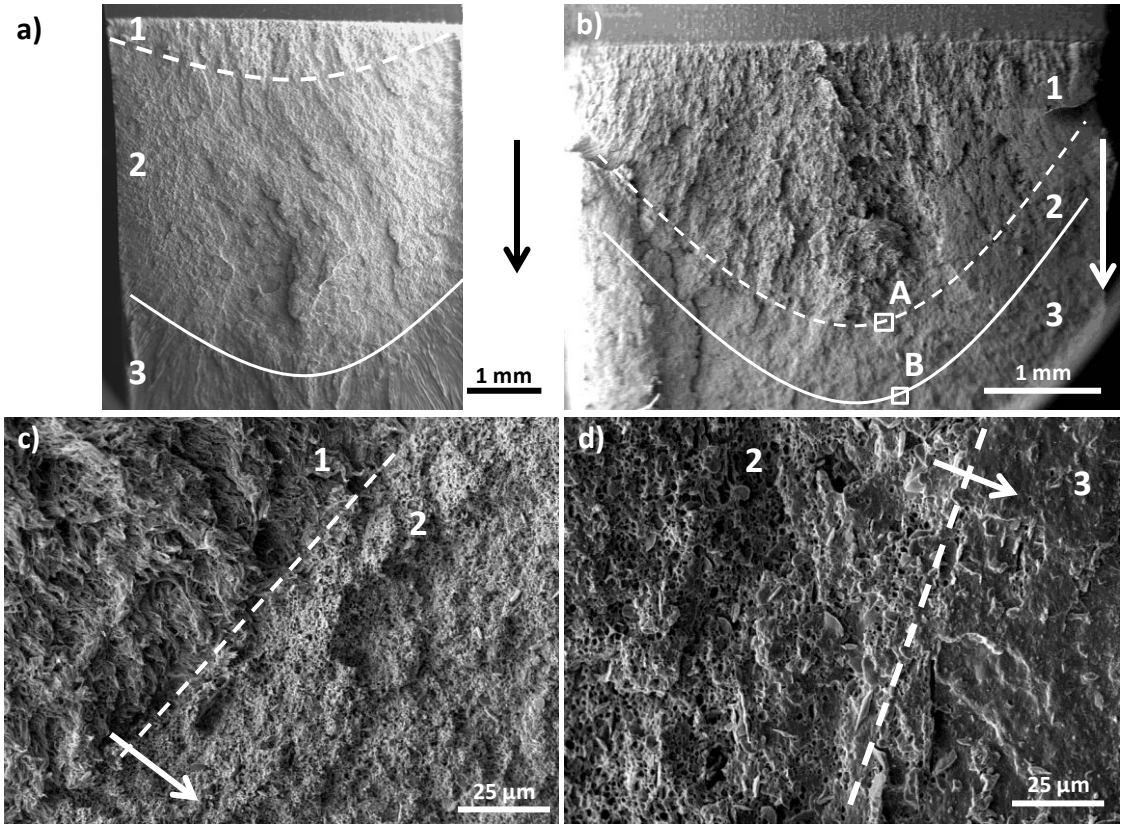

Figure 3.5 Fracture surface of neat PP a) and 0.5 wt.% GNP/PP nanocomposite (a–c). The white arrow indicates the crack-growth direction, the dashed line indicates the transition between the ductile tearing zone 1 and the plastic deformation zone ahead of the crack tip (zone 2). An area similar to that marked by the square A is shown in c). The second line indicates the transition between the plastic deformation zone (2) and the unaffected polymer (3). An area similar to that marked by the square B is shown in d).

The first two regions are characteristic of the fracture mechanism of PP known as crazing, which leads to the ductile tearing of the polymer by void nucleation and growth [12,38,39]. In neat PP, the voids that were nucleated at the intercrystalline regions of the polymer are the weakest points of the material [12,40]. The fracture surfaces of the neat PP and the nanocomposite with the highest fracture toughness, 1wt.% GNP, were compared (Figure 3.6a and b). By the addition of 1 wt.% GNP, the stretched fibrils generated during the fracture process are oriented in the crack-propagation direction; in addition to this it seems that there is a higher number of fibrils with a slightly longer length than is the case for neat PP. This result seems to indicate that these fibrils have been highly elongated up to failure, which leads to an improvement in fracture toughness due to the consumption of fracture energy [12,41]. The extensive plastic deformation suffered by the polymer in the region

ahead the crack tip can be noted from the DIC analysis, which shows a larger deformation area. As the DSC results do not show an increase in the degree of crystallinity, the apparently higher nucleation of voids and deformation of the polymer around them seems to be promoted by the addition of GNPs and the weak interface generated. In Figure 3.6c and d, it can be observed GNP agglomerates that have been debonded from the PP matrix.

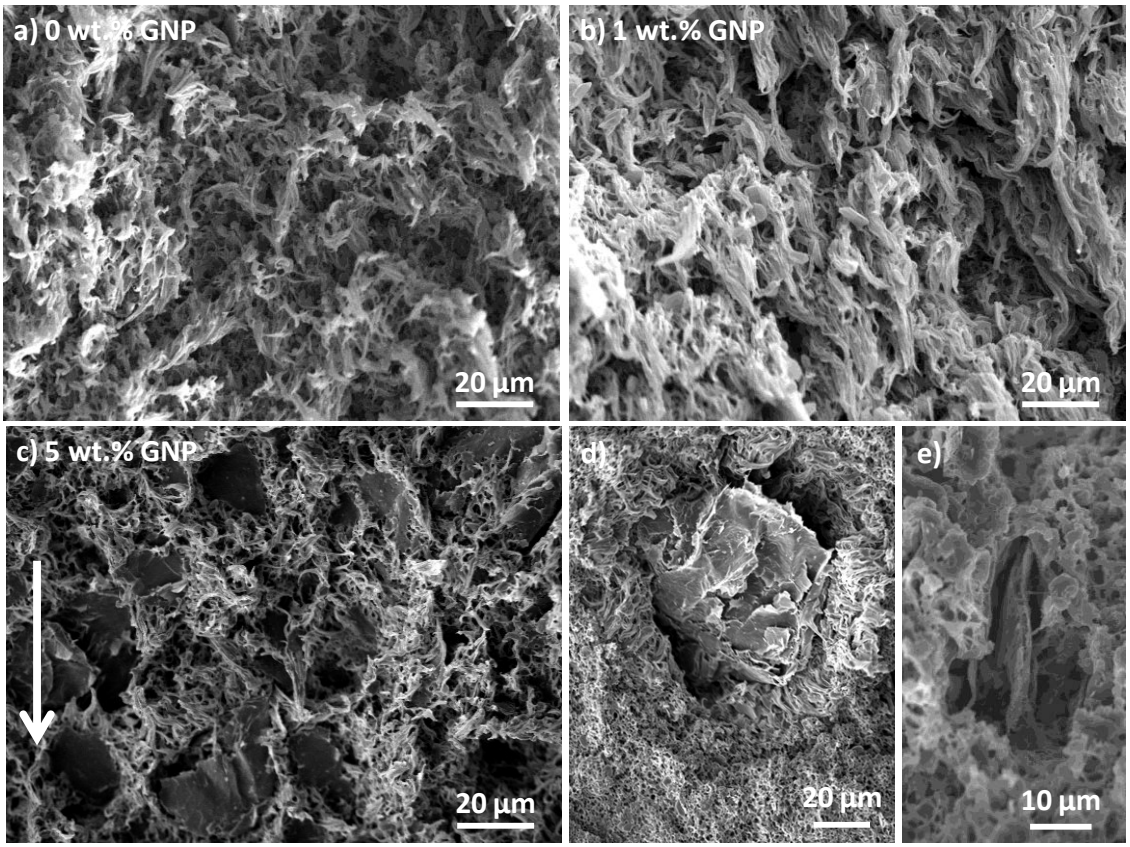

Figure 3.6 Ductile-tearing region (zone 1) in the fracture surface of the neat PP a), 1 wt.% GNP b) and 5wt.% GNP c) nanocomposites. The arrow indicates the crack-growth direction. In b) the extensive plastic deformation of the fibrils can be observed. Large GNP agglomerates can be seen in c). In c) and d) debonded agglomerates in the 1 wt.% nanocomposites are shown.

However, as the nanofiller content increases so does the number and/or size of agglomerates, as discussed earlier. This result can be seen in Figure 3.6c, where the fracture surface of the nanocomposite with 5 wt.% of GNP is shown. The surface is similar to that of the neat PP but contains GNP agglomerates, which seems to reduce the number of stretched polymeric fibrils; these are shorter and not oriented in the crack-growth direction (compared to the fibrils of the 1 wt.% GNP nanocomposite fracture surface), and thus do not provide evidence of extensive

plastic deformation. This result may indicate that as these bigger agglomerates are debonded, the stretched polymer around the agglomerate fails prior to experience extremely high elongation, because its deformability is restricted by the neighbouring agglomerates. The presence of large agglomerates within the polymeric matrix may be responsible for the reduction in deformability, represented by strain at break, of nanocomposites [10,42,43]. This result is in good agreement with the results obtained from the DIC analysis, which shows a reduction in the size of the plastic deformation zone for the nanocomposite with 5 wt.% GNPs. Thus, an extensive plastic deformation upon the addition of the optimal amount of GNPs, which is promoted by nucleation of voids, can be identified as the mechanism responsible for the improvement of the fracture toughness.

3.4 Conclusions

Graphite nanoplates were added to the PP matrix by following an industrial approach known as the masterbatch technique. The addition of GNPs does not affect the PP matrix, as all the nanocomposites have practically the same glass transition, melting, and crystallization temperatures as well as degrees of crystallinity. The results obtained from the flexural tests show slight or no improvement in strength and modulus upon the addition of the nanofiller, which could be attributed to the weak interactions between filler and matrix and also the presence of GNP agglomerates and/or a poor dispersion of the filler.

To measure the fracture toughness, the load separation S_{pb} parameter method was successfully applied in nanocomposites for the first time. The fracture toughness, measured as J_{IC}, is improved by the addition of GNPs up to a value of 2.5 wt.%. The highest fracture toughness value was obtained for the 1 wt.% GNP/PP nanocomposite (25% improvement over the neat PP specimens), which is also the material with the largest plastic deformation zone. At a 5 wt.% content of GNPs, the fracture toughness sharply decreases, which is attributed to the presence of large GNP agglomerates that constrain the plastic flow of polymeric fibrils [42].

The presence of the GNPs promotes an intrinsic toughening mechanism that is mainly dependent on the matrix nature. The mechanical properties of the GNPs

seem to be irrelevant; only their weight fraction, dispersion, and/or size are important in this mechanism. The addition of GNPs, up to an optimal amount, promotes the void nucleation, which then triggers the plastic deformation. However, for higher loadings, the GNPs are poorly dispersed, which has a detrimental effect on the fracture behaviour and makes the crack propagation easier.

3.5 Acknowledgments

This work was supported by the European Commission under the 7th Framework Program, NFRP project (PICIG12-GA-2012-33924). R.G.V. gratefully acknowledges the Spanish Ministry of Science and Innovation for financial funding through the Ramon y Cajal Fellowship. J.P.F-B is grateful for support from the "Marie Curie" Amarout Programme. The authors would like to thank A. Salazar (URJC) for discussions about fracture test methodology.

3.6 References

[1] Paton KR, Varrla E, Backes C, Smith RJ, Khan U, O'Neill A, et al. Scalable production of large quantities of defect-free few-layer graphene by shear exfoliation in liquids. Nat Mater 2014;advance online publication. doi:10.1038/nmat3944.

[2] Park S, Ruoff RS. Chemical methods for the production of graphenes. Nat Nanotechnol 2009;4:217–24. doi:10.1038/nnano.2009.58.

[3] Guzmán de Villoria R, Miravete A. Mechanical model to evaluate the effect of the dispersion in nanocomposites. Acta Mater 2007;55:3025–31. doi:10.1016/j.actamat.2007.01.007.

[4] Hussain F, Hojjati M, Okamoto M, Gorga RE. Review article: polymer-matrix nanocomposites, processing, manufacturing, and application: an overview. J Compos Mater 2006;40:1511–75.

[5] Thostenson ET, Li C, Chou T-W. Nanocomposites in context. Compos Sci Technol 2005;65:491–516. doi:10.1016/j.compscitech.2004.11.003.

[6] Chatterjee S, Nüesch FA, Chu BTT. Comparing carbon nanotubes and graphene nanoplatelets as reinforcements in polyamide 12 composites. Nanotechnology 2011;22:275714. doi:10.1088/0957-4484/22/27/275714.

[7] Vallés C, Kinloch IA, Young RJ, Wilson NR, Rourke JP. Graphene oxide and base-washed graphene oxide as reinforcements in PMMA nanocomposites. Compos Sci Technol 2013;88:158–64. doi:10.1016/j.compscitech.2013.08.030.

[8] Chandrasekaran S, Sato N, Tölle F, Mülhaupt R, Fiedler B, Schulte K. Fracture toughness and failure mechanism of graphene based epoxy composites. Compos Sci Technol n.d. doi:10.1016/j.compscitech.2014.03.014.

[9] Raza MA, Westwood A, Brown A, Hondow N, Stirling C. Characterisation of graphite nanoplatelets and the physical properties of graphite nanoplatelet/silicone composites for thermal interface applications. Carbon 2011;49:4269–79. doi:10.1016/j.carbon.2011.06.002.

[10] Duguay AJ, Nader JW, Kiziltas A, Gardner DJ, Dagher HJ. Exfoliated graphite nanoplatelet-filled impact modified polypropylene nanocomposites: influence of

particle diameter, filler loading, and coupling agent on the mechanical properties. Appl Nanosci 2014;4:279–91. doi:10.1007/s13204-013-0204-2.
[11] Young RJ, Kinloch IA, Gong L, Novoselov KS. The mechanics of graphene nanocomposites: A review. Compos Sci Technol 2012;72:1459–76. doi:10.1016/j.compscitech.2012.05.005.
[12] Sugimoto M, Ishikawa M, Hatada K. Toughness of polypropylene. Polymer 1995;36:3675–82. doi:10.1016/0032-3861(95)93769-I.
[13] Argon AS, Cohen RE. Toughenability of polymers. Polymer 2003;44:6013–32. doi:10.1016/S0032-3861(03)00546-9.
[14] Bartczak Z, Argon AS, Cohen RE, Weinberg M. Toughness mechanism in semi-crystalline polymer blends: II. High-density polyethylene toughened with calcium carbonate filler particles. Polymer 1999;40:2347–65. doi:10.1016/S0032-3861(98)00444-3.
[15] Ganß M, Satapathy BK, Thunga M, Weidisch R, Pötschke P, Jehnichen D. Structural interpretations of deformation and fracture behavior of polypropylene/multi-walled carbon nanotube composites. Acta Mater 2008;56:2247–61. doi:10.1016/j.actamat.2008.01.010.
[16] Thio YS, Argon AS, Cohen RE, Weinberg M. Toughening of isotactic polypropylene with CaCO3 particles. Polymer 2002;43:3661–74. doi:10.1016/S0032-3861(02)00193-3.
[17] Landes JD, Begley JA. Test results from J-integral studies: an attempt to establish a JIC testing procedure. Fract Anal ASTM STP 1974;560:170–86.
[18] Hale GE, Ramsteiner F. J-Fracture toughness of polymers at slow speed. In: D.R. Moore AP and JGW, editor. Eur. Struct. Integr. Soc., vol. Volume 28, Elsevier; 2001, p. 123–57.
[19] Sharobeam MH, Landes JD. The load separation criterion and methodology in ductile fracture mechanics. Int J Fract 1991;47:81–104. doi:10.1007/BF00032571.
[20] Sharobeam MH, Landes JD. The load separation and η pl. Int J Fract 1993;59:213–26. doi:10.1007/BF00012362.
[21] Salazar A, Rodríguez J. The use of the load separation parameter Spb method to determine the J–R curves of polypropylenes. Polym Test 2008;27:977–84. doi:10.1016/j.polymertesting.2008.08.013.
[22] Baldi F, Agnelli S, Riccò T. On the determination of the point of fracture initiation by the load separation criterion in J-testing of ductile polymers. Polym Test 2013;32:1326–33. doi:10.1016/j.polymertesting.2013.08.007.
[23] Kalaitzidou K, Fukushima H, Drzal LT. A new compounding method for exfoliated graphite–polypropylene nanocomposites with enhanced flexural properties and lower percolation threshold. Compos Sci Technol 2007;67:2045–51. doi:10.1016/j.compscitech.2006.11.014.
[24] Alig I, Pötschke P, Lellinger D, Skipa T, Pegel S, Kasaliwal GR, et al. Establishment, morphology and properties of carbon nanotube networks in polymer melts. Polymer 2012;53:4–28. doi:10.1016/j.polymer.2011.10.063.
[25] Villmow T, Pegel S, Pötschke P, Wagenknecht U. Influence of injection molding parameters on the electrical resistivity of polycarbonate filled with multi-walled carbon nanotubes. Compos Sci Technol 2008;68:777–89. doi:10.1016/j.compscitech.2007.08.031.
[26] Villmow T, Pötschke P, Pegel S, Häussler L, Kretzschmar B. Influence of twin-screw extrusion conditions on the dispersion of multi-walled carbon nanotubes in a poly(lactic acid) matrix. Polymer 2008;49:3500–9. doi:10.1016/j.polymer.2008.06.010.
[27] Kim S, Do I, Drzal LT. Multifunctional xGnP/LLDPE Nanocomposites Prepared by Solution Compounding Using Various Screw Rotating Systems. Macromol Mater Eng 2009;294:196–205. doi:10.1002/mame.200800319.
[28] Tanahashi M. Development of Fabrication Methods of Filler/Polymer Nanocomposites: With Focus on Simple Melt-Compounding-Based Approach without Surface Modification of Nanofillers. Materials 2010;3:1593–619. doi:10.3390/ma3031593.
[29] Villmow T, Kretzschmar B, Pötschke P. Influence of screw configuration, residence time, and specific mechanical energy in twin-screw extrusion of polycaprolactone/multi-walled carbon nanotube composites. Compos Sci Technol 2010;70:2045–55. doi:10.1016/j.compscitech.2010.07.021.
[30] Pötschke P, Krause B, Buschhorn ST, Köpke U, Müller MT, Villmow T, et al. Improvement of carbon nanotube dispersion in thermoplastic composites using a three roll mill at

elevated temperatures. Compos Sci Technol 2013;74:78–84. doi:10.1016/j.compscitech.2012.10.010.
[31] Jamali S, Paiva MC, Covas JA. Dispersion and re-agglomeration phenomena during melt mixing of polypropylene with multi-wall carbon nanotubes. Polym Test 2013;32:701–7. doi:10.1016/j.polymertesting.2013.03.005.
[32] Li Y, Zhu J, Wei S, Ryu J, Sun L, Guo Z. Poly (propylene)/Graphene Nanoplatelet Nanocomposites: Melt Rheological Behavior and Thermal, Electrical, and Electronic Properties. Macromol Chem Phys 2011;212:1951–9.
[33] Kalaitzidou K, Fukushima H, Askeland P, Drzal LT. The nucleating effect of exfoliated graphite nanoplatelets and their influence on the crystal structure and electrical conductivity of polypropylene nanocomposites. J Mater Sci 2008;43:2895–907. doi:10.1007/s10853-007-1876-3.
[34] Ryan KP, Cadek M, Nicolosi V, Blond D, Ruether M, Armstrong G, et al. Carbon nanotubes for reinforcement of plastics? A case study with poly(vinyl alcohol). Compos Sci Technol 2007;67:1640–9. doi:10.1016/j.compscitech.2006.07.006.
[35] Brandrup J, Immergut EH, Grulke EA, Abe A, Bloch DR. Polymer handbook. vol. 1999. Wiley New York; 1999.
[36] Arranz-Andrés J, Peña B, Benavente R, Pérez E, Cerrada ML. Influence of isotacticity and molecular weight on the properties of metallocenic isotactic polypropylene. Eur Polym J 2007;43:2357–70. doi:10.1016/j.eurpolymj.2007.03.034.
[37] Tanniru M, Yuan Q, Misra RDK. On significant retention of impact strength in clay–reinforced high-density polyethylene (HDPE) nanocomposites. Polymer 2006;47:2133–46. doi:10.1016/j.polymer.2006.01.063.
[38] Anderson TL. Fracture Mechanics: Fundamentals and Applications, Third Edition. CRC Press; 2005.
[39] Deblieck RAC, van Beek DJM, Remerie K, Ward IM. Failure mechanisms in polyolefines: The role of crazing, shear yielding and the entanglement network. Polymer 2011;52:2979–90. doi:10.1016/j.polymer.2011.03.055.
[40] Arencón D, Velasco JI. Fracture Toughness of Polypropylene-Based Particulate Composites. Materials 2009;2:2046–94. doi:10.3390/ma2042046.
[41] Chan C-M, Wu J, Li J-X, Cheung Y-K. Polypropylene/calcium carbonate nanocomposites. Polymer 2002;43:2981–92. doi:10.1016/S0032-3861(02)00120-9.
[42] Premalal HGB, Ismail H, Baharin A. Comparison of the mechanical properties of rice husk powder filled polypropylene composites with talc filled polypropylene composites. Polym Test 2002;21:833–9. doi:10.1016/S0142-9418(02)00018-1.
[43] Yu Z-Z, Yan C, Yang M, Mai Y-W. Mechanical and dynamic mechanical properties of nylon 66/montmorillonite nanocomposites fabricated by melt compounding. Polym Int 2004;53:1093–8. doi:10.1002/pi.1498.

4 The effect of a semi-industrial masterbatch process on the carbon nanotube agglomerates and its influence in the properties of thermoplastic carbon nanotube composites

4.1 Introduction

It has been reported that addition of a small amount of nanofillers can lead to significant enhancement of properties in polymeric materials. Consequently, extensive research has been carried out in the field of nanocomposites that consist of a polymeric matrix and carbon-based nanofillers, such as carbon nanotubes (CNTs) [1–3] and nanofibers [4,5], graphene [3,6,7], graphite nanoplates [8–10], among others. To take advantage of these nanofillers, a homogeneous dispersion of the nanofiller in the matrix is necessary [11]. For thermoplastic polymers, solution mixing [12] or in situ polymerization [13] are probably the most effective techniques for nanosized filler dispersion. However, these techniques require a lot of reagents (monomers, solvents, chemical products for functionalization), are very time consuming (solvent removal, polymerization reaction, functionalization or grafting reaction), and typically environmentally unfriendly.

From an industrial perspective, melt compounding is a highly desirable processing technique approach to produce thermoplastic nanocomposites because it is compatible with conventional processing techniques used in the thermoplastic industry, such as extrusion or injection moulding. Most of the studies reported used injection-moulding machines and a few grams of material, the processing characteristics of which do not correspond to industrial equipment [14–23]. The injection pressure, mould temperatures, and volume of sample are some of the parameters that will affect the characteristics of the material obtained. For CNTs thermoplastic composites, these process parameters affects the dispersion of the

nanofiller on the polymer matrix: CNTs agglomerate disentanglement and orientation, break-up and orientation of dispersed individual CNTs [24,25], formation of new secondary agglomerates [26,27], etc. For example, injection-moulded samples use to have anisotropic properties dependant on the polymer chains and filler processing-induced orientation [28–30].

However, the majority of these studies only analysed the electrical properties of thin films of CNTs composites but just a few of them also included mechanical -tensile and flexural- properties (strength, modulus and/or strain at break) and impact resistance properties [31–34]. As it is well known, impact tests cannot evaluate how a material will resist crack initiation and growth when loaded at low speed, i.e. quasi-statically. Recently, we performed one of the few studies in fracture toughness with a PP matrix reinforced with graphite nanoplates (GNP) [35].

In this work, we have prepared and characterized PP/CNTs composites made by direct dilution of a highly loaded masterbatch. A highly concentrated mixture of polymer and nanofiller (masterbatch) is produced by extrusion compounding, followed by a direct dilution to achieve the desired concentration by injection moulding of the required amount of masterbatch pellets into the polymer matrix to achieve the nanocomposite with the desired nanofiller content. The use of masterbatches is highly desired by plastic converters as it avoids the direct handling of hazardous materials, this is more remarked when dealing with CNTs and other nanomaterials. The effect of the direct dilution on the injection machine will be evaluated in the present work to determine the limitations and drawbacks of the proposed solution. The aim of the present work is to demonstrate the feasibility of using a direct dilution of a CNT masterbatch on an injection machine. In general in literature there are several examples that are focused on the determination on how the filler agglomerates undergo dispersion by rupture and erosion mechanisms, which usually occur simultaneously [14,36,37]. These processes are based on the determination of the optimal conditions in the extruder, optimizing temperatures, profiles, etc. [38,39]. Although these studies have demonstrated that optimal conditions resulted in better performances, the effect of the extra steps required and the costs makes this process not always the

most efficient. There are examples in literature that are focused on the determination of the use of the direct dilution of masterbatches in injection processes [40]. From an industrial point of view the elimination of extra steps in the use of nanocomposites is envisaged for the industry as it reduces costs and negative impacts. The present works aims to determine the potential use of direct dilution of masterbatches as a cost effective process for nanocomposites adoption. In our study the results pointed out some benefits of the direct dilution as the electrical conductivity obtained are among the highest described in literature for PP nanocomposites.

The CNT dispersion was studied by scanning and transmission electron microscopy (SEM and TEM). The anisotropy of the injection-moulded specimens was analysed by measuring the electrical conductivity in three dimensions.

Analysis of the fracture behaviour of the PP/CNTs composites produced was also carried out by applying the same method as in our previous work, the S_{pb} parameter method [35]. The fracture study included a digital image correlation (DIC) analysis of the deformation zone in front of the crack tip, during fracture tests, and a fracture surface analysis by SEM.

4.2 Experimental

4.2.1 Materials

Commercially available PP impact copolymer (Hifax EP3080), acquired from Lyondell Basell, with a density of 900 kg/m^3 and a melt flow index (230°C/2.16 kg) of 7.5 g/10min (ISO 1133), was used for the production of the PP/CNTs nanocomposites. The commercially-acquired 90% purified multi-walled CNTs (NC7000), produced by catalytic chemical vapour deposition, were available commercially from Nanocyl S.A., and were used with no further treatment. The individual CNT had an average diameter of 9.5 nm and an average length of 1.5μm.

Masterbatch production by extrusion-compounding

A polypropylene masterbatch with 10 wt.% of CNTs was prepared by using an industrial extrusion-compounding machine (Coperion ZSK 26) equipped with a 26

mm diameter co-rotating twin-screw and with two Brabender gravimetric feeders. The optimal conditions were selected using different screw configurations, processing conditions and evaluating their results on CNT dispersion. Temperature profile and high shear screw profile were used to ensure proper dispersion. The polymer pellets and the powdery CNTs were introduced by the main feeder and the side feeder, respectively. The molten polymer and nanofiller were mixed at a screw speed of 500 rpm. The temperature of the resulting mixture was increased from 170°C in the feeding zone to 190°C at the nozzle. The compounding was extruded through a 2 mm diameter die at a constant output rate of 5 kg/h to give 10 kg of masterbatch. The extrudate strand was quenched immediately in a water bath at room temperature, dried and cut into small pellets. For the pure PP samples, PP pellets were also extruded following the same process.

Sample preparation by injection-moulding

Dog-bone shaped specimens (type 1A) for tensile tests, under ISO 527 [41,42], and specimens for flexural tests, under ISO 178 [43], were injected into a specific mould made in tool steel 1.2790, at a temperature of 30°C. The masterbatch pellets were dried at 80°C for 4 hours prior to processing. Composites were prepared by diluting the masterbatch with neat PP until the desired concentration (0.5, 1.0, 2.5 and 5.0 wt.%) and the specimens produced by injection moulding through a JSW 85 EL II injection machine with a 35 mm diameter reciprocating screw, at a screw speed of 131 rpm. The temperature of the mixture was increased from 225°C at the barrel to 255°C at the nozzle. Pure PP samples were also prepared using the extruded PP to be used as reference.

4.2.2 Morphological analysis of the samples

The microstructural analysis of the as received flexural test specimens was performed by scanning electron microscopy (Helios NanoLab 600i). To analyse the agglomerates in the transverse direction the specimen, two notches were machined on both sides of specimen to create a flat crack surface. The specimen was cooled in liquid nitrogen and immediately broken transversally into two halves at high speed by impacting it with a hammer. A similar process have been followed to analyse the agglomerates in the longitudinal direction of the specimen.

The surfaces of the broken specimens were analysed by SEM using both secondary and backscattered electron detectors (Figure 4.1). To study the CNTs agglomerates morphology, it has been measured from SEM micrographs the equivalent planar diameter d = $(4\times area/\pi)^{1/2}$, and the shape factor defined as:

$$F = \frac{4\pi\ x\ area}{perimeter^2} \qquad \text{Eq. 4.1}$$

Note that F ranges between 1 and 0. F=1 corresponds to a circle and it decreases as particles becomes elongated. Such measurements were performed parallel and perpendicular to the injection flow direction.

Thin samples (40 nm thickness) were also prepared by ultra-microtomy under cryogenic conditions and observed by Transmission electron microscopy (TEM, JEOL-2000 FXIIa).

4.2.3 Electrical conductivity characterization

The electrical conductivity of the injection-moulded nanocomposites was measured in the three dimensions of the sample. To perform these measurements, cubic samples with a side of 5 mm were cut from the prismatic bars injected for flexural tests. The faces perpendicular to the desired direction, in which the electrical conductivity was to be measured, were subjected to a polishing process to ensure a smooth surface. The samples were then cleaned in an ultrasound bath with ethanol to remove the abrasive particles left behind as a result of the polishing process. The polished surfaces were coated with silver paint to ensure good contact between the sample surface and the electrode. The sample was sandwiched between two copper electrodes connected to a digital multimeter (Agilent 34410A 6 1/2 Digit multimeter). At least three samples were measured per material. The electrical conductivity (σ) was calculated following Eq. 4.2:

$$\sigma = \frac{L}{RA} \qquad \text{Eq. 4.2}$$

Where L is the length of the specimen (distance between the surfaces coated with silver paste), R is the resistance measured by the multimeter and A is the area of the sample (area of the faces coated with silver paste).

4.2.4 Mechanical and thermal characterization

Analysis of tensile and flexural properties was conducted under ambient conditions with a Zwick Roell Z 10KN. At least 10 specimens were measured for each composite. Tensile tests were carried out in accordance with standard ISO 527 with an initial gauge length of 50mm and a crosshead speed of 1 mm/min during linear tensile stretching, which was increased to 50 mm/min until failure. Flexural tests were carried out in accordance with standard ISO 178 with a cross-head speed of 2 mm/min. Specimens were tested in a three-point bending configuration with a distance of 57 mm between supports.

Differential scanning calorimetry (DSC) measurements were performed on samples cut from the dog-bone specimens and measured on a DSC Q200 (TA Instruments). During analysis, samples were heated 20–220°C at a rate of 10°C/min, held at 220°C for 0.5 min and then cooled to 20°C at a rate of 10°C/min. Then, after being kept at 20°C for 0.5 min, samples were heated to 220°C at a rate of 10 °C/min [35]. The crystallinity of the nanocomposites has been determined by the integration of the melting region of the DSC curve on the second heating curve in order to suppress any thermal history.

Analysis of the quasi-static fracture behaviour of PP nanocomposites was carried out by following a three-point bending test, with a span to width ratio of 4, by using single edge-notch bending specimens with a length of 62.6 mm, a width of 13 mm, and a thickness of 5 mm. To apply the S_{pb} parameter, blunt-notched and pre-cracked specimens have to be tested. A detailed explanation of the S_{pb} parameter method can be found elsewhere [44–47].

To analyse the PP/CNTs nanocomposites, one blunt-notched reference specimen and two pre-cracked specimens were tested for each concentration. The reference specimens had blunt notches 10.5±0.1 mm in length, which were made with a disk-cutting machine. The pre-cracked specimens were prepared from an initial blunt

notch, of 3.0±0.2 mm by sharpening the notch by tapping with a razor blade to extend the crack length to 3.9±0.2 mm. Fracture tests were performed by an universal electromechanical testing machine (Instron 3384) at room temperature and with a crosshead speed of 1 mm/min [35,44].

4.2.5 Fractographic analysis and digital image correlation

After fracture tests, the specimens were cooled down in liquid nitrogen and immediately shattered to generate a brittle fracture surface to allow easy identification of the ductile fracture surface generated during the fracture test. The surfaces of the broken specimens were sputter-coated with a thin layer of gold (~ 20 nm) and analysed by SEM (EVO MA15, Zeiss) [35].

To identify the plastic deformation zone that is generated in front of the crack tip during the fracture toughness test, one side of every specimen was painted white and a random black speckle pattern was painted for DIC analysis [35]. Images were recorded every 3 s during the test. The area of interest was located immediately in front of the root of the blunt notch (13x6.5 mm^2). Evaluation of the acquired images was carried out using the Vic-2D 2009 software (VicSNAP, Correlated Solutions Inc.).

4.3 Results

4.3.1 CNT dispersion and electrical conductivity

SEM of the cryogenically fractured surface of all the samples were analysed. The neat PP sample showed some micron-scaled platelets. These platelets were composed of silicon and oxygen among other elements, which have been added to enhance the processability or heat stability of the raw material.

For all the composite samples, CNT agglomerates were observed (Figure 4.1). The surface image of the 5 wt.% CNT composite is shown in Figure 4.1b, in which large agglomerates wide were observed. These agglomerates may have been formed during the re-melting corresponding to the injection-moulding step, as the re-agglomeration process of CNTs can be thermally activated and accelerated by shear flow [37,48].

Interestingly, these agglomerates seem to have a preferred orientation as seen in Figure 4.1. It is well known that the injection process produces an anisotropy in the filler distribution, for CNTs [28–30], carbon nanofibres [21], talc [49], and short carbon and glass fibre [50] polymer composites. Because of the high shear forces produced during injection and the high viscosity of the molten polymer, the agglomerates seems to be elongated following the polymer flow [24]. The shape factor have been calculated for the 5 and 10 wt.% CNT samples. For the other materials, it have not been possible to find enough agglomerates to have a statistic.

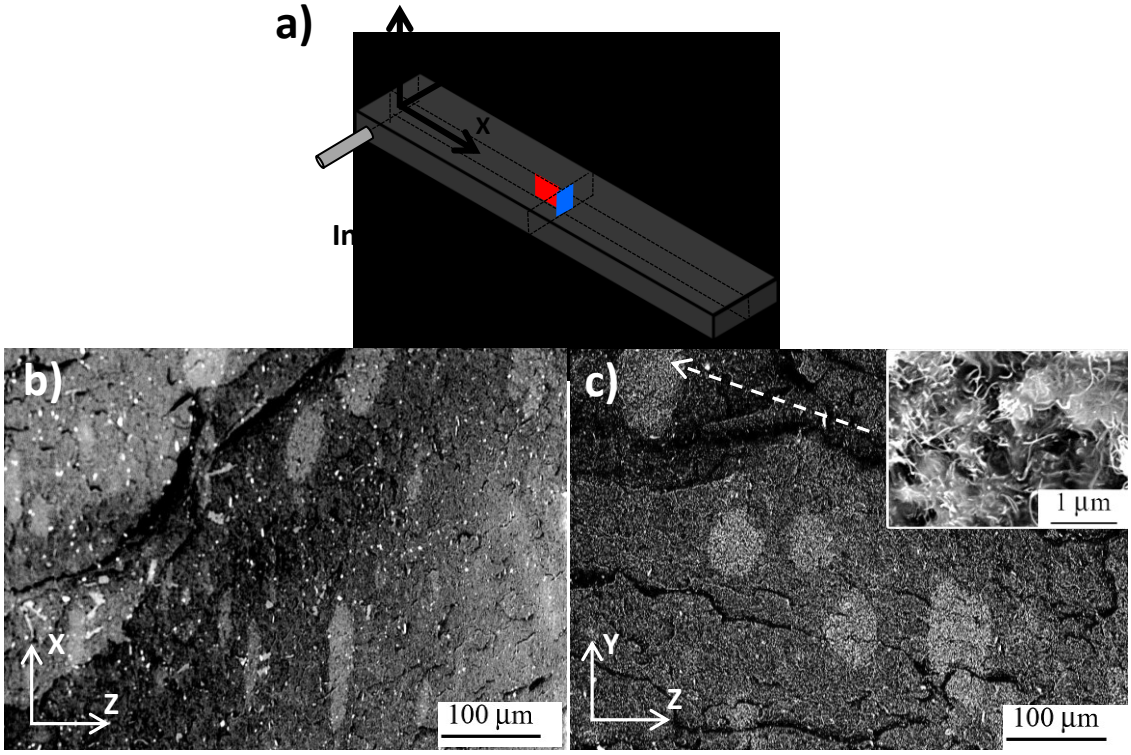

Figure 4.1 a) Scheme of the surfaces analyzed. b) and c) Backscattered electron SEM micrographs of the cryogenically fractured surfaces of a 5wt.% CNTs specimen observed along and perpendicular to the injection direction, respectively. The CNTs agglomerates are clearly aligned along the longitudinal direction (red surface, X-axis). Inset shows a high-magnification image of an agglomerate.

No significant changes have been found in the agglomerate size for both the 5 and 10 wt.% CNT composites. As the 5 wt.% CNT sample have been diluted with raw PP, it seems that during the dilution process there are not build-up or destruction [26] of agglomerates. On the other hand, the shape factor remained unaffected by the dilution process, with a value of 0.4 and 0.8 along the longitudinal and

transverse direction respectively, for both 5 and 10 wt.% composites (Table 4.1 and Figure 4.1a). This indicates a clear elongation of CNTs agglomerates along the injection flow direction (F=0.4) compared to the transverse direction (F=0.8), which is undoubtedly generated by the geometry of the injection process.

Table 4.1 Size and shape factor of the CNTs agglomerates presented in the longitudinal (longit.) and transverse direction (trans.)

Material	Direction	Agglomerate size (μm)	Shape factor
PP + 5 CNTs	Longit.	40.8 ± 13.7	0.42 ± 0.07
PP + 10 CNTs	Longit.	41.8 ± 15.5	0.44 ± 0.08
PP + 5 CNTs	Trans.	45.2 ± 20.8	0.81 ± 0.03
PP + 10 CNTs	Trans.	44.1 ± 17.4	0.80 ± 0.04

The TEM micrographs confirmed a good dispersion and homogeneous distribution of the CNTs within the composite for all the samples (Figure 4.2). No significant changes have been found for the agglomerates presented in the undiluted and diluted samples indicating that the direct dilution of the masterbatch on the injection process results effective. Thus, we can conclude that the presented strategy can be directly implemented by the plastic sector as no specific dispersion approaches are required. The benefits of using masterbatches in direct dilution had been already highlighted in the introduction.

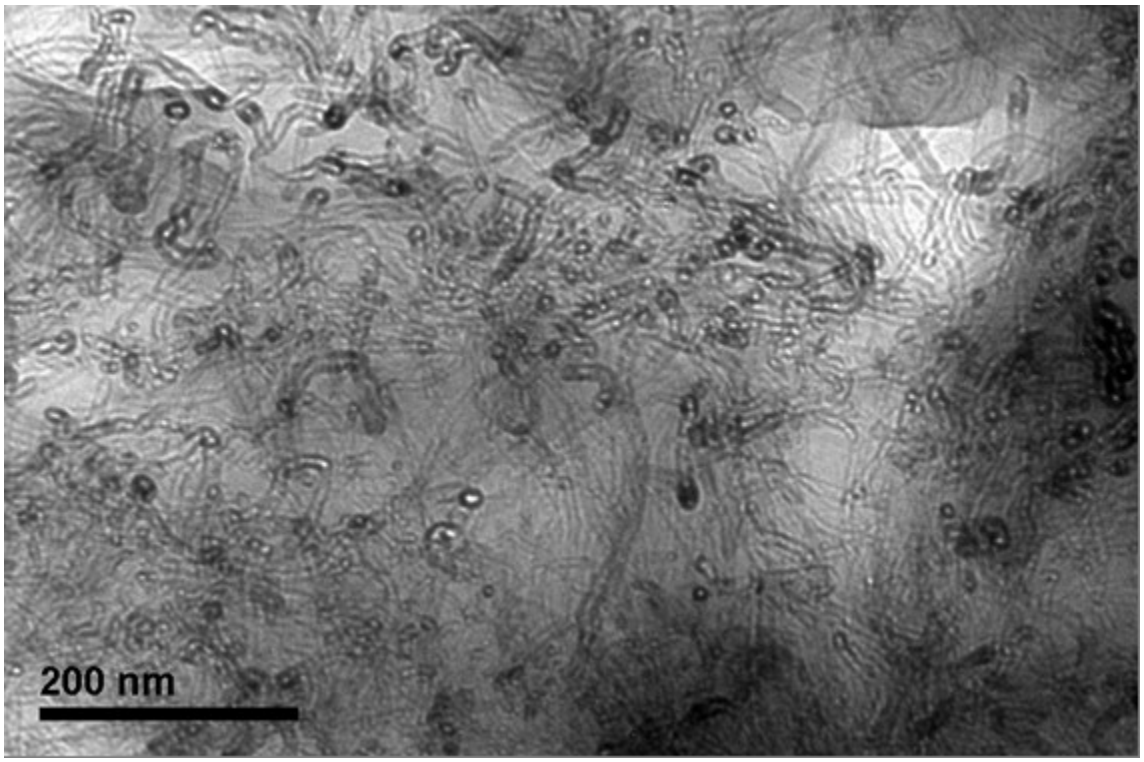

Figure 4.2 TEM micrograph of a thin film obtained by ultra-microtomy of nanocomposite with 10 wt.% concentration. The micrograph shows the dispersion degree of the CNTs obtained in the masterbatch with individual tubes and small aggregates and the presence of larger aggregates

As expected, CNT orientation affects the properties of the sample. For electrical conductivity, highly anisotropy behaviour has been measured. Depending on the direction of the sample (Figure 4.3), the amount of filler at which the material experiences a sharp increase in the electrical conductivity, known as the percolation threshold, is 2.5-5 wt.% of CNTs for the X and Y direction and 5-10 wt.% of CNTs for the Z direction. The electrical conductivity obtained for the 10 wt.% sample is comparable to other CNTs composites [2,20,23,29,34,51–54]. At the present work, the high conductivity obtained at industrial scale is relevant for industrial applications. This value may result from the large elongated agglomerates formed and the anisotropy effect, in which the conductivity in the X direction is 6 x 10^{-2} S/cm, but only 2x10^{-2} S/cm and 2x10^{-5} S/cm in the Y and Z directions, respectively.

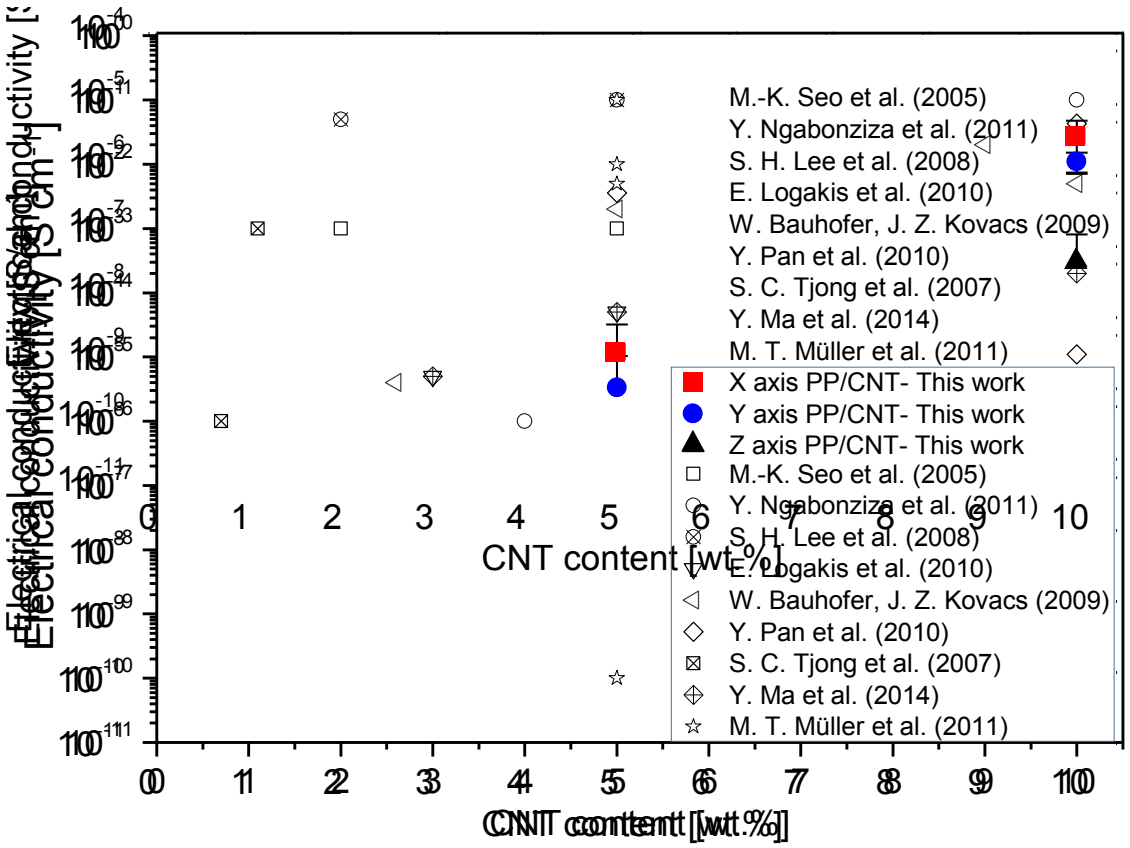

Figure 4.3 Electrical conductivity measurements obtained in this work for the PP/CNTs composites, compared to some values reported for PP composites made by melt mixing [2,20,23,29,34,51–54]. A schematic representation of the injection moulded bars and the three directions for which electrical conductivity was measured are shown. The injection-moulding direction corresponds to the X axis, the width corresponds to the Y axis, and the thickness corresponds to the Z axis. The values of electrical conductivity obtained are comparable to those reported in works that have use treated CNTs [34], different injection moulding velocities [29], two-roll mill [53] or small-scale mixing machines [20,23].

4.3.2 Mechanical properties

The tensile modulus and tensile strength increases with CNT content (Figure 4.4a). The tensile strength improvements (10% for the composite with 10 wt.% CNT) seem to indicate that the debonding of particles does no takes place prior to the start of plastic deformation [55]. Both the flexural modulus and flexural strength show similar trends with slight increases too with CNT weight fraction (Figure 4.2b).

This modest enhancement in mechanical properties, relative to some reported in the literature [33,56], can be attributed, among others, to the presence of

agglomerates and the relatively weak effect of the CNTs on crystallization behaviour [12]. The melting temperature (T_m) of neat PP is 164.1°C, whereas for the PP/CNTs composites it is 163.8±0.1°C. The crystallization temperature (T_c) of neat PP is 123.6°C, which is similar to the T_c of the composites 124.1±0.3°C. From calculations we find that the degree of crystallinity (X_c) [35] is almost the same for the PP and PP/CNTs samples (27.7 and 28.6%±2.1%, respectively). There is no significant effect of the CNTs on the melting and crystallization of PP [28,34,56]. Thus, based on the results obtained, there is no nucleating effect and change on the crystalline phase of the polymeric matrix.

In Figure 4.4c, the average value of the fracture toughness, J_{IC}, calculated from the two specimens tested for each CNT content is presented. The best result, a fracture toughness a 55% higher than that of neat PP, with a loading of just 0.5 wt.% CNTs, is larger than the highest improvement obtained for PP/GNPs composites [35]. Ganß et al. [28] analysed the resistance to quasi-static crack growth initiation on PP/CNTs composites in which the CNTs have a higher dispersion degree than those in the present study. They found that resistance decreased with addition of up to 5 wt.% CNTs, except for 1.5 wt.% at which an increase of 25% was measured. This effect was attributed to hindrance of the ductile yield as a result of polymer wrapping and the immobilized polymer layer at the polymer-nanofiller interface. However, in the present study, the J_{IC} values obtained by application of the S_{pb} parameter method show that by increasing the amount of CNTs from 0.5 to 10 wt.%, the improvements were not as good as those achieved for 0.5 wt.% CNTs, even though the composites have a higher fracture toughness than the neat matrix.

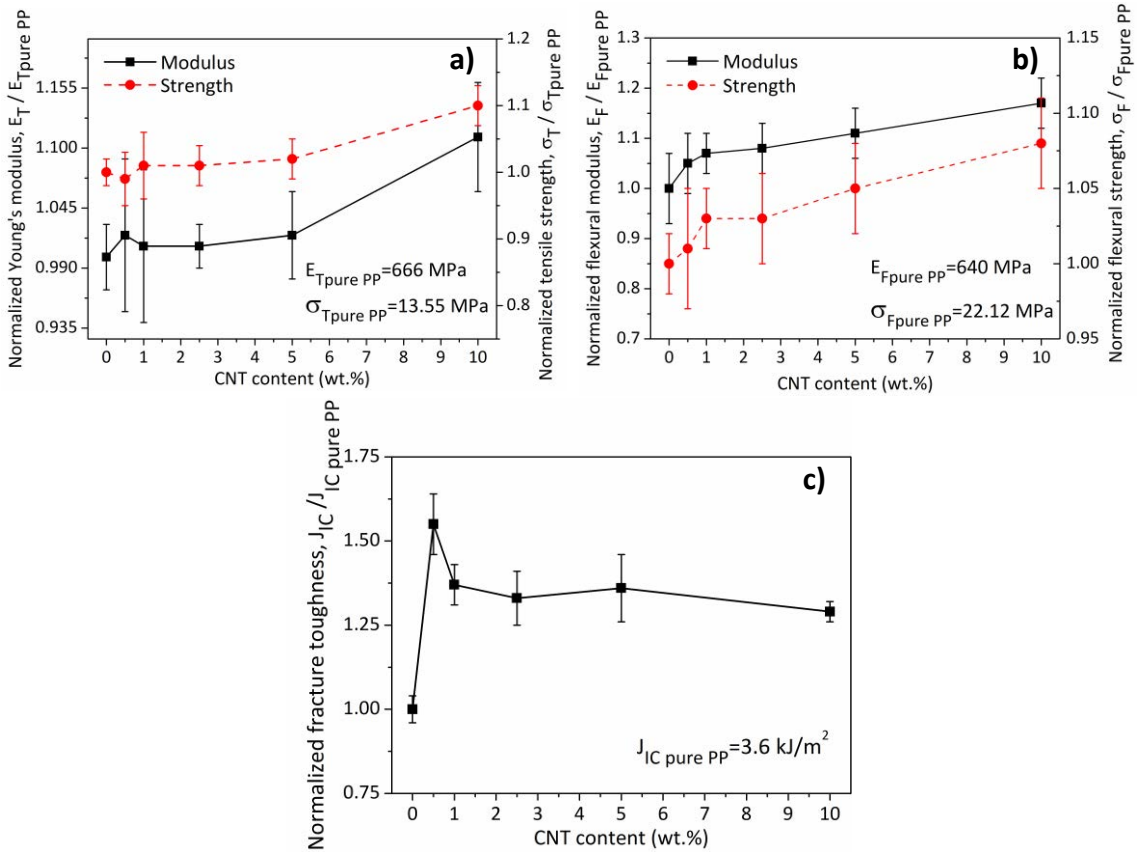

Figure 4.4 a) Normalized tensile modulus and strength; b) normalized flexural modulus and strength as a function of nanofiller content for PP/CNTs nanocomposites: c) Crack growth initiation energy, JIC, for PP/CNTs nanocomposites. The fracture toughness increases with the addition of CNTs. The maximum increase is achieved for a nanocomposite is 0.5 wt.% CNTs, which has a value 55% higher than neat PP.

4.3.3 Digital image correlation (DIC) and SEM analysis of fracture surfaces

Pictures taken during the fracture tests were processed by DIC to obtain the strain field in the principal direction, ε_1. This is the direction in which the major principal stresses take place and, in the testing configuration of the fracture tests, this direction is approximately equal to the longitudinal direction of the single edge-notched bend specimen (Figure 4.5a). A comparison performed between the full-field total strain obtained for PP (Figure 4.5b) and the nanocomposites with 0.5 and 10 wt.% of CNTs (Figure 4.5c and d, respectively) at the moment of the fracture initiation shows a change in size of the deformation zone in front of the crack tip. The strain provided has both an elastic and plastic component. However,

to identify the crack growth initiation by the S_{pb} parameter method, it is necessary to fully reach the plastic zone [45,46]. Because this requirement was met for all the materials analysed, the plastic component is assumed to be the predominant component of the deformation shown in Figure 4.5. It is well known that the shape of the plastic zone in front of the crack tip changes with the transition from plain stress conditions at the specimen surface, to plain strain conditions at the mid-thickness section [57]. However, for this comparison it is assumed that the plastic deformation zone has a cylindrical shape along the thickness of the single edge-notched bend specimen.

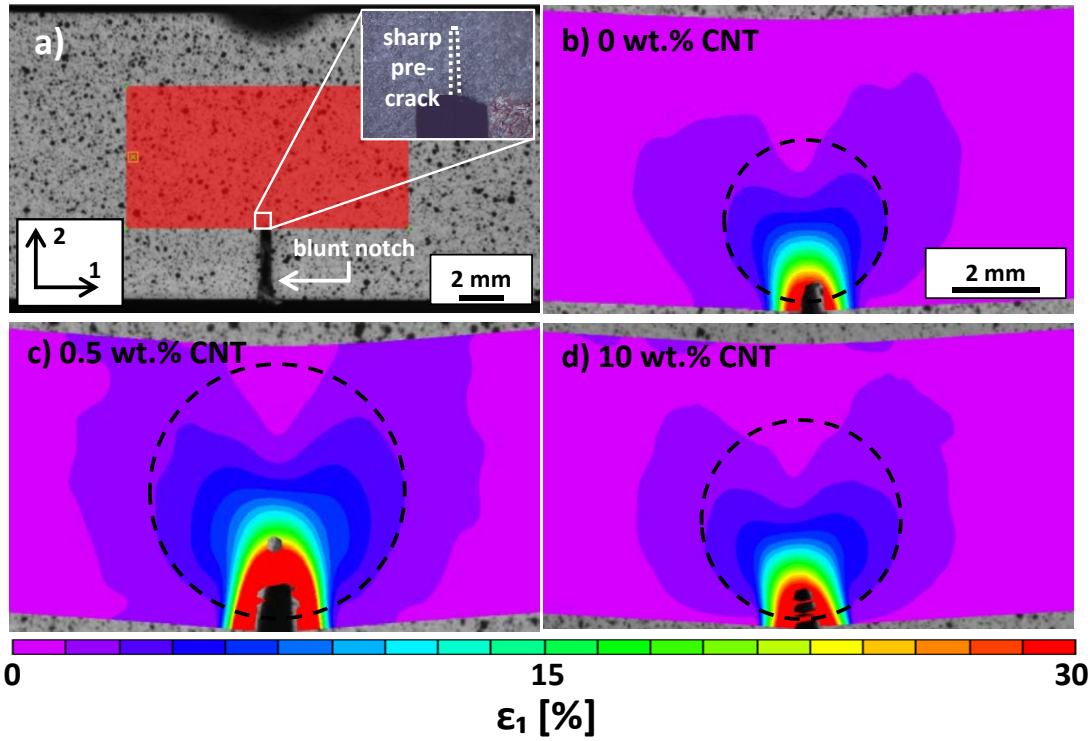

Figure 4.5 Results obtained from DIC analysis. a) Area of interest analysed by DIC. The inset shows the root of the blunt notch and the sharp pre-crack (indicated by the dotted line). The principal direction is approximately equal to the longitudinal direction of the single edge-notched bend specimen; b) Strain field in the principal direction, ε1, obtained by DIC at the moment of fracture initiation during the fracture toughness tests for neat PP; c) Nanocomposite with 0.5 wt.% of CNTs, which is the material with the highest fracture toughness; and d) 10 wt.% CNT nanocomposite.

In the PP matrix, the region of the specimen with a deformation smaller or equal to 4.5% is 54 mm^3 (Figure 4.5b). The volume of this region increases by 145% to 132 mm^3 in the nanocomposite with 0.5 wt.% of CNTs (Figure 4.5c). This increase in size may indicate that large plastic strain has taken place in the zone in front of the

crack tip. In the case of the 10 wt.% CNT nanocomposite (Figure 4.5d), the size of this region increases by 50% relative to neat PP, with a volume of approximately 80 mm^3. These results are in agreement with those obtained in our previous work for PP/graphite nanoplates composites [35] in which an increase in fracture toughness corresponds to an increase in size of the deformed region.

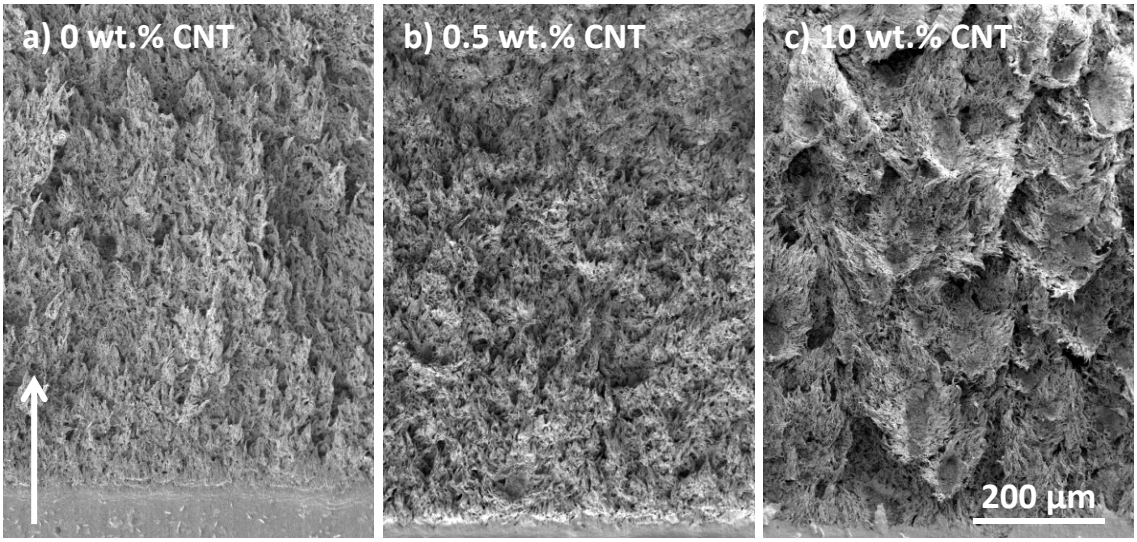

Figure 4.6 Ductile tearing region in the fracture surface of a) neat PP; b) 0.5 wt.% CNT nanocomposite; and c) 10 wt.% CNT nanocomposite in which large CNT agglomerates can be seen. The arrow indicates the crack growth direction.

Once the fracture toughness tests were complete, the fracture surfaces of the specimens were analysed by SEM. By observation of the fracture surface of PP (Figure 4.6a) the failure mechanism was seen to be polymer ductile tearing by void nucleation and growth. This mechanism was also observed in the fracture surfaces of nanocomposites (Figure 4.6b and c). The fracture mechanism of the nanocomposites is matrix ductile tearing, which has been reported for PP composites with graphite nanoplates [35], Al_2O_3 nanoparticles, SiO_2 nanoparticles, nanoclays, $CaCO_3$ microparticles [58], and PE composites with $CaCO_3$ microparticles [59]. However, relative to our previous work on PP/graphite nanoplatelets composites, the CNT agglomerates were not completely debonded after the fracture test, as confirmed by SEM (Figure 4.7). It seems that stress concentrates around the CNT agglomerate during fracture tests, which acts as a soft particle during this process [60,61]. Thus, the high stress state generated is released by deformation of the polymer around the agglomerate. The polymer

around the CNTs agglomerates can be deformed plastically into fibrils, however the CNTs of the surface of the agglomerate remained bonded to the polymer (Figure 4.7a). As the polymer around the agglomerate plastically deforms, there is somehow a slight load transmission from the matrix to the CNTs. The process allows dissipation of energy, which may explain the improvement of the fracture toughness of the PP/CNTs composites relative to neat PP. It is known that the number and size of nanofiller agglomerates increase with increased nanofiller loading [28,56,62]. Thus, after the fracture toughness reaches its maximum at 0.5 wt.% CNTs, the JIC decreases because this value is the result of two important facts: the energy dissipated by deformation of the polymer around the agglomerates versus the effect of the larger agglomerates as sources of secondary cracks [59]. For CNT weight fractions higher than 0.5%, the net balance between both effects seems to be positive because all the values for fracture toughness are higher than that of neat PP.

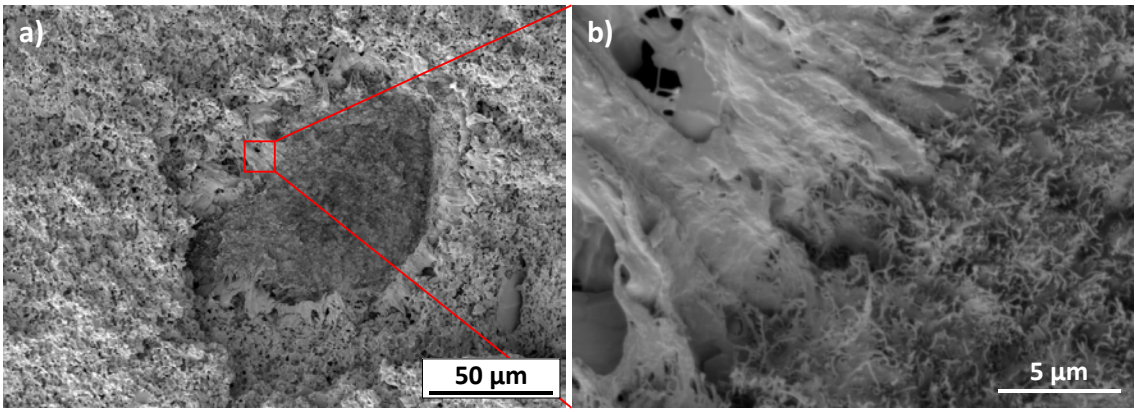

Figure 4.7 a) SEM image of a CNT agglomerate located within the deformation zone in front of the crack tip in a 0.5 wt.% CNT composite; b) Inset from a) in which the external CNTs of the agglomerate are still bonded to the plastically deformed polymer around the agglomerate.

4.4 Conclusions

Commercial-grade CNTs were efficiently integrated into a PP matrix by following a solvent-free approach known as the masterbatch technique. The obtained materials show good and homogeneous distribution of the CNT, however it was not possible to completely break up and disperse these agglomerates in the matrix. Despite the presence of these agglomerates, the electrical conductivity obtained above the percolation threshold is among the highest conductivities reported in

the literature [2,20,23,29,34,51–54]. The electrical conductivity also shows that the processing method induced a certain anisotropy to the samples obtained, which is in agreement with the elongation of the agglomerates presented in matrix. Also the agglomerate size and orientation seem not to be affected by the dilution process.

Moderate improvements in tensile and flexural properties as CNT content increases indicates that the addition of CNTs does not significantly affect the PP matrix, because all the materials have almost the same glass transition, melting and crystallization temperatures as well as similar degrees of crystallinity.

Addition of CNTs improves the fracture toughness of PP, for all nanofiller loadings up to 55% higher for the 0.5wt.% PP/CNTs composite, which turned out to have the largest deformation zone. It was seen that CNT agglomerates promote plastic deformation of the matrix during the fracture process, similarly as the cavitation or debonding mechanism of microparticles dispersed in a thermoplastic polymer. This, along with the slight load transfer from the matrix to the CNTs, during deformation, explains the enhancement in fracture toughness.

4.5 Acknowledgements

This work was supported by the European Commission under the 7th Framework Program, NFRP project (PICIG12-GA-2012- 33924), ROBOHEALTH-A project (DPI2013-47944-C4-1-R) funded by Spanish Ministry of Economy and Competitiveness and from the RoboCity2030-II-CM project (S2009/DPI-1559), funded by Programas de Actividades I+D en la Comunidad de Madrid and cofunded by Structural Funds of the EU. R.G.V. gratefully acknowledges the Spanish Ministry of Science and Innovation for funding through the Ramon y Cajal Fellowship. L.C.H-R acknowledges the support from the Spanish Ministry of Education through the FPU programme (FPU14/06843). The authors would also thank to the Ministerio de Economía y Competitividad for the Torres Quevedo Grant of Pere Castell (PTQ12-05223). The authors would like to thank J.P. Fernández-Blázquez for his help with DSC measurements and A. Salazar (URJC) for discussions of fracture test methodology.

4.6 References

[1] Coleman, J. N., Khan, U., Blau, W. J. & Gun'ko, Y. K. Small but strong: a review of the mechanical properties of carbon nanotube–polymer composites. Carbon 44, 1624–1652 (2006).

[2] Bauhofer, W. & Kovacs, J. Z. A review and analysis of electrical percolation in carbon nanotube polymer composites. Compos. Sci. Technol. 69, 1486–1498 (2009).

[3] Mittal, G., Dhand, V., Rhee, K. Y., Park, S.-J. & Lee, W. R. A review on carbon nanotubes and graphene as fillers in reinforced polymer nanocomposites. J. Ind. Eng. Chem. 21, 11–25 (2015).

[4] Al-Saleh, M. H. & Sundararaj, U. Review of the mechanical properties of carbon nanofiber/polymer composites. Compos. Part Appl. Sci. Manuf. 42, 2126–2142 (2011).

[5] Al-Saleh, M. H. & Sundararaj, U. A review of vapor grown carbon nanofiber/polymer conductive composites. Carbon 47, 2–22 (2009).

[6] Kuilla, T. et al. Recent advances in graphene based polymer composites. Prog. Polym. Sci. 35, 1350–1375 (2010).

[7] Potts, J. R., Dreyer, D. R., Bielawski, C. W. & Ruoff, R. S. Graphene-based polymer nanocomposites. Polymer 52, 5–25 (2011).

[8] Li, B. & Zhong, W.-H. Review on polymer/graphite nanoplatelet nanocomposites. J. Mater. Sci. 46, 5595–5614 (2011).

[9] Sengupta, R., Bhattacharya, M., Bandyopadhyay, S. & Bhowmick, A. K. A review on the mechanical and electrical properties of graphite and modified graphite reinforced polymer composites. Prog. Polym. Sci. 36, 638–670 (2011).

[10] Jang, B. Z. & Zhamu, A. Processing of nanographene platelets (NGPs) and NGP nanocomposites: a review. J. Mater. Sci. 43, 5092–5101 (2008).

[11] Guzmán de Villoria, R. & Miravete, A. Mechanical model to evaluate the effect of the dispersion in nanocomposites. Acta Mater. 55, 3025–3031 (2007).

[12] Ryan, K. P. et al. Carbon nanotubes for reinforcement of plastics? A case study with poly(vinyl alcohol). Compos. Sci. Technol. 67, 1640–1649 (2007).

[13] Funck, A. & Kaminsky, W. Polypropylene carbon nanotube composites by in situ polymerization. Compos. Sci. Technol. 67, 906–915 (2007).

[14] Kasaliwal, G. R., Pegel, S., Göldel, A., Pötschke, P. & Heinrich, G. Analysis of agglomerate dispersion mechanisms of multiwalled carbon nanotubes during melt mixing in polycarbonate. Polymer 51, 2708–2720 (2010).

[15] Alig, I., Skipa, T., Lellinger, D. & Pötschke, P. Destruction and formation of a carbon nanotube network in polymer melts: Rheology and conductivity spectroscopy. Polymer 49, 3524–3532 (2008).

[16] Alig, I., Lellinger, D., Engel, M., Skipa, T. & Pötschke, P. Destruction and formation of a conductive carbon nanotube network in polymer melts: In-line experiments. Polymer 49, 1902–1909 (2008).

[17] Razavi-Nouri, M., Ghorbanzadeh-Ahangari, M., Fereidoon, A. & Jahanshahi, M. Effect of carbon nanotubes content on crystallization kinetics and morphology of polypropylene. Polym. Test. 28, 46–52 (2009).

[18] Manchado, M. A. L., Valentini, L., Biagiotti, J. & Kenny, J. M. Thermal and mechanical properties of single-walled carbon nanotubes–polypropylene composites prepared by melt processing. Carbon 43, 1499–1505 (2005).

[19] Chan, C.-M., Wu, J., Li, J.-X. & Cheung, Y.-K. Polypropylene/calcium carbonate nanocomposites. Polymer 43, 2981–2992 (2002).

[20] Logakis, E. et al. Structure–property relationships in isotactic polypropylene/multi-walled carbon nanotubes nanocomposites. Compos. Sci. Technol. 70, 328–335 (2010).

[21] Kuriger, R. J., Alam, M. K., Anderson, D. P. & Jacobsen, R. L. Processing and characterization of aligned vapor grown carbon fiber reinforced polypropylene. Compos. Part Appl. Sci. Manuf. 33, 53–62 (2002).

[22] Kalaitzidou, K., Fukushima, H. & Drzal, L. T. A new compounding method for exfoliated graphite–polypropylene nanocomposites with enhanced flexural properties and lower percolation threshold. Compos. Sci. Technol. 67, 2045–2051 (2007).
[23] Pan, Y., Li, L., Chan, S. H. & Zhao, J. Correlation between dispersion state and electrical conductivity of MWCNTs/PP composites prepared by melt blending. Compos. Part Appl. Sci. Manuf. 41, 419–426 (2010).
[24] Abbasi, S., Carreau, P. J. & Derdouri, A. Flow induced orientation of multiwalled carbon nanotubes in polycarbonate nanocomposites: Rheology, conductivity and mechanical properties. Polymer 51, 922–935 (2010).
[25] Pegel, S. et al. Dispersion, agglomeration, and network formation of multiwalled carbon nanotubes in polycarbonate melts. Polymer 49, 974–984 (2008).
[26] Skipa, T., Lellinger, D., Böhm, W., Saphiannikova, M. & Alig, I. Influence of shear deformation on carbon nanotube networks in polycarbonate melts: Interplay between build-up and destruction of agglomerates. Polymer 51, 201–210 (2010).
[27] Socher, R., Krause, B., Müller, M. T., Boldt, R. & Pötschke, P. The influence of matrix viscosity on MWCNT dispersion and electrical properties in different thermoplastic nanocomposites. Polymer 53, 495–504 (2012).
[28] Ganß, M. et al. Structural interpretations of deformation and fracture behavior of polypropylene/multi-walled carbon nanotube composites. Acta Mater. 56, 2247–2261 (2008).
[29] Ngabonziza, Y., Li, J. & Barry, C. F. Electrical conductivity and mechanical properties of multiwalled carbon nanotube-reinforced polypropylene nanocomposites. Acta Mech. 220, 289–298 (2011).
[30] Villmow, T., Pegel, S., Pötschke, P. & Wagenknecht, U. Influence of injection molding parameters on the electrical resistivity of polycarbonate filled with multi-walled carbon nanotubes. Compos. Sci. Technol. 68, 777–789 (2008).
[31] Yuan, Q. & Misra, R. D. K. Impact fracture behavior of clay–reinforced polypropylene nanocomposites. Polymer 47, 4421–4433 (2006).
[32] Zhang, H. & Zhang, Z. Impact behaviour of polypropylene filled with multi-walled carbon nanotubes. Eur. Polym. J. 43, 3197–3207 (2007).
[33] Prashantha, K. et al. Masterbatch-based multi-walled carbon nanotube filled polypropylene nanocomposites: Assessment of rheological and mechanical properties. Compos. Sci. Technol. 69, 1756–1763 (2009).
[34] Seo, M.-K., Lee, J.-R. & Park, S.-J. Crystallization kinetics and interfacial behaviors of polypropylene composites reinforced with multi-walled carbon nanotubes. Mater. Sci. Eng. A 404, 79–84 (2005).
[35] Herrera-Ramírez, L. C., Castell, P., Fernández-Blázquez, J. P., Fernández, Á. & Guzmán de Villoria, R. How do graphite nanoplates affect the fracture toughness of polypropylene composites? Compos. Sci. Technol. 111, 9–16 (2015).
[36] McNally, T. & Pötschke, P. Polymer-carbon nanotube composites: Preparation, properties and applications. (Elsevier, 2011).
[37] Alig, I. et al. Establishment, morphology and properties of carbon nanotube networks in polymer melts. Polymer 53, 4–28 (2012).
[38] Kasaliwal, G., Göldel, A. & Pötschke, P. Influence of processing conditions in small-scale melt mixing and compression molding on the resistivity and morphology of polycarbonate–MWNT composites. J. Appl. Polym. Sci. 112, 3494–3509 (2009).
[39] Manas-Zloczower, I. & Feke, D. Dispersive mixing of solid additives. Mix. Compd. Polym. Theory Pract. Ed Manas-Zloczower 183–216 (2009).
[40] Wegrzyn, M., Juan, S., Benedito, A. & Giménez, E. The influence of injection molding parameters on electrical properties of PC/ABS-MWCNT nanocomposites. J. Appl. Polym. Sci. 130, 2152–2158 (2013).
[41] ISO 527-1: Plastics. Determination of tensile properties. Part 1: General principles. (2012).
[42] ISO 527-2: Plastics. Determination of tensile properties. Part 2: Test conditions for moulding and extrusion plastics. (2012).
[43] ISO 178: Plastics. Determination of flexural properties. (2010).
[44] Salazar, A. & Rodríguez, J. The use of the load separation parameter Spb method to determine the J–R curves of polypropylenes. Polym. Test. 27, 977–984 (2008).

[45] Sharobeam, M. H. & Landes, J. D. The load separation criterion and methodology in ductile fracture mechanics. Int. J. Fract. 47, 81–104 (1991).
[46] Sharobeam, M. H. & Landes, J. D. The load separation and η pl. Int. J. Fract. 59, 213–226 (1993).
[47] Baldi, F., Agnelli, S. & Riccò, T. On the determination of the point of fracture initiation by the load separation criterion in J-testing of ductile polymers. Polym. Test. 32, 1326–1333 (2013).
[48] Jamali, S., Paiva, M. C. & Covas, J. A. Dispersion and re-agglomeration phenomena during melt mixing of polypropylene with multi-wall carbon nanotubes. Polym. Test. 32, 701–707 (2013).
[49] Díez-Gutiérrez, S., Rodríguez-Pérez, M. A., De Saja, J. A. & Velasco, J. I. Dynamic mechanical analysis of injection-moulded discs of polypropylene and untreated and silane-treated talc-filled polypropylene composites. Polymer 40, 5345–5353 (1999).
[50] Fu, S.-Y., Mai, Y.-W., Lauke, B. & Yue, C.-Y. Synergistic effect on the fracture toughness of hybrid short glass fiber and short carbon fiber reinforced polypropylene composites. Mater. Sci. Eng. A 323, 326–335 (2002).
[51] Lee, S. H., Kim, M. W., Kim, S. H. & Youn, J. R. Rheological and electrical properties of polypropylene/MWCNT composites prepared with MWCNT masterbatch chips. Eur. Polym. J. 44, 1620–1630 (2008).
[52] Tjong, S. C., Liang, G. D. & Bao, S. P. Electrical behavior of polypropylene/multiwalled carbon nanotube nanocomposites with low percolation threshold. Scr. Mater. 57, 461–464 (2007).
[53] Ma, Y. et al. Electrically conductive and super-tough polypropylene/carbon nanotube nanocomposites prepared by melt compounding. Compos. Part B Eng. 56, 384–391 (2014).
[54] Müller, M. T., Krause, B., Kretzschmar, B. & Pötschke, P. Influence of feeding conditions in twin-screw extrusion of PP/MWCNT composites on electrical and mechanical properties. Compos. Sci. Technol. 71, 1535–1542 (2011).
[55] Thio, Y. S., Argon, A. S., Cohen, R. E. & Weinberg, M. Toughening of isotactic polypropylene with CaCO3 particles. Polymer 43, 3661–3674 (2002).
[56] Yang, B.-X., Shi, J.-H., Pramoda, K. P. & Goh, S. H. Enhancement of the mechanical properties of polypropylene using polypropylene-grafted multiwalled carbon nanotubes. Compos. Sci. Technol. 68, 2490–2497 (2008).
[57] Anderson, T. L. Fracture Mechanics: Fundamentals and Applications, Third Edition. (CRC Press, 2005).
[58] Pérez, E., Alvarez, V., Pérez, C. J. & Bernal, C. A comparative study of the effect of different rigid fillers on the fracture and failure behavior of polypropylene based composites. Compos. Part B Eng. 52, 72–83 (2013).
[59] Bartczak, Z., Argon, A. S., Cohen, R. E. & Weinberg, M. Toughness mechanism in semi-crystalline polymer blends: II. High-density polyethylene toughened with calcium carbonate filler particles. Polymer 40, 2347–2365 (1999).
[60] Kim, G.-M. & Michler, G. H. Micromechanical deformation processes in toughened and particle-filled semicrystalline polymers: Part 1. Characterization of deformation processes in dependence on phase morphology. Polymer 39, 5689–5697 (1998).
[61] Kim, G.-M. & Michler, G. H. Micromechanical deformation processes in toughened and particle filled semicrystalline polymers: Part 2. model representation for micromechanical deformation processes. Polymer 39, 5699–5703 (1998).
[62] Esawi, A. M. K., Salem, H. G., Hussein, H. M. & Ramadan, A. R. Effect of processing technique on the dispersion of carbon nanotubes within polypropylene carbon nanotube-composites and its effect on their mechanical properties. Polym. Compos. 31, 772–780 (2010).

5 Polypropylene composites with enhanced mechanical and thermal properties thanks to a novel carbon microfiller

5.1 Introduction

Polymer nanocomposites have focused tremendous scientific interest because significant mechanical properties improvements can be obtained upon the addition of small amounts of nano-scaled fillers [1–3], compared to conventional composites with micron-scaled fillers. In the last decade, carbon-based nanomaterials as carbon nanotubes (CNTs) and graphene have been extensively used as fillers in polymer nanocomposites due to their outstanding mechanical, thermal and electrical properties [4]. However, one of the main challenges is to achieve a large scale production of high quality nanofillers. Therefore, the development of carbon materials which could be produced at industrial scales [5–7] is envisaged as an attractive approach that could represent a significant advance in the field of commercially available high-performance multifunctional composites.

Moreover, in order to fully take advantage of the outstanding mechanical, thermal and electrical properties of fillers, as graphene or graphite nanoplatelets, the paramount concern is to achieve a homogeneous filler dispersion and a strong interaction filler-matrix to enhance the stress transfer. However, it is clear that using as-received nanofillers and applying conventional processing techniques to obtain polymer composites usually results in an agglomerated morphology of the nanofiller and modest mechanical properties improvements [8,9]. Thus, an alternative for the processing of polymer composites would be the use of micron-scaled carbon fillers that could be easily dispersed within the matrix without the agglomeration tendency of the nanofillers.

In this work, a novel carbon-based micron-sized material was used as filler to produce polypropylene (PP) composites and its effect on the mechanical and thermal properties of the resulting composites was analysed. Polypropylene was chosen as matrix as it is a widely used commodity thermoplastic polymer. Its simplicity of processing, low cost and relatively good physical, chemical and mechanical properties makes it the ideal candidate to be used for industrial applications (household goods, food packaging, automobile, etc.) [10]. The carbon micron-scaled material was directly synthesized by a chemical vapour deposition process, using commercially available nickel microparticles as catalyst. The potential of the carbon material to be produced at large-scale has been previously reported [11]. Although having a high degree of heterogeneity, the synthesised carbon material showed interesting structures consisting in micron-scaled fibre-like structures with a highly rough surface morphology. This feature could improve the stress transfer from the matrix to the filler due to the mechanical interlocking with the polymer chains [12–14]. Therefore, the synthesized carbon material also shows potential as reinforcement for polymer composites.

PP composites were produced following a simple masterbatch technique as this approach has proved effective in improving the dispersion of fillers such as CNTs, graphite nanoplatelets or glass microspheres [15–17] compared to traditional melt mixing approach. The scale-up of this approach to a semi-industrial level was previously reported for the processing of PP composites with GNP and CNTs, which exhibited acceptable mechanical properties [8,9].

The masterbatch approach resulted in the break-up of the as-synthesized structures, although the resulting carbon microfiller (CMF) showed good degree of dispersion within the matrix. Consequently, a 25% increase in flexural modulus and 7% increase in flexural strength are obtained for the composite with the 8.9 wt.% of carbon microfiller. Furthermore, this material exhibited and enhanced thermal stability and conductivity. The obtained results makes the CMF/PP composite very attractive for the development of commercially available polymer composites with enhanced mechanical and thermal behaviour.

5.2 Experimental procedure

5.2.1 Synthesis of carbon microfiller

Nickel particles (Alfa Aesar), with an average particle size of 3.4 ± 2.2 μm [18] and 99.9% purity, were used to synthesize the carbon-based micro-filler by means of a chemical vapour deposition (CVD) process. The particles were used as received, i.e. with no further treatment.

The Ni microparticles (50 mg) were placed in an alumina boat, which was positioned in the middle of a quartz tube, heated by a mobile horizontal tube furnace that allows fast heat and cool down rates. A detailed explanation of the CVD system can be found elsewhere [19]. The particles were first conditioned for the growth of the carbon arms. This conditioning was done by heating particles at 550 °C, under a flow of 100 sccm of H_2 and 400 sccm of Ar, for 5 min. Afterwards, for the carbon nanostructures growth, the temperature was maintained at 550 °C and a flow of 100 sccm of H_2, 400 sccm of Ar and 150 sccm of C_2H_4 was settled for 360 min. After this process, the furnace was cooled down under a flow of 1000 sccm of Ar. The material obtained after this process was the carbon micron-scaled material.

5.2.2 Preparation of composites

A commercial polypropylene homopolymer (ISPLEN® PP070G2M, Repsol), with a density of 905 kg/m^3 and a melt flow index (230°C/2.16 kg) of 12 g/10 min. Due to the different morphology of the material after the processing of composites, compared to the as-synthesized morphology, the filler is referred to as carbon microfiller (CMF). PP composites with 0.5, 1, 5 and 10 wt.% of CMF were processed.

Polypropylene masterbatches containing 5 and 10 wt.% of CMF were produced using a co-rotating twin-screw micro-compounder (MC 15 Xplore) with a chamber capacity of 15 cm^3. The as-received PP granules and the as-synthesized carbon material were dried at 100 °C for 4 h prior to masterbatch processing. The PP and the powdery filler were premixed and fed together in the hopper. The

compounding was done at a temperature of 210 °C for 5 min, with a screw speed of 150 rpm. The extruded strand was cut into pellets.

Composites with filler content of 0.5 and 1 wt.% of CMF were produced by diluting pellets of masterbatch (5 wt.% of CMF) with neat PP pellets, dried at 100 °C for 4 h, to achieve the desired filler content. The dilution process was done applying the same parameters and equipment as in the masterbatch processing (210 °C for 5 min, with a screw speed of 150 rpm). The composites with the highest CMF content, i.e. 5 and 10 wt.%, were obtained by re-processing the masterbatches with the same parameters as those used in the dilution step (210 °C for 5 min, with a screw speed of 150 rpm).

For comparison, neat PP was processed by following the same processing steps as those used for the composite, i.e. 2 cycles in the micro-compounder at 210 °C for 5 min, with a screw speed of 150 rpm. The extruded strand was cut into pellets.

Afterwards, prismatic bars with dimensions of 150×13×4 mm^3 and discs, diameter of 30 mm and a thickness of 3.2 mm, were produced by compression moulding at 200 °C.

5.2.3 Characterization of carbon micron-scaled material

The morphology of the as-received Ni microparticles and the synthesized carbon micron-scaled material were analysed by scanning electron microscopy (field emission gun-SEM Helios NanoLab 600i, FEI). For SEM, the particles were lightly pressed onto an adhesive carbon tape.

The thermal stability, in air and nitrogen, of the as received Ni particles and the synthesized material, as well as its carbon content, was characterized by thermo-gravimetric analysis (TGA) (Q50, TA Instruments). Approximately 10 mg of powdery material was heated at 10°C/min from room temperature to 800°C, under air or nitrogen atmosphere, respectively.

The synthesized carbon material was placed on thin aluminium foils and analysed by Raman spectroscopy (Micro-Raman spectrometer Renishaw PLC), using a DPSS Nd:YAG green laser (532nm wavelength). At least four spectra were obtained for

15s exposure, 5 accumulations, over a range of 200-3500cm^{-1} and at a laser power of 5%.

5.2.4 Characterization of composites

Dispersion of the carbon microfiller, thermal stability and density of composites

The degree of dispersion of the carbon microfiller was analysed by SEM. Specimens of the resulting composites were embedded in epoxy resin and polished with grinding paper, diamond paste and alumina suspension (0.3 μm). The surfaces of the samples were sputter-coated with a thin layer of gold to prevent charging.

The thermal stability of composites in air and nitrogen was characterized by thermo-gravimetric analysis (Q50, TA Instruments). Samples, 10 mg, were extracted from the produced specimens and heated at 10°C/min from room temperature to 800°C, under nitrogen atmosphere, respectively. Three measurements, for each filler content, were performed.

The density of the resulting composites was measured following the ASTM D792-13 standard [20], through the application of the Archimedes' principle. At least three cylindrical samples with a diameter of 30 mm and a thickness of 3 mm, for each filler content, were first weighted in air and then in distilled water. The theoretical density of composites was also obtained, by applying the rule of mixtures, in order to compare the values obtained with the experimentally measured densities of composites.

Differential scanning calorimetry, X-ray diffraction and dynamic mechanical analysis

Differential scanning calorimetry (DSC) was performed on a DSC Q200 (TA Instruments), to analyse the effect of the filler on the crystallization behaviour and degree of crystallinity of the PP matrix. Three measurements per material were performed. During which, the samples were heated from 20 to 220 °C at a rate of 10 °C/min, held at 220 °C for 0.5 min to remove thermal history and cooled to 20

°C at a rate of 10 °C/min. Then, after being kept at 20 °C for 0.5 min, the samples were heated to 220 °C at a rate of 10 °C/min.

X-ray diffraction (XRD) patterns were recorded (Empyrean, PANalytical) operating with a Cu Kα radiation source (wavelength λ= 1.5406 Å). The x-ray beam was generated at a voltage of 45 kV and a current of 40 mA. The measurements were performed over the range 2θ=10° to 60°, with a step of 0.026°, on the surface of the moulded discs with a diameter of 30 mm and a thickness of 3 mm.

Dynamic mechanical analysis (DMA) were carried out by using specimens with dimensions of 17.5×12.65×3.2 mm^3 in single cantilever mode. The tests were performed on a Q800 (TA Instruments) in a temperature range of –150 to 180 °C, at a frequency of 1 Hz, and at a heating rate of 1.5 °C/min.

Thermal conductivity measurement

The thermal conductivity of the neat PP and the CMF composites was measured at room temperature applying a transient plane source technique. For each material at least three measurements were performed, using cylindrical shaped samples, with a diameter of 30 mm and a thickness of 3 mm, in a hot disk thermal constants analyser TPS 2500 S (Hot Disk AB). In this technique, a thin heater/sensor, with a radius of 0.536 mm, was clamped between two identical samples. Then, the heater/sensor element was first used as a heat source to increase the temperature of the surrounding sample by applying an output power of 0.01 W. Afterwards, the temperature increase was monitored over a period of time of 3 s by measuring the resistance of the heater/sensor. In order to minimize the effect of the interfacial thermal resistance, the surfaces of the cylindrical samples were polished. A detailed description of the transient plane source technique and its theoretical background can be found in [53–55].

Flexural and fracture characterization

The flexural tests were conducted under ambient conditions, using an Instron 5966 (500 N load cell). At least five specimens of each composition were tested in a three-point bending configuration with 50 mm between supports. Tests were carried out at a cross-head speed of 1.25 mm/min.

For the fracture characterization of the resulting composites, three-point bending tests (Instron 5966) were carried out at room temperature. Single-edge-notch bending (SENB) specimens, with dimensions of 65×12.5×3.5 mm^3, were tested with a span-to-width ratio of 4 at a cross-head speed of 1 mm/min.

The SENB samples were prepares as reported in previous works [8,9]. Briefly, samples were notched with a wire-cutting machine. Then, a sharp pre-crack was generated by tapping with a razor blade before testing such that the ratio of specimen width to crack length was between 0.45 and 0.55. In order to construct the *J-R* curve of composites, the crack length of the specimens being tested was followed by taking images every second.

5.3 Results and discussion

5.3.1 Synthesis and characterization of carbon micron-scaled material

The material obtained by chemical vapour deposition, the carbon micron-scaled material, was used as filler in the processing of PP-matrix composites. The amount of Ni microparticles placed in the alumina boat for each CVD batch was 55 mg. The pre-treatment was carried out at 550°C, for 5 min; while the growth step is done at 550°C, for 6 hours, with a flow of ethylene of 150 ml/min. Further details of this process can be found elsewhere [11].

The morphology of the as-received Ni microparticles was analysed by SEM (Annex A: Supplementary information). The microparticles are almost spherical, with a diameter of 3.4 ± 2.2 μm. From the TGA performed under air atmosphere (Annex A: Supplementary information) of the as-received particles it was observed that the oxidation starts at 400°C, resulting in a weight increase of 26.4% at 900°C.

The synthesized material exhibited a high degree of heterogeneity (Figure 5.1). The different structures where divided in two groups. The first morphology consisted in sub-micron sized structures (Figure 5.1a, white arrow, and b). However, the main characteristic of the synthesized material was the micron-sized fibre-like structures, as those observed in Figure 5.1a and c, which grew from

nickel microparticles (white arrow in Figure 5.1c). By analysing these fibre-like structures at higher magnification it was found that their surface exhibited a high roughness degree (Figure 5.1d).

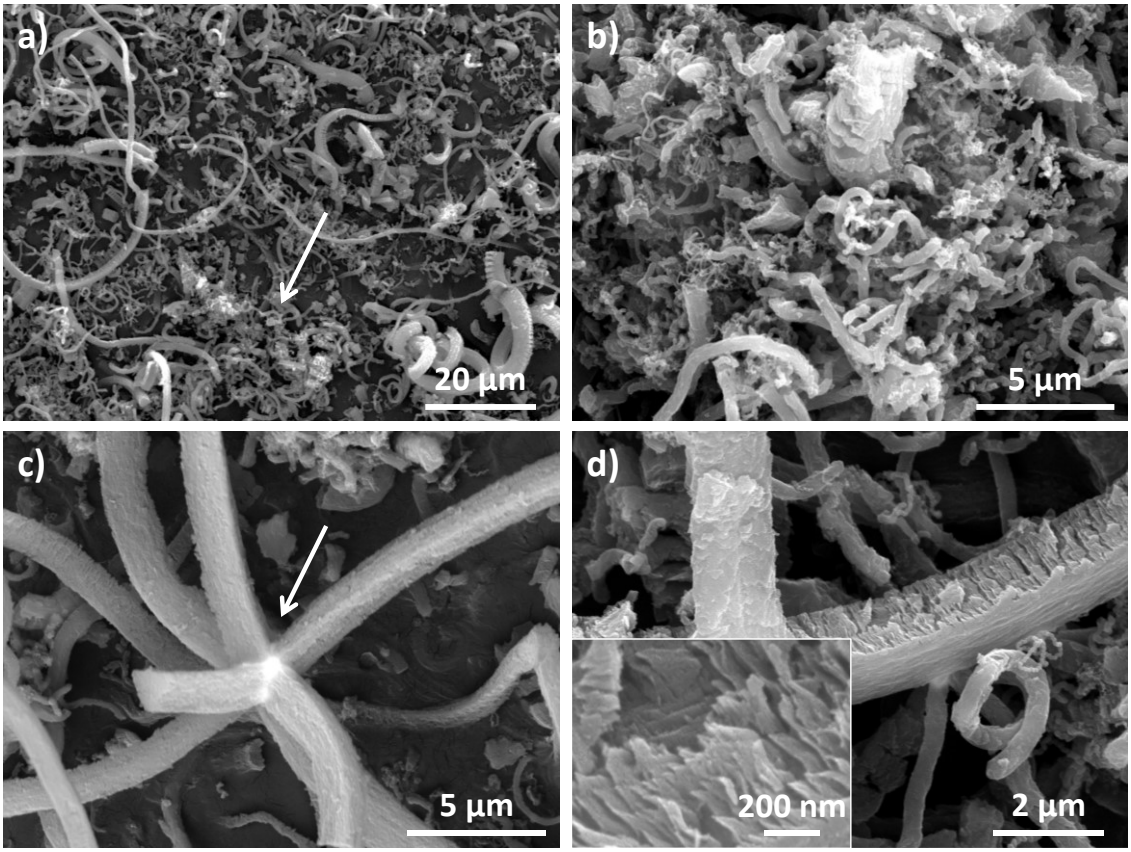

Figure 5.1 SEM images of the synthesized carbon microfiller a) low magnification image showing the heterogeneity of the filler, b) sub-micron sized filler, similar to that indicated by the arrow in a), c) nickel particle (indicated by the arrow) with micron-sized fibre-like structures, which had grown from it; and d) high magnification image of a fibre-like structure, the inset shows a structure that seems to be formed by layers.

The carbon content of the as-synthesized material was analysed by TGA performed under air atmosphere (Annex A: Supplementary information). The oxidation of the carbon-based material takes place in a single process, which is started at *ca.* 550°C. The temperature at which the highest rate of sample's weight loss takes place, i.e. oxidation temperature, corresponds to the maximum of the degradation peak in the first derivative of the weight curve, which is located at *ca.* 575°C. The carbon filler presented in this work has an excellent thermal stability, which can be compared to other carbon-based materials as MWNTs, with oxidation temperatures usually in the range from 400 to 600°C [21,22]. The residue left in air

at 900°C, *ca.* 2 wt.%, corresponds to the Ni microparticles. However it should be taken into account that during this analysis the microparticles have undergone oxidation. Taking into account this effect, it was obtained that the carbon micron-scaled material was composed by a 98.5 wt.% of carbon. In the case of the thermal stability in nitrogen, it was obtained that the synthesized carbon material was thermally stable up to 900°C, suffering a weight loss of just 3% at this temperature.

5.3.2 Characterization of composites

Composite processing and thermal stability

From the analysis by SEM of the polished surfaces (Figure 5.2), an important consequence of the processing on the morphology of the carbon material was observed. The micron-sized fibre-like structures (Figure 5.1a and c) were broken, resulting in structures with a lateral size less than ca. 10 μm, which will be referred to as carbon microfiller. It is worth to note that the processing approach resulted in a good dispersion of the carbon microfiller, as it was homogeneously distributed within the matrix (Figure 5.2c). From Figure 5.2d, it seems that the structural integrity of the carbon filler was lower than the adhesion with to the Ni particle, as some short carbon structures (dashed line in Figure 5.2d) remained attached to the Ni particle.

The effect of the carbon microfiller on the thermal decomposition of PP in nitrogen was analysed by TGA (Figure 5.3a). The curve obtained for neat PP indicate that the non-oxidative thermal decomposition takes place in a single process, which starts at approximately 350°C. All the composites exhibited a similar behaviour, however, as the amount of CMF increased the temperature at which the decomposition starts increased. Therefore, to further characterize the stabilizing effect of the carbon microfiller, the temperature at which a weight loss of 5% takes place ($T_{5\%}$) and the temperature at a maximum rate of weight loss (T_P) were identified for neat PP and the composites (Figure 5.3b). As it can be observed a considerable improvement of $T_{5\%}$ is obtained upon the addition of the carbon microfiller. The largest increase, approximately 50°C compared to the $T_{5\%}$ of PP, is obtained for the 8.9 wt.% CMF composites. However, with just a 0.6 wt.% of filler, an increase of *ca.* 7°C was obtained. An increasing trend of T_P as the CMF content

increases is also observed. Although in this case, the effect of the filler addition is less pronounced than in the case of the $T_{5\%}$.

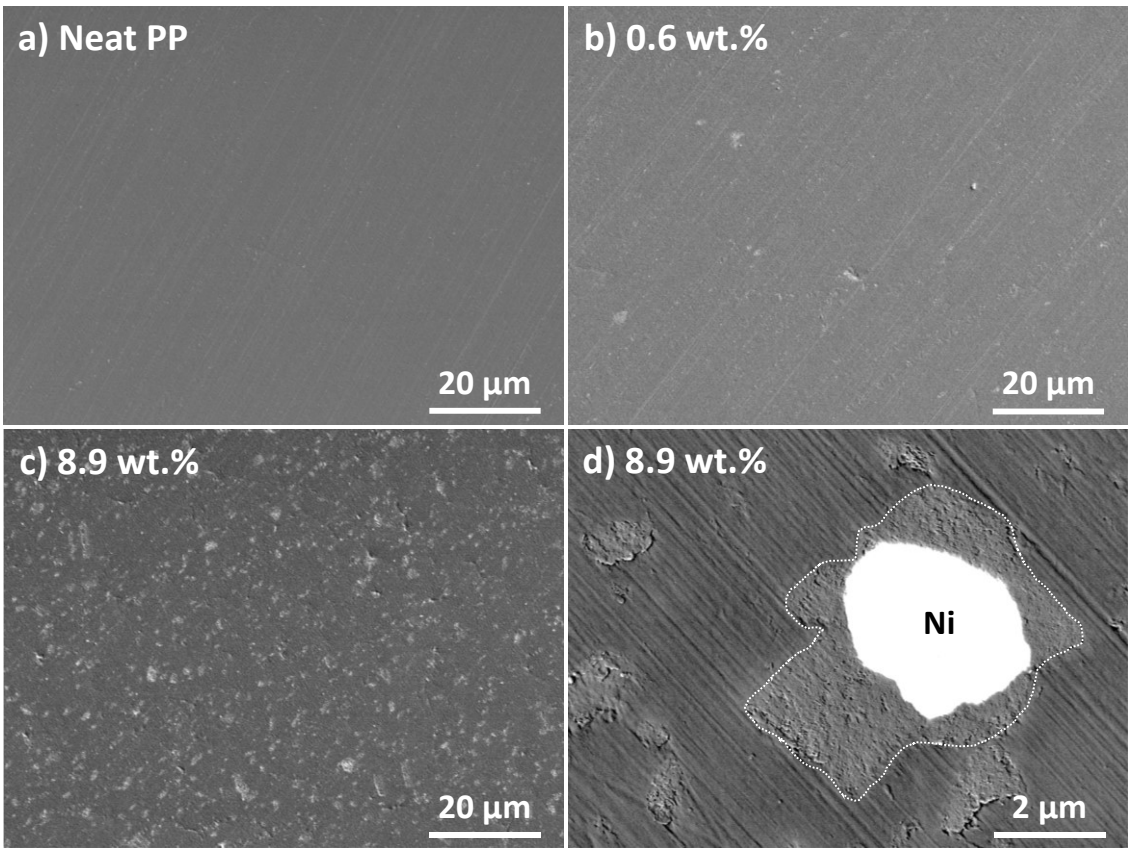

Figure 5.2 SEM images of the polished surfaces of a) neat PP and composites with b) 0.6 and c-d) 8.9 wt.% of CMF. The dashed line in d) indicates the short carbon structures that remained attached to the Ni particle.

As it was observed in Figure 5.2c, the CMF is homogeneously distributed within the PP matrix. This carbon microfiller network could restrict the emission of decomposition gases during the thermal degradation, thus resulting in a delayed degradation, i.e. shift of $T_{5\%}$ toward higher temperatures, of the matrix [25–28]. As the filler content increase so does the network density. Therefore, the barrier effect would be more pronounced for the samples with higher filler content, which is in agreement with the observed behaviour. Another explanation could be the absorption of free radicals, generated during the decomposition of PP, by the surface of the carbon microfiller [26,29,30]. Another effect that could account for the increased thermal stability is the physical adsorption of PP chains at the rough surfaces of the filler (Figure 5.1d). Thus the degradation of the polymer around the

filler is delayed, compared to the bulk polymer, which could be observed by the increase in T_P [28,31].

Nonetheless, the stabilising effect of the carbon microfiller reported in this work is in agreement with that found for PP composites with carbon-based fillers [28,30,32–34]. Furthermore, an increase of 23 and 35°C was obtained for 8.4 and 12.3 wt.% of graphene [32] and graphite nanoplatelets [33], respectively. In this work, the increase was 50°C for 8.9 wt.% of carbon microfiller, thus the higher stabilising effect of this filler, compared to graphene or graphite nanoplatelets, is demonstrated.

The densities of PP and composites were measured and are available in the Annex A: Supplementary information. Moreover, the theoretical density of composites was calculated applying the rule of mixtures. For this analysis, the weight fractions of carbon microfiller on composites was obtained from the residues of TGA, the density of the matrix was the measured for neat PP, ρ_m=0.906 g/cm^3; and the density of the carbon microfiller was ρ_{CMF}=2.024 g/cm^3, which was calculated assuming a carbon density of 2 g/cm^3 [35] and a Ni content of 1.5 wt.%, ρ_{Ni}=8.908 g/cm^3 as provided by the manufacturer. The experimental values fitted well with the theoretical linear behaviour as the filler content increases.

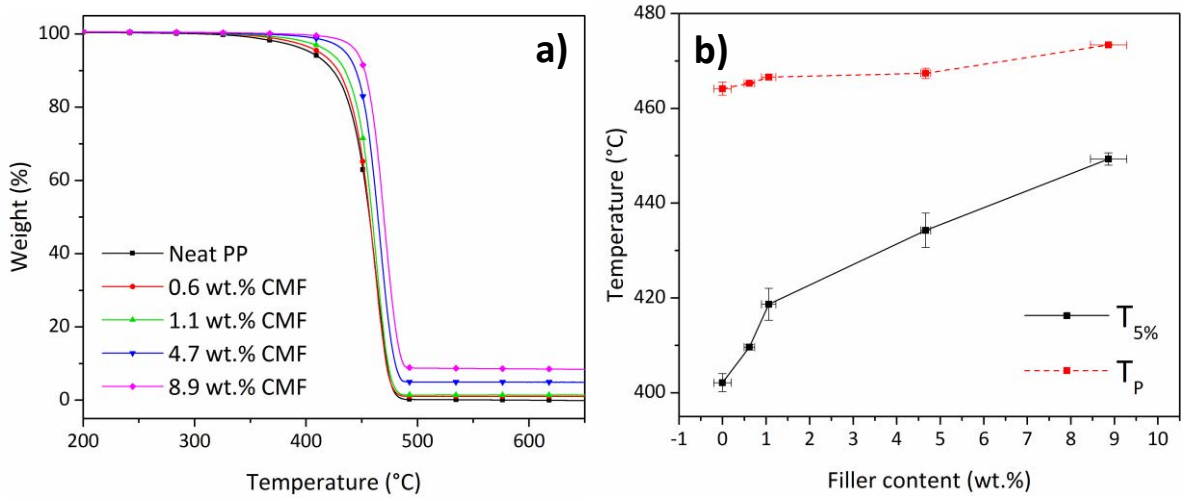

Figure 5.3 a) Curves obtained from the TGA, corresponding to the weight (%) (in nitrogen, at a heating rate of 10 °C/min) of the neat PP and the composites with CMF, b) Temperature at a weight

loss of 5% ($T_{5\%}$) and temperature at maximum rate of weight loss (T_P) as a function of the filler content, obtained from TGA.

DSC, XRD and DMA

Differential scanning calorimetry measurements were performed to study the effect of the carbon micro filler on the melting and crystallization behaviour of the PP matrix. The melting and crystallisation temperatures were taken as those of the maximum in the endothermic and exothermic peaks, respectively, in the heat flow curve. The melting temperature, for the first and second heating, are given in the Annex A: Supplementary information. It was observed that the addition of the carbon microfiller have no effect on the melting temperature of the PP matrix. The degree of crystallinity (X_c) of neat PP and composites was calculated by following [8,36]:

$$X_C(\%) = \frac{\Delta H_s}{(1-\phi)\Delta H_0} \times 100 \qquad \text{Eq. 5.1}$$

where ΔH_s is the enthalpy of fusion of the sample (obtained by integration of melting peak [37]), ϕ is the weight fraction of filler, and ΔH_0 is the enthalpy of fusion of 100 % crystalline PP, taken as 209 J/g [8,38].

The X_c obtained from the first heating (Annex A: Supplementary information) did not significantly change upon the addition of CMF. This means that degree of crystallinity of the PP matrix after the processing of composites was not affected by the CMF. Furthermore, after removing the thermal history and subjecting the sample to a controlled crystallization process, the degree of crystallinity obtained from the second heating showed no effect of the carbon microfiller. This effect is in agreement with that reported for PP composites with carbon-based fillers as GNPs [8,26,39], graphite [33] or CNTs [36,40], which showed no or a slight effect of the filler on the degree of crystallinity of the PP matrix.

The non-isothermal crystallisation process, i.e. cooling curve, is shown in Figure 5.4. In this case, the T_c gradually increases as the CMF content increases; having the composite with a 8.9 wt.% of CMF a crystallisation temperature 7°C higher than that of neat PP (Figure 5.4a). This considerable effect indicates that the CMF

acts as nucleating agent of the crystallisation process of the PP matrix [32,36,39,41,42].

To further analyse the effect of the CMF on the crystalline structure of PP, X-ray diffraction measurements were carried out (Figure 5.4b). For neat PP, the peaks that appears at approximately 14, 17, 18.5, 21, 22, 25.5 and 28.5° correspond to the planes (1 1 0), (0 4 0), (1 3 0), (1 1 1), (1 3 1)+(0 4 1), (0 6 0) and (2 2 0), respectively, of the α-phase (monoclinic unit cell). The XRD patterns of PP and the CMF composites showed the complete absence of the β- and γ-phase [43], as no additional peaks was observed (Figure 5.4b). Therefore, the carbon microfiller acted as a purely α-nucleating agent during the crystallisation of PP. However, a change on the intensities of the peaks was observed upon the addition of the CMF. The ratio between the intensities of the (1 1 0) and the (0 4 0) planes indicates the orientation of the *a* and *b* axes of the α-phase unit cell. If the ratio is less than 1.3, the *b* axis lies predominantly parallel to the surface under analysis. If the ratio is higher than 1.5, then the *a* axis lies parallel to the analysed surface. Finally, a ratio between 1.3 and 1.5 indicates an isotropic mixture of crystallites [44–46]. In the case of neat PP, a I_{110}/I_{040}=1.18 was obtained, indicating an orientation of the *b* axis parallel to the surface of the moulded disc. Furthermore, this ratio decreases with increasing the CMF content, having the 8.9 wt.% composite an I_{110}/I_{040}=1.00. This seems to indicate that the CMF induces an orientation of the α crystallites in the plane of the moulded discs. This effect was previously reported for PP filled with talc [44], magnesium hydroxide [46] or graphite nanoplatelets [39].

The effect of the CMF on the thermo-mechanical behaviour of PP was analysed by dynamic mechanical analysis. Figure 5.4c show the storage modulus (E') and tan δ curves, respectively, of neat PP and CMF composites as a function of the temperature. As it can be observed, the storage modulus of neat PP decreased with increasing temperature, suffering a drastic drop in the region near 0°C, which is associated with the glass transition of PP. The behaviour of CMF composites is similar to that of neat PP, although it was found that the E' of composites increases with increasing the CMF content. This behaviour is indicative of a reinforcing effect of the carbon microfiller. Any reinforcing effect resulting from a variation in the degree of crystallinity or in the crystalline phase was excluded, taking into account

the results obtained by DSC and XRD. It is worth noting that the reinforcing effect can be observed in both the glassy, at -150°C, and rubbery state, at 50°C, (Annex A: Supplementary information).

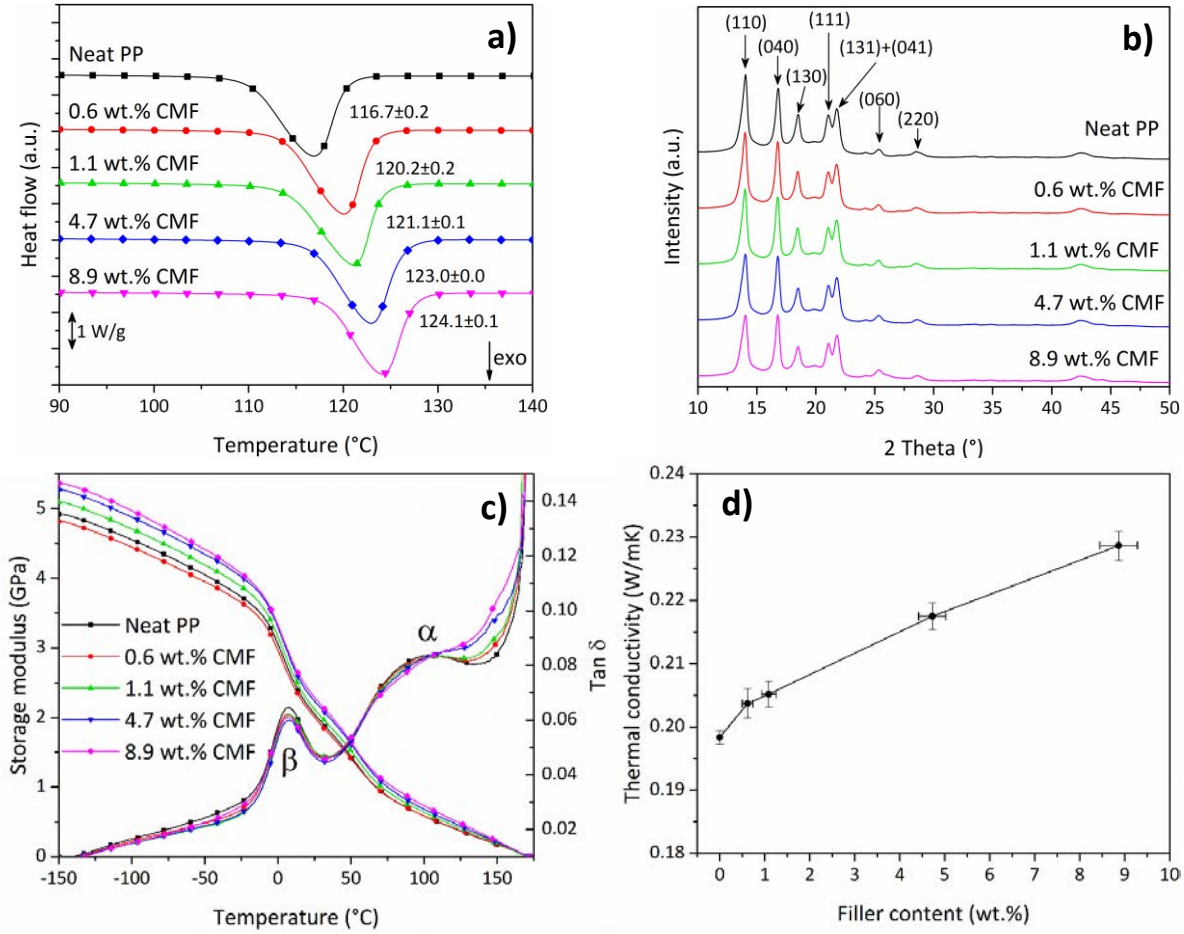

Figure 5.4 a) DSC thermograms showing the non-isothermal crystallization (at a cooling rate of 10 °C/min) of PP and CMF composites. b) XRD patterns of neat PP and CMF composites. The planes associated with the main peaks are indicated with arrows. c) Storage modulus and tan δ (at a frequency of 1 Hz), as a function of temperature. d) thermal conductivity of neat PP and composites with CMF.

In the tan *δ* curve (Figure 5.4c), two of the three relaxation processes of PP could be observed [47,48]. The γ relaxation peak, which appears at *ca.* -50 °C, was not observed probably due to overlapping with the β relaxation. The γ relaxation peak is related to local motions within the amorphous phase of PP. The β relaxation peak is associated with the glass transition of the amorphous phase of PP. As it can be observed, the intensity and position of the peak are not significantly affected upon the addition of CMF, being located between 7.5 and 8.5 °C for neat PP and CMF composites. Thus, the CMF is not significantly affecting the amorphous phase

of PP [8,32,41]. The α relaxation peak is related with motions within the crystalline phase of PP, particularly to the diffusion of defects in the crystals. In this case, the addition of CMF seems to be restricting the movement within the crystalline phase as the position of the α peak of composites shifts to higher temperature, overlapping with the onset of melting, and its intensity decreases [32]. Therefore, taking into account the results obtained by DSC and DMA it can be said that the addition of the carbon microfiller affects the crystalline phase of PP, while the amorphous phase remains unaffected.

Thermal conductivity

The effect of the carbon microfiller on the thermal behaviour of resulting materials was analysed by measuring the thermal conductivity of neat PP and CMF composites, the results are shown in Figure 5.4d. As it can be observed, the thermal conductivity of neat PP is 0.198 W/mK, while the thermal conductivity of CMF composites increased with increasing the filler content. The highest improvement was obtained for the composite with a 8.9 wt.% of CMF, which has a thermal conductivity a 15% higher than that of neat PP.

This improvement seems to be low compared to that achieved in PP composites with graphene or exfoliated graphite nanoplatelets, where approximately a 100% increase was obtained for composites with 5 wt.% of filler [41,49]; however, it should be taken into account that graphene is amongst the materials with the highest thermal conductivities, i.e. 5000 W/mK [50]. The filler presented in this work is highly heterogeneous (Figure 5.1) and, as observed by transmission electron microscopy [11], the fibre-like structures have voids or discontinuities in the centre. Therefore, it seems reasonable to assume that the thermal conductivity of the carbon microfiller to be lower than that of graphene or exfoliated graphite nanoplatelets. Nonetheless, based on our results, it can be said that the addition of the carbon microfiller results in PP composites with improved thermal conductivity, compared to neat PP.

Flexural and fracture characterization

Results obtained from the flexural characterization, performed by three-point bending tests, are presented in Figure 5.5. The stiffening effect of the carbon microfiller on the PP composites is clear as the flexural modulus exhibited approximately a linear increase with increasing the filler content. This effect is in agreement with the reinforcing effect obtained from the analysis of the storage modulus, in the rubbery state, by DMA (Annex A: Supplementary information). This effect could be explained in terms of a certain degree of mechanical interlocking between the polymer and the highly rough surface of the matrix, which improve the stress transfer from the matrix to the filler [8,9].

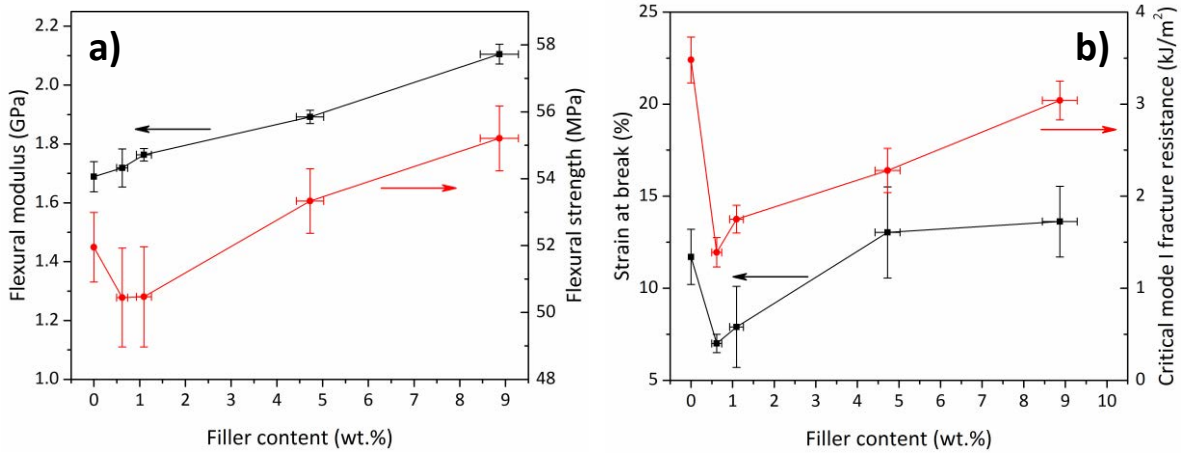

Figure 5.5 a) Flexural modulus and strength and b) strain at break, obtained from the flexural tests, and mode I fracture toughness of neat PP and CMF composites.

In the case of the flexural strength, the addition of a small amount of CMF, i.e. 0.6 and 1.1 wt.%, seems to have no or a somewhat detrimental effect. Nonetheless, for higher filler contents the flexural strength increased. The composite with 8.9 wt.% of CMF presented the best flexural properties, having an improvement in flexural modulus and strength of 25 and 7%, respectively, compared to neat PP.

The strain at break followed a trend similar to that of flexural strength. At filler contents of 0.6 and 1.1 wt.%, it drastically decreased. However, for the composites with 4.7 and 8.9 wt.% of CMF, the strain at break was slightly higher than that of neat PP. The obtained results are comparable to those obtained for PP/graphene composites [32], where a good dispersion of the filler was achieved.

The effect of the carbon microfiller on the fracture behaviour of the PP matrix was performed by testing single-edge notched specimens in a three-point bending configuration. The resistance of the polymer to slow stable crack grow after initiation from a sharp pre-crack, i.e. J-R curve, was obtained for PP and CMF composites. The value of J at a crack extension of 0.2 mm was taken as the critical mode I fracture resistance, J_{IC} [51]. The obtained results are shown in Figure 5.5b. As it can be observed, the J_{IC} follows the same trend as the strain at break, upon the addition of the carbon microfiller. This result was expected as the strain at break is a measure of the ductility of the samples, i.e. their ability to withstand plastic deformation until failure.

The fracture surfaces of neat PP and CMF composites were analysed by scanning electron microscopy. From the images taken at low magnification (Figure 5.6a, c and e), it was observed that neat PP exhibits features that indicates a certain degree of plastic deformation during the fracture process. In the CMF composites, the size of the fracture features decreases with increasing the filler content. Higher magnification images are shown in Figure 5.6b, d and f. These features (indicated by a dotted line in Figure 5.6b) may be indicative of a fracture mechanism consisting in the ductile tearing of polymer through spherulites [52]. In the case of the composite with 0.6 wt.% of CMF, the same failure mechanism was observed. However, the size of the features seemed to be more heterogeneous (indicated by a dotted line in Figure 5.6d), compared to the neat PP. The fracture surface of the composite with 8.9 wt.% of CMF, showed plastic deformation of the matrix; although no features similar to those in were observed (Figure 5.6f). The stretched polymeric fibrils attached to the surface of a carbon microfiller (Figure 5.7) are indicative of a strong interaction between the filler and the PP matrix, what could result in a mechanical interlocking effect.

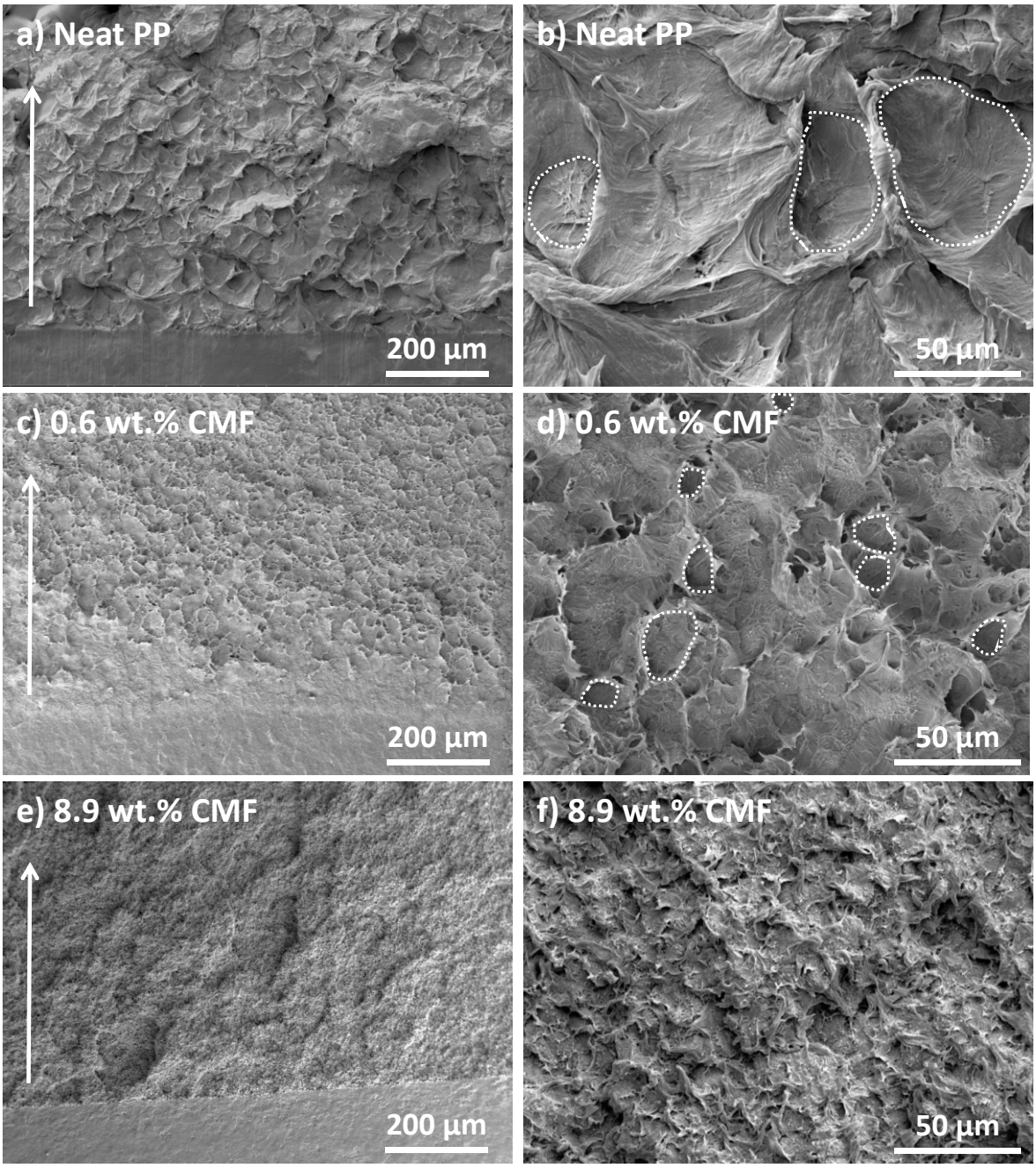

Figure 5.6 Fracture surfaces of a-b) neat PP and composites with c-d) 0.6 and e-f) 8.9 wt.% of carbon microfiller. The white arrow indicates the crack-growth direction. The characteristic features, which could be related to spherulites, are encircled by a dotted line.

As obtained by DSC, the CMF act as nucleating agent for the PP matrix. Although no new crystalline phases were nucleated (Figure 5.4b), the addition of CMF could alter the size of the crystallites of the PP in the composites [39,42]. It has been reported that the spherulite size affects the mechanical properties of PP [52–56]. Thus, it is clear that further work should be done to understand the effect of the

carbon microfiller on the crystalline morphology of PP and, therefore, fully understand the mechanical behaviour of the CMF composites.

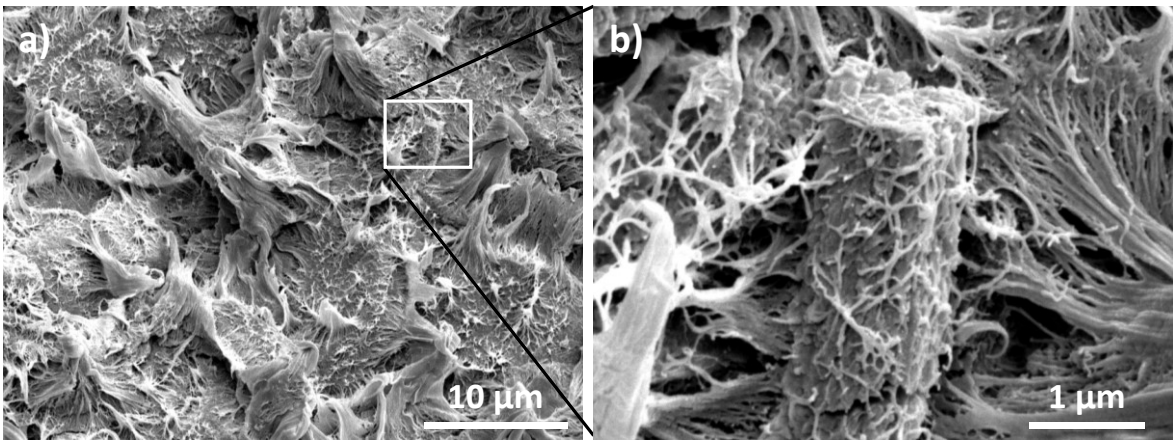

Figure 5.7 a) High magnification SEM image of the fracture surface of the composite with 8.9 wt.% of CMF. b) detailed image, of the inset in a), where stretched polymeric fibrils, attached to the CMF, could be observed.

5.4 Conclusions

In this work, the potential of a novel carbon microfiller to be used as filler for polypropylene composites is explored. From the analysis of the filler morphology it is clear that further characterization should be done to identify the different synthesised structures and how to control it by adjusting the parameters of the chemical vapour deposition process. Nonetheless, the synthesized carbon structures showed potential to be used as fillers for mechanical reinforcing of polymeric matrices.

The composites were produced by preparing and diluting a masterbatch through melt mixing. This processing technique result in the break-up of the micron-sized fibre-like structures, which were obtained after the synthesis process. Furthermore, it proved to be effective for the processing of CMF composites, as the resulting carbon microfiller exhibited a good dispersion degree within the PP matrix.

The resulting composites exhibited enhanced thermal stability and flexural modulus, what could be due to the interaction between the polymer and the highly rough surface of the microfiller. It was found that the carbon microfiller improved

the thermal conductivity of the resulting composites and also acted as nucleating agent for the crystallization of PP, inducing a certain degree of orientation on the α crystallites, however the degree of crystallinity and the crystalline phase, as well as the amorphous region of the matrix were not affected by the filler.

Further characterization work would be required in order to identify the effect of the filler on the crystalline morphology and understand the plastic deformation behaviour (strain at break and fracture resistance) of the of CMF composites. This, along with the potential of the filler to be produced at large-scale, make the presented carbon microfiller composite a good candidate to be a commercially available polypropylene material with enhanced mechanical and thermal behaviour.

5.5 Acknowledgements

This work was supported by the European Commission under the 7th Framework Program, NFRP project (PICIG12-GA-2012-33924). R. G. V. gratefully acknowledges the Spanish Ministry of Science and Innovation for financial funding through the Ramon y Cajal Fellowship. L. C. H-R acknowledges the support from the Spanish Ministry of Education through the FPU programme (FPU14/06843).

5.6 References

[1] B.-X. Yang, J.-H. Shi, K.P. Pramoda, S.H. Goh, Enhancement of the mechanical properties of polypropylene using polypropylene-grafted multiwalled carbon nanotubes, Compos. Sci. Technol. 68 (2008) 2490–2497. doi:10.1016/j.compscitech.2008.05.001.

[2] M.Z. Rong, M.Q. Zhang, Y.X. Zheng, H.M. Zeng, R. Walter, K. Friedrich, Structure–property relationships of irradiation grafted nano-inorganic particle filled polypropylene composites, Polymer. 42 (2001) 167–183. doi:10.1016/S0032-3861(00)00325-6.

[3] C.-M. Chan, J. Wu, J.-X. Li, Y.-K. Cheung, Polypropylene/calcium carbonate nanocomposites, Polymer. 43 (2002) 2981–2992. doi:10.1016/S0032-3861(02)00120-9.

[4] G. Mittal, V. Dhand, K.Y. Rhee, S.-J. Park, W.R. Lee, A review on carbon nanotubes and graphene as fillers in reinforced polymer nanocomposites, J. Ind. Eng. Chem. 21 (2015) 11–25. doi:10.1016/j.jiec.2014.03.022.

[5] K.R. Paton, E. Varrla, C. Backes, R.J. Smith, U. Khan, A. O'Neill, C. Boland, M. Lotya, O.M. Istrate, P. King, T. Higgins, S. Barwich, P. May, P. Puczkarski, I. Ahmed, M. Moebius, H. Pettersson, E. Long, J. Coelho, S.E. O'Brien, E.K. McGuire, B.M. Sanchez, G.S. Duesberg, N. McEvoy, T.J. Pennycook, C. Downing, A. Crossley, V. Nicolosi, J.N. Coleman, Scalable production of large quantities of defect-free few-layer graphene by shear exfoliation in liquids, Nat. Mater. advance online publication (2014). doi:10.1038/nmat3944.

[6] M. Endo, T. Hayashi, Y.-A. Kim, Large-scale production of carbon nanotubes and their applications, Pure Appl. Chem. 78 (2009) 1703–1713. doi:10.1351/pac200678091703.

[7] Y.Z. Jin, C. Gao, W.K. Hsu, Y. Zhu, A. Huczko, M. Bystrzejewski, M. Roe, C.Y. Lee, S. Acquah, H. Kroto, D.R.M. Walton, Large-scale synthesis and characterization of carbon spheres prepared by direct pyrolysis of hydrocarbons, Carbon. 43 (2005) 1944–1953. doi:10.1016/j.carbon.2005.03.002.
[8] L.C. Herrera-Ramírez, P. Castell, J.P. Fernández-Blázquez, Á. Fernández, R. Guzmán de Villoria, How do graphite nanoplates affect the fracture toughness of polypropylene composites?, Compos. Sci. Technol. 111 (2015) 9–16. doi:10.1016/j.compscitech.2015.02.017.
[9] L.C. Herrera-Ramírez, P. Castell, M. Castillo-Rodríguez, Á. Fernández, R. Guzman de Villoria, The effect of a semi-industrial masterbatch process on the carbon nanotube agglomerates and its influence in the properties of thermoplastic carbon nanotube composites, J. Polym. Sci. Part B Polym. Phys. 55 (2017) 189–197. doi:10.1002/polb.24258.
[10] H. Karian, Handbook of Polypropylene and Polypropylene Composites, Revised and Expanded, CRC Press, 2003.
[11] P. Romero, I. Martin-Gullon, R. Guzman de Villoria, Temperature effect on the synthesis of multi-armed carbon fibres and core-shell nanoparticles by chemical vapor deposition on nickel powders, Submitt. Manuscr. (2017).
[12] A. Kumar, D.K. Chouhan, P.S. Alegaonkar, T.U. Patro, Graphene-like nanocarbon: An effective nanofiller for improving the mechanical and thermal properties of polymer at low weight fractions, Compos. Sci. Technol. 127 (2016) 79–87. doi:10.1016/j.compscitech.2016.02.028.
[13] M.A. Rafiee, J. Rafiee, Z. Wang, H. Song, Z.-Z. Yu, N. Koratkar, Enhanced Mechanical Properties of Nanocomposites at Low Graphene Content, ACS Nano. 3 (2009) 3884–3890. doi:10.1021/nn9010472.
[14] T. Ramanathan, A.A. Abdala, S. Stankovich, D.A. Dikin, M. Herrera-Alonso, R.D. Piner, D.H. Adamson, H.C. Schniepp, X. Chen, R.S. Ruoff, Functionalized graphene sheets for polymer nanocomposites, Nat. Nanotechnol. 3 (2008) 327–331.
[15] K. Prashantha, J. Soulestin, M.F. Lacrampe, P. Krawczak, G. Dupin, M. Claes, Masterbatch-based multi-walled carbon nanotube filled polypropylene nanocomposites: Assessment of rheological and mechanical properties, Compos. Sci. Technol. 69 (2009) 1756–1763. doi:10.1016/j.compscitech.2008.10.005.
[16] Y.-C. Li, G.-H. Chen, HDPE/expanded graphite nanocomposites prepared via masterbatch process, Polym. Eng. Sci. 47 (2007) 882–888.
[17] J. Li, X. Luo, X. Lin, Preparation and characterization of hollow glass microsphere reinforced poly(butylene succinate) composites, Mater. Des. 46 (2013) 902–909. doi:10.1016/j.matdes.2012.11.054.
[18] Pablo Romero Rodríguez, Synthesis of carbon nanomaterials by catalytic chemical vapor deposition: growth mechanisms on metal powders and foils, PhD Thesis, Universidad Carlos III de Madrid, 2017.
[19] P. Romero, R. Oro, M. Campos, J.M. Torralba, R. Guzman de Villoria, Simultaneous synthesis of vertically aligned carbon nanotubes and amorphous carbon thin films on stainless steel, Carbon. 82 (2015) 31–38. doi:10.1016/j.carbon.2014.10.020.
[20] ASTM D792-13, Standard Test Methods for Density and Specific Gravity (Relative Density) of Plastics by Displacement, ASTM International, West Conshohocken, PA, (2013). doi:10.1520/D0792.
[21] J.H. Lehman, M. Terrones, E. Mansfield, K.E. Hurst, V. Meunier, Evaluating the characteristics of multiwall carbon nanotubes, Carbon. 49 (2011) 2581–2602. doi:10.1016/j.carbon.2011.03.028.
[22] B. Scheibe, E. Borowiak-Palen, R.J. Kalenczuk, Oxidation and reduction of multiwalled carbon nanotubes — preparation and characterization, Mater. Charact. 61 (2010) 185–191. doi:10.1016/j.matchar.2009.11.008.
[23] A.C. Ferrari, D.M. Basko, Raman spectroscopy as a versatile tool for studying the properties of graphene, Nat. Nanotechnol. 8 (2013) 235–246. doi:10.1038/nnano.2013.46.
[24] R.A. DiLeo, B.J. Landi, R.P. Raffaelle, Purity assessment of multiwalled carbon nanotubes by Raman spectroscopy, J. Appl. Phys. 101 (2007) 064307. doi:10.1063/1.2712152.

[25] C. Vallés, I.A. Kinloch, R.J. Young, N.R. Wilson, J.P. Rourke, Graphene oxide and base-washed graphene oxide as reinforcements in PMMA nanocomposites, Compos. Sci. Technol. 88 (2013) 158–164. doi:10.1016/j.compscitech.2013.08.030.
[26] Y. Li, J. Zhu, S. Wei, J. Ryu, L. Sun, Z. Guo, Poly (propylene)/Graphene Nanoplatelet Nanocomposites: Melt Rheological Behavior and Thermal, Electrical, and Electronic Properties, Macromol. Chem. Phys. 212 (2011) 1951–1959.
[27] Y. Zhan, Y. Lei, F. Meng, J. Zhong, R. Zhao, X. Liu, Electrical, thermal, and mechanical properties of polyarylene ether nitriles/graphite nanosheets nanocomposites prepared by masterbatch route, J. Mater. Sci. 46 (2011) 824–831. doi:10.1007/s10853-010-4823-7.
[28] T.Y. Zhou, G.C.P. Tsui, J.Z. Liang, S.Y. Zou, C.Y. Tang, V. Mišković-Stanković, Thermal properties and thermal stability of PP/MWCNT composites, Compos. Part B Eng. 90 (2016) 107–114. doi:10.1016/j.compositesb.2015.12.013.
[29] A.K. Barick, D.K. Tripathy, Effect of nanofiber on material properties of vapor-grown carbon nanofiber reinforced thermoplastic polyurethane (TPU/CNF) nanocomposites prepared by melt compounding, Compos. Part Appl. Sci. Manuf. 41 (2010) 1471–1482. doi:10.1016/j.compositesa.2010.06.009.
[30] C.-C. Chu, K.L. White, P. Liu, X. Zhang, H.-J. Sue, Electrical conductivity and thermal stability of polypropylene containing well-dispersed multi-walled carbon nanotubes disentangled with exfoliated nanoplatelets, Carbon. 50 (2012) 4711–4721. doi:10.1016/j.carbon.2012.05.063.
[31] J. Yang, Y. Lin, J. Wang, M. Lai, J. Li, J. Liu, X. Tong, H. Cheng, Morphology, thermal stability, and dynamic mechanical properties of atactic polypropylene/carbon nanotube composites, J. Appl. Polym. Sci. 98 (2005) 1087–1091. doi:10.1002/app.21206.
[32] M.A. Milani, D. González, R. Quijada, N.R.S. Basso, M.L. Cerrada, D.S. Azambuja, G.B. Galland, Polypropylene/graphene nanosheet nanocomposites by in situ polymerization: Synthesis, characterization and fundamental properties, Compos. Sci. Technol. 84 (2013) 1–7. doi:10.1016/j.compscitech.2013.05.001.
[33] K. Wakabayashi, P.J. Brunner, J. Masuda, S.A. Hewlett, J.M. Torkelson, Polypropylene-graphite nanocomposites made by solid-state shear pulverization: Effects of significantly exfoliated, unmodified graphite content on physical, mechanical and electrical properties, Polymer. 51 (2010) 5525–5531. doi:10.1016/j.polymer.2010.09.007.
[34] T. Kashiwagi, E. Grulke, J. Hilding, R. Harris, W. Awad, J. Douglas, others, Thermal degradation and flammability properties of poly (propylene)/carbon nanotube composites, Macromol. Rapid Commun. 23 (2002) 761–765.
[35] A. Yasmin, I.M. Daniel, Mechanical and thermal properties of graphite platelet/epoxy composites, Polymer. 45 (2004) 8211–8219. doi:10.1016/j.polymer.2004.09.054.
[36] E. Logakis, E. Pollatos, C. Pandis, V. Peoglos, I. Zuburtikudis, C.G. Delides, A. Vatalis, M. Gjoka, E. Syskakis, K. Viras, P. Pissis, Structure–property relationships in isotactic polypropylene/multi-walled carbon nanotubes nanocomposites, Compos. Sci. Technol. 70 (2010) 328–335. doi:10.1016/j.compscitech.2009.10.023.
[37] K.P. Ryan, M. Cadek, V. Nicolosi, D. Blond, M. Ruether, G. Armstrong, H. Swan, A. Fonseca, J.B. Nagy, W.K. Maser, W.J. Blau, J.N. Coleman, Carbon nanotubes for reinforcement of plastics? A case study with poly(vinyl alcohol), Compos. Sci. Technol. 67 (2007) 1640–1649. doi:10.1016/j.compscitech.2006.07.006.
[38] J. Brandrup, E.H. Immergut, E.A. Grulke, A. Abe, D.R. Bloch, Polymer handbook, Wiley New York, 1999.
[39] K. Kalaitzidou, H. Fukushima, P. Askeland, L.T. Drzal, The nucleating effect of exfoliated graphite nanoplatelets and their influence on the crystal structure and electrical conductivity of polypropylene nanocomposites, J. Mater. Sci. 43 (2008) 2895–2907. doi:10.1007/s10853-007-1876-3.
[40] H. Zhang, Z. Zhang, Impact behaviour of polypropylene filled with multi-walled carbon nanotubes, Eur. Polym. J. 43 (2007) 3197–3207. doi:10.1016/j.eurpolymj.2007.05.010.
[41] P. Song, Z. Cao, Y. Cai, L. Zhao, Z. Fang, S. Fu, Fabrication of exfoliated graphene-based polypropylene nanocomposites with enhanced mechanical and thermal properties, Polymer. 52 (2011) 4001–4010. doi:10.1016/j.polymer.2011.06.045.
[42] M. Ganß, B.K. Satapathy, M. Thunga, R. Weidisch, P. Pötschke, D. Jehnichen, Structural interpretations of deformation and fracture behavior of polypropylene/multi-walled

carbon nanotube composites, Acta Mater. 56 (2008) 2247–2261. doi:10.1016/j.actamat.2008.01.010.
[43] S. Brückner, S.V. Meille, V. Petraccone, B. Pirozzi, Polymorphism in isotactic polypropylene, Prog. Polym. Sci. 16 (1991) 361–404. doi:10.1016/0079-6700(91)90023-E.
[44] F. Rybnikář, Orientation in composite of polypropylene and talc, J. Appl. Polym. Sci. 38 (1989) 1479–1490. doi:10.1002/app.1989.070380806.
[45] H. Xia, Q. Wang, K. Li, G.-H. Hu, Preparation of polypropylene/carbon nanotube composite powder with a solid-state mechanochemical pulverization process, J. Appl. Polym. Sci. 93 (2004) 378–386. doi:10.1002/app.20435.
[46] M. Cook, J.F. Harper, The influence of magnesium hydroxide morphology on the crystallinity and properties of filled polypropylene, Adv. Polym. Technol. 17 (1998) 53–62. doi:10.1002/(SICI)1098-2329(199821)17:1<53::AID-ADV5>3.0.CO;2-H.
[47] C. Jourdan, J.Y. Cavaille, J. Perez, Mechanical relaxations in polypropylene: A new experimental and theoretical approach, J. Polym. Sci. Part B Polym. Phys. 27 (1989) 2361–2384. doi:10.1002/polb.1989.090271115.
[48] J. Arranz-Andrés, B. Peña, R. Benavente, E. Pérez, M.L. Cerrada, Influence of isotacticity and molecular weight on the properties of metallocenic isotactic polypropylene, Eur. Polym. J. 43 (2007) 2357–2370. doi:10.1016/j.eurpolymj.2007.03.034.
[49] K. Kalaitzidou, H. Fukushima, L.T. Drzal, Multifunctional polypropylene composites produced by incorporation of exfoliated graphite nanoplatelets, Carbon. 45 (2007) 1446–1452. doi:10.1016/j.carbon.2007.03.029.
[50] A.A. Balandin, S. Ghosh, W. Bao, I. Calizo, D. Teweldebrhan, F. Miao, C.N. Lau, Superior Thermal Conductivity of Single-Layer Graphene, Nano Lett. 8 (2008) 902–907. doi:10.1021/nl0731872.
[51] G.E. Hale, F. Ramsteiner, J-Fracture toughness of polymers at slow speed, in: D.R. Moore, A. Pavan, J.G. Williams (Eds.), Eur. Struct. Integr. Soc., Elsevier, 2001: pp. 123–157.
[52] J.L. Way, J.R. Atkinson, J. Nutting, The effect of spherulite size on the fracture morphology of polypropylene, J. Mater. Sci. 9 (1974) 293–299. doi:10.1007/BF00550954.
[53] T. Xu, J. Yu, Z. Jin, Effects of crystalline morphology on the impact behavior of polypropylene, Mater. Des. 22 (2001) 27–31. doi:10.1016/S0261-3069(00)00033-9.
[54] A. van der Wal, J.J. Mulder, R.J. Gaymans, Fracture of polypropylene: The effect of crystallinity, Polymer. 39 (1998) 5477–5481. doi:10.1016/S0032-3861(97)10279-8.
[55] M. Ouederni, P.J. Phillips, Influence of morphology on the fracture toughness of isotactic polypropylene, J. Polym. Sci. Part B Polym. Phys. 33 (1995) 1313–1322.
[56] K. Friedrich, Strength and fracture of crystalline isotactic polypropylene and the effect of molecular and morphological parameters, in: Anwendungsbezogene Phys. Charakt. Von Polym. Insbes. Im Festen Zustand, Springer, 1979: pp. 299–309.

6 Alumina nanoparticle/carbon nanotube hybrid filler and its application to epoxy composites

6.1 Introduction

High performance polymer nanocomposites are focusing a vast amount of research effort due to their potential to develop novel functionalities and, thus, satisfy the demand of industries, such the aerospace, for materials with sensing and actuating abilities, while maintaining their structural integrity [1].

Epoxy resins have been extensively used as matrix in polymer composites due to their high specific strength and stiffness, chemical stability, low cost an ease of processing [2,3]. However, their main drawbacks are their electrical and thermal insulating behaviour and low fracture toughness. An approach followed to overcome these problems was the development of epoxy-based nanocomposites with different fillers, depending on which properties need to be improved [4–6]. Regarding the fracture toughness of epoxy, it has been demonstrated that significant mechanical properties improvements are achieved by adding rigid nanoparticles [7–9]. Generally, these rigid particles are made of metal oxides, as alumina or silica. Moreover, in the case of alumina, since it has a higher thermal conductivity (30 W/mK [10]), than the polymer matrix (0.1-1 W/mK [11]), the addition of alumina nanoparticles to a polymeric matrix results in composites with improved thermal conductivity [12,13]. However, the resulting composites are electrically insulating.

Carbon nanotubes (CNTs) have been extensively used as fillers to obtain electrically conductive polymer-matrix composites, due to their outstanding electrical, thermal and mechanical properties [6,14,15]. Nonetheless, one of the main challenges in the processing of CNT composites is to achieve the required dispersion degree and interfacial CNT-matrix to fully harness the properties of the CNTs [16].

When a desired combination of properties is needed, two different materials, with a determined shape and size, can be combined to obtain a single hybrid filler [17]. The effects of the hybrid fillers can be observed on improved electrical [18–20], thermal [21,22] and mechanical [18,21,23] properties, or new functionalities as self-sensing behaviour [24,25]. The development of hybrid fillers resulting from the combination of CNTs attached to fibres [26], platelets [23,27] or particles [28,29] has proved to be an effective approach to avoid the agglomeration of CNTs, achieving an homogeneous CNT dispersion within the matrix and strengthening the interaction between the filler, to which CNTs are attached, and the matrix.

Another advantage of using hybrid fillers is the reported synergistic effect on the formation of a conducting thermal and electrical network through the composite, compared to the composites with the single fillers [30,31]. However, there is scarce literature reporting nano-scaled hybrid fillers [32], being most of the available literature focused on multi-scaled hybrid fillers consisting in CNTs grafted on micron-sized platelets [23,27], in-plane size in the range of microns, or micron-scaled particles [28,29].

Thus, in this work, we report the development of a hybrid material consisting in alumina nanoparticles surrounded by an entangled network of CNTs. This is achieved by pre-treating the nanoparticles with a catalyst precursor by a cost-effective method [26], followed by a chemical vapour deposition process to synthesize the CNTs. The resulting hybrid filler was dispersed in the epoxy matrix by three-roll milling, as it has been identified as an effective approach to disperse relatively high amounts of CNTs in thermosetting resins [33].

The resulting composites showed a slightly enhanced interaction of the hybrid filler with the matrix, i.e. composites with higher T_g, compared to the plain nanoparticles without carbon nanotubes. The mechanical properties were similar to that of the composite with alumina nanoparticles. However, the electrical conductivity was enhanced to $1 \pm 0.3 \times 10^{-3}$ S/m and the thermal conductivity a 7.4%, compared to neat epoxy, for the composite with 5 wt.% of hybrid nanoparticles, which corresponds to a carbon nanotube content of 1 wt.%. Therefore, this work shows the potential to develop nano-scaled hybrid materials

to be used as fillers for polymer composites with desired thermal or electrical properties.

6.2 Experimental procedure

6.2.1 Synthesis of hybrid material

Alumina spherical nanoparticles, (NanoDur, Nanophase Technologies Corporation) were used as substrate for the synthesis of carbon nanotubes and as filler for epoxy nanocomposites. The nanoparticles are crystalline and non-porous, with an average particle size of 50 nm and a specific surface area of 30 m^2/g. Iron nitrate nonahydrate ($Fe(NO_3)_3 \cdot 9H_2O$) (Sigma-Aldrich, >98% purity) was used as catalyst precursor for the synthesis of carbon nanotubes.

The as-received nanoparticles (NPs) were treated with the catalyst precursor by applying a scalable low-cost method, proposed in [26]. The powdery nanoparticles (0.025 g) were added to a solution (500 ml) of iron nitrate dissolved in 2-propanol, with a concentration of 50 mM, followed by sonication for 15 min and mechanical mixing for 2 hours. The resulting mixture was filtered overnight and dried at 150°C for 3 hours.

For the carbon nanotube synthesis, 0.5 g of nanoparticles treated with the catalyst precursor were loaded in an alumina boat, which was placed in the centre of a quartz tube. Heated by a mobile horizontal tube furnace. Further explanation of the chemical vapour deposition system can be found elsewhere [34]. In first place, the furnace is purged with 1000 sccm (sccm stands for cm^3/min at a standard temperature and pressure) of Ar for 5 min. After purging, the pre-treatment of the catalyst precursor is performed to create nanoscale clusters that would act as catalyst for the CNT growth at a temperature. The pre-treatment step involved setting a flow of 400 sccm of H_2 and 100 sccm of Ar, while moving the furnace, at a temperature of 650°C, so that the alumina boat could be heated. After the pre-treatment, the CNT growth was initiated by setting a flow of 100 sccm of H_2, 400 sccm of Ar and 200 sccm of C_2H_4, for 2 minutes. After this process, the furnace was cooled down under a flow of 1000 sccm of Ar. The material was obtained after this

process, consisting in alumina nanoparticles and carbon nanotubes, is referred to as hybrid nanoparticles (h-NPs).

6.2.2 Preparation of nanocomposites

The resin used as matrix in this work was a mono-component epoxy system (HexFlow RTM6, Hexcel Corporation) designed for resin transfer moulding and infusion processes in the aerospace industry. The technique chosen to disperse the as-synthesized hybrid nanoparticles in the epoxy resin was the three-roll milling (Exakt 80E, Germany). Afterwards, the resulting mixture was heated to 90°C to decrease its viscosity and then degassed for 1 hour. The degassed mixture was poured into steel moulds and cured for 2 hours at 180°C, as recommended by the manufacturer.

6.2.3 Characterization of fillers

Morphology

The as-received nanoparticles and the as-synthesized hybrid nanoparticles were analysed by scanning (field emission gun-SEM Helios NanoLab 600i, FEI) and transmission electron microscopy (Talos F200X, FEI). The elemental composition of the as-received NPs was confirmed by energy dispersive spectroscopy (EDS). For scanning electron microscopy (SEM) the NPs and h-NPs were lightly pressed onto an adhesive carbon tape. For transmission electron microscopy (TEM), a small amount of the hybrid material and as-received NPs was dispersed in isopropanol by means of an ultrasonic probe (VC 505 Ultrasonic processor), for 3 min and 1s pulse at 20% amplitude. A drop of the resulting solutions was carefully deposited on a TEM carbon coated Cu grid (LC300-Cu, EMS) and left to dry in a fume hood. The samples were viewed at an acceleration voltage of 200 kV.

Thermo-gravimetric analysis, Raman spectroscopy and BET surface area

The thermal stability of the as-received NPs and the thermal stability and carbon content of the h-NPs was studied using a thermogravimetric analyser Q50 (TA Instruments). Approximately 10 mg of powdery nanomaterial were heated under air atmosphere, at a heating rate of 10°C/min from room temperature to 800°C.

Raman spectroscopy was carried out using a Micro-Raman spectrometer Renishaw PLC, equipped with a DPSS Nd:YAG green laser (532 nm wavelength). The as-received NPs and the synthesized hybrid fillers were placed on thin aluminium foils and three measurements were performed per sample. Spectra were obtained for 10 s of exposure, 10 accumulations, in the range of 500-3500 cm-1 and at a laser power of 5%.

The specific surface area of the NPs and h-NPs were calculated by applying the BET (Brunauer-Emmett-Teller) method. The measurements of the isothermal adsorption of nitrogen at -196 °C were performed using a Gemini VII 2390 surface area analyser. Prior to the analysis, samples were subjected to a 120°C for 90 min to remove the adsorbed humidity.

6.2.4 Characterization of nanocomposites

Morphology, thermogravimetric analysis, differential scanning calorimetry and dynamic mechanical analysis

The morphology of the resulting composites was assessed by analysing the fracture surfaces of the tested specimens by scanning electron microscopy (Helios NanoLab 600i, FEI). The surfaces of the samples were sputter-coated with a thin layer of gold to avoid electrostatic charge of the sample during the analysis.

Thermo-gravimetric analysis (Q50, TA Instruments) was performed to study the thermal stability of the resulting nanocomposites. Samples (approximately 10 mg) were extracted from the cured specimens and heated at 10°C/min from room temperature to 800°C, under air atmosphere.

In this work, DSC was performed (DSC Q200, TA Instruments) to determine the degree of cure of the sample, α, as well as its glass transition temperature. During the measurements, the samples were heated from 20 to 310°C at a heating rate of 10°C/min, held at 310°C for 0.5 min and then cooled down to 20°C at a cooling rate of 10°C/min. Then, after being kept at 20°C during 0.5 min, the samples were heated to 310°C at a heating rate of 10°C/min. The degree of cure was calculated by applying the following equation [35]:

$$\alpha = 1 - \frac{\Delta H_r}{\Delta H_T} \qquad \text{Eq. 6.1}$$

Where ΔH_r is the residual heat of cure of the cured sample (obtained by integration of the exothermic peak in the first heating curve) obtained during the first heating curve, ΔH_T is the total enthalpy of the cure reaction, which was obtained from a cure process of an uncured sample in the DSC.

Dynamic mechanical analysis (DMA) were carried out by using specimens with dimensions of 17.5×12.7×3 mm^3 in single cantilever mode. The tests were performed on a Q800 (TA Instruments) in the temperature range from 20 to 270°C, at a frequency of 1 Hz, and a heating rate of 3°C/min.

Mechanical characterization of nanocomposites

Characterization of flexural properties was conducted under ambient conditions by using an Instron 5966, equipped with a 500 N load cell. At least four specimens of each composition were tested in a three-point bending configuration with 52 mm between supports. Tests were carried out at a cross-head speed of 2 mm/min.

The characterization of the fracture behaviour of nanocomposites was carried out at room temperature, using a Zwick universal testing machine with a 2.5 kN load cell. The tests were carried out following the ASTM D5045 standard. Single-edge-notch specimens, with dimensions of 50×8×4 mm^3 were loaded in three-point bending with a span-to-width ratio of 4 and a cross-head speed of 1 mm/min. The samples were pre-cracked before testing such that the ratio of specimen width to crack length was between 0.45 and 0.55, as specified in the standard.

Thermal and electrical conductivity measurement

The thermal conductivity of the resulting nanocomposites was measure at room temperature applying a transient plane source technique. For each filler content and neat resin at least three measurements were performed. Cylindrical shaped samples, with a diameter of 30 mm and a thickness of 3 mm, were measured in a hot disk thermal constants analyser TPS 2500 S (Hot Disk AB). In this technique, a thin heater/sensor, with a radius of 2.001 mm, was clamped between two identical samples. Then, the heater/sensor element was first used as a heat source to

increase the temperature of the surrounding sample by applying an output power of 0.01 W. Afterwards, the temperature increase was monitored over a period of time of 20 s by measuring the resistance of the heater/sensor. In order to minimize the effect of the interfacial thermal resistance, the surfaces of the cylindrical samples were polished. A detailed description of the transient plane source technique and its theoretical background can be found in [36].

To perform the DC electrical conductivity measurements, the disc-shaped specimens used for the thermal conductivity measurements were cut into 3×3×3 mm^3 parallelepiped samples. Two opposite faces were coated with silver paint as non-guarded electrodes. The voltage applied to the electrodes was increased from 15 to 40 V, and the slope of the intensity-voltage curve (Keithley SMU 2450 Graphical series SourceMeter) was fitted with the least-squares method. Electrical conductivity was calculated from the measured slope of the V-I curve and the sample dimensions.

6.3 Results

6.3.1 Characterization of hybrid nanoparticles

The morphology of the as-received nanoparticles and as-synthesized hybrid nanoparticles was analysed by SEM and TEM (Figure 6.1 and Annex B: Supplementary information). As it can be observed in the Figure 6.1a, the as-received NPs are in an agglomerated state (Annex B: Supplementary information). After the CVD process, the NPs remain agglomerated; however, the entangled network of synthesised CNTs can be observed (Figure 6.1a).

By TEM it was observed that the NPs have a spherical shape (Supplementary information), which they maintained after the CVD process (Figure 6.1c). It was also observed that the CNTs have grown forming an entangled network around the NPs. The synthesised CNTs were identified as multi-walled CNTs (Figure 6.1d).

It is worth noting that as the diameter of the spherical particles decrease from several hundreds of microns to several nanometres, the alignment of the CNTs

decrease and they are not attached to the surface of the particle due to their large curvature [37].

Form the thermogravimetric analysis (Annex B: Supplementary Information) it was obtained that the carbon content in the hybrid filler was approximately 20 wt.%.

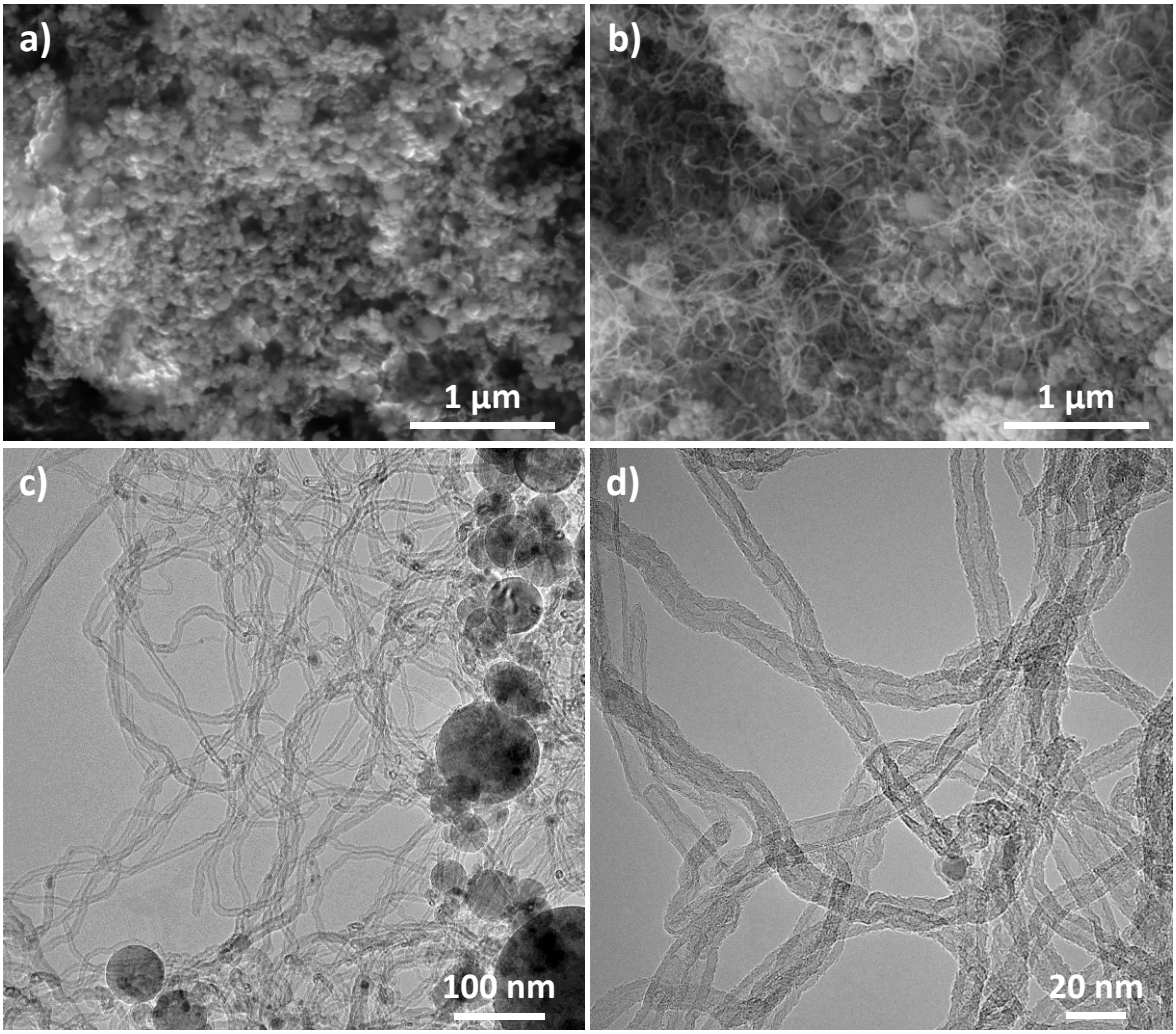

Figure 6.1 SEM images of the a) as-received alumina nanoparticles and b) hybrid nanoparticles, composed by alumina nanoparticles and carbon nanotubes, obtained after the CVD process. c) TEM image of the hybrid nanoparticles, d) higher magnification TEM image showing some carbon nanotubes synthesised by CVD process.

6.3.2 Characterization of nanocomposites

Nanocomposite processing

The morphology of the resulting nanocomposites was analysed by SEM of the fractured surfaces of processed samples (Figure 6.2 and Annex B: Supplementary information). It was found that for low fillers contents, i.e. of up to 2 wt.%, the dispersion degree of both the hybrid filler and the alumina nanoparticles were relatively homogeneous, as it can be observed for the 0.5 wt.% composites (Figure 6.2a and b). For the nanocomposites with 5 wt.% of NPs and h-NPs, agglomerates with a size in the range of several tenths of microns were observed (Figure 6.2c and d). However, the number of observed agglomerates was higher for the 5 wt.% h-NP composite than for the 5 wt.% NP composite.

Higher magnification SEM images of the NP and h-NPs are available in the Supplementary information. From the observation of these images the adhesion between the NPs and the matrix seems to be weak, as the nanoparticle seem to be debonded.

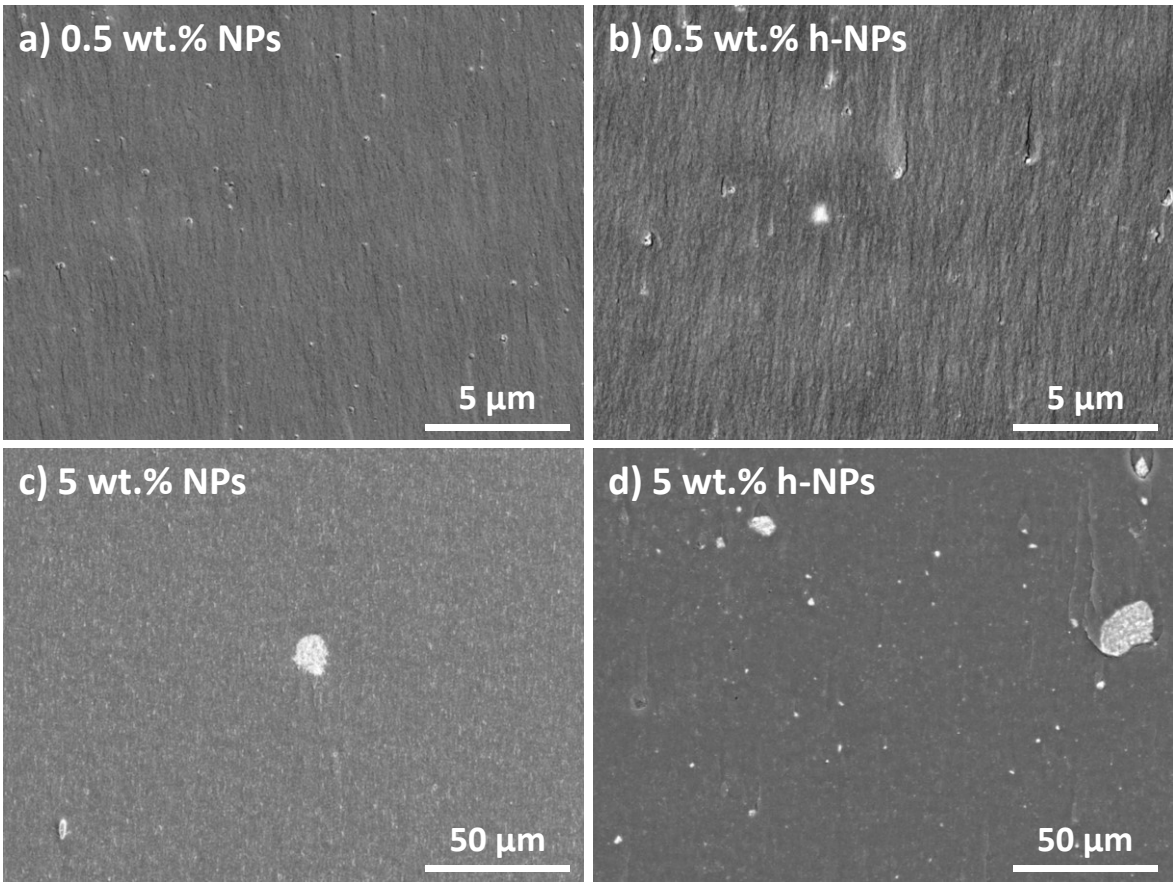

Figure 6.2 Low magnification SEM images of the nanocomposites with a 0.5 wt.% of a) NPs and b) h-NPs and with 5 wt.% of c) NPs and d) h-NPs, where the dispersion of the filler can be observed.

Thermogravimetric analysis

The effect of the addition of hybrid nanoparticles on the thermal stability in oxidant atmosphere of the epoxy resin was analysed by TGA (Figure 6.3) and compared with the results obtained for the NP composites. The onset of degradation of the neat resin takes place at 310°C and the temperature at which a weight loss of 5% takes place ($Td_{5\%}$) is 337°C. The decomposition process is divided in two steps, with their corresponding peaks in the first derivative of weight curve at 385°C and 568°C, respectively (Annex B: Supplementary information).

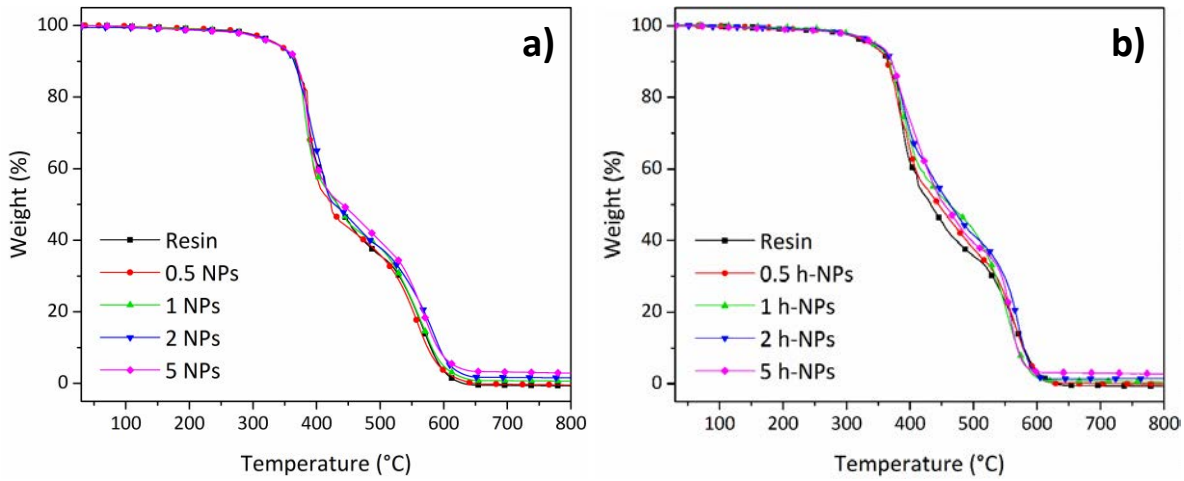

Figure 6.3 Curves obtained from the TGA, corresponding to the weight (%) of the neat resin and the a) NP and b) h-NP composites.

As it can be observed in Figure 6.3a and c and in the values listed in Table 6.1, the addition of the alumina nanoparticles has a slight detrimental effect on the thermal stability of the matrix of the resulting nanocomposites. This is in agreement with the results reported for epoxy composites with nanosized alumina particles that showed no [38–40] or a slight effect [41,42] of the nanofiller on the decomposition behaviour of the matrix. When the results obtained for the h-NPs composites were analysed, it was found that the decomposition behaviour of the epoxy matrix was somewhat improved. The $Td_{5\%}$ is 10 and 13°C higher than those of neat epoxy and 5 wt.% NP composite, respectively.

In [43,44] the addition of CNTs or CNFs to an epoxy resin resulted in nanocomposites with similar temperatures at the onset of degradation. In polymer composites with CNFs [45] and CNTs [46], the filler improved the thermal stability. This effect was attributed to the capture of free radicals, generated during the thermo-oxidation process, by the CNT surface. In this work, the stabilizing effect of the hybrid particles, likely due to the presence of CNTs, is reported. As proposed by Goyat *et al.* [47,48], the addition of nanofillers can also affect the thermal stability by changing the crosslinking degree or the thermal conductivity of the resulting composite; or by binding with the network side-chains. These parameters will be discussed in the following sections.

Table 6.1 Temperature at a loss of weight of 5 wt.% ($Td_{5\%}$) and residue left at 800°C by the neat resin and nanocomposites obtained from TGA; calculated filler content, degree of cure

and glass transition temperature of neat resin and composites obtained from the DSC curves.

Sample	$Td_{5\%}$ (°C)	Residue (wt.%)	Filler content (wt.%)	Degree of cure, α	Onset T_g , 1st heating (°C)
Resin	337	0.00	0.00	0.95	189
0.5 NPs	337	0.36	0.36	0.95	189
1 NPs	335	1.25	1.25	0.95	190
2 NPs	335	2.47	2.47	0.94	189
5 NPs	334	4.22	4.22	0.95	190
0.5 h-NPs	339	0.40	0.50	0.94	192
1 h-NPs	342	0.77	0.96	0.93	194
2 h-NPs	345	1.80	2.25	0.94	193
5 h-NPs	347	3.51	4.38	0.93	192

The amount of residue left after the TGA of composites was used to assess the amount of filler present in the nanocomposite. As obtained by TGA, the as-received NPs are thermally stable up to 900°C (Figure 6.3a), while the synthesized CNTs are completely oxidized at approximately 625°C. Thus, it has been assumed that the residue at 700°C corresponds exclusively to the NPs as at this temperature the resin left no measurable residue. The hybrid nanoparticles content was calculated taking into account that the NPs represent the 80 wt.% of the hybrid material. The obtained values are listed in Table 6.1. As it can be observed, the actual values of the filler content are close to the theoretical ones. For the sake of simplicity, the nanocomposites are named as per their theoretical amount of filler. Furthermore, the volume fractions of nanoparticles and carbon nanotubes on the resulting composites were calculated and are available in the Annex B: Supplementary information.

Differential scanning calorimetry

The DSC curves obtained in the first and second heating for the neat resin and the NP and h-NP composites are presented in the Annex B: Supplementary information.

As it can be observed in the graphs of the first heating (Annex B: Supplementary information), there is an exothermic peak for the neat resin and the nanocomposites, which is indicative of an incomplete cure of the sample [49]. The integration of the exothermic peak gives the residual heat of cure, ΔH_r. It was obtained that the total enthalpy of the cure reaction, at a heating rate of 10°C/min up to 310°C, of the neat epoxy resin was 457 J/g. The degree of cure of the resulting nanocomposites, as well as that of neat resin, was calculated in order to detect any possible effect of the filler on the result after the cure reaction (Table 6.1). It was obtained that the addition of the hybrid filler or the alumina nanoparticles to the epoxy resin does not significantly change the resulting cross-linking degree, determined by the degree of cure, of the composites after being processed following the cure cycle recommended by the manufacturer.

In the first heating curve, the endothermic shift in the heat flow curve, which is related with the glass transition of the resin, overlaps the exothermic cure peak. Thus, an exact value of the T_g from the first heating curve could not be obtained. However, it can be observed that the h-NPs composites exhibits a somewhat higher onset of T_g than the neat epoxy and the composites with as-received nanoparticles (Table 6.1).

The effect observed for the NP composites is in agreement with that reported for epoxy composites with alumina NPs [42], where the addition of up to 5 wt.% of NPs had no effect on the degree of cure. Furthermore, in the case of epoxy composites with alumina NPs [50], similar to those used in this work, the sample with 5 wt.% of filler exhibited the same T_g as the neat resin; and the DSC showed that the samples were completely cured.

In one hand, the shift of T_g to higher temperatures could be indicative of attractive matrix-particle interaction, which hinders the movement of polymer chains [51]. On the other hand, the shift of T_g to lower temperatures could be related with a reduced crosslinking degree of the epoxy matrix [48,52], an increase of the free volume of the resin [51] or particle agglomeration [53]. Thus, it can be said that in the NP composites obtained in this work, the nanoparticles does not have a strong interaction with the matrix.

In this work, the CNTs growth by the CVD process, comprised the 20 wt.% of the hybrid material, which possess with a specific surface area if 83 m^2/g, compared to 30 m^2/g of alumina nanoparticles (Annex B: Supplementary information). Thus, the increased values of the T_g of the h-NP composites compared to the NP composites could be attributed to the stronger interaction between the CNT and the matrix, than interaction between the NP and the matrix, and/or the increased specific surface area of the hybrid filler [9].

Dynamic mechanical analysis

The storage modulus and the tan δ of the NP and h-NP composites are shown in Figure 6.4a and b, respectively. The glass transition temperatures, obtained from the different curves are available in the Supplementary information. The values obtained from the storage modulus show a slight effect on T_g as the amount of hybrid filler increases, being the T_g of the 5 wt.% h-NP composite 3°C higher than that of the neat resin. If the glass transition obtained from the tan δ curves is analysed, no significant effect due to the addition of h-NPs is observed. In the case of the NP composites, no change in the different values of T_g is observed as the NP content increases. The trend followed by the T_g upon the addition of NPs or h-NPs is similar to that obtained by DSC.

The difference between the effect of the hybrid filler on the T_g values obtained from the E' or tan δ curves could be explained due to a weak interaction between the filler and the matrix. As the material approaches the T_g region (T_g onset) from lower temperatures, the presence of h-NPs seems to weakly restrict the movement of polymeric chains. However, when the material has reached certain temperature, i.e. T_g tan δ, polymer chains have energy enough to move, overcoming the hindering effect of the filler.

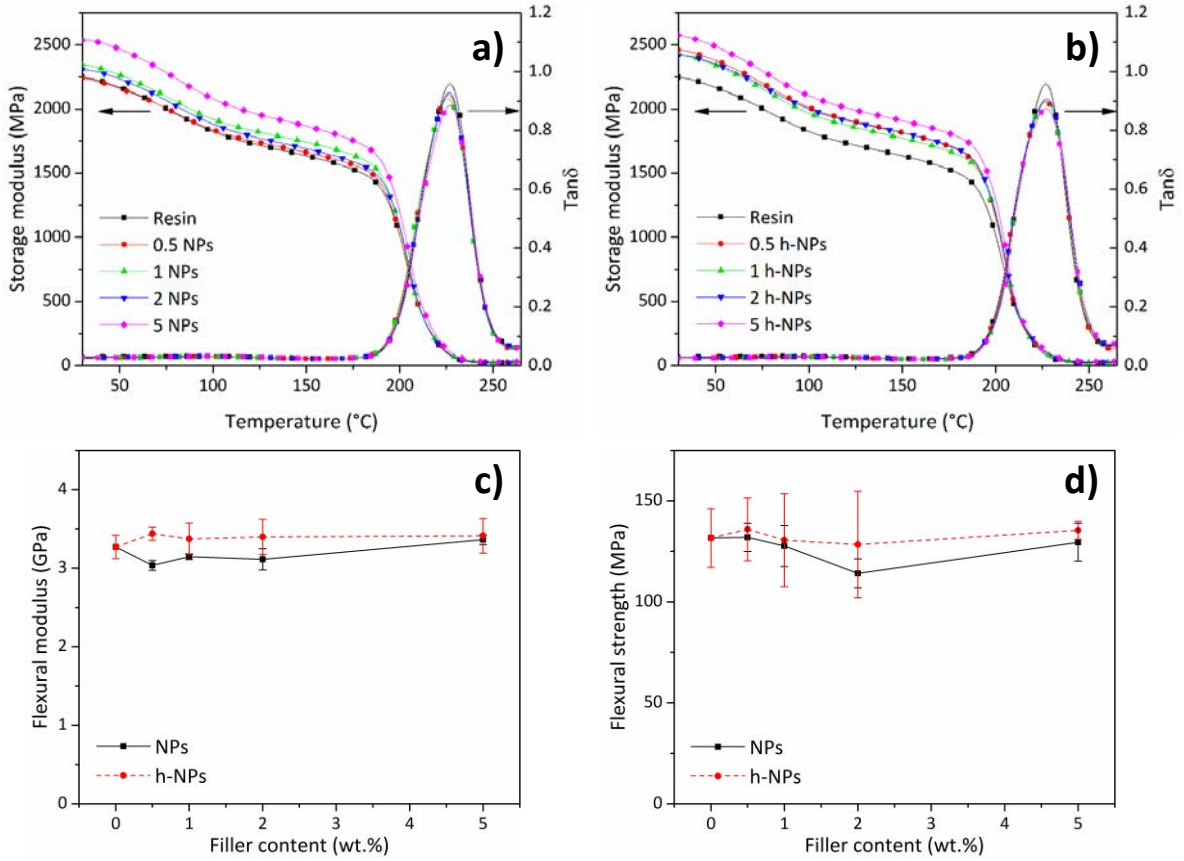

Figure 6.4 Storage modulus and tan δ (at a frequency of 1 Hz) of a) NP and b) h-NP composites as a function of the temperature. c) Flexural modulus and d) strength of NP and h-NP composites as a function of the filler content.

In the tan δ curve another peak apart from the T_g peak related with the α relaxation, can be observed in the range between 50 and 150°C (Annex B: Supplementary information). This peak is associated with a sub-T_g relaxation, known as as ω relaxation [54], due to molecular rearrangement of the crosslinked network due to the sorption of moisture [55]. As it can be observed, there is no effect of the NPs nor the h-NPs on the ω relaxation of the epoxy matrix. However, it is clear that the value of the tan δ is lower in the case of the NP and h-NP composites than in the neat matrix. The value of tan δ is related with the damping behaviour of the material [56]. The reduction found in this work is in agreement with the observed behaviour in composites with fillers that are relatively stiffer than the matrix [43,45,57].

Regarding the storage modulus, at temperatures below T_g onset E', the addition of h-NPs resulted in an increased modulus; being significantly higher the

improvement obtained for the 5 wt.% h-NP composite. In the case of the NP composites, the highest increase in E' was obtained for a 5 wt.% of NPs, while for the rest of composites a lower reinforcing effect was obtained. The reinforcing effect of both the NPs and h-NPs was expected from results obtained for epoxy composites with carbon nanomaterials [43,44], silica NPs [58] or alumina microparticles [57] and nanoparticles [59,60].

The results indicate that the reinforcing effect of the hybrid filler was stronger than the reinforcing effect of the alumina nanoparticles. A possible explanation for the more efficient reinforcing effect of the h-NPs than the NPs could be the somewhat stronger interaction of the hybrid material with the matrix, due to the CNTs. This would be in agreement with the results obtained from DSC.

Flexural properties

The results obtained from the flexural characterization of the h-NP and NP composites, by three-point bending tests, are shown in Figure 6.4c and d.

From the analysis of the flexural modulus (Figure 6.4c), it is obtained a behaviour similar to that found in the storage modulus by DMA. The stiffening effect of the filler is higher in the h-NP composites than in the NPs. The possible reasons to explain the higher stiffening effect of the hybrid filler could be the interaction between the filler and the matrix, as found by DMA and DSC; and/or the higher specific surface area of the hybrid filler compared to the as-received NPs. Lim *et al.* compared in [61] the effect of filler's shape on the resulting mechanical properties of epoxy/alumina nanoparticles composites. They found that for the nanocomposites with rod-shape particles with a mean diameter of 6 nm, but having the highest specific surface area, the modulus was unaffected up to a filler content of 2.5 wt.%. However, for the rest of fillers (10 nm platelet-shape and 12 nm rod shape), a considerable improvement was obtained at all filler contents. They attributed this effect to a higher efficiency in the stress transfer of the platelet-shaped filler than the rod-shaped filler. Therefore, the reduced stiffening effect of the NPs, compared to the h-NPs, could be explained in terms of a weak nanoparticle-matrix interaction, which results in a poor stress transfer. However,

it could be said that the flexural modulus is not significantly affected by the addition of alumina nanoparticles nor the hybrid material.

Furthermore, in the case of the flexural strength (Figure 6.4d) there is no difference between the NP and the h-NP composites, which have a similar behaviour to that of neat resin. The high dispersion of results may be due to the presence of agglomerates, localized heterogeneous dispersion of the filler or inappropriate preparation of the tested samples.

Fracture behaviour

The addition of hybrid nanoparticles to the epoxy resin resulted in composites with similar fracture behaviour than the NP composites, as shown in Figure 6.5, which is better than that of neat resin. However, it seems that the effect of the CNTs in the hybrid material is negligible during the fracture process of composites. In order to further understand this process, the fracture surfaces of the samples were analysed.

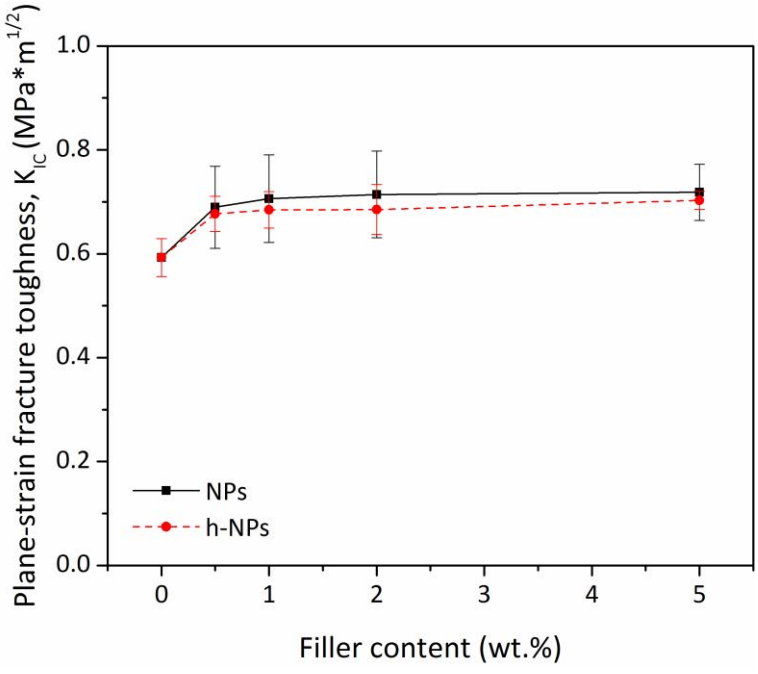

Figure 6.5 a) Mode I fracture toughness of NP and h-NP composites as a function of the filler content.

In Figure 6.6 are shown the SEM images of the fracture surfaces, in the region immediately ahead the pre-crack, of the neat resin and the composites with 5 wt.%

of NPs and h-NPs. At low magnification (Figure 6.6a, c and e), the neat resin and both types of composites exhibits a relatively plane surface. By analysing images at higher magnification (Figure 6.6b, e and f), it was observed that neat resin presents a mirror-like fracture, characterized by a smooth surface, which is the typical surface of a brittle fracture (Figure 6.6b) [50]. However, when the surfaces of the composites were analysed, an increased surface roughness was observed due to the presence of alumina nanoparticles, in the NP composites; and alumina nanoparticles and carbon nanotubes, in the h-NP composites. Thus, the increased fracture surface roughness seems to indicate that crack deflection is the main toughening mechanism in the resulting composites [50,62].

By further analysis of the fracture surfaces of the NP composites, the following toughening mechanisms were identified (Figure 6.7). The first mechanism was crack deflection/pinning, indicated with the number 1 in Figure 6.7. Crack pinning is identified by the tails. In a growing crack, when the crack front reaches a rigid particle, it cannot break the particle and it remains pinned, thus the crack bows out, creating secondary cracks. After passing the particles, the secondary cracks unify generating the tails [63]. The crack deflection was observed by an increase in the surface roughness when compared to the smooth surface of the resin (inset in Figure 6.6b). However, these mechanisms are not the main toughening mechanism as in the case of a nanofiller, their size is not the adequate to pin or mechanically interact, i.e. deflect, the growing crack [58,62]. Thus, the main toughening mechanism were identified to be particle debonding and plastic void growth (indicated by numbers 2 and 3, respectively, in Figure 6.7). The high stress state that takes place in the region ahead the crack tip is slightly released by the debonding of the rigid particles. The stress state is further released by void growth due to the plastic deformation of the matrix [7–9,62]. This mechanism absorbs higher energy, compared to the debonding.

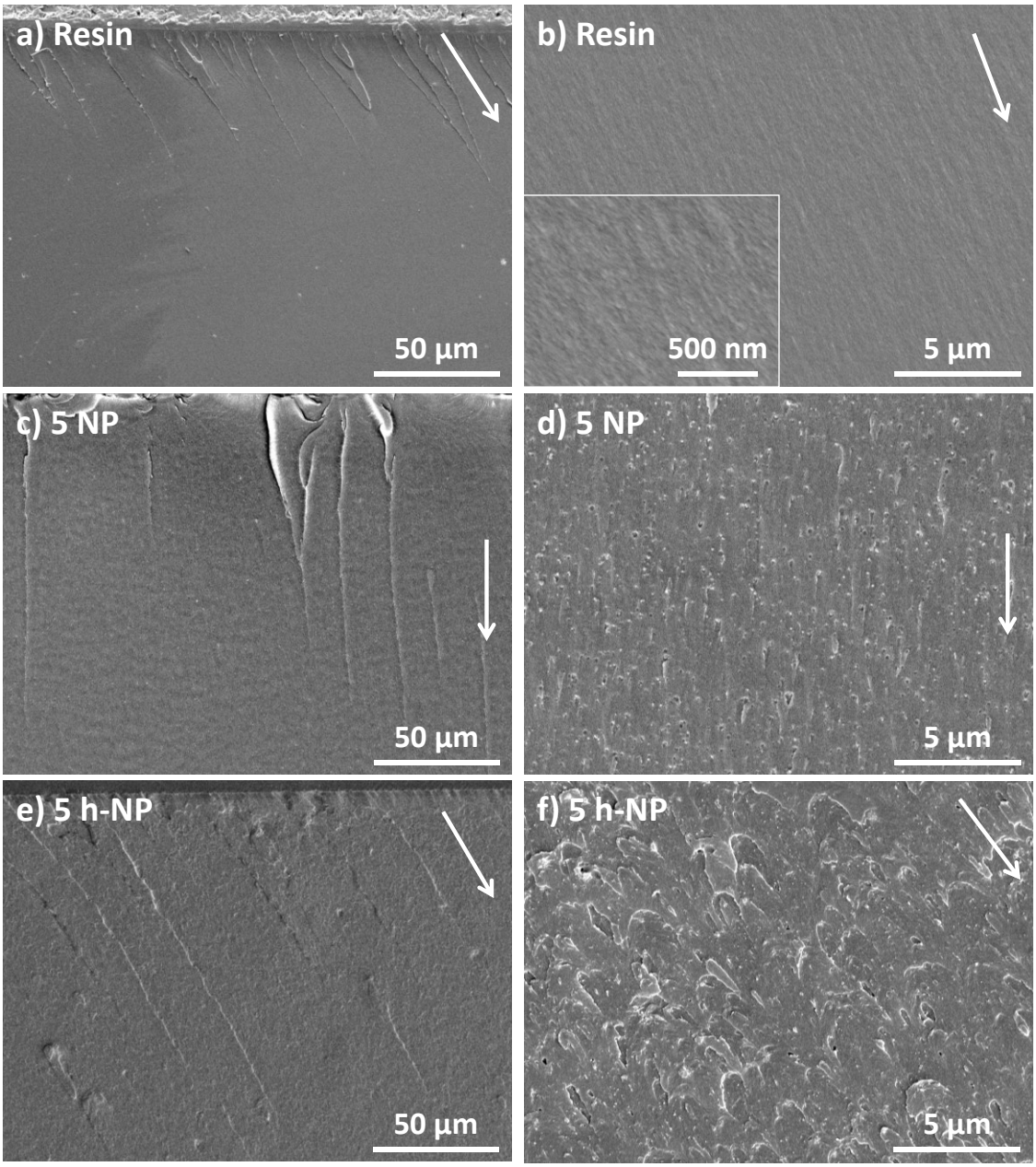

Figure 6.6 SEM images of the fracture surfaces of a-b) neat resin and the composites with 5 wt.% of c-d) nanoparticles and e-f) hybrid nanoparticles. The inset in b) shows a high magnification SEM image of the region showed in b). The white arrow indicate crack propagation direction. An increase in the fracture surface roughness of composites compared with the neat resin can be observed.

In the case of the h-NP composites, the main toughening mechanisms were found to be crack pinning and deflection, as shown in Figure 6.6f and Figure 6.7c. As in the NP composites, an increased surface roughness, compared to that of neat resin (inset in Figure 6.6b), can be observed. Additional toughening mechanism were particle debonding and void growth (numbers 2 and 3 in Figure 6.7d). Some CNTs could be observed in Figure 6.7c and d (indicated by dashed arrows). Mirjalili and

Hubert [64] found that no significant enhancement in fracture toughness can be achieved in composites with randomly dispersed CNTs at volume fractions lower than 2%. In this work the volume fraction of CNTs was calculated to be approximately 0.6% (Annex B: Supplementary information).Therefore, the negligible toughening effect of the CNTs reported in this work is in agreement with previously reported results [64].

The fracture behaviour of h-NP composites is dominated by the presence of alumina nanoparticles. For the same filler content, the h-NP composites have lower amount of alumina nanoparticles than the NP composites. Therefore, the overall fracture behaviour of h-NPs composites is similar to that of the composites with NPs, having higher values of fracture toughness than neat resin at all filler contents.

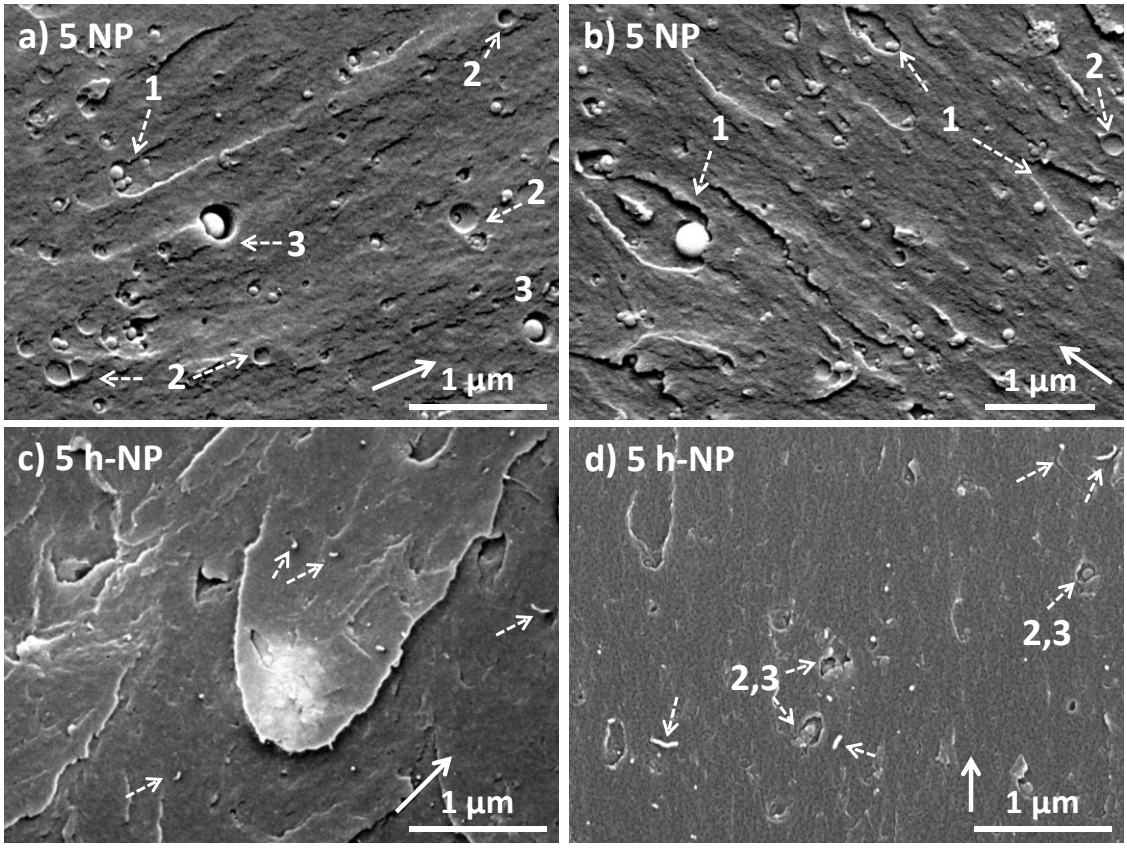

Figure 6.7 High magnification SEM images of the fracture surfaces of composites with 5 wt.% of a-b) NPs and c-d) h-NPs. The white solid arrows, near the scale, indicate crack growth direction. The toughening mechanism consisting in crack deflection (surface roughness), crack pinning (1), particle debonding (2), plastic void growth (3). CNTs can be observed in c and d) indicated by dashed arrows.

Thermal and electrical conductivity

The thermal conductivity of the NP and h-NP composites were analysed (Figure 6.8) by the hot disk technique. The thermal conductivity of alumina is k_{NP}=30 W/mK [10], while CNTs are supposed to have a thermal conductivity, k_{CNT}, between 2000 and 3000 W/mK [14], which are relatively higher than that found in this work for neat resin, k_m=0.23 W/mK. Thus, the addition of NPs and h-NPs is expected to result in composites with an increased thermal conductivity. If the results of the NP and h-NPs are compared, it seems that the thermal conductivities of the later are somewhat higher that the former, likely due to the presence of CNTs. For a filler content of 5 wt.% of NPs and h-NPs, the thermal conductivity increase a 5.1 and 7.4%, respectively, compared to the neat resin. However, the obtained results showed only slight improvements for high filler contents. In [21], it was reported a 20% increment in the thermal conductivity for an epoxy filled with 5 wt.% of hybrid alumina/CNT. In this case, the hybrid consists in micron-sized particles with a CNT content of *ca.* 12 wt.% [28]. A possible explanation for the low values of thermal conductivity obtained may be due to the reduced size of the filler that results in a higher surface area, which has an associated interfacial thermal resistance, than in the case of micron-sized fillers [11].

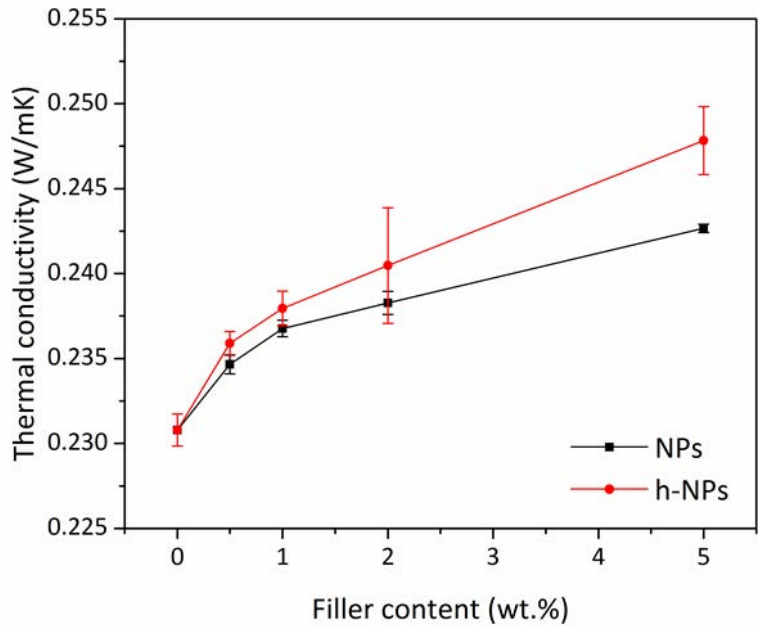

Figure 6.8 Thermal conductivity of NP and h-NP composites as a function of the filler content.

The electrical conductivity of the neat resin, the NP composites and the h-NP composites up to 2 wt.% filler was lower than 1×10^{-7} S/m, which is the minimum value that can be measured with the equipment and the sample dimensions used. However, for the 5 wt.% h-NP composite a conductivity of $1 \pm 0.3 \times 10^{-3}$ S/m. Thus, it was found that the percolation threshold of the h-NP composites was between 2 and 5 wt.% of hybrid filler. If the results obtained from the TGA of the hybrid filler are taken into account, it could be said that the percolation threshold is between 0.4 and 1 wt.% of CNTs or 0.24 and 0.58 vol.% of CNTs (Annex B: Supplementary information).

6.4 Conclusions

An approach to develop a nano-scaled hybrid material is reported in this work. The approach consists in treating the as-received nanoparticles with a catalyst precursor by a low-cost method, followed by a chemical vapour deposition process. This approach allows the direct synthesis of an entangled network of carbon nanotubes surrounding the alumina nanoparticles. The amount and characteristics of the resulting CNTs can be tuned by adjusting the parameters of the CVD process.

It was obtained that the resulting hybrid filler had a somewhat better interaction with the matrix, compared to the interaction between the as-received nanoparticles and the epoxy. This effect was observed in the slight shift to higher temperatures of the T_g. Furthermore, the h-NPs did not modify the processing of the epoxy resin, as after following the cure cycle recommended by the manufacturer, the degree of cure was the similar to that of the neat epoxy. The enhanced filler-matrix interaction in the h-NP composites was pointed as the responsible for the stabilizing effect on the thermal decomposition of nanocomposites.

Regarding the mechanical properties, the hybrid nanoparticles exhibited a slightly better stiffening effect than the as-received nanoparticles. However, the effect of the hybrid nanomaterial and the alumina nanoparticles on the flexural properties of the epoxy matrix was not significant.

The increase in the fracture toughness, compared to the neat epoxy, were similar for both nanocomposites. However, it seems that the toughening mechanisms that took place during the fracture process of the composites changed from the NP to the h-NP composites. Being the particle debonding and plastic void growth the main mechanism in the NP composites; and crack pinning and deflection in the h-NP composites.

The nanocomposites with 5 wt.% of h-NPs exhibited higher thermal conductivity than the nanocomposites with the same content of NPs, and an electrical conductivity of $1 \pm 0.3 \times 10^{-3}$ S/m, while the later remained as insulators.

Therefore, the results obtained in this work showed the potential to develop nano-scaled hybrid materials to be used as fillers for composite materials with improved mechanical, thermal and electrical properties. However, further work should be done to improve the mechanical reinforcing efficiency and the formation of a thermally and electrically conducting network through the matrix.

6.5 Acknowledgements

This work was supported by the European Commission under the 7th Framework Program, NFRP project (PICIG12-GA-2012-33924). R. G. V. gratefully acknowledges the Spanish Ministry of Science and Innovation for financial funding through the Ramon y Cajal Fellowship. L. C. H-R acknowledges the support from the Spanish Ministry of Education through the FPU programme (FPU14/06843).

6.6 References

[1] C. González, J.J. Vilatela, J.M. Molina-Aldareguía, C.S. Lopes, J. LLorca, Structural composites for multifunctional applications: Current challenges and future trends, Prog. Mater. Sci. 89 (2017) 194–251. doi:10.1016/j.pmatsci.2017.04.005.

[2] G.M. Odegard, A. Bandyopadhyay, Physical aging of epoxy polymers and their composites, J. Polym. Sci. Part B Polym. Phys. 49 (2011) 1695–1716. doi:10.1002/polb.22384.

[3] P. Mohan, A Critical Review: The Modification, Properties, and Applications of Epoxy Resins, Polym.-Plast. Technol. Eng. 52 (2013) 107–125. doi:10.1080/03602559.2012.727057.

[4] N. Domun, H. Hadavinia, T. Zhang, T. Sainsbury, G.H. Liaghat, S. Vahid, Improving the fracture toughness and the strength of epoxy using nanomaterials – a review of the current status, Nanoscale. 7 (2015) 10294–10329. doi:10.1039/C5NR01354B.

[5] H. Chen, V.V. Ginzburg, J. Yang, Y. Yang, W. Liu, Y. Huang, L. Du, B. Chen, Thermal conductivity of polymer-based composites: Fundamentals and applications, Prog. Polym. Sci. 59 (2016) 41–85. doi:10.1016/j.progpolymsci.2016.03.001.

[6] W. Bauhofer, J.Z. Kovacs, A review and analysis of electrical percolation in carbon nanotube polymer composites, Compos. Sci. Technol. 69 (2009) 1486–1498. doi:10.1016/j.compscitech.2008.06.018.
[7] T.H. Hsieh, A.J. Kinloch, K. Masania, A.C. Taylor, S. Sprenger, The mechanisms and mechanics of the toughening of epoxy polymers modified with silica nanoparticles, Polymer. 51 (2010) 6284–6294. doi:10.1016/j.polymer.2010.10.048.
[8] J.G. Williams, Particle toughening of polymers by plastic void growth, Compos. Sci. Technol. 70 (2010) 885–891. doi:10.1016/j.compscitech.2009.12.024.
[9] B. Wetzel, P. Rosso, F. Haupert, K. Friedrich, Epoxy nanocomposites – fracture and toughening mechanisms, Eng. Fract. Mech. 73 (2006) 2375–2398. doi:10.1016/j.engfracmech.2006.05.018.
[10] G. Wypych, 5 - PHYSICAL PROPERTIES OF FILLERS AND FILLED MATERIALS, in: Handb. Fill. Fourth Ed., ChemTec Publishing, 2016: pp. 303–371. doi:10.1016/B978-1-895198-91-1.50007-5.
[11] H. Chen, V.V. Ginzburg, J. Yang, Y. Yang, W. Liu, Y. Huang, L. Du, B. Chen, Thermal conductivity of polymer-based composites: Fundamentals and applications, Prog. Polym. Sci. 59 (2016) 41–85. doi:10.1016/j.progpolymsci.2016.03.001.
[12] J.-F. Fu, L.-Y. Shi, Q.-D. Zhong, Y. Chen, L.-Y. Chen, Thermally conductive and electrically insulative nanocomposites based on hyperbranched epoxy and nano-Al2O3 particles modified epoxy resin, Polym. Adv. Technol. 22 (2011) 1032–1041. doi:10.1002/pat.1638.
[13] W. Zhou, S. Qi, C. Tu, H. Zhao, C. Wang, J. Kou, Effect of the particle size of Al2O3 on the properties of filled heat-conductive silicone rubber, J. Appl. Polym. Sci. 104 (2007) 1312–1318. doi:10.1002/app.25789.
[14] Z. Han, A. Fina, Thermal conductivity of carbon nanotubes and their polymer nanocomposites: A review, Prog. Polym. Sci. 36 (2011) 914–944. doi:10.1016/j.progpolymsci.2010.11.004.
[15] J.N. Coleman, U. Khan, W.J. Blau, Y.K. Gun'ko, Small but strong: a review of the mechanical properties of carbon nanotube–polymer composites, Carbon. 44 (2006) 1624–1652.
[16] P.-C. Ma, N.A. Siddiqui, G. Marom, J.-K. Kim, Dispersion and functionalization of carbon nanotubes for polymer-based nanocomposites: A review, Compos. Part Appl. Sci. Manuf. 41 (2010) 1345–1367. doi:10.1016/j.compositesa.2010.07.003.
[17] M.F. Ashby, Y.J.M. Bréchet, Designing hybrid materials, Acta Mater. 51 (2003) 5801–5821. doi:10.1016/S1359-6454(03)00441-5.
[18] M.R. Zakaria, H. Md. Akil, M.H. Abdul Kudus, A.H. Kadarman, Improving flexural and dielectric properties of MWCNT/epoxy nanocomposites by introducing advanced hybrid filler system, Compos. Struct. 132 (2015) 50–64. doi:10.1016/j.compstruct.2015.05.020.
[19] R.N. Othman, I.A. Kinloch, A.N. Wilkinson, Synthesis and characterisation of silica–carbon nanotube hybrid microparticles and their effect on the electrical properties of poly(vinyl alcohol) composites, Carbon. 60 (2013) 461–470. doi:10.1016/j.carbon.2013.04.062.
[20] L.C. Herrera-Ramírez, M. Cano, R. Guzman de Villoria, Low thermal and high electrical conductivity in hollow glass microspheres covered with carbon nanofiber–polymer composites, Compos. Sci. Technol. 151 (2017) 211–218. doi:10.1016/j.compscitech.2017.08.020.
[21] M.R. Zakaria, H.M. Akil, M.H.A. Kudus, S.S.M. Saleh, Enhancement of tensile and thermal properties of epoxy nanocomposites through chemical hybridization of carbon nanotubes and alumina, Compos. Part Appl. Sci. Manuf. 66 (2014) 109–116. doi:10.1016/j.compositesa.2014.07.008.
[22] M. Bozlar, D. He, J. Bai, Y. Chalopin, N. Mingo, S. Volz, Carbon Nanotube Microarchitectures for Enhanced Thermal Conduction at Ultralow Mass Fraction in Polymer Composites, Adv. Mater. 22 (2010) 1654–1658. doi:10.1002/adma.200901955.
[23] W. Li, A. Dichiara, J. Bai, Carbon nanotube–graphene nanoplatelet hybrids as high-performance multifunctional reinforcements in epoxy composites, Compos. Sci. Technol. 74 (2013) 221–227. doi:10.1016/j.compscitech.2012.11.015.
[24] H. Zhao, J. Bai, Highly Sensitive Piezo-Resistive Graphite Nanoplatelet–Carbon Nanotube Hybrids/Polydimethylsilicone Composites with Improved Conductive Network

Construction, ACS Appl. Mater. Interfaces. 7 (2015) 9652–9659. doi:10.1021/acsami.5b01413.
[25] W. Li, J. Yuan, A. Dichiara, Y. Lin, J. Bai, The use of vertically aligned carbon nanotubes grown on SiC for in situ sensing of elastic and plastic deformation in electrically percolative epoxy composites, Carbon. 50 (2012) 4298–4301. doi:10.1016/j.carbon.2012.05.011.
[26] N. Yamamoto, A. John Hart, E.J. Garcia, S.S. Wicks, H.M. Duong, A.H. Slocum, B.L. Wardle, High-yield growth and morphology control of aligned carbon nanotubes on ceramic fibers for multifunctional enhancement of structural composites, Carbon. 47 (2009) 551–560. doi:10.1016/j.carbon.2008.10.030.
[27] W.-D. Zhang, I.Y. Phang, T.X. Liu, Growth of Carbon Nanotubes on Clay: Unique Nanostructured Filler for High-Performance Polymer Nanocomposites, Adv. Mater. 18 (2006) 73–77. doi:10.1002/adma.200501217.
[28] M.H.A. Kudus, H.M. Akil, H. Mohamad, L.E. Loon, Effect of catalyst calcination temperature on the synthesis of MWCNT–alumina hybrid compound using methane decomposition method, J. Alloys Compd. 509 (2011) 2784–2788. doi:10.1016/j.jallcom.2010.11.099.
[29] D. He, M. Bozlar, M. Genestoux, J. Bai, Diameter- and length-dependent self-organizations of multi-walled carbon nanotubes on spherical alumina microparticles, Carbon. 48 (2010) 1159–1170. doi:10.1016/j.carbon.2009.11.039.
[30] S. Chatterjee, F. Nafezarefi, N.H. Tai, L. Schlagenhauf, F.A. Nüesch, B.T.T. Chu, Size and synergy effects of nanofiller hybrids including graphene nanoplatelets and carbon nanotubes in mechanical properties of epoxy composites, Carbon. 50 (2012) 5380–5386. doi:10.1016/j.carbon.2012.07.021.
[31] T. Wei, L. Song, C. Zheng, K. Wang, J. Yan, B. Shao, Z.-J. Fan, The synergy of a three filler combination in the conductivity of epoxy composites, Mater. Lett. 64 (2010) 2376–2379. doi:10.1016/j.matlet.2010.07.061.
[32] K. Yang, M. Gu, Enhanced thermal conductivity of epoxy nanocomposites filled with hybrid filler system of triethylenetetramine-functionalized multi-walled carbon nanotube/silane-modified nano-sized silicon carbide, Compos. Part Appl. Sci. Manuf. 41 (2010) 215–221. doi:10.1016/j.compositesa.2009.10.019.
[33] F.H. Gojny, M.H.G. Wichmann, U. Köpke, B. Fiedler, K. Schulte, Carbon nanotube-reinforced epoxy-composites: enhanced stiffness and fracture toughness at low nanotube content, Compos. Sci. Technol. 64 (2004) 2363–2371. doi:10.1016/j.compscitech.2004.04.002.
[34] P. Romero, R. Oro, M. Campos, J.M. Torralba, R. Guzman de Villoria, Simultaneous synthesis of vertically aligned carbon nanotubes and amorphous carbon thin films on stainless steel, Carbon. 82 (2015) 31–38. doi:10.1016/j.carbon.2014.10.020.
[35] J. Moosburger-Will, M. Greisel, M.G.R. Sause, R. Horny, S. Horn, Influence of partial cross-linking degree on basic physical properties of RTM6 epoxy resin, J. Appl. Polym. Sci. 130 (2013) 4338–4346. doi:10.1002/app.39722.
[36] S.E. Gustafsson, Transient plane source techniques for thermal conductivity and thermal diffusivity measurements of solid materials, Rev. Sci. Instrum. 62 (1991) 797.
[37] S. Agrawal, A. Kumar, M.J. Frederick, G. Ramanath, Hybrid Microstructures from Aligned Carbon Nanotubes and Silica Particles, Small. 1 (2005) 823–826. doi:10.1002/smll.200500023.
[38] W. Jiang, F.-L. Jin, S.-J. Park, Thermo-mechanical behaviors of epoxy resins reinforced with nano-Al2O3 particles, J. Ind. Eng. Chem. 18 (2012) 594–596. doi:10.1016/j.jiec.2011.11.140.
[39] F.-L. Jin, S.-J. Park, Thermal properties of epoxy resin/filler hybrid composites, Polym. Degrad. Stab. 97 (2012) 2148–2153. doi:10.1016/j.polymdegradstab.2012.08.015.
[40] Z. Guo, T. Pereira, O. Choi, Y. Wang, H.T. Hahn, Surface functionalized alumina nanoparticle filled polymeric nanocomposites with enhanced mechanical properties, J. Mater. Chem. 16 (2006) 2800. doi:10.1039/b603020c.
[41] A. Mohanty, V.K. Srivastava, Dielectric breakdown performance of alumina/epoxy resin nanocomposites under high voltage application, Mater. Des. 47 (2013) 711–716. doi:10.1016/j.matdes.2012.12.052.

[42] C.-H. Chen, J.-Y. Jian, F.-S. Yen, Preparation and characterization of epoxy/γ-aluminum oxide nanocomposites, Compos. Part Appl. Sci. Manuf. 40 (2009) 463–468. doi:10.1016/j.compositesa.2009.01.010.
[43] Y. Zhou, F. Pervin, L. Lewis, S. Jeelani, Experimental study on the thermal and mechanical properties of multi-walled carbon nanotube-reinforced epoxy, Mater. Sci. Eng. A. 452–453 (2007) 657–664. doi:10.1016/j.msea.2006.11.066.
[44] Y. Zhou, F. Pervin, V.K. Rangari, S. Jeelani, Fabrication and evaluation of carbon nano fiber filled carbon/epoxy composite, Mater. Sci. Eng. A. 426 (2006) 221–228. doi:10.1016/j.msea.2006.04.031.
[45] Y.-K. Choi, K. Sugimoto, S.-M. Song, Y. Gotoh, Y. Ohkoshi, M. Endo, Mechanical and physical properties of epoxy composites reinforced by vapor grown carbon nanofibers, Carbon. 43 (2005) 2199–2208. doi:10.1016/j.carbon.2005.03.036.
[46] C.-C. Chu, K.L. White, P. Liu, X. Zhang, H.-J. Sue, Electrical conductivity and thermal stability of polypropylene containing well-dispersed multi-walled carbon nanotubes disentangled with exfoliated nanoplatelets, Carbon. 50 (2012) 4711–4721. doi:10.1016/j.carbon.2012.05.063.
[47] M.S. Goyat, S. Suresh, S. Bahl, S. Halder, P.K. Ghosh, Thermomechanical response and toughening mechanisms of a carbon nano bead reinforced epoxy composite, Mater. Chem. Phys. (n.d.). doi:10.1016/j.matchemphys.2015.09.038.
[48] M.S. Goyat, S. Ray, P.K. Ghosh, Innovative application of ultrasonic mixing to produce homogeneously mixed nanoparticulate-epoxy composite of improved physical properties, Compos. Part Appl. Sci. Manuf. 42 (2011) 1421–1431. doi:10.1016/j.compositesa.2011.06.006.
[49] S. Mutlur, "Thermal Analysis of Composites Using DSC", Advanced Topics in Characterization of Composites, Trafford Publishing, Victoria, BC, Canada, 2004.
[50] S. Zhao, L.S. Schadler, R. Duncan, H. Hillborg, T. Auletta, Mechanisms leading to improved mechanical performance in nanoscale alumina filled epoxy, Compos. Sci. Technol. 68 (2008) 2965–2975. doi:10.1016/j.compscitech.2008.01.009.
[51] P. Rittigstein, J.M. Torkelson, Polymer–nanoparticle interfacial interactions in polymer nanocomposites: Confinement effects on glass transition temperature and suppression of physical aging, J. Polym. Sci. Part B Polym. Phys. 44 (2006) 2935–2943. doi:10.1002/polb.20925.
[52] J.D. Fidelus, E. Wiesel, F.H. Gojny, K. Schulte, H.D. Wagner, Thermo-mechanical properties of randomly oriented carbon/epoxy nanocomposites, Compos. Part Appl. Sci. Manuf. 36 (2005) 1555–1561. doi:10.1016/j.compositesa.2005.02.006.
[53] R. Qiao, H. Deng, K.W. Putz, L.C. Brinson, Effect of particle agglomeration and interphase on the glass transition temperature of polymer nanocomposites, J. Polym. Sci. Part B Polym. Phys. 49 (2011) 740–748. doi:10.1002/polb.22236.
[54] D. Colombini, J.J. Martinez-Vega, G. Merle, Influence of hydrothermal ageing and thermal treatments on the viscoelastic behavior of DGEBA-MCDEA epoxy resin, Polym. Bull. 48 (2002) 75–82. doi:10.1007/s00289-002-0009-z.
[55] W.J. Mikols, J.C. Seferis, A. Apicella, L. Nicolais, Evaluation of structural changes in epoxy systems by moisture sorption-desorption and dynamic mechanical studies, Polym. Compos. 3 (1982) 118–124. doi:10.1002/pc.750030304.
[56] R.L. Poveda, S. Achar, N. Gupta, Viscoelastic properties of carbon nanofiber reinforced multiscale syntactic foam, Compos. Part B Eng. 58 (2014) 208–216. doi:10.1016/j.compositesb.2013.10.079.
[57] L.M. McGrath, R.S. Parnas, S.H. King, J.L. Schroeder, D.A. Fischer, J.L. Lenhart, Investigation of the thermal, mechanical, and fracture properties of alumina–epoxy composites, Polymer. 49 (2008) 999–1014. doi:10.1016/j.polymer.2007.12.014.
[58] B.B. Johnsen, A.J. Kinloch, R.D. Mohammed, A.C. Taylor, S. Sprenger, Toughening mechanisms of nanoparticle-modified epoxy polymers, Polymer. 48 (2007) 530–541. doi:10.1016/j.polymer.2006.11.038.
[59] A. Omrani, A.A. Rostami, Understanding the effect of nano-Al2O3 addition upon the properties of epoxy-based hybrid composites, Mater. Sci. Eng. A. 517 (2009) 185–190. doi:10.1016/j.msea.2009.03.076.
[60] A. Omrani, L.C. Simon, A.A. Rostami, The effects of alumina nanoparticle on the properties of an epoxy resin system, Mater. Chem. Phys. 114 (2009) 145–150. doi:10.1016/j.matchemphys.2008.08.090.

[61] S.H. Lim, K.Y. Zeng, C.B. He, Morphology, tensile and fracture characteristics of epoxy-alumina nanocomposites, Mater. Sci. Eng. A. 527 (2010) 5670–5676. doi:10.1016/j.msea.2010.05.038.
[62] M. Quaresimin, M. Salviato, M. Zappalorto, 4 - Toughening mechanisms in nanoparticle polymer composites: experimental evidences and modeling, in: Q.Q. Ye (Ed.), Toughening Mech. Compos. Mater., Woodhead Publishing, 2015: pp. 113–133.
[63] F.F. Lange, The interaction of a crack front with a second-phase dispersion, Philos. Mag. 22 (1970) 0983–0992. doi:10.1080/14786437008221068.
[64] V. Mirjalili, P. Hubert, Modelling of the carbon nanotube bridging effect on the toughening of polymers and experimental verification, Compos. Sci. Technol. 70 (2010) 1537–1543. doi:10.1016/j.compscitech.2010.05.016.

7 Low thermal and high electrical conductivity in hollow glass microspheres covered with carbon nanofiber–polymer composites

7.1 Introduction

There is a need for high-performance polymers with high electrical and low thermal conductivity for aerospace, marine and energy applications. However, this combination of properties is really hard to obtain in a single material.

By adding conducting fillers [1–4] to a polymer matrix, the thermal and electrical conductivity of the resulting composite can be increased. Once these fillers form a conductive network within the polymeric matrix, the electrons can flow through the composite, increasing the thermal and electrical conductivity of the composite. When electrically insulating fillers are added to a polymer [5–8] the thermal conductivity of the composite is modified but not the electrical conductivity.

Opposed effects on the thermal and electrical conductivity can also be obtained by combining insulating and conducting fillers that are added to the matrix. By adding carbon-based nanomaterials and electrically insulating fillers to a polymer matrix; composites with improved thermal conductivity and high electrical resistivity are obtained [9–11]. This approach, based on the combination of fillers has been followed in the present work using hollow glass microspheres (HGMs) and carbon nanofibers.

Composites containing hollow glass microspheres (HGMs) are very attractive due to their light weight, high thermal stability, and low thermal conductivity [12–15]. Depending on the density (wall thickness) of the HGMs, stiffer composites can be obtained. However, as the interaction between the matrix and HGMs is generally poor, the resultant composites suffer reduced strength, compared with the raw matrix [16,17]. On the other hand, the addition of HGMs to a polymer, e.g., epoxy

resin, results in a material with the same electrically insulating behaviour as the matrix but with reduced thermal conductivity [8,12].

Carbon-based nanostructures, such as graphene, graphite nanoplates, graphite oxide, carbon nanofibers (CNFs) and nanotubes were extensively studied due to their outstanding mechanical, thermal and electrical properties, which make these nanosized structures ideal as nanofillers for aerospace or high-performance composites. To take advantage of both the low density and thermal conductivity of HGMs and the high mechanical and electrical conductivity of carbon-based nanofillers, both micro- and nano-sized fillers can be combined in a single composite material; for example, when 0.3 vol.% of CNFs is added to an epoxy composite with 50 vol.% of HGMs (0.46 g/cm^3), the tensile modulus and strength are increased by 10 and 29%, respectively, compared to the unmodified HGM composite [18]. For an epoxy composite with 10 wt.% of CNFs and 15 vol.% of HGMs (0.22 g/cm^3) the electrical resistance is reduced by 85% while the dielectric constant is increased by four orders of magnitude, compared to the neat resin [19]. The effect of CNFs on the viscoelastic properties [20], as well as on the degradation due to moisture exposure [21] or thermal expansion [22], was also studied.

Several groups have directly grown CNTs on micron-diameter fibres [23–25] and solid particles of different sizes and materials, such as alumina/iron oxide nanoparticles [26], ceramic spheres [27], alumina microparticles [28,29] or silica microparticles [30,31]. However, to our knowledge, there is scarce literature on the growth of carbon nanotubes or nanofibers on micron-scaled hollow glass spheres [32] and only the mechanical (compression) and thermomechanical (dynamic mechanical analysis) properties of the produced composites were characterized.

Here we present a method to develop a hybrid composite material with an unusual combination of properties such as improved electrical conductivity and low thermal conductivity. We tailored the composite properties by using a hybrid filler based on carbon nanofibers that were directly synthesized by chemical vapour deposition on micron-sized hollow glass spheres. We also compared our

experimental results with analytical models and found a good correlation between the results obtained from both approaches.

7.2 Methods

7.2.1 Synthesis of hybrid HGM-CNF particles

Carbon nanofibers were synthesized on the surface of hollow glass microspheres (K20 Glass bubbles, 3M) by means of a chemical vapour deposition process. The catalyst precursor for the growth of carbon nanofibers was iron nitrate nonahydrate ($Fe(NO_3)_3 \cdot 9H_2O$) (Sigma-Aldrich, >98% purity). To coat the surface with the catalyst precursor [24], the microspheres were added to a solution of 50 mM iron nitrate in isopropanol and mechanically mixed for 2 h. Then, the mixture was filtered for overnight and dried at 150°C for 3 h. After this process, the catalyst precursor-coated HGMs were stored until they were used as substrate for the growth of CNFs.

The treated microspheres were placed in an alumina boat, which was positioned in the middle of a quartz tube and heated by a mobile horizontal tube furnace that allows fast heating and cooling rates. A detailed explanation of the CVD system can be found elsewhere [33]. For the conditioning of the catalyst, the furnace was heated to 600°C and a flow of 100 sccm of H_2 and 400 sccm of Ar was passed through the quartz tube for 20 min. Afterwards, for the carbon nanofibers growth, the temperature was maintained at 600°C and a flow of 100 sccm of H_2, 400 sccm of Ar and 200 sccm of C_2H_4 was maintained for 20 min. After this process, the furnace was cooled down under a flow of 1000 sccm of Ar.

7.2.2 Composite preparation

The resin used as matrix for the preparation of composites was a high-temperature urethane acrylate resin (Crestapol 1234, Scott Bader Company Ltd.). Methyl-ethyl-ketone peroxide solution in diisobuthyl phthalate (Butanox LPT) was used as catalyst (2% by weight of resin) and a solution of cobalt octoate in styrene (Accelerator G) was used as accelerator (2% by weight of resin).

Composites containing 0, 2, 5 and 10 wt.% of HGM and the hybrid material, obtained by the CVD process (HGMs-CNFs), were produced. Resin, catalyst and accelerator were hand-mixed and degassed for 1 min. Then, the appropriate amount of filler was added to the resin and stirred by hand. Finally, the resulting mixture was cast in a silicone mould and cured at room temperature for 48 h, followed by a post-curing cycle of 5 h at 80°C and 3 h at 195°C.

7.2.3 Characterization

Morphology and Raman spectroscopy

The morphologies of the as-received HGMs and the synthesized HGM-CNF particles were analysed by scanning (SEM equipped with an energy-dispersive spectrometer, EVO MA15, Zeiss) and transmission electron microscopy (TEM, JEOL JEM 3000F). The elemental composition of the as-received HGMs was analysed by energy-dispersive spectroscopy (EDS). For SEM and EDS, the particles were lightly pressed onto an adhesive carbon tape and for TEM, a small amount of the hybrid material was dispersed in isopropanol by means of an ultrasonic probe. A drop of the resulting solution was carefully deposited on a TEM carbon-coated Cu grid (LC300-Cu, EMS).

The morphology of the resulting composites was assessed by analysing the fracture surfaces of the manually fractured specimens by light microscopy and scanning electron microscopy (Helios NanoLab 600i, FEI). For SEM, the surfaces of the samples were sputter-coated with a thin layer of gold to avoid electrostatic charge of the sample during the analysis.

The as-received HGMs and the synthesized hybrid fillers were placed on top of thin aluminium foils and analysed by Raman spectroscopy (Micro-Raman spectrometer Renishaw PLC), using a DPSS Nd:YAG green laser (532nm wavelength). Three measurements were performed per sample. Spectra were obtained for an exposure of 15 s, 5 accumulations, in the range of 200 – 3500 cm^{-1}, applying a laser power of 5%.

Thermogravimetric analysis and density measurement

The thermal stability of HGMs and the carbon content of the HGMs-CNFs, as well as the thermal stability of the resulting composites, were analysed by using a thermogravimetric analysis (Q50 TA Instruments), during which the samples were heated under air, at a heating rate of 10°C/min, from room temperature to 800°C. The residue obtained after the thermogravimetric analysis was used to calculate the actual amount of HGMs and HGMs-CNFs added to the composites. The procedure followed is explained in the Annex A.

The density of the resulting composites was measured by following the ASTM D792-13 standard [34], through the application of the Archimedes' principle. At least three cylindrical samples for each filler content, were first weighted in air and then in distilled water at 24°C. The theoretical density of composites was also obtained, by applying the rule of mixtures, to compare the experimentally measured densities of the composites with their theoretical densities. The HGM and HGM-CNF weight fractions used to calculate the theoretical densities were those obtained by TGA, as mentioned above. The equations used for the calculation of the filler volume fraction and the theoretical density are available in the Annex A.

Thermal conductivity analysis

The thermal conductivity and diffusivity and the volumetric heat capacity of the resulting composites were measured at room temperature by applying a transient plane source technique (TPS 2500 S, Hot Disk AB). A thin heater/sensor, with a radius of 2.001 mm, was placed between two identical samples (30 mm diameter and 3 mm thick). The heater/sensor element was first used as a heat source to increase the temperature of the surrounding sample by applying an output power of 0.01 W. Afterwards, the temperature increase was monitored over a period of time of 20 s by measuring the resistance of the heater/sensor. A detailed description of the transient plane source technique, as well as its theoretical background, can be found in references [35–37]. For each filler content and neat resin at least three measurements were performed. To minimize the effect of the

interfacial thermal resistance, the surfaces of the cylindrical samples were polished.

To further analyse the thermal conductivity of the composites, Maxwell's model was applied to predict the theoretical thermal conductivities of HGM and HGM-CNF composites.

Electrical conductivity analysis

To perform the DC electrical conductivity measurements, the disc-shaped specimens used for the thermal conductivity measurements were cut into 3×3×3 mm^3 parallelepiped samples. The electrical resistance was measured in the in-plane and the through-thickness direction of the samples (Annex A). The corresponding two opposite faces were subjected to a polishing process to ensure a smooth surface. The polished surfaces were coated with silver paint as non-guarded electrodes. The voltage (V) applied to the electrodes was increased between 15 and 40 V, and the I–V slope (Keithley SMU 2450 Graphical series SourceMeter) was fitted with the least-squares method. Electrical conductivity was calculated by normalizing measured slope with sample geometry. An estimation of the percolation threshold for the HGM-CNF composites was obtained. The procedure and equations applied are available in the Annex A. Three samples were measured per volume fraction of filler.

7.3 Results and Discussion

7.3.1 Characterization of the fillers

Hollow glass microspheres

The EDS analysis of the as-received HGMs, presented in Figure 7.1a, revealed that the chemical composition of the particles resemble that of soda-lime-borosilicate glass. The SEM images showed that the as-received HGMs have a size distribution of between approximately 20 and 100 μm. The microspheres were homogeneously dispersed on the carbon adhesive tape and no agglomerates were observed. Only a few of the as-received HGMs were broken (inset in Figure 7.1a). The HGMs are

thermally stable up to 800°C, which is well above the CVD synthesis temperature (600°C), as measured by TGA (Figure 7.2).

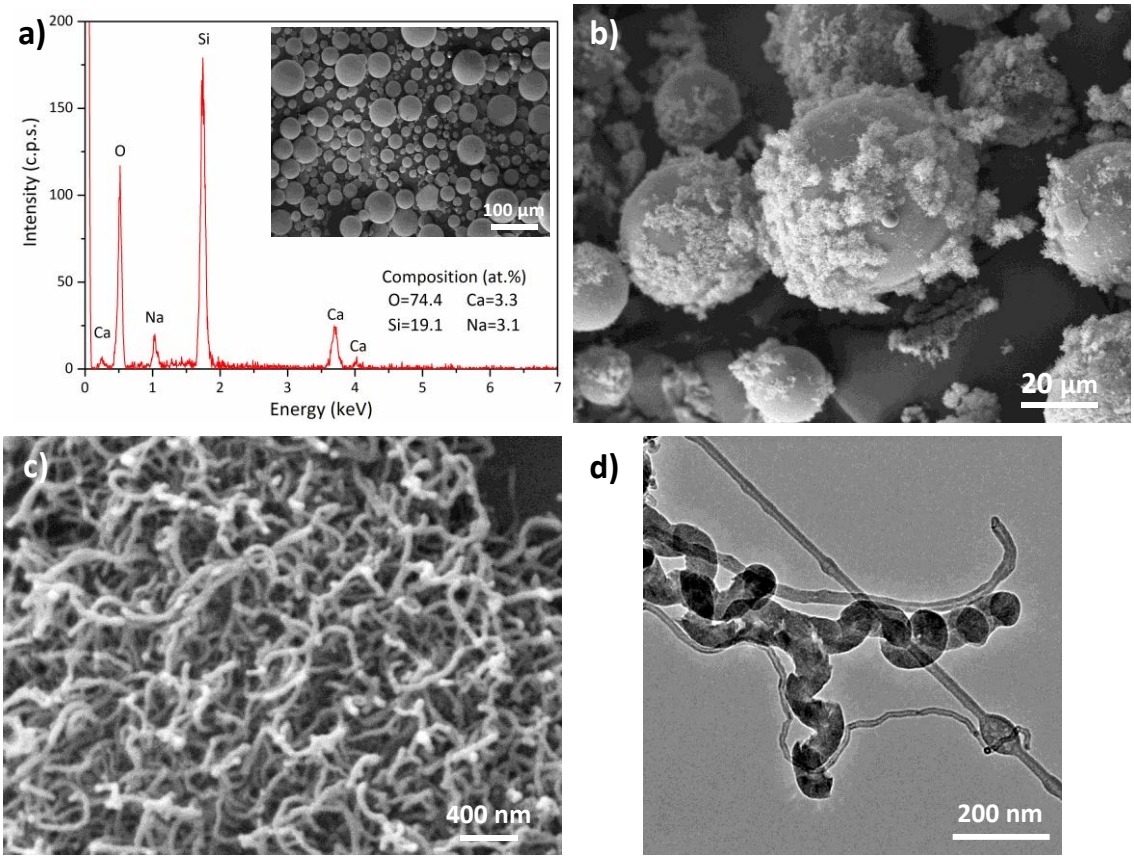

Figure 7.1 a) EDS of the as-received HGMs, performed to analyse the chemical composition (in at.%) of the as-received microspheres. The inset shows a SEM image of the as-received HGMs. b) SEM images of the HGMs after the CVD process; the carbon-based nanostructures cover the surface of the HGMs, although not completely. c) High-magnification SEM images of the synthesized carbon nanofibers. d) TEM images of CNFs in the resulting hybrid material.

Hollow glass microspheres–carbon nanofibers

After the synthesis process, the glass microspheres maintained their spherical shape, as the softening temperature of the particles, i.e., the temperature at which the viscosity of the material reaches a value high enough to allow the deformation of the particle under its own weight [38], was not reached during the CVD process. A certain amount of carbon-based nanostructures, grown by the CVD process, seems to be covering the surface of HGMs (Figure 7.1b), although not completely. By SEM and TEM observation, it was found that the synthesized nanostructures were highly heterogeneous. Although most of the synthesized structures (Figure

7.1c) were identified as carbon nanofibers (Figure 7.1d), a small amount of different carbon-based architectures was also observed in the hybrid material obtained after CVD: hollow carbon nanofibers, nanotubes, and graphitic particles (see Annex C: Supplementary information).

From the TGA measurements of the HGM-CNF samples (Figure 7.2) we obtained the carbon content of hybrid fillers and the thermal stability of the carbon nanostructures. The temperature at which the CNFs started to decompose (onset temperature), was *ca.* 535°C, similar to onset temperatures for MWNTs (400–600°C) [39,40]. It was obtained that CNFs constituted 25 wt.% of the total amount of the HGM-CNF material.

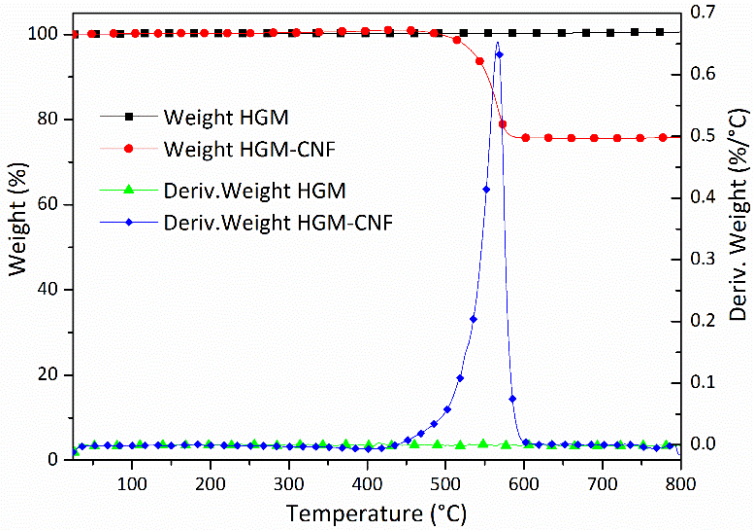

Figure 7.2 Weight change and derivative of weight change, as a function of the temperature, of the HGMs and the HGMs-CNFs. The thermal stability up to 800 °C is confirmed for the HGMs. The amount of CNFs, obtained by CVD, is 25 wt.% of the hybrid HGM-CNF material.

7.3.2 Characterization of composites

Morphology, thermal stability and density

The morphology of the composites was characterized by optical and electronic microscopy of the fractured surfaces. The filler was homogeneously dispersed within the matrix of both HGM and HGM-CNF composites (Figure 7.3a-b and Annex C: Supplementary information), which was not expected as both fillers were dispersed by hand-stirring. A few microspheres appeared to be damaged, probably due to sample preparation and the manufacturing process. In the HGM-CNFs

composites, most of the synthesized CNFs remained located around the HGMs (Figure 7.3c-d), and thus was part of the interphase between the matrix and HGMs.

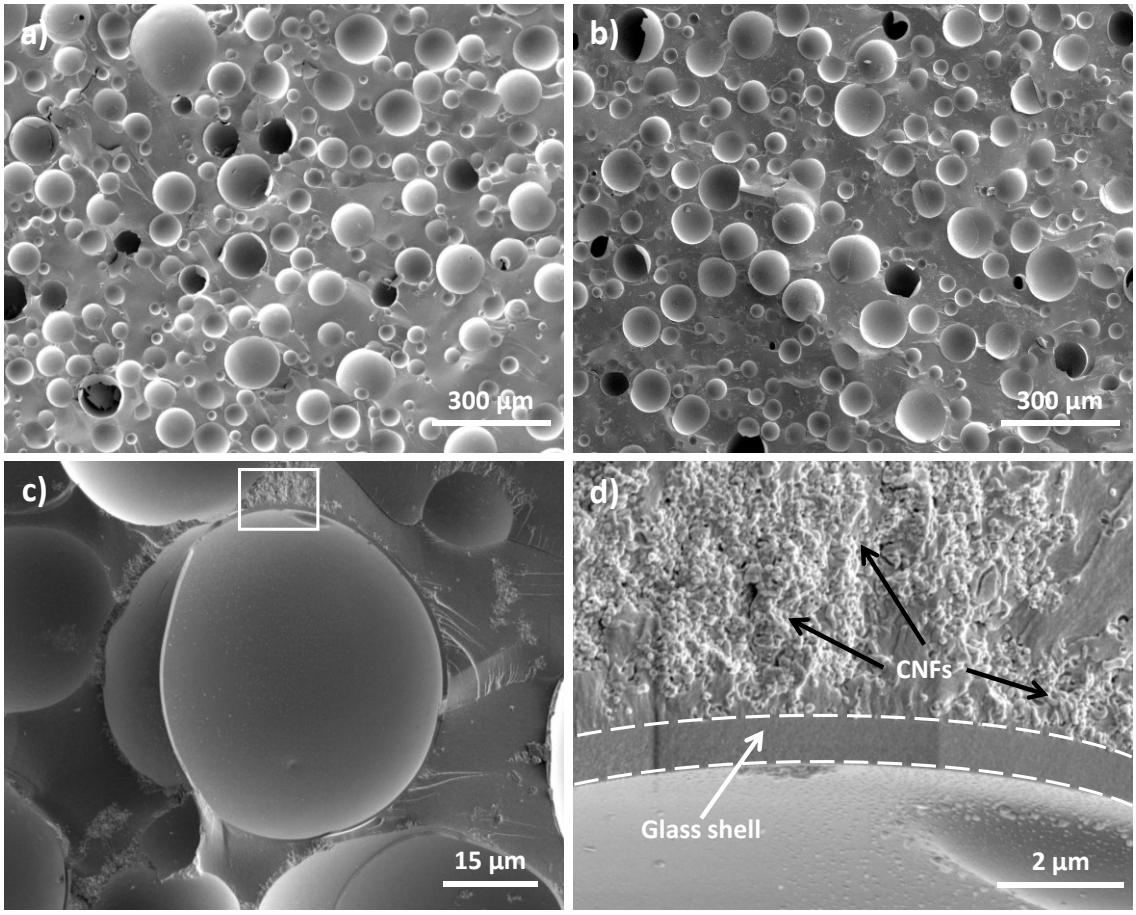

Figure 7.3 SEM images of the fractured surfaces of the a) 10 wt.% HGM and b) 10 wt.% HGM-CNF composites; there is a homogeneous dispersion of the HGMs. c) A broken HGM shown in the 10 wt.% HGM-CNF composite and d) the magnified view showing the glass shell and the synthesized CNFs on the HGM surface, which make up part of the HGM-matrix interface. Some CNF agglomerates are dispersed within the matrix and located near the HGM-CNFs.

The thermal stability of composites was analysed by thermogravimetric analysis carried out in air. The TGA curves of the samples, presented in Figure 7.4, were used to analyse the thermal stability of the resulting composites and to confirm the amount of filler added to the matrix. As observed, the onset temperature of thermal degradation of the resin (357°C) is not significantly affected by the addition of HGMs (360–361°C for all the composites). In the case of the HGM-CNF composites, the onset temperature of thermal degradation was only slightly reduced by the addition of further CNFs; it was 361, 358 and 355°C for the 2, 5 and 10 wt.% HGM-CNF composites, respectively.

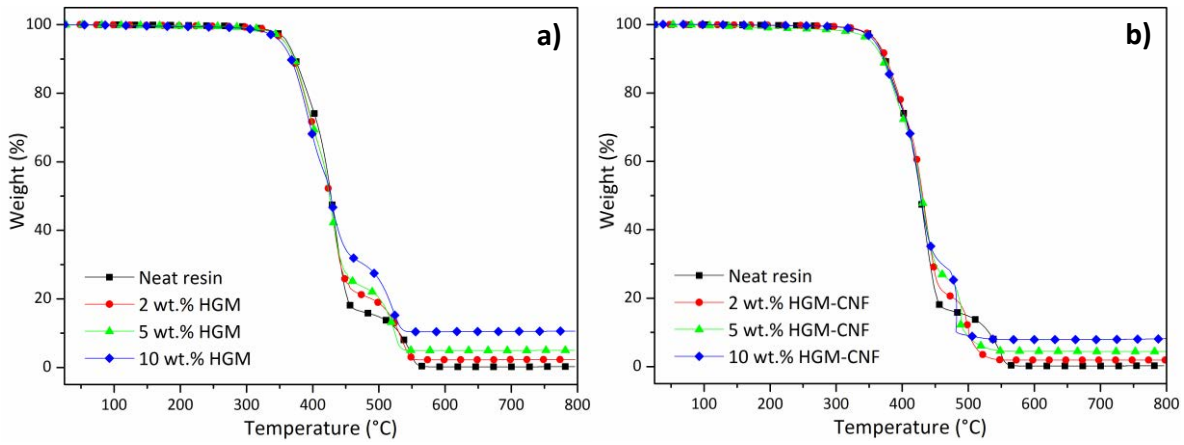

Figure 7.4 Weight change, as a function of the temperature, of the a) HGM and b) HGM-CNF composites. The residue left at 650 °C (Table 7.1), after the degradation process of polymer and CNFs has finished, was used to confirm the amount of HGMs that were added to the composites.

Table 7.1 Analysis of the filler amount and density of the resulting composites. Residue, at 650 °C, obtained after the thermogravimetric analysis of neat resin, HGM, and HGM-CNF composites. The experimental densities were measured according to the ASTM D792-13 standard [34].

Filler amount (wt.%)		Residue (wt.%)	Experimental wt.% HGM/ wt.% CNF	Experimental density (g/cm^3)
0		0.2	-/-	1.159
HGMs	2	2.2	2.1/-	1.056
	5	4.9	4.8/-	0.921
	10	10.4	10.3/-	0.752
HGMs-CNFs	2	1.9	1.7/0.6	1.101
	5	3.9	3.7/1.2	1.004
	10	7.9	7.7/2.6	0.823

The results obtained from the TGA allowed us to confirm the filler content by measuring the residue left at 650 °C, after the degradation process of polymer and CNFs have finished (Table 7.1). The addition of HGMs and HGMs-CNFs to the polymeric matrix led to a decrease in the density of the material. As expected, the lowest densities were obtained for the composites with the largest amounts of filler, which were 35% (10% wt. HGM) and 29% (10 wt.% HGM-CNF) lower than

the density of the neat matrix. The differences between the theoretical (Table 7.1) and the experimental amount of filler could be attributed to errors during weighing the filler to be mixed with the resin, porosity of the matrix, or localized heterogeneous dispersion of the filler within the matrix [41,42].

Thermal behavior

The effect of the HGMs and the HGMs-CNFs on the thermal behaviour of the neat resin was analysed by the hot-disk technique. The values obtained for the thermal conductivity, k, and thermal diffusivity, λ, are shown in Figure 7.5 and Figure 7.6. The thermal conductivity of composites decreases with an increased amount of HGMs and HGMs-CNFs added. The neat resin had a thermal conductivity, k_m, of 0.228 W/mK.

For composite materials formed by two phases, i.e. resin and HGMs, Maxwell model was applied to analyse the effective thermal conductivity of the HGM composites. Maxwell model assumes randomly dispersed and non-interacting spheres [43], thus it is only valid for low volume fractions of filler (<10 vol.%) [44]. As observed in Figure 7.5a, the results obtained by the application of Maxwell's equation are well in agreement with those experimentally obtained.

For the HGM-CNF composites, the thermal conductivity of the resulting material decreased with the addition of filler. Nevertheless, the thermal conductivity of HGM-CNFs composites is higher than that of the HGM composites for the same amount of filler. This higher thermal conductivity of HGM-CNF composites than HGM composites should be due to the high thermal conductivity of the CNFs [45] and the lower content of HGM per volume fraction of HGM–CNF (Figure 7.5), compared with the HGM composite with the same wt.% of filler. For the 10 wt.% HGM composite (*ca.* 40 vol.% HGM) we obtained a thermal conductivity that was 31% lower than for the neat resin, which is in agreement with the values reported for HGM–epoxy [14]. In the case of the composite with 10 wt.% of HGMs-CNFs (*ca.* 34 vol.% HGM) the measured thermal conductivity (0.172 W/mK) is 25% lower than that of neat resin. The same reduction has also been reported for 30 vol.% of HGMs in epoxy composites [14]. It is clear that, regardless of the presence of CNFs

within the matrix, the main contribution to the thermal conductivity of the composite is the presence of HGMs.

We also applied the Maxwell model to estimate the thermal conductivity of the resulting HGM-CNF composites. This estimation was done by adjusting the theoretical values obtained from the Maxwell equation (Annex C: Supplementary information) to the experimental thermal conductivity values of the HGM-CNF composites. As mentioned, the Maxwell model is only valid for low volume fractions of filler, thus the value of $k_{HGM-CNF}$ used for the application of the series and parallel models corresponded to the composite with 2 wt,% of HGM, i.e., $k_{HGM-CNF}$= 0.104 W/mK (Annex C: Supplementary information). The obtained results are in agreement with the experimental values, as observed in Figure 7.5b.

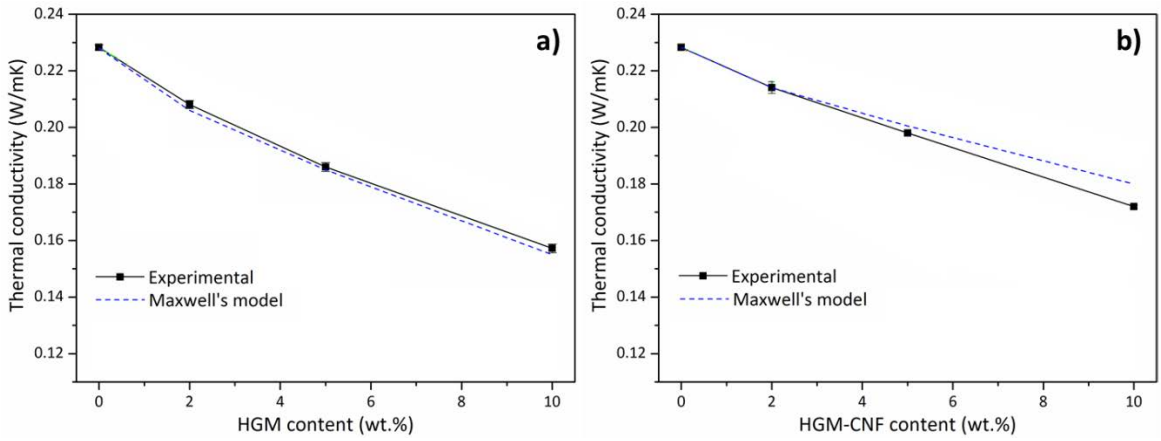

Figure 7.5 Analysis of the thermal conductivity of the a) HGM and b) HGM-CNF composites. The experimental results were obtained from the measurements of a hot disk process. The values obtained by the application of the series, parallel and Maxwell's models are also shown for comparison with the experimental values.

Along with the addition of HGMs, there are several mechanisms that account for the reduction of the thermal conductivity of HGM-CNF composites. The structure and quality of the CNFs affect the resulting thermal conductivity as defects and presence of amorphous carbon can strongly affect heat conduction [46]. Thermal conductivity is reduced due to the presence of contacts between CNFs and between HGMs and the effect of the interfacial thermal resistance or Kapitza resistance between the CNFs and the matrix, the CNFs and the HGMs, and HGMs and the matrix, which were not taken into account in the applied models [47–50].

The thermal diffusivity, λ, of an homogeneous and isotropic material is given by the ratio between its thermal conductivity and the product of its density and specific heat capacity, c, Eq. 7.1.

$$\lambda = \frac{k}{\rho c} \qquad \text{Eq. 7.1}$$

Thus, the thermal diffusivity, λ, can be understood as the ratio between the ability of heat to flow through the material and its ability to store thermal energy [51].

In the case of HGM composites, it can be observed that the 2 wt.% composite have a λ=0.166 mm²/s, which does not significantly differs from that of neat resin (0.167 mm²/s). However, for the 5 and 10 wt.% composite, λ increases reaching a maximum value of 0.184 mm²/s for the 10 wt.%.

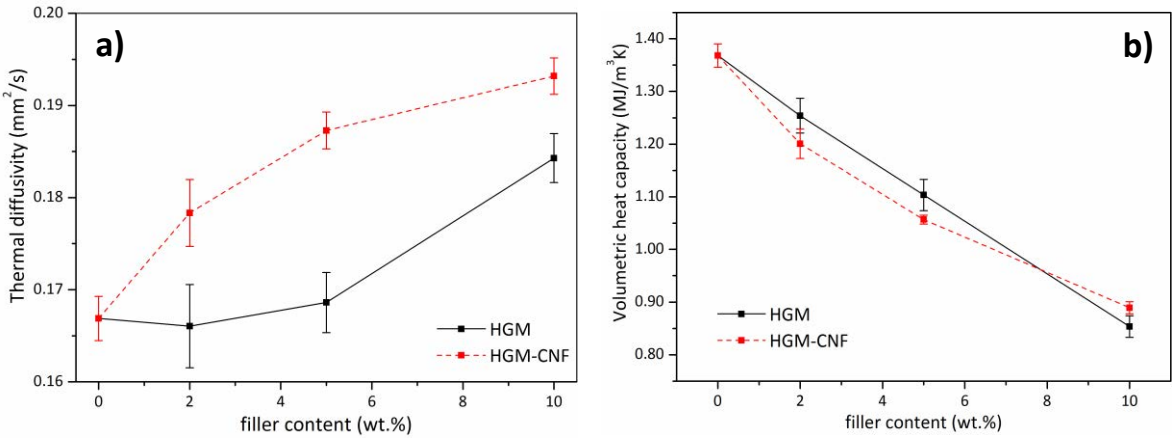

Figure 7.6 a) Thermal diffusivity and b) volumetric heat capacity of the HGM and HGM-CNF composites, obtained by hot disk technique.

A HGM consists in a spherical glass shell filled by a gas. The thermal diffusivity of glass is approximately 0.56 mm²/s, while light gases such as air or He typically have higher thermal diffusivity (22 and 137 mm²/s, respectively) [51]. Thus, it is reasonable to assume that the thermal diffusivity of HGMs is higher than that of neat resin. This explains the increase in thermal diffusivity of the resulting composites when the HGMs are dispersed within the polymeric matrix. On the other hand, in the case of the HGM-CNF composites, the thermal diffusivity of the samples rapidly increases as the amount of hybrid microspheres increases (Figure

7.6a). According to results reported for polymers filled with CNTs [52–55], the addition of CNTs resulted in an increased thermal diffusivity of the composite.

The ability to store thermal energy is expressed by the volumetric heat capacity, ρc. For the matrix, it was found that $\rho c = 1.37 \times 10^{-6}$ J/m^{3}K. The value of ρc for the HGMs is unknown. However, it is known that glass has a ρc of 1.98×10^{-6} J/m^{3}K while light gases presents extremely low values of volumetric heat capacity, i.e. 1.2×10^{-8} for air and 1.1×10^{-8} for Ar [51].

Thus, the HGM composites exhibit a lower ability to store thermal energy than the matrix (Figure 7.6b). From the volumetric heat capacity values measured for the HGM-CNF composites, it was obtained that the behaviour was similar to that of the HGM composites, although the values were slightly lower than in the HGM composites, probably due to the CNFs. Further work should be done to understand the behaviour and properties of the hybrid material.

Electrical conductivity

The electrical conductivity of the resin, the HGM composites and the 2 and 5 wt.% HGM-CNF was lower than 1×10^{-7} S/m, which is the minimum value that can be measured with the equipment and the sample dimensions used. In the case of the HGM-CNF composites, an electrical conductivity of $7\pm3\times10^{-4}$ S/m and $3\pm2\times10^{-4}$ S/m was obtained for the 10 wt.% HGM-CNF composite in the through-thickness and in-plane directions, respectively (Annex C: Supplementary information). Taking into account the results obtained from the TGA of the hybrid materials obtained by CVD, this result implies that the critical amount of HGM-CNF at which takes place the formation of a continuous electrically conducting network within the resin [45] is between about 1.25 and 2.5 wt.% of CNFs, which corresponds to the composites with 5 and 10 wt.% of HGMs-CNFs, respectively. By assuming that the CNFs synthesized by CVD had mainly grown on the surface of the HGMs, an HGM-CNF can be modelled as a hybrid particle of single-phase material. The theoretical percolation threshold should be 4.9 wt.%. The followed procedure and the applied equations are available in the Annex C: Supplementary information. The experimental percolation threshold obtained in this work is higher than the theoretical value; this could be because the CNFs do not completely cover the

surface of the HGMs, or due to the size distribution of HGM. The obtained result is a good first approximation to the experimental percolation threshold obtained in this study, which is located between 5 and 10 wt.% of HGMs-CNFs.

7.4 Conclusions

The thermal and electrical behaviour of as-received HGMs and synthesized HGMs-CNF composites were studied to assess the effect of the HGMs on the resin and the effect of the CNFs on the HGM composites. These HGMs-CNFs mainly consist of HGMs surrounded by carbon nanofibers and were synthesized in our lab by using chemical vapour deposition.

Both types of composites were directly prepared by hand mixing. Although the hybrid microspheres have carbon-based nanomaterials, no further dispersing step or dispersing aiding agents were needed. The quality of both composites, in terms of matrix porosity and filler dispersion, was similar to that in the reported literature.

By adding 10% wt. HGM-CNFs to a high temperature resin (thermal stability up to *ca.* 350 °C) we can obtain a low density (0.823 g/cm^3), low thermally (0.172 W/mK) and good electrically conducting ($7\pm3\times10^{-4}$ S/m) composite. This material presents an unusual combination of properties, such as a low thermal conductivity and a relatively high electrical conductivity. This new generation of hybrid nanofillers paves the way to unique composite materials with properties that are currently hard to combine in a single material.

7.5 Acknowledgments

This work was supported by the European Commission under the 7th Framework Program, NFRP project (PICIG12-GA-2012-33924), ROBOHEALTH-A project (DPI2013-47944-C4-1-R) funded by Spanish Ministry of Economy and Competitiveness and from the RoboCity2030-II-CM project (S2009/DPI-1559), funded by "Programas de Actividades I+D en la Comunidad de Madrid" and co-funded by Structural Funds of the EU. R. G. V. gratefully acknowledges the Spanish Ministry of Science and Innovation for financial funding through the Ramon y Cajal

Fellowship. L. C. H-R acknowledges the support from the Spanish Ministry of Education through the FPU programme (FPU14/06843). The authors would like to acknowledge 3M for providing the hollow glass microspheres, Scott Bader for providing the resin and J. C. Fernandez for the as-received HGM composite preparation.

7.6 References

[1] I. Krupa, V. Cecen, A. Boudenne, J. Prokeš, I. Novák, The mechanical and adhesive properties of electrically and thermally conductive polymeric composites based on high density polyethylene filled with nickel powder, Mater. Des. 51 (2013) 620–628. doi:10.1016/j.matdes.2013.03.067.

[2] Y.P. Mamunya, V.V. Davydenko, P. Pissis, E.V. Lebedev, Electrical and thermal conductivity of polymers filled with metal powders, Eur. Polym. J. 38 (2002) 1887–1897. doi:10.1016/S0014-3057(02)00064-2.

[3] A. Yu, P. Ramesh, X. Sun, E. Bekyarova, M.E. Itkis, R.C. Haddon, Enhanced Thermal Conductivity in a Hybrid Graphite Nanoplatelet - Carbon Nanotube Filler for Epoxy Composites, Adv. Mater. 20 (2008) 4740–4744. doi:10.1002/adma.200800401.

[4] S.Y. Kwon, I.M. Kwon, Y.-G. Kim, S. Lee, Y.-S. Seo, A large increase in the thermal conductivity of carbon nanotube/polymer composites produced by percolation phenomena, Carbon. 55 (2013) 285–290. doi:10.1016/j.carbon.2012.12.063.

[5] H. Chen, V.V. Ginzburg, J. Yang, Y. Yang, W. Liu, Y. Huang, L. Du, B. Chen, Thermal conductivity of polymer-based composites: Fundamentals and applications, Prog. Polym. Sci. 59 (2016) 41–85. doi:10.1016/j.progpolymsci.2016.03.001.

[6] Y. Hu, G. Du, N. Chen, A novel approach for Al2O3/epoxy composites with high strength and thermal conductivity, Compos. Sci. Technol. 124 (2016) 36–43. doi:10.1016/j.compscitech.2016.01.010.

[7] M. Donnay, S. Tzavalas, E. Logakis, Boron nitride filled epoxy with improved thermal conductivity and dielectric breakdown strength, Compos. Sci. Technol. 110 (2015) 152–158. doi:10.1016/j.compscitech.2015.02.006.

[8] K.C. Yung, B.L. Zhu, T.M. Yue, C.S. Xie, Preparation and properties of hollow glass microsphere-filled epoxy-matrix composites, Compos. Sci. Technol. 69 (2009) 260–264. doi:10.1016/j.compscitech.2008.10.014.

[9] R. Sun, H. Yao, H.-B. Zhang, Y. Li, Y.-W. Mai, Z.-Z. Yu, Decoration of defect-free graphene nanoplatelets with alumina for thermally conductive and electrically insulating epoxy composites, Compos. Sci. Technol. 137 (2016) 16–23. doi:10.1016/j.compscitech.2016.10.017.

[10] J.-W. Zha, T.-X. Zhu, Y.-H. Wu, S.-J. Wang, R.K.Y. Li, Z.-M. Dang, Tuning of thermal and dielectric properties for epoxy composites filled with electrospun alumina fibers and graphene nanoplatelets through hybridization, J Mater Chem C. 3 (2015) 7195–7202. doi:10.1039/C5TC01552A.

[11] W. Cui, F. Du, J. Zhao, W. Zhang, Y. Yang, X. Xie, Y.-W. Mai, Improving thermal conductivity while retaining high electrical resistivity of epoxy composites by incorporating silica-coated multi-walled carbon nanotubes, Carbon. 49 (2011) 495–500. doi:10.1016/j.carbon.2010.09.047.

[12] N. Gupta, D. Pinisetty, A Review of Thermal Conductivity of Polymer Matrix Syntactic Foams—Effect of Hollow Particle Wall Thickness and Volume Fraction, JOM. 65 (2013) 234–245. doi:10.1007/s11837-012-0512-0.

[13] B.L. Zhu, H. Zheng, J. Wang, J. Ma, J. Wu, R. Wu, Tailoring of thermal and dielectric properties of LDPE-matrix composites by the volume fraction, density, and surface modification of hollow glass microsphere filler, Compos. Part B Eng. 58 (2014) 91–102. doi:10.1016/j.compositesb.2013.10.029.

[14] B. Zhu, J. Ma, J. Wang, J. Wu, D. Peng, Thermal, dielectric and compressive properties of hollow glass microsphere filled epoxy-matrix composites, J. Reinf. Plast. Compos. 31 (2012) 1311–1326. doi:10.1177/0731684412452918.
[15] J.Z. Liang, F.H. Li, Heat transfer in polymer composites filled with inorganic hollow micro-spheres: A theoretical model, Polym. Test. 26 (2007) 1025–1030. doi:10.1016/j.polymertesting.2007.07.002.
[16] N. Gupta, R. Ye, M. Porfiri, Comparison of tensile and compressive characteristics of vinyl ester/glass microballoon syntactic foams, Compos. Part B Eng. 41 (2010) 236–245. doi:10.1016/j.compositesb.2009.07.004.
[17] N. Gupta, R. Nagorny, Tensile properties of glass microballoon-epoxy resin syntactic foams, J. Appl. Polym. Sci. 102 (2006) 1254–1261. doi:10.1002/app.23548.
[18] M. Colloca, N. Gupta, M. Porfiri, Tensile properties of carbon nanofiber reinforced multiscale syntactic foams, Compos. Part B Eng. 44 (2013) 584–591. doi:10.1016/j.compositesb.2012.02.030.
[19] R.L. Poveda, N. Gupta, Electrical properties of carbon nanofiber reinforced multiscale polymer composites, Mater. Des. 56 (2014) 416–422. doi:10.1016/j.matdes.2013.11.074.
[20] R.L. Poveda, S. Achar, N. Gupta, Viscoelastic properties of carbon nanofiber reinforced multiscale syntactic foam, Compos. Part B Eng. 58 (2014) 208–216. doi:10.1016/j.compositesb.2013.10.079.
[21] R.L. Poveda, G. Dorogokupets, N. Gupta, Carbon nanofiber reinforced syntactic foams: Degradation mechanism for long term moisture exposure and residual compressive properties, Polym. Degrad. Stab. 98 (2013) 2041–2053. doi:10.1016/j.polymdegradstab.2013.07.007.
[22] R.L. Poveda, S. Achar, N. Gupta, Thermal Expansion of Carbon Nanofiber-Reinforced Multiscale Polymer Composites, JOM. 64 (2012) 1148–1157. doi:10.1007/s11837-012-0402-5.
[23] H. Qian, A. Bismarck, E.S. Greenhalgh, M.S.P. Shaffer, Synthesis and characterisation of carbon nanotubes grown on silica fibres by injection CVD, Carbon. 48 (2010) 277–286. doi:10.1016/j.carbon.2009.09.029.
[24] S.S. Wicks, R.G. de Villoria, B.L. Wardle, Interlaminar and intralaminar reinforcement of composite laminates with aligned carbon nanotubes, Compos. Sci. Technol. 70 (2010) 20–28. doi:10.1016/j.compscitech.2009.09.001.
[25] N. Yamamoto, A. John Hart, E.J. Garcia, S.S. Wicks, H.M. Duong, A.H. Slocum, B.L. Wardle, High-yield growth and morphology control of aligned carbon nanotubes on ceramic fibers for multifunctional enhancement of structural composites, Carbon. 47 (2009) 551–560. doi:10.1016/j.carbon.2008.10.030.
[26] Z.H. Han, B. Yang, S.H. Kim, M.R. Zachariah, Application of hybrid sphere/carbon nanotube particles in nanofluids, Nanotechnology. 18 (2007) 105701.
[27] Q. Zhang, J. Huang, F. Wei, G. Xu, Y. Wang, W. Qian, D. Wang, Large scale production of carbon nanotube arrays on the sphere surface from liquefied petroleum gas at low cost, Chin. Sci. Bull. 52 (2007) 2896–2902. doi:10.1007/s11434-007-0458-8.
[28] D. He, M. Bozlar, M. Genestoux, J. Bai, Diameter- and length-dependent self-organizations of multi-walled carbon nanotubes on spherical alumina microparticles, Carbon. 48 (2010) 1159–1170. doi:10.1016/j.carbon.2009.11.039.
[29] D. He, H. Li, J. Bai, Experimental and numerical investigation of the position-dependent growth of carbon nanotube–alumina microparticle hybrid structures in a horizontal CVD reactor, Carbon. 49 (2011) 5359–5372. doi:10.1016/j.carbon.2011.08.003.
[30] R.N. Othman, I.A. Kinloch, A.N. Wilkinson, Synthesis and characterisation of silica–carbon nanotube hybrid microparticles and their effect on the electrical properties of poly(vinyl alcohol) composites, Carbon. 60 (2013) 461–470. doi:10.1016/j.carbon.2013.04.062.
[31] S. Huang, Growing carbon nanotubes on patterned submicron-size SiO2 spheres, Carbon. 41 (2003) 2347–2352. doi:10.1016/S0008-6223(03)00275-6.
[32] E.F. Zegeye, E. Woldesenbet, Processing and mechanical characterization of carbon nanotube reinforced syntactic foams, J. Reinf. Plast. Compos. 31 (2012) 1045–1052. doi:10.1177/0731684412452919.

[33] P. Romero, R. Oro, M. Campos, J.M. Torralba, R. Guzman de Villoria, Simultaneous synthesis of vertically aligned carbon nanotubes and amorphous carbon thin films on stainless steel, Carbon. 82 (2015) 31–38. doi:10.1016/j.carbon.2014.10.020.
[34] ASTM D792-13, Standard Test Methods for Density and Specific Gravity (Relative Density) of Plastics by Displacement, ASTM International, West Conshohocken, PA, (2013). doi:10.1520/D0792.
[35] S.E. Gustafsson, Transient plane source techniques for thermal conductivity and thermal diffusivity measurements of solid materials, Rev. Sci. Instrum. 62 (1991) 797.
[36] Y. He, Rapid thermal conductivity measurement with a hot disk sensor: Part 1. Theoretical considerations, Thermochim. Acta. 436 (2005) 122–129. doi:10.1016/j.tca.2005.06.026.
[37] S.A. Al-Ajlan, Measurements of thermal properties of insulation materials by using transient plane source technique, Appl. Therm. Eng. 26 (2006) 2184–2191. doi:10.1016/j.applthermaleng.2006.04.006.
[38] J.E. Shelby, Introduction to Glass Science and Technology, Royal Society of Chemistry, 2005.
[39] J.H. Lehman, M. Terrones, E. Mansfield, K.E. Hurst, V. Meunier, Evaluating the characteristics of multiwall carbon nanotubes, Carbon. 49 (2011) 2581–2602. doi:10.1016/j.carbon.2011.03.028.
[40] B. Scheibe, E. Borowiak-Palen, R.J. Kalenczuk, Oxidation and reduction of multiwalled carbon nanotubes — preparation and characterization, Mater. Charact. 61 (2010) 185–191. doi:10.1016/j.matchar.2009.11.008.
[41] J. Li, X. Luo, X. Lin, Preparation and characterization of hollow glass microsphere reinforced poly(butylene succinate) composites, Mater. Des. 46 (2013) 902–909. doi:10.1016/j.matdes.2012.11.054.
[42] T.C. Lin, N. Gupta, A. Talalayev, Thermoanalytical characterization of epoxy matrix-glass microballoon syntactic foams, J. Mater. Sci. 44 (2009) 1520–1527. doi:10.1007/s10853-008-3074-3.
[43] J.C. Maxwell, A treatise on electricity and magnetism, Oxford : Clarendon Press, 1873. http://archive.org/details/electricandmagne01maxwrich (accessed September 25, 2015).
[44] H. Zhou, S. Zhang, M. Yang, The effect of heat-transfer passages on the effective thermal conductivity of high filler loading composite materials, Compos. Sci. Technol. 67 (2007) 1035–1040. doi:10.1016/j.compscitech.2006.06.004.
[45] M.H. Al-Saleh, U. Sundararaj, A review of vapor grown carbon nanofiber/polymer conductive composites, Carbon. 47 (2009) 2–22. doi:10.1016/j.carbon.2008.09.039.
[46] A.A. Balandin, Thermal properties of graphene and nanostructured carbon materials, Nat. Mater. 10 (2011) 569–581. doi:10.1038/nmat3064.
[47] F. Gong, H.M. Duong, D.V. Papavassiliou, Inter-Carbon Nanotube Contact and Thermal Resistances in Heat Transport of Three-Phase Composites, J. Phys. Chem. C. 119 (2015) 7614–7620. doi:10.1021/acs.jpcc.5b00651.
[48] F. Gong, K. Bui, D.V. Papavassiliou, H.M. Duong, Thermal transport phenomena and limitations in heterogeneous polymer composites containing carbon nanotubes and inorganic nanoparticles, Carbon. 78 (2014) 305–316. doi:10.1016/j.carbon.2014.07.007.
[49] R.S. Prasher, X.J. Hu, Y. Chalopin, N. Mingo, K. Lofgreen, S. Volz, F. Cleri, P. Keblinski, Turning Carbon Nanotubes from Exceptional Heat Conductors into Insulators, Phys. Rev. Lett. 102 (2009). doi:10.1103/PhysRevLett.102.105901.
[50] C.-W. Nan, R. Birringer, D.R. Clarke, H. Gleiter, Effective thermal conductivity of particulate composites with interfacial thermal resistance, J. Appl. Phys. 81 (1997) 6692.
[51] A. Salazar, On thermal diffusivity, Eur. J. Phys. 24 (2003) 351. doi:10.1088/0143-0807/24/4/353.
[52] V. Datsyuk, M. Lisunova, M. Kasimir, S. Trotsenko, K. Gharagozloo-Hubmann, I. Firkowska, S. Reich, Thermal transport of oil and polymer composites filled with carbon nanotubes, Appl. Phys. A. 105 (2011) 781–788. doi:10.1007/s00339-011-6667-7.
[53] M. Akoshima, H. Abe, T. Baba, Thermal Diffusivity of Carbon Materials as Candidate Reference Materials, Int. J. Thermophys. 36 (2014) 2507–2517. doi:10.1007/s10765-014-1624-2.

[54] J. Chiguma, E. Johnson, P. Shah, N. Gornopolskaya, W.E. Jones Jr., Thermal Diffusivity and Thermal Conductivity of Epoxy-Based Nanocomposites by the Laser Flash and Differential Scanning Calorimetry Techniques, Open J. Compos. Mater. 03 (2013) 51–62. doi:10.4236/ojcm.2013.33007.
[55] Y. Xu, G. Ray, B. Abdel-Magid, Thermal behavior of single-walled carbon nanotube polymer–matrix composites, Compos. Part Appl. Sci. Manuf. 37 (2006) 114–121. doi:10.1016/j.compositesa.2005.04.009.

8 Concluding remarks and future work

The development of industries as aerospace or energy require the development of a new generation of polymer composites. These materials should have improved mechanical properties, compared to conventional composites, and at the same time should have the desired levels of thermal and electrical conductivity, depending on the application for which they are required. Two-dimensional fibre-reinforced polymers are widely used in industries as transport (aerospace, marine, automobile), sport or even civil engineering. They are designed to maximize the in-plane specific stiffness and specific strength. However, they suffer from low mechanical properties and lack of multifunctionality (i.e. thermal and electrical conductivity) in the through-thickness direction.

The modification of polymeric matrix with carbon-based fillers to obtain hybrid fibre-reinforced polymers is a promising approach for the development of multifunctional composites.

In this thesis, the effect of three different fillers on the properties of polypropylene has been studied. In first place, it was concluded that the proposed processing approach, based on the masterbatch technique, was not appropriate for the individual homogeneous dispersion of nanofillers, e.g. graphite nanoplatelets and carbon nanotubes. Agglomerates or clusters of GNPs and CNTs were observed on the resulting composites. Regarding the novel micron-scale carbon filler, the masterbatch processing resulted in the break-up of the as-synthesized structures. Nonetheless, the resulting carbon microfiller was homogeneously dispersed within the matrix.

Regarding the mechanical properties it can be said that CNTs exhibited the best reinforcing and toughening performance (Figure 8.1), although it should be kept in mind that the composites have different matrices.

The flexural modulus (Figure 8.1a) and strength (Figure 8.1b) increased with increasing the CNT content. Enhancements of 17 and 8% in flexural modulus and strength, respectively, were achieved for the composite with 10 wt.% of CNTs. Concerning the fracture behaviour, an improvement of more than 50%, compared to unmodified PP, can be obtained upon the addition of just 0.5 wt.% of CNTs.

From the observation of Figure 8.1a and b, it can be said that the flexural modulus of the CMF composites follows a similar behaviour to that of the CNT composites. However, the behaviour of the flexural strength of the CMF composites is similar to that of the GNP composites. In order to fully understand the behaviour of the CMF composites, further work must be done to further characterize the filler and their effect on the morphology of the resulting composites, i.e. crystalline structure, as well as their mechanical behaviour.

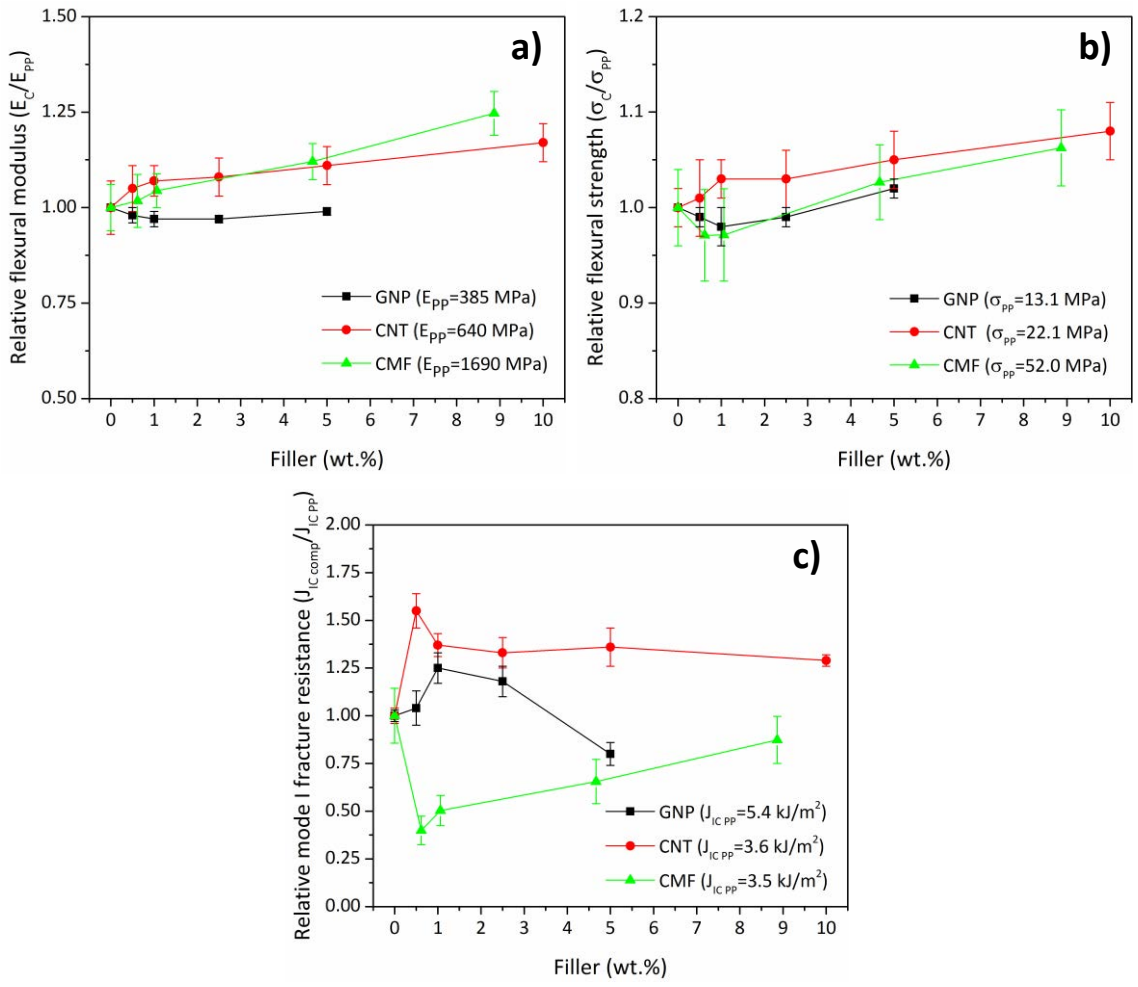

Figure 8.1 Relative mechancial properties of PP composites with GNPs, CNTs and CMF: a) Flexural modulus, b) Flexural strength and c) Mode I fracture resistance.

Regarding the electrical conductivity, the percolation threshold was not reached in the GNP nor in the CMF composites. Although in the case of the CNT composites, the electrical conductivity of the composites with the highest filler content was among the highest of those available in previously reported results. The characterisation of the thermal behaviour of the CMF composites showed that the thermal conductivity increased with increasing the filler content, up to a 15% for the composite with 8.9 wt.% of CMF. The thermal behaviour of the polypropylene composites with GNPs and CNTs was not analysed in this thesis, thus it is proposed as future work.

The second main objective of this thesis was the development of hybrid fillers through the synthesis of carbon structures by chemical vapour deposition, using different particles as substrates. It was concluded that by appropriately selecting the substrate particles, different resulting properties can be achieved.

In one hand, using nanoparticles as substrate, the synthesis of carbon nanotubes was performed. In this case, due to the size of the nanoparticles, the CNTs formed and entangled network with the nanoparticles, rather than being attached to them. The homogeneous dispersion of the resulting hybrid nanofiller proved to be difficult, as confirmed by the agglomerates observed in the composites with the highest filler contents. This poor dispersion resulted in epoxy composites with similar or slightly improved mechanical behaviour, compared to neat epoxy. Nonetheless, the addition of the hybrid material to an epoxy result resulted in composites with improved thermal and electrical conductivity. However, further work can be done to achieve a homogeneous dispersion of the hybrid filler and/or the interaction between the filler and the matrix. This would lead to composites with significantly higher improvements in mechanical properties. Moreover, the formation of a contacting network could be achieved at lower filler contents, resulting in an improved thermal and electrical behaviour.

On the other hand, using micron-scaled hollow particles as substrate, carbon nanofibers were grown. The resulting hybrid filler could be easily dispersed within the matrix. Since the carbon nanofibers were mainly attached to the surface of the microspheres, the resulting morphology favoured the homogeneous dispersion of

the hybrid filler. The combination of the low density, thermal insulating microspheres with the electrically conducting carbon nanofiller resulted in a hybrid filler that was used to obtain lightweight, thermal insulating and electrically conducting polymer composites. Further work should be done to increase the yield obtained after each CVD process. This would allow to further characterize the effect of the hybrid filler on the polymeric resin, e.g. the mechanical properties of the resulting composites.

To sum it up, the hybrid fillers developed in this thesis proved to be promising materials to be used for the development of polymer composites with improved mechanical behaviour, while having the desired levels of thermal and electrical conductivity. In the case of the composites with the nanoscaled fillers (alumina nanoparticles, hybrid nanoparticles, GNPs or CNTs), it was concluded that the dispersion should be improved to fully take advantage of the properties of the filler. Nevertheless, it can be said that the presented polymer composites showed potential to be used as modified matrices for the development of hybrid fibre-reinforced polymers.

Annex A: Supplementary Information for Chapter 5

A1 Results

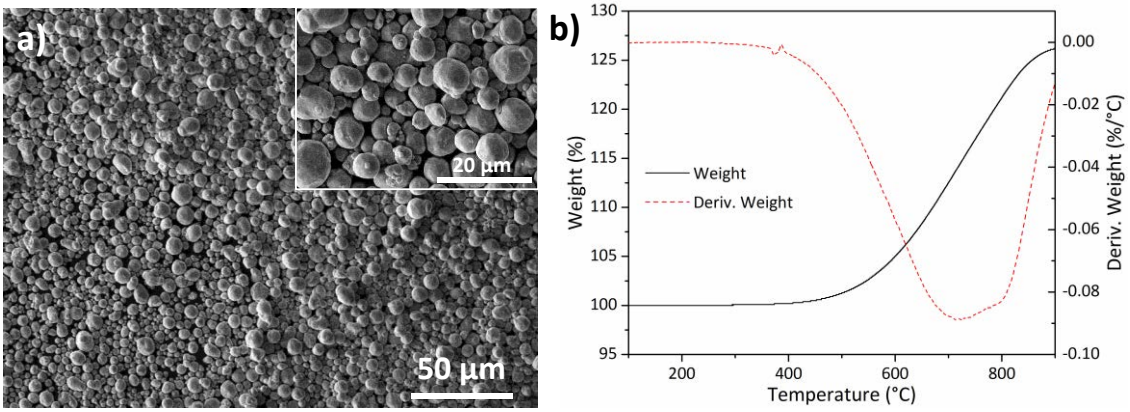

Figure A.1 a) SEM image of the as-received Ni microparticles and b) curves obtained from the TGA performed in air, corresponding to the weight (%) and first derivative of the weight (%/°C) of the as received microparticles.

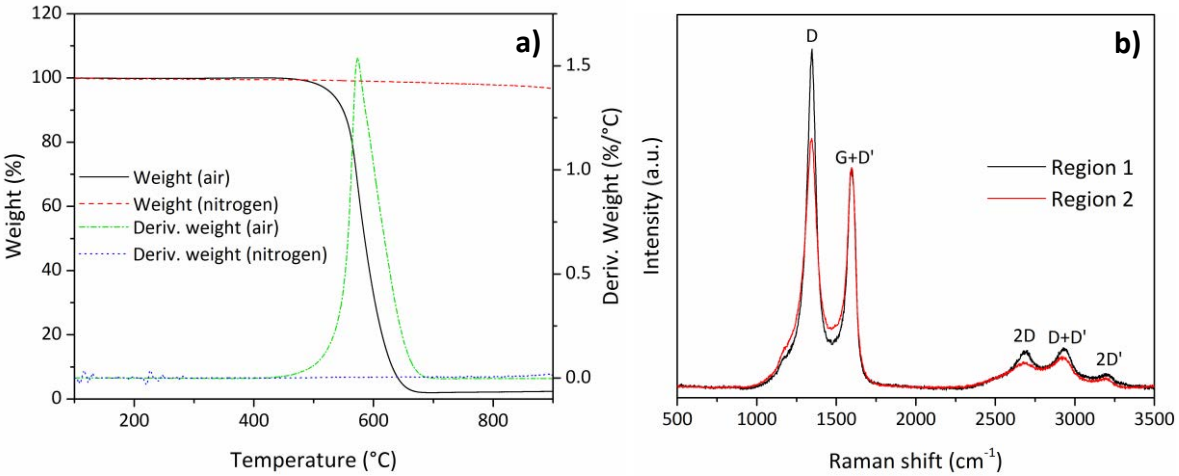

Figure A.2 a) Curves obtained from the TGA performed under air and nitrogen, corresponding to the weight (%) and first derivative of the weight (%/°C) of the CMF. b) Raman spectra of hybrid microparticles showing the characteristic peaks of carbon-based materials. Region 1 is a spectra aquired for the micron-sized fibre-like structures, and region 2 is a spectra aquired for the sub-micron sized structures.

Raman spectra, in the range from 500 to 3500 cm^{-1}, were acquired to study the quality of the synthesized carbon microfiller (Figure A.2b). The characteristic peaks of carbon allotropes can be observed in the acquired spectra [1]. The

relative quality of the two different morphologies identified in the synthesized filler is analysed by comparing their I_D/I_G ratio [2]. For the micron-sized fibre-like fillers (region 1 in Figure A.2) the I_D/I_G ratio was 1.53±0.03, while for the sub-micron sized structures I_D/I_G=1.12±0.09 (region 2 in Figure A.2). Therefore, it was obtained that the structures with a sub-micron size have higher quality than the fibre-like structures with a size in the range of microns.

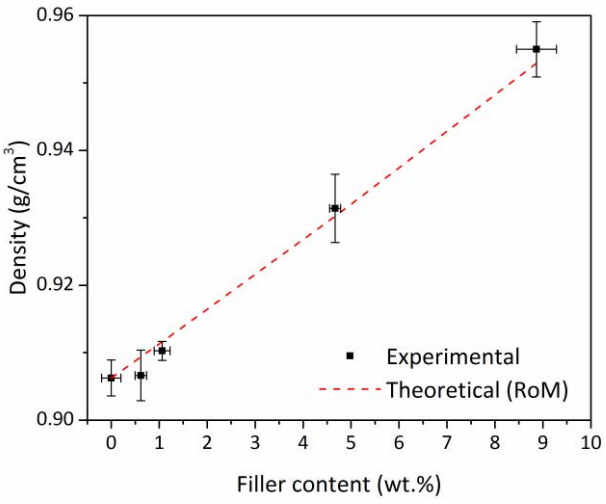

Figure A.3 Measured densities of PP and composites and theoretical values obtained by the rule of mixtures as a function of the filler content, obtained from TGA.

Table A.1 Melting temperature (T_m), degree of crystallinity (X_C) and crystallisation temperature (T_c) of neat PP and CMF composites, obtained by DSC.

CMF content (wt.%)	T_m (°C)		X_C (%)		T_c (°C)
	1st heating	2nd heating	1st heating	2nd heating	
0	164.6±1.1	161.8±0.6	46.5±0.6	45.5±0.5	116.7±0.2
0.6	165.0±0.4	162.0±0.9	47.0±1.3	46.1±1.1	120.2±0.2
1.1	165.4±0.9	162.4±0.6	47.1±0.8	46.6±1.0	121.1±0.1
4.7	165.8±1.2	162.7±0.5	47.2±1.1	47.2±0.4	123.0±0.0
8.9	165.7±1.1	164.2±0.2	48.0±0.6	47.3±0.4	124.1±0.1

Table A.2 Storage modulus (E'), in the glassy state and in the rubbery state, of neat PP and CMF composites. In parentheses are indicated the increment (in %) compared to the neat PP

CMF content (wt.%)	E' glassy state, at -150 °C (MPa), increment (%)	E' rubbery state, at 50 °C (MPa), increment (%)
0	4916 (-)	1419 (-)
0.6	4812 (-2.1)	1393 (-1.8)
1.1	5091 (+3.6)	1510 (+6.4)
4.7	5267 (+7.1)	1616 (+13.9)
8.9	5398 (+9.8)	1751 (+23.4)

A2 References

[1] A.C. Ferrari, D.M. Basko, Raman spectroscopy as a versatile tool for studying the properties of graphene, Nat. Nanotechnol. 8 (2013) 235–246. doi:10.1038/nnano.2013.46.

[2] R.A. DiLeo, B.J. Landi, R.P. Raffaelle, Purity assessment of multiwalled carbon nanotubes by Raman spectroscopy, J. Appl. Phys. 101 (2007) 064307. doi:10.1063/1.2712152.

Annex B: Supplementary Information for Chapter 6

B1 Synthesis and characterization of hybrid nanoparticles

The effect of the duration of the pre-treatment of the catalyst precursor was analysed. The aim of the pre-treatment is to decompose and reduce the Fe-salt used as catalyst precursor to obtain Fe nanoparticles required for the CNT growth [1–4]. The pre-treatment and growth temperature was 650 °C and the growth reaction time was 1 min. Four CVD processes with conditioning treatments of 5, 7, 10 and 20 min were carried out. The amount of alumina nanoparticles placed in the alumina boat for each CVD batch was 50 mg.

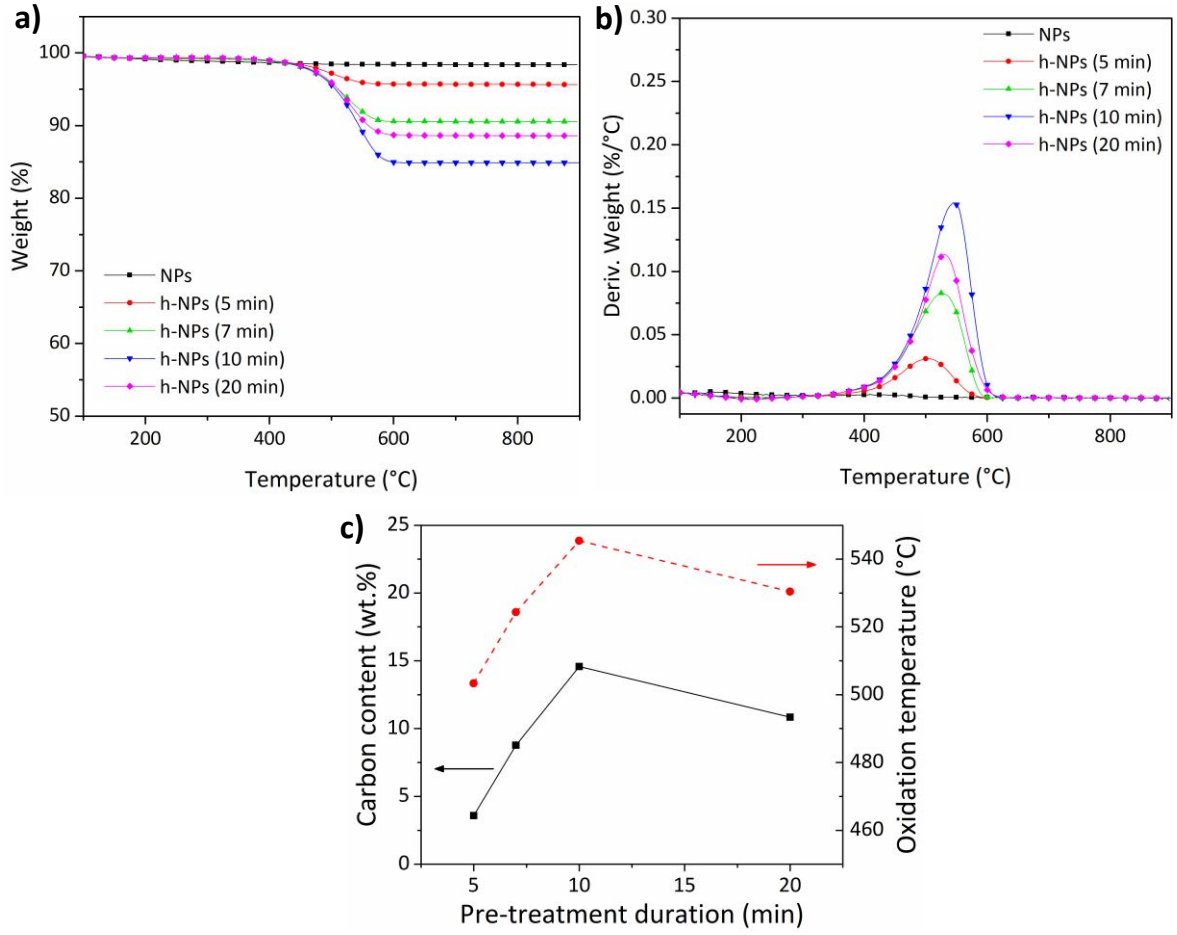

Figure B.1 Curves obtained from the TGA, corresponding to the a) weight (%) and b) first derivative of the weight (%/°C) of hybrid nanoparticles obtained after a CVD process with a catalyst precursor

pre-treatments of 5, 7, 10 and 20 min. c) carbon content and oxidation temperature, respectively, as a function of the pre-treatment duration.

The carbon content and oxidation temperature, T_o, of the CNTs in the hybrid material obtained after the CVD processes were calculated from the obtained TGA curves (Figure B.1). The decomposition temperatures of MWNTs are usually in the range from 400 to 600 °C [5,6]. As it can be observed in Figure B.1a the alumina nanoparticles are thermally stable up to 900 °C. Therefore, the weight loss of the samples upon heating during the TGA is associated with the decomposition of CNTs and the lost wt.% is taken as the CNT content of the hybrid material.

The temperature at which the highest rate of sample's weight loss takes place is the oxidation temperature and it corresponds to the maximum of the degradation peak in the first derivative of the weight curve (Figure B.1b). It can be observed in Figure B.1c, as the duration of the catalyst precursor treatment under H_2 increases from 5 to 10 min, the amount of carbon in hybrid materials increases, reaching a maximum value of 14.6 wt.% of C. However, for a catalyst precursor treatment of 20 min, just a 10.8 wt.% of carbon is obtained for the h-NPs.

The oxidation temperature of the synthesized CNTs (Figure B.1c) is located in the range from 500 to 550 °C and it follows a similar trend to that of the carbon content, i.e. T_o reaches its maximum for the h-NPs obtained after the CVD process with a catalyst pre-treatment of 10 min.

When comparing carbon-based nanomaterials, a higher decomposition temperature is indicative of purer or less defective material [5–8]. Regarding this parameter, in order of increasing temperature, amorphous carbon decomposes first, followed by SWNTs and, finally, the MWNTs and graphitic particles. Thus, the decomposition temperatures obtained in this work are similar to those corresponding to MWNTs, which generally are between 400 and 600 °C [5,6].

The results obtained from the BET surface area analysis showed that the as-received alumina nanoparticles have a specific surface area of 29.8 m^2/g, in agreement with the value provided by the manufacturer. The specific surface area obtained for the h-NPs are shown in Figure B.2d. It can be observed that the

specific surface area of h-NPs follows the same trend as that of the carbon content as a function of the pre-treatment duration.

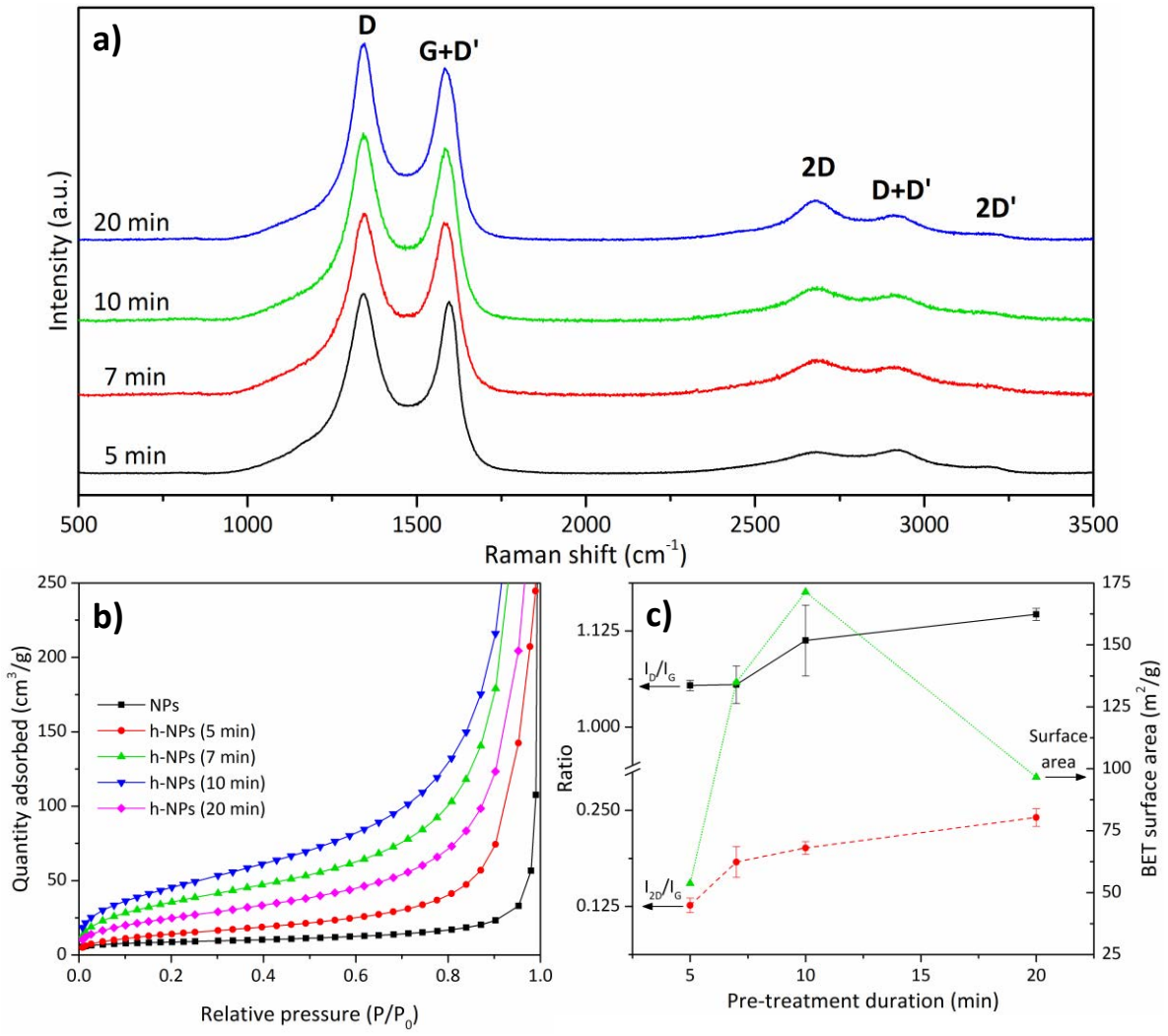

Figure B.2 a) Raman spectra of hybrid nanoparticles obtained after a CVD process with a catalyst precursor pre-treatments of 5, 7, 10 and 20 min. b) isothermal adsorption curves obtained from the BET surface area measurements and c) I_D/I_G and I_{2D}/I_G ratios obtained from the peaks in the Raman spectra (left axis); and BET surface area of h-NPs (right axis).

Raman spectroscopy was performed to study the quality of the synthesized CNTs. The spectra were acquired in the range from 500 to 3500 cm^{-1} (Figure B.2a). The characteristic peaks associated with the presence of carbon allotropes [5,9,10] can be observed in the acquired spectra.

The ratio between the intensity of the D peak to the intensity of the G peak (I_D/I_G) has been extensively used as a way to assess the purity or quality of carbon nanotubes [5,11,12]. In this work, the I_D/I_G ratio of the h-NPs increases as the pre-

treatment duration increases, from 1.05, for 5 min of pre-treatment, to 1.15, for 20 min of pre-treatment. Alternatively, it has been proposed that the ratio I_{2D}/I_G could also be used to qualitatively quantify the amount of CNTs in a sample, as the 2D peak intensity is drastically enhanced by the presence of CNTs while being less sensitive to defects than the D peak [11]. Thus, it is observed that the I_{2D}/I_G ratio experiences a similar trend to that of the I_D/I_G ratio; varying from 0.13 (5 min of pre-treatment) to 0.24 (20 min of pre-treatment). However, the relative variation is significantly higher than that experienced by the former ratio.

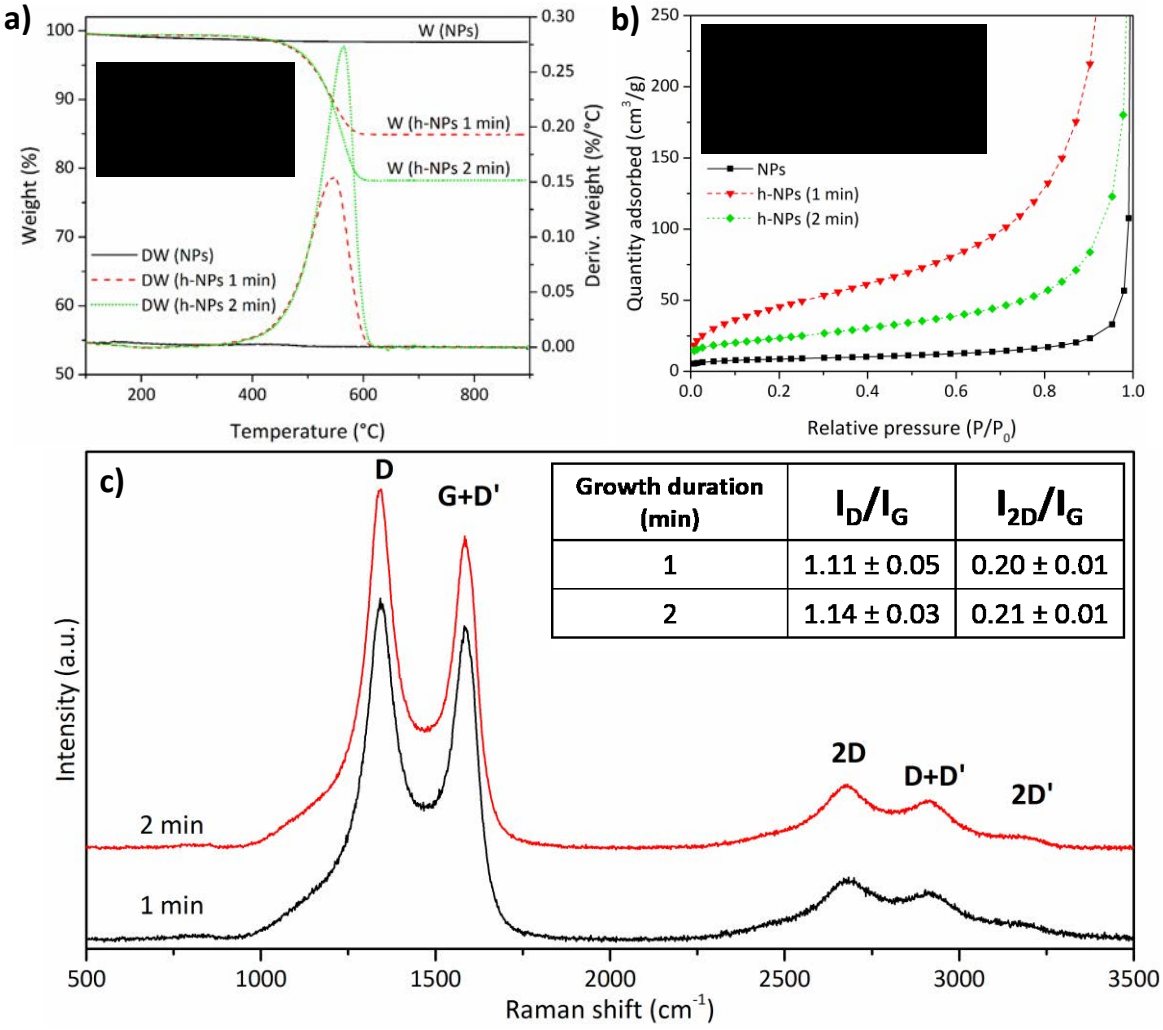

Figure B.3 Curves obtained from the TGA, corresponding to the a) weight (%) and first derivative of the weight (%/°C), b) isothermal adsorption curves obtained from the BET surface area measurements and c) Raman spectra of hybrid nanoparticles obtained after a CVD process with growth steps of 1 and 2 min. The tables give in a) the carbon content and oxidation temperature, in b) the specific surface area and in c) the I_D/I_G and I_{2D}/I_G ratios obtained from the peaks in the Raman spectra, for the h-NPs obtained after growth steps of 1 and 2 min of duration.

In [13] the authors had synthesized CNTs on ceramic microspheres, obtaining an I_D/I_G value of 0.72 for a growth temperature of 800 °C. When this temperature is reduced to 700 °C, the I_D/I_G value increases up to 1.35. The authors attributed this increase due to a higher defect density. In a work reporting the growth of CNTs on alumina microparticles it was found that the I_D/I_G value of the CNTs decreases with increasing the temperature of synthesis [14].

Regarding the quality of the synthesized CNTs, analysed by Raman spectroscopy, it seems that as the pre-treatment duration increase the amount of CNTs also increase, however the quality of these CNTs decrease.

Thus, taking into account the above presented results it was decided that a pre-treatment of the catalyst of 10 min of duration was the optimal for the subsequent CNT growth as it provides the highest amount of carbon nanotubes, which are also the most thermally stable. Moreover, the chosen pre-treatment gives as a result the h-NPs with the highest surface area.

For the synthesis of h-NPs to be used as filler in epoxy composites, the duration of the growth step was increased from 1 to 2 min, in order to obtain a higher amount of CNTs (Figure B.3a). This was successfully achieved as the carbon content after a growth step of 2 min is 21 wt.%. However, increasing the growth duration results in a reduction of the specific surface area, as observed in Figure B.3b. Regarding the quality, it can be observed that both hybrid materials exhibits similar Raman spectra, thus, similar I_D/I_G and I_{2D}/I_G ratios (Figure B.3c).

B2 Nanocomposite characterisation

The morphology of the as-received alumina nanoparticles was analysed by SEM (Figure B.4a) and TEM (Figure B.5). Furthermore, an SEM image of the agglomerated hybrid material is shown in Figure B.4b.

High magnification SEM images of the NP and h-NP composites are shown in Figure B.6. In the NP composite, the individual spherical nanoparticles can be observed. From the observation of Figure B.6c the adhesion between the NPs and

the matrix seems to be weak, as the nanoparticle seem to be debonded. In the h-NP composites, the individual NPs can also be observed in Figure B.6d. Furthermore, in this image carbon nanotubes which are not attached to the nanoparticles are indicated by the white arrows.

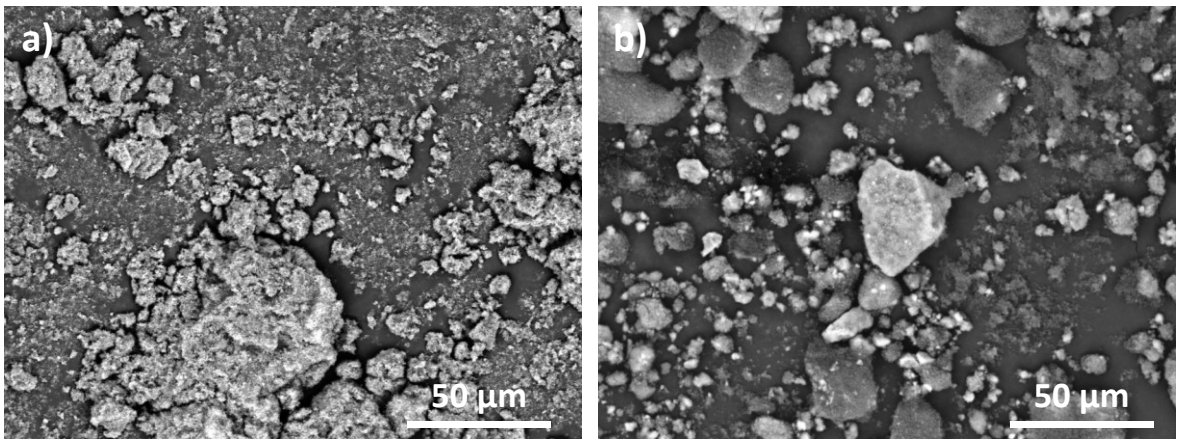

Figure B.4 Low magnification SEM images of the a) as-received alumina nanoparticles and b) hybrid nanoparticles, composed by alumina nanoparticles and carbon nanotubes, obtained after the CVD process.

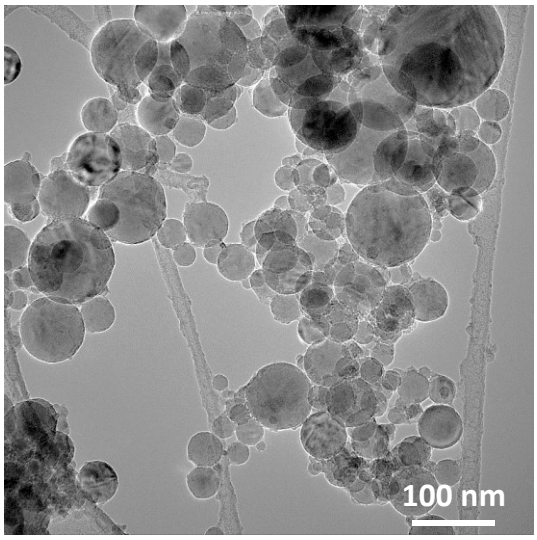

Figure B.5 TEM image of the as-received nanoparticles.

The NP and CNT volume fractions, ϕ_{NP} and ϕ_{CNF}, respectively; were estimated using a matrix density of ρ_m =1.14 g/cm^3, an alumina density of ρ_{NP} =3.97 g/cm^3, as provided by the manufacturer, and a CNT density of ρ_{CNT} =1.9 g/cm^3 [15]. The values were obtained applying the rule of mixtures (Eq. B.1 and Eq. B.2):

$$\phi_{NP} = \frac{w_{NP}}{w_{NP} + w_m \frac{\rho_{NP}}{\rho_m} + w_{CNT} \frac{\rho_{NP}}{\rho_{CNT}}} \quad \text{Eq. B.1}$$

$$\phi_{CNF} = \frac{w_{CNT}}{w_{CNT} + w_m \frac{\rho_{CNT}}{\rho_m} + w_{NP} \frac{\rho_{CNT}}{\rho_{NP}}} \quad \text{Eq. B.2}$$

Where w_m, w_{NP} and w_{CNT} are the matrix, nanoparticles and CNT weight fraction, respectively. In the case of the h-NP composites, it was taken into account the results obtained by TGA which indicated that $w_{CNT} = 0.8\, w_{h-NP}$. The calculated filler volume fractions are given in Table B.1.

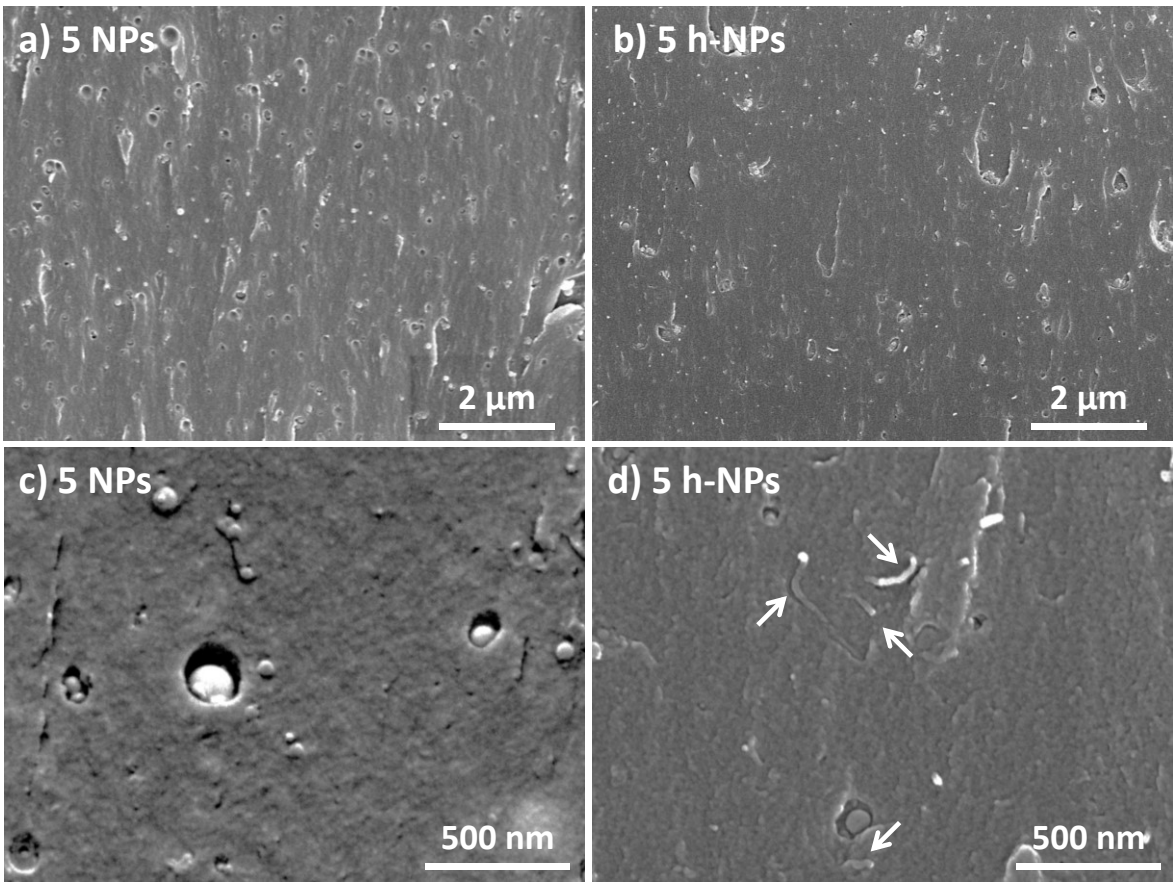

Figure B.6 High magnification SEM images of the nanocomposites with a 0.5 wt.% of a) NPs and b) h-NPs and with 5 wt.% of c) NPs and d) h-NPs, where the dispersion of the filler can be observed. In c) and d) the individual NPs and CNTs dispersed within the matrix could be observed.

The glass transition temperatures, calculated from the different curves obtained by DMA, are listed in Table B.2.

The curves obtained from the TGA, corresponding to the first derivative of the weight (%/°C) of the neat resin and the NP and h-NP composites are presented in Figure B.7.

Table B.1 Estimated volume fractions of nanoparticles and carbon nanotubes on the resulting nanocomposites.

Sample	Total nanofiller content (wt.%)	NP content (vol.%)	CNT content (vol.%)
0.5 NPs	0.5	0.14	-
1 NPs	1	0.29	-
2 NPs	2	0.58	-
5 NPs	5	1.49	-
0.5 h-NPs	0.5	0.12	0.06
1 h-NPs	1	0.23	0.12
2 h-NPs	2	0.47	0.24
5 h-NPs	5	1.19	0.58

Table B.2 Glass transition temperature of neat resin, NP and h-NPs composites obtained from the storage modulus and tan δ curves.

Sample	T_g onset (°C)	T_g E' (°C)	T_g tanδ (°C)
Resin	192.2	203.7	227.1
0.5 NPs	191.8	202.9	226.5
1 NPs	192.2	203.6	226.0
2 NPs	193.2	204.3	226.6
5 NPs	193.2	204.8	227.0
0.5 h-NPs	193.2	204.5	227.0
1 h-NPs	194.5	205.6	226.9
2 h-NPs	194.5	205.3	227.3
5 h-NPs	195.4	206.3	227.0

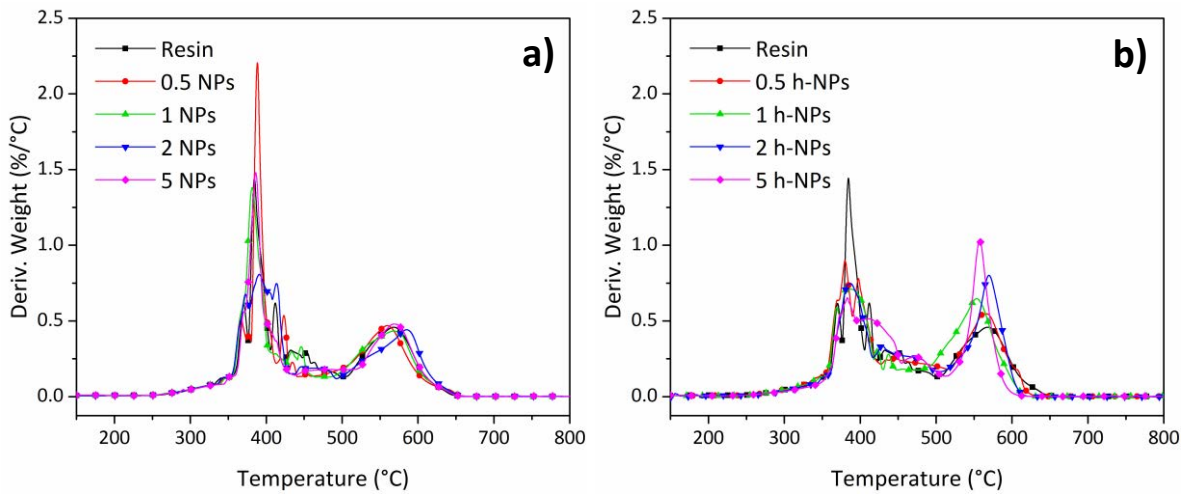

Figure B.7 Curves obtained from the TGA, corresponding to the first derivative of the weight (%/°C) of the neat resin and the a) NP and b) h-NP composites.

In Figure B.8 it can be observed the DSC thermograms showing the first and second heating cycles for NP and h-NP composites.

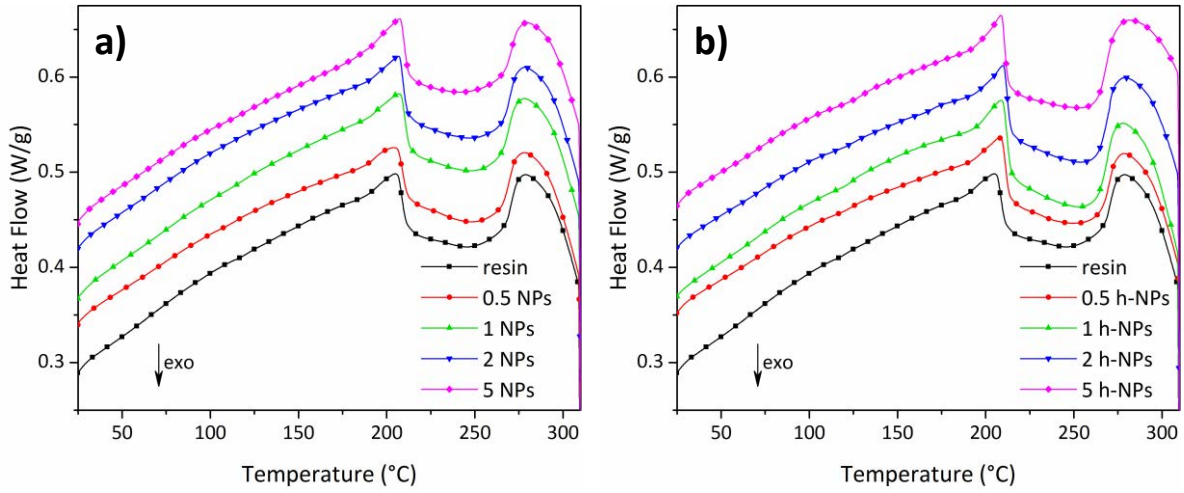

Figure B.8 DSC thermograms showing the first heating curve of a) NP and b) h-NP composites.

The sub-T_g relaxation, known as ω relaxation, observed in the range between 50 and 150°C is shown in Figure B.9.

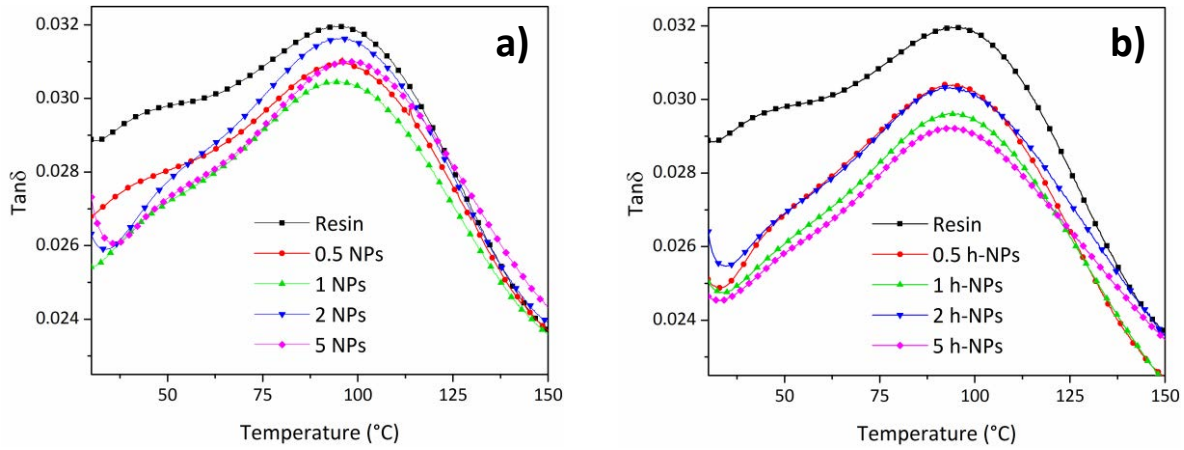

Figure B.9 Tan δ (at a frequency of 1 Hz) showing the ω relaxation of the a) NP and b) h-NP composites.

B3 References

[1] N. Yamamoto, A. John Hart, E.J. Garcia, S.S. Wicks, H.M. Duong, A.H. Slocum, B.L. Wardle, High-yield growth and morphology control of aligned carbon nanotubes on ceramic fibers for multifunctional enhancement of structural composites, Carbon. 47 (2009) 551–560. doi:10.1016/j.carbon.2008.10.030.

[2] G.D. Nessim, A.J. Hart, J.S. Kim, D. Acquaviva, J. Oh, C.D. Morgan, M. Seita, J.S. Leib, C.V. Thompson, Tuning of Vertically-Aligned Carbon Nanotube Diameter and Areal Density through Catalyst Pre-Treatment, Nano Lett. 8 (2008) 3587–3593. doi:10.1021/nl801437c.

[3] E. Terrado, M. Redrado, E. Muñoz, W.K. Maser, A.M. Benito, M.T. Martínez, Aligned carbon nanotubes grown on alumina and quartz substrates by a simple thermal CVD process, Diam. Relat. Mater. 15 (2006) 1059–1063. doi:10.1016/j.diamond.2005.10.071.

[4] O.A. Nerushev, M. Sveningsson, L.K.L. Falk, F. Rohmund, Carbon nanotube films obtained by thermal chemical vapour deposition, J. Mater. Chem. 11 (2001) 1122–1132. doi:10.1039/b009775f.

[5] J.H. Lehman, M. Terrones, E. Mansfield, K.E. Hurst, V. Meunier, Evaluating the characteristics of multiwall carbon nanotubes, Carbon. 49 (2011) 2581–2602. doi:10.1016/j.carbon.2011.03.028.

[6] B. Scheibe, E. Borowiak-Palen, R.J. Kalenczuk, Oxidation and reduction of multiwalled carbon nanotubes — preparation and characterization, Mater. Charact. 61 (2010) 185–191. doi:10.1016/j.matchar.2009.11.008.

[7] S. Arepalli, P. Nikolaev, O. Gorelik, V.G. Hadjiev, W. Holmes, B. Files, L. Yowell, Protocol for the characterization of single-wall carbon nanotube material quality, Carbon. 42 (2004) 1783–1791. doi:10.1016/j.carbon.2004.03.038.

[8] D. Bom, R. Andrews, D. Jacques, J. Anthony, B. Chen, M.S. Meier, J.P. Selegue, Thermogravimetric Analysis of the Oxidation of Multiwalled Carbon Nanotubes: Evidence for the Role of Defect Sites in Carbon Nanotube Chemistry, Nano Lett. 2 (2002) 615–619. doi:10.1021/nl020297u.

[9] A.C. Ferrari, D.M. Basko, Raman spectroscopy as a versatile tool for studying the properties of graphene, Nat. Nanotechnol. 8 (2013) 235–246. doi:10.1038/nnano.2013.46.

[10] B.L. Crossley, N.E. Glauvitz, B.T. Quinton, R.A. Coutu, P.J. Collins, Characterizing Multi-Walled Carbon Nanotube Synthesis for Field Emission Applications, in: J.M. Marulanda (Ed.), Carbon Nanotub. Appl. Electron Devices, InTech, 2011.

[11] R.A. DiLeo, B.J. Landi, R.P. Raffaelle, Purity assessment of multiwalled carbon nanotubes by Raman spectroscopy, J. Appl. Phys. 101 (2007) 064307. doi:10.1063/1.2712152.
[12] A.C. Ferrari, J. Robertson, Raman spectroscopy of amorphous, nanostructured, diamond–like carbon, and nanodiamond, Philos. Trans. R. Soc. Lond. Math. Phys. Eng. Sci. 362 (2004) 2477–2512. doi:10.1098/rsta.2004.1452.
[13] Q. Zhang, J. Huang, F. Wei, G. Xu, Y. Wang, W. Qian, D. Wang, Large scale production of carbon nanotube arrays on the sphere surface from liquefied petroleum gas at low cost, Chin. Sci. Bull. 52 (2007) 2896–2902. doi:10.1007/s11434-007-0458-8.
[14] D. He, M. Bozlar, M. Genestoux, J. Bai, Diameter- and length-dependent self-organizations of multi-walled carbon nanotubes on spherical alumina microparticles, Carbon. 48 (2010) 1159–1170. doi:10.1016/j.carbon.2009.11.039.
[15] T.M. Herceg, S.-H. Yoon, M.S.Z. Abidin, E.S. Greenhalgh, A. Bismarck, M.S.P. Shaffer, Thermosetting nanocomposites with high carbon nanotube loadings processed by a scalable powder based method, Compos. Sci. Technol. 127 (2016) 62–70. doi:10.1016/j.compscitech.2016.01.017.

Annex C: Supplementary Information for Chapter 7

C1 Morphology and Raman spectroscopy of the synthesized carbon-based structures

The morphology of the carbon-based materials, which were synthesized by the chemical vapour deposition process, were analysed by using transmission electron microscopy. The predominant material observed was amorphous carbon nanofibers (Figure C.1a and b), although hollow carbon nanofibers (Figure C.1c and d), carbon nanotubes (Figure C.1e and f), and graphitic particles (Figure C.1g and h) were also identified.

The Raman spectrum of the synthesized hybrid fillers (Figure C.2) presents three main peaks associated with the presence of sp2-bonded carbon allotropes [1–3]. The peak that appears at ca. 1340 cm–1 is the D peak, which is a disorder-induced peak caused by the presence of defects in the graphitic structure of the CNFs [1]. The peak at ca. 1590 cm–1 is a combination of the G peak, which arises from the tangential vibrations of carbon atoms and is indicative of a graphitized carbon structure, and the D′ peak, which is a double resonance process that arises from the presence of defects [1]. At ca. 2680 cm–1 the 2D peak appears; this is the D peak overtone, which results from a second-order scattering process, and is indicative of long-range order in the carbon-based structures synthesized. The peak that appears at ca. 2920 cm–1 is known as the D + D′ peak because it originates from a two-phonon defect-assisted process that involves one intervalley and one intravalley phonon. The 2D′ peak, at ca. 3180 cm–1, is the second-order D′ peak overtone.

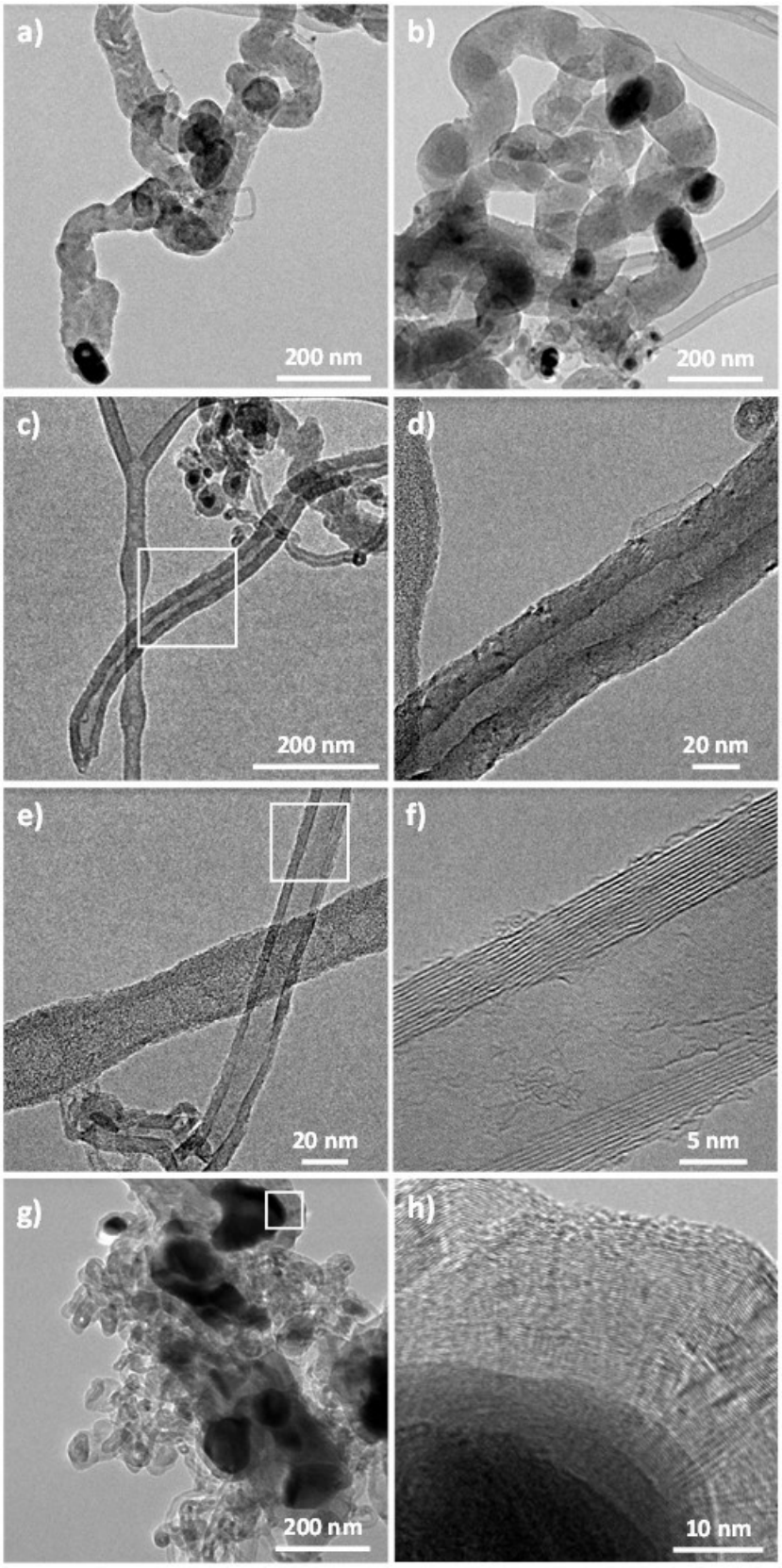

Figure C.1 Different carbon structures identified by TEM. a) and b) show different amorphous carbon nanofibers. c) Hollow carbon nanofiber, d) shows the boxed area of (c), magnified, where the nanofiber walls can be observed at higher magnification. In e) a CNT is shown; the graphitic walls

can be observed in f). In g) graphitic particles may be formed by concentric graphitic layers around catalyst particles. A higher magnification image, corresponding to the inset in g), is shown in h).

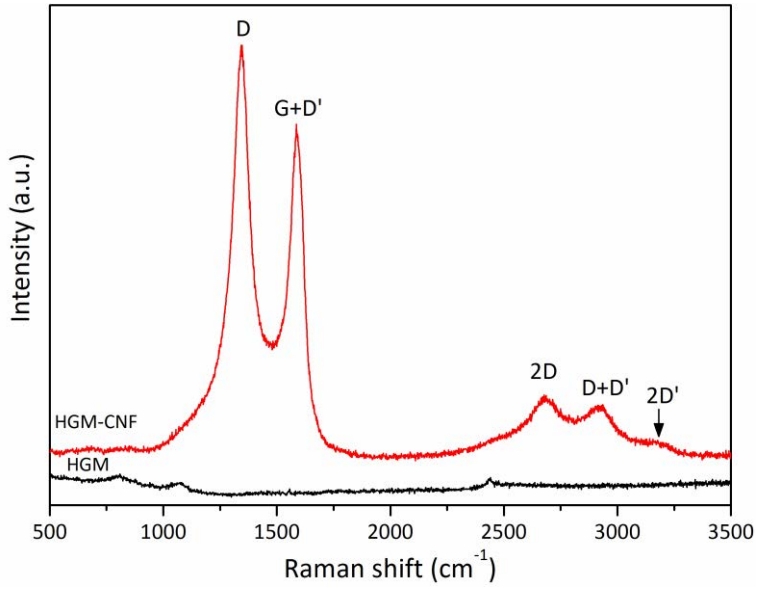

Figure C.2 Raman spectra of the as-received HGMs and the HGMs-CNFs, showing the characteristic D, G, and 2D peaks of carbon-based nanomaterials.

The ratio between the intensity of the D peak to the intensity of the G peak (ID/IG) was extensively used as a way to assess the purity or quality of carbon nanotubes [3,4]. In reference [5] the authors synthesized CNT on ceramic microspheres and obtained an ID/IG value of 0.72 for a growth temperature of 800 °C. When this temperature was reduced to 700 °C, the ID/IG value increased up to 1.35. The authors attributed this increase due to a higher defect density. He et al. reported [6] the growth of CNT on alumina microparticles and they found that the ID/IG value of the CNTs decreases with increasing the temperature of synthesis. Nguyen et al. [7] studied the synthesis of CNTs on stainless steel nanoparticles. They also reported that the degree of graphitization of the CNTs increases with increasing the growth temperature, with ID/IG values of approximately 1.15, 0.95, 0.9 and 0.7 for growth temperatures of 600, 650, 750 and 800 °C, respectively. Othman et al. [4] characterized the growth of CNTs on silica microparticles at 760 °C, by varying the synthesis time. From the Raman spectra, they deduced that the intensity of the D peak was similar to that of the G peak, ID/IG ≈1, as observed in the above-mentioned works. In the present study, a ID/IG value of 1.14 ± 0.8 was obtained.

This is in good agreement with the values reported in the available literature for similar growth temperatures (600 °C in this work).

C2 Density of hybrid microspheres

Assuming that a hybrid microsphere is composed of a HGM that is completely covered by a layer of CNFs, then the volume fraction of CNFs, over the total volume of the HGM-CNF, is given by Eq. C.1:

$$\phi_{CNF} = \frac{w_{CNF}}{w_{CNF} + (1 - w_{CNF})\frac{\rho_{CNF}}{\rho_{HGM}}} \quad \text{Eq. C.1}$$

Where w_{CNF} is the weight fraction corresponding to the CNFs, which is 0.25, as obtained from the TGA (Figure 7.2); ρ_{HGM} is the density of HGMs, and ρ_{CNF} is the density of CNFs, which is taken as 2.0 g/cm^3 [8].

The theoretical density of the hybrid microspheres, $\rho_{HGM-CNF}$=0.258 g/cm^3, can be obtained by application of the rule of mixtures [9,10], Eq. C.2:

$$\rho_{HGM-CNF} = \phi_{HGM}\rho_{HGM} + \phi_{CNF}\rho_{CNF} \quad \text{Eq. C.2}$$

C3 Density and morphology of composites

As obtained by TGA (Figure 7.2), HGMs do not exhibit weight changes when heated up to 800 °C. Thus, it is assumed that the residue left after the TGA of composites corresponds to the HGMs that were added to the matrix for the production of composites. For the neat resin, a residue of 0.2 wt.% is obtained. Thus, the following expression is used to determine the amount of HGMs, taking into account the residue that corresponds to the matrix [11]:

$$w_{HGM} = r_c - r_m w_m \quad \text{Eq. C.3}$$

where w_{HGM} and w_m are the weight fraction of HGMs and matrix, respectively, and r_c and r_m are the residue obtained by TGA for the composites and the matrix, respectively. In the case of the HGM-CNF composites, the TGA results (Figure 7.2) showed that the amount of CNFs grown by CVD was approximately 25 wt.% of the HGMs-CNFs. Thus, the value of w_{HGM} was divided by 0.75, to obtain the total content of HGMs-CNFs that was added to the matrix.

The experimental density of composite materials was calculated by applying the following equation, Eq. C.4:

$$\rho_m = \frac{W_a}{W_a - W_w}\rho_w \qquad \text{Eq. C.4}$$

where ρ_m is the measured density of the material and ρ_w is the density of distilled water or absolute ethanol at 24 °C, and W_a and W_w are the weight of the sample in air and immersed in water or ethanol, respectively.

The theoretical density of the composite materials is obtained by application of the rule of mixtures [9,10], Eq. C.5:

$$\rho_C = \phi_m\rho_m + \phi_f\rho_f \qquad \text{Eq. C.5}$$

The filler's volume fraction, ϕ_f, of composites was obtained by applying the following equation [12,13], Eq. C.6:

$$\phi_f = \frac{w_f}{w_f + (1 - w_f)\frac{\rho_f}{\rho_m}} \qquad \text{Eq. C.6}$$

where w_f and w_m are the weight fraction of filler and matrix, and ρ_f and ρ_m are the density of filler and matrix, respectively. w_f and w_m are the weight fractions obtained by TGA (Table C.1).

Generally, the experimental density of the composites is lower than the theoretically calculated density. Some authors explain this difference in terms of

porosity, which tends to lower the density, or by break up of HGMs, which tends to increase it [11,14,15]. The porosity is the air entrapped within the resin at the moment of the mixing step, during the processing of the composite. During the processing, some HGMs may be broken due to mixing forces. The difference between the theoretical and the experimental density, in volume fraction, is calculated as follows (Eq. C.7):

$$\Phi_p = \frac{\rho_{th} - \rho_e}{\rho_{th}} \times 100 \qquad \text{Eq. C.7}$$

where ρ_{th} and ρ_e are the theoretical and experimental density of the composites. The value of Φ_p is –0.2, 2.3 and 3.2 vol.% for the 2, 5, and 10 wt.% HGM composites, respectively. For the HGM-CNF composites, Φ_p is –2.6, –1.6 and 3.5 vol.% for the composites with 2, 5, and 10 wt.% of HGM-CNF. Φ_p, considered to be matrix porosity, increases with an increasing amount of filler. The matrix porosity reaches its maximum for the composites with the highest amount of filler, i.e. 10 wt.%. This seems reasonable because the composite processing becomes more difficult as the amount of filler increases, due to the drastic increase in the mixture viscosity. The negative values may be produced by HGM fracture during processing or error in the estimation of the CNF density.

Table C.1 Theoretical density calculated for the different composites and difference between the theoretical and the experimental density

Filler amount (wt.%)		Theoretical density (g/cm^3)	Difference (vol.%)
0		-	0.0
HGMs	2	1.054	–0.2
	5	0.943	2.3
	10	0.776	3.2
HGM-CNFs	2	1.073	–2.6
	5	0.988	–1.6
	10	0.853	3.5

In the case of epoxy composites, Lin *et al.* [11] reported matrix porosities between 2.0 and 6.3 vol.%, for composites with 30 and 40 vol.% of HGMs. Tagliavia *et al.* [16] and Gupta *et al.* [17] produced composites consisting of a vinyl ester matrix with HGMs. For a 30 and 40 vol.% of HGMs, the composites had porosity values between 2.6 and 9.3 vol.% [16], and 0.0 and 8.7 vol.% [17]. , Shunmugasamy *et al.* [15,18] reported, for a 30 and 40 vol.% of HGMs dispersed within a vinyl ester resin, porosity values of between 1.2 and 4.6 vol.%. In the case of composites with HGMs and CNFs, Poveda *et al.* [19] produced composites with 1 wt.% of CNFs and 30 to 50 vol.% of HGMs, obtaining porosity values between 0.7 and 3.7 vol.%. All of these works used HGMs (3M Glass microspheres) similar to those in the present study. The HGMs have densities (g/cm^3)/average diameter (μm) ratios of 0.220/35, 0.320/40, 0.370/40, 0.380/40 and 0.460/40. In this work, the composites with the highest amount of filler have 10.4 wt.% of HGM and 10.3 wt.% of HGM-CNF, which corresponds to 40 and 34 vol.%, respectively. As discussed above, the values of matrix porosity obtained for the materials produced in the present study are comparable to those in the available literature for similar composites [11,15–19].

The two different directions defined in this work, for the samples produced, can be observed in Figure C.3.

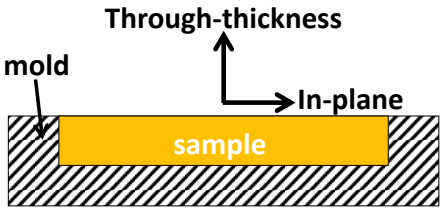

Figure C.3 Schematic representation of the two different directions defined for all the samples processed.

The distribution of the as-received and hybrid microspheres, for all the composites processed in this work, can be observed in Figure C.4. The white arrow indicates the through-thickness direction.

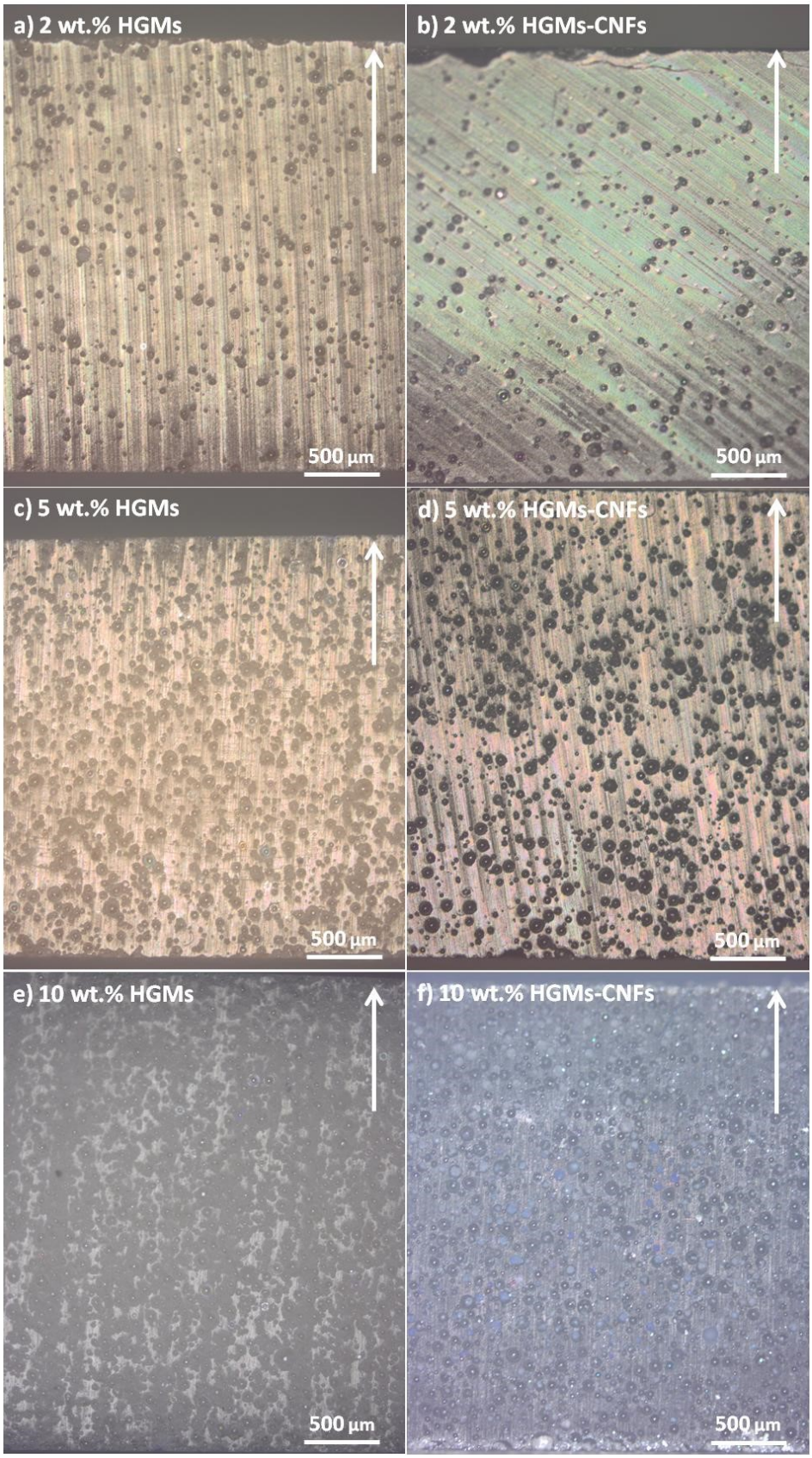

Figure C.4 Light microscope image showing the transverse section of the composites. a) 2, c) 5 and e) 10 wt.% of HGMs. And the composites with b) 2, d) 5 and f) 10 wt.% of HGMs-CNFs. The arrow indicates the top surface of the sample.

In Figure C.5 SEM images are shown of the hand-fractured surfaces of composites with HGM and HGM-CNFs. In these images the dispersion of the filler can be observed.

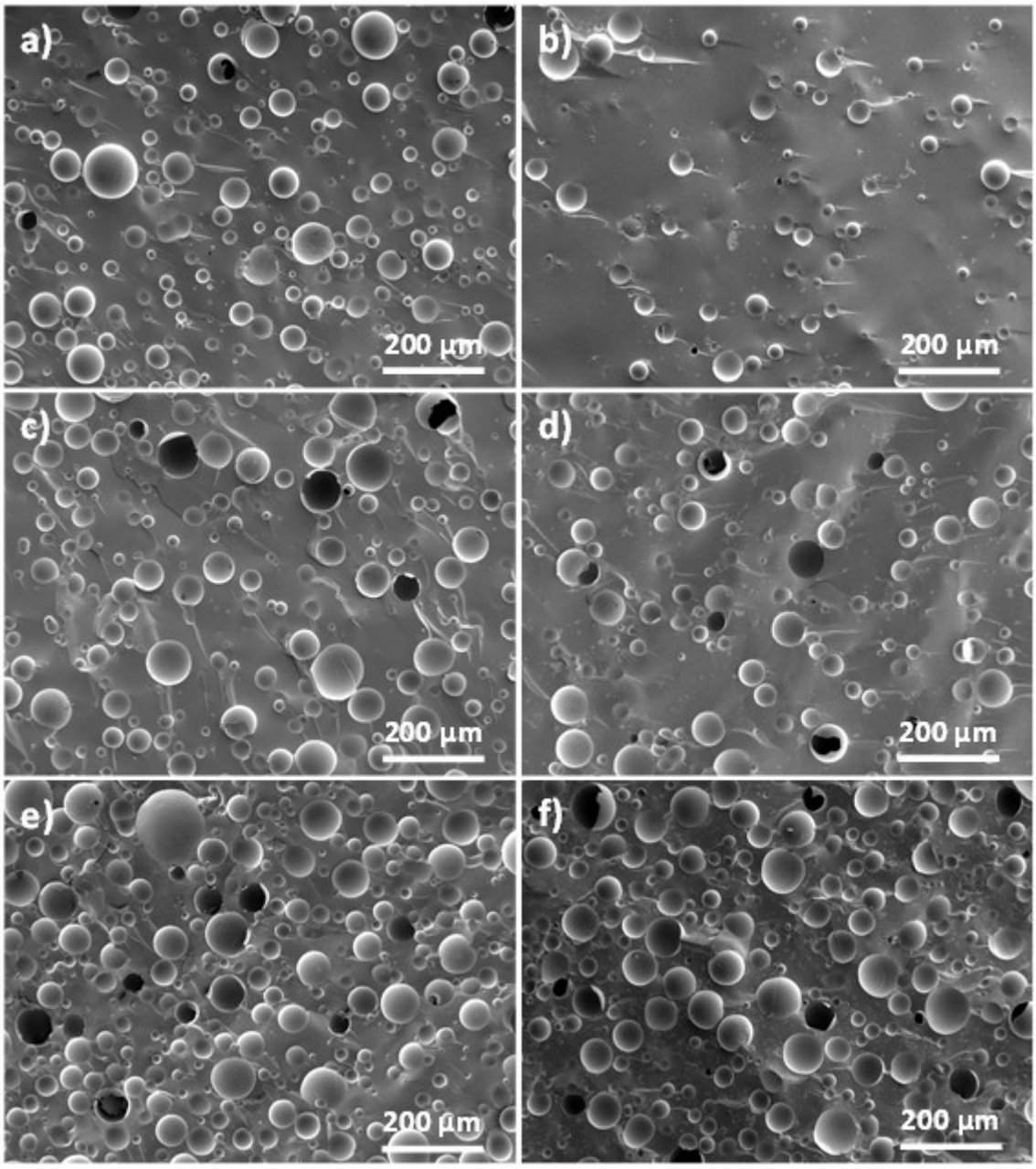

Figure C.5 SEM images showing the dispersion of the processed composites. a) 2 wt.% HGM b) 2 wt.% HGM-CNF, c) 5 wt.% HGM, d)5 wt.% HGM-CNF, e) 10 wt.% HGM and f) 10 wt.% HGM-CNF.

C4 Thermal conductivity of composites

The series, parallel, and Maxwell models were applied to calculate the theoretical thermal conductivity of the resulting HGM-CNF composites.

The parallel circuit model, applied to a composite material (Eq. C.8), represents the formation of a thermally conductive network that is parallel to the direction of heat flow. As this network offers the minimum resistance to heat transfer, this model gives the upper bound of the effective thermal conductivity that can be achieved for the resulting composite. The effective thermal conductivity of the composite, k_c, is given by Eq. C.8:

$$k_c = \phi_m k_m + \phi_f k_f \quad \text{Eq. C.8}$$

where ϕ_m and k_m are the volume fraction and thermal conductivity of the matrix, respectively; and ϕ_f and k_f are the volume fraction and thermal conductivity of the dispersed phase, i.e. filler [20–22]. In this work k_{HGM} has a value of 0.07 W/mK, as provided by the HGM's manufacturer.

The series circuit model (Eq. C.9) represents a configuration where the phases of the composite are arranged perpendicular to the heat flow. This configuration provides the maximum insulating behavior, thus representing the lower bound for the effective thermal conductivity of the composite.

$$k_c = \frac{1}{\frac{\phi_m}{k_m} + \frac{\phi_f}{k_f}} \quad \text{Eq. C.9}$$

The Maxwell model, applied to predict the thermal conductivity of a material consisting in randomly dispersed and noninteracting spheres within a continuous phase [23], is given by Eq. C.10:

$$k_c = k_m \left(\frac{2k_m + k_f - 2\phi_f (k_m - k_f)}{2k_m + k_f + \phi_f (k_m - k_f)} \right) \quad \text{Eq. C.10}$$

Assuming that the HGM-CNF composites follows the Maxwell model, Eq. C.10 was used to obtain the effective thermal conductivity of the HGMs-CNFs as follows, Eq. C.11:

$$k_{HGM-CNF} = \frac{2k_m(1-\phi_{HGM-CNF}) - k_c(2+\phi_{HGM-CNF})}{\frac{k_c}{k_m}(1-\phi_{HGM-CNF}) - 2\phi_{HGM-CNF} - 1} \quad \text{Eq. C.11}$$

C5 Electrical conductivity of HGM-CNF composites

To further understand the electrical behavior of our material, we performed some simple calculations. First, we assumed that all of the HGMs are completely covered by the CNFs, that the thickness of the layer of CNFs is constant and that the HGM-CNF particles have the same particle size. In this case we can assume that, as reported for a particulate-filled continuum matrix composite [24], the percolation threshold corresponds to a volume fraction of HGM-CNF, $\phi_{th/HGM-CNF}$, of 0.187. The weight fraction of HGM-CNF corresponding to the percolation threshold can be obtained from the following equation:

$$w_{HGM-CNF} = \frac{\phi_{th/HGM-CNF}\frac{\rho_{HGM-CNF}}{\rho_m}}{1-\left(1-\frac{\rho_{HGM-CNF}}{\rho_m}\right)\phi_{th/HGM-CNF}} \quad \text{Eq. C.12}$$

The calculated weight fraction, corresponding to the percolation threshold is 4.9 wt% of HGMs-CNFs. The results obtained from the electrical conductivity measurements indicates that the percolation threshold of the HGMs-CNF composites was between a 5 and a 10 wt.% of HGMs-CNFs. Thus, the result obtained from the simple approximation presented above is in agreement with the experimental results.

C6 References

[1] A.C. Ferrari, D.M. Basko, Raman spectroscopy as a versatile tool for studying the properties of graphene, Nat. Nanotechnol. 8 (2013) 235–246. doi:10.1038/nnano.2013.46.

[2] B.L. Crossley, N.E. Glauvitz, B.T. Quinton, R.A. Coutu, P.J. Collins, Characterizing Multi-Walled Carbon Nanotube Synthesis for Field Emission Applications, in: J.M. Marulanda (Ed.), Carbon Nanotub. Appl. Electron Devices, InTech, 2011.

[3] J.H. Lehman, M. Terrones, E. Mansfield, K.E. Hurst, V. Meunier, Evaluating the characteristics of multiwall carbon nanotubes, Carbon. 49 (2011) 2581–2602. doi:10.1016/j.carbon.2011.03.028.
[4] R.N. Othman, I.A. Kinloch, A.N. Wilkinson, Synthesis and characterisation of silica–carbon nanotube hybrid microparticles and their effect on the electrical properties of poly(vinyl alcohol) composites, Carbon. 60 (2013) 461–470. doi:10.1016/j.carbon.2013.04.062.
[5] Q. Zhang, J. Huang, F. Wei, G. Xu, Y. Wang, W. Qian, D. Wang, Large scale production of carbon nanotube arrays on the sphere surface from liquefied petroleum gas at low cost, Chin. Sci. Bull. 52 (2007) 2896–2902. doi:10.1007/s11434-007-0458-8.
[6] D. He, M. Bozlar, M. Genestoux, J. Bai, Diameter- and length-dependent self-organizations of multi-walled carbon nanotubes on spherical alumina microparticles, Carbon. 48 (2010) 1159–1170. doi:10.1016/j.carbon.2009.11.039.
[7] X.H. Nguyen, Y.B. Lee, C.H. Lee, D.-S. Lim, Synthesis of sea urchin-like particles of carbon nanotubes directly grown on stainless steel cores and their effect on the mechanical properties of polymer composites, Carbon. 48 (2010) 2910–2916. doi:10.1016/j.carbon.2010.04.027.
[8] M.H. Al-Saleh, U. Sundararaj, Review of the mechanical properties of carbon nanofiber/polymer composites, Compos. Part Appl. Sci. Manuf. 42 (2011) 2126–2142. doi:10.1016/j.compositesa.2011.08.005.
[9] D. Hull, T.W. Clyne, An Introduction to Composite Materials, Second Edition, 2nd ed., Cambridge University Press, 1996. http://proquest.safaribooksonline.com.strauss.uc3m.es:8080/9781107384859 (accessed January 14, 2016).
[10] C. Swetha, R. Kumar, Quasi-static uni-axial compression behaviour of hollow glass microspheres/epoxy based syntactic foams, Mater. Des. 32 (2011) 4152–4163. doi:10.1016/j.matdes.2011.04.058.
[11] T.C. Lin, N. Gupta, A. Talalayev, Thermoanalytical characterization of epoxy matrix-glass microballoon syntactic foams, J. Mater. Sci. 44 (2009) 1520–1527. doi:10.1007/s10853-008-3074-3.
[12] B.L. Zhu, H. Zheng, J. Wang, J. Ma, J. Wu, R. Wu, Tailoring of thermal and dielectric properties of LDPE-matrix composites by the volume fraction, density, and surface modification of hollow glass microsphere filler, Compos. Part B Eng. 58 (2014) 91–102. doi:10.1016/j.compositesb.2013.10.029.
[13] K.C. Yung, B.L. Zhu, T.M. Yue, C.S. Xie, Preparation and properties of hollow glass microsphere-filled epoxy-matrix composites, Compos. Sci. Technol. 69 (2009) 260–264. doi:10.1016/j.compscitech.2008.10.014.
[14] G. Hu, D. Yu, Tensile, thermal and dynamic mechanical properties of hollow polymer particle-filled epoxy syntactic foam, Mater. Sci. Eng. A. 528 (2011) 5177–5183. doi:10.1016/j.msea.2011.03.071.
[15] V.C. Shunmugasamy, D. Pinisetty, N. Gupta, Viscoelastic properties of hollow glass particle filled vinyl ester matrix syntactic foams: effect of temperature and loading frequency, J. Mater. Sci. 48 (2013) 1685–1701. doi:10.1007/s10853-012-6927-8.
[16] G. Tagliavia, M. Porfiri, N. Gupta, Analysis of flexural properties of hollow-particle filled composites, Compos. Part B Eng. 41 (2010) 86–93. doi:10.1016/j.compositesb.2009.03.004.
[17] N. Gupta, R. Ye, M. Porfiri, Comparison of tensile and compressive characteristics of vinyl ester/glass microballoon syntactic foams, Compos. Part B Eng. 41 (2010) 236–245. doi:10.1016/j.compositesb.2009.07.004.
[18] V.C. Shunmugasamy, D. Pinisetty, N. Gupta, Electrical properties of hollow glass particle filled vinyl ester matrix syntactic foams, J. Mater. Sci. 49 (2014) 180–190. doi:10.1007/s10853-013-7691-0.
[19] R.L. Poveda, G. Dorogokupets, N. Gupta, Carbon nanofiber reinforced syntactic foams: Degradation mechanism for long term moisture exposure and residual compressive properties, Polym. Degrad. Stab. 98 (2013) 2041–2053. doi:10.1016/j.polymdegradstab.2013.07.007.
[20] A. Agrawal, A. Satapathy, Thermal and dielectric behavior of epoxy composites filled with ceramic micro particulates, J. Compos. Mater. (2013). doi:10.1177/0021998313513205.

[21] Z. Han, A. Fina, Thermal conductivity of carbon nanotubes and their polymer nanocomposites: A review, Prog. Polym. Sci. 36 (2011) 914–944. doi:10.1016/j.progpolymsci.2010.11.004.
[22] F.H. Gojny, M.H.G. Wichmann, B. Fiedler, I.A. Kinloch, W. Bauhofer, A.H. Windle, K. Schulte, Evaluation and identification of electrical and thermal conduction mechanisms in carbon nanotube/epoxy composites, Polymer. 47 (2006) 2036–2045. doi:10.1016/j.polymer.2006.01.029.
[23] J.C. Maxwell, A treatise on electricity and magnetism, Oxford : Clarendon Press, 1873. http://archive.org/details/electricandmagne01maxwrich (accessed September 25, 2015).
[24] C.-H. Kuo, P.K. Gupta, Rigidity and conductivity percolation thresholds in particulate composites, Acta Metall. Mater. 43 (1995) 397–403. doi:10.1016/0956-7151(95)90296-1.